UNIVERSITY OF SOUTHAMPTON

Observations of Oceanic Potential Vorticity and its Relationship with Other Tracers

by

Anne Inglis Morrison

Doctor of Philosophy

School of Ocean and Earth Sciences, Faculty of Science

September 1999

UNIVERSITY OF SOUTHAMPTON

ABSTRACT

FACULTY OF SCIENCE

OCEAN AND EARTH SCIENCES

Doctor of Philosophy

Observations of oceanic potential vorticity and its relationship with other tracers.

by Anne Inglis Morrison

Driven by interest in measuring the oceanic velocity field from space, sea surface temperature (SST) has been suggested as a proxy for potential vorticity (PV), which may then be inverted to give velocity. However, little is known about the relationships between PV and other water mass tracers, as these have not previously been thoroughly examined. In this thesis, the inter-relationships between PV, SST, potential temperature and salinity in three quite different frontal regions of the ocean are investigated. The regions studied were in the North-east Atlantic, the Sargasso Sea and the Bellingshausen Sea (Southern Ocean).

The only earlier work known in this field was by Fischer et al. (1989), which found a near-linear relationship between PV and isopycnic potential temperature on a shallow isopycnal in the North Atlantic. This relationship was also evident in climatological values of PV and temperature in the North Atlantic. The results from the three regions considered in this thesis vary considerably, and are believed to be due to different frontal dynamics and water mass formation mechanisms. All the North-east Atlantic results are in close agreement, despite differences in measurement scales and the year of survey.

The reasons for different relationships occurring are examined. Theories for setting PV and tracer values are investigated, and in particular the models of Woods (1985) and Spall (1995) are found to explain the relationships found in the North-east Atlantic and Sargasso Sea, respectively. However, a combination of these models, applied to different scales of motion, is needed to explain the Bellingshausen Sea results. Preliminary work is carried out using a one-dimensional computer model to follow the development of the relationship in the north-east Atlantic.

CONTENTS

LIST OF FIGURES

ACKNOWLEDGEMENTS

I would like to thank Prof. Ian Robinson and Dr Meric Srokosz for their supervision and encouragement during the course of this work.

This thesis could not have been carried out without the data, which were collected during three cruises, and I would like to record my thanks to those scientists and ships' crew and technicians who did this. I am also grateful to Meric, and to David Turner (Principal Scientist), for allowing me to take part in Discovery Cruise 198.

Many other people gave me help, advice and information, and were generally willing to discuss various aspects of the work. The most significant of these were Raymond Pollard, Jane Read, George Nurser, Ian Totterdell and Yanli Jia. Other members of the James Rennell Division of Southampton Oceanography Centre also helped me, and I apologise for not listing them all by name, but it was much appreciated.

Finally, I would like to thank my friends and family for putting up with my preoccupation in the last few months. Without your support, I could not have done it. And without David's dedicated support, I would not have done it. Thank you.

LIST OF ABBREVIATIONS USED

θ-S	Potential temperature - Salinity
ACC	Antarctic Circumpolar Current
ADCP	Acoustic Doppler Current Profiler
ATSR	Along-Track Scanning Radiometer
AVHRR	Advanced Very High Resolution Radiometer
CTD	Conductivity-Temperature-Depth
CWB	Continental Water Boundary
CZCS	Coastal Zone Color Scanner
ENAW	Eastern North Atlantic Water
FASINEX	Frontal Air-Sea INteraction EXperiment
FLW89	Fischer, J., H. Leach and J. D. Woods (1989) A synoptic map of isopycnic potential vorticity in the seasonal thermocline. *J. Phys. Oceanogr.*, **19**, 519-531.
GPS	Global Positioning System
IPV	Isopycnic Potential Vorticity
LPS83	Luyten, J., J. Pedlosky and H. Stommel (1983) The ventilated thermocline. *J. Phys. Oceanogr.*, **13(2)**, 292-309.
MLD	Mixed Layer Depth
NAC	North Atlantic Current
NACW	North Atlantic Central Water
PF	Polar Front
PV	Potential Vorticity
PVU	Potential Vorticity Unit, equivalent to 10^{-9} m^{-1} s^{-1}
RRS	Royal Research Ship
RY82	Rhines, P. and W. Young (1982a) Homogenization of potential vorticity in planetary gyres. *J. Fluid. Mech.*, **122**, 347-367.
SFZ	Subtropical Frontal Zone
SPF	Southern Polar Front
SST	Sea Surface Temperature
STERNA '92	Bellingshausen Sea survey (not an acronym)
STCZ	Sub-Tropical Convergence Zone
TSG	ThermoSalinoGraph
Vivaldi '91	North-east Atlantic Ocean survey (not an acronym)
WNAW	Western North Atlantic Water
WOCE	World Ocean Circulation Experiment

Chapter 1. INTRODUCTION

1.1 WHAT IS THIS THESIS ABOUT?

Interest in ocean dynamics has developed for many reasons, not least of which is that the ocean plays an important role in setting the weather and climate over land and sea (Apel, 1987). Commercial shipping uses knowledge of the velocity and position of currents to make their operations safer, cheaper and quicker, while scientific researchers need to know about currents to understand the transport of heat, nutrients and pollutants. These applications require knowledge of climatic ocean dynamics, and short- to medium-range forecasts of the ocean's state, while studies of global environmental change require forecasts on longer time-scales.

In the last few decades, ocean models have been developed to study the ocean's effect on long-term climate change, and to look at dynamics on various temporal and spatial scales (Bryan, 1969, Cox and Bryan, 1984, Oberhuber, 1990). These ocean models use approximate forms of the basic equations that govern ocean dynamics, and are integrated forward in time from a set of initial conditions, to give an estimate of the physical state of the ocean at a later time. The equations used in these models are gradually developing towards being more representative of the observed dynamics in the ocean, which are not yet fully understood. The initial conditions, such as the initial velocity field, need to be as accurate and precise as possible, because subsequent integration of a model is dependent on these. As computer technology improves and models are developed, they are based on grids of finer resolution, and the initialisation fields must adequately represent the dynamics at these finer resolutions (Robinson, 1996).

Initial velocity fields are mainly derived from historical hydrographic data collected '*in situ*' from ships or buoys in the region of interest (Smeed, *et al.*, 1991, Smeed, *et al.*, 1992). Hydrographic data are sparse in location and time, more so in some regions than others, and are therefore not ideal for use in initialisation of models. Satellite data have introduced the possibility of improving the initial fields, by specifying the initial velocity field in more detail than can be derived from hydrographic data. Satellite-borne instruments can survey large areas of ocean, at least quasi-synoptically, and a single satellite can achieve global coverage in a fairly short time. Satellites follow repeated orbits, meaning that a particular patch of sea can be surveyed regularly, say monthly or seasonally, for a length of time up to the lifetime of the satellite. That is to say, data may be available over all areas of the ocean, at all times of the year, over many years: a situation which cannot be achieved by hydrographic surveys alone. However, current practice does not fully exploit the advantages of satellite data.

The velocity field of the ocean cannot directly be measured from satellites and must be inferred from some other measurement such as sea surface temperature (SST) or sea surface height. Although it is possible to measure the varying part of the surface geostrophic current with a satellite altimeter, the mean ocean circulation cannot be easily separated from the geoid signal (Marshall, 1985). Until this happens through determining the geoid directly by measuring the Earth's gravitational field, other techniques have been developed to get round the problem. One such method uses hydrography at the time of one satellite pass to determine the absolute current, which can then be inferred by subsequent passes which measure the variability of the current (Challenor, *et al.*, 1996). For many applications, velocity variability is all that is required, and using satellite altimetry, relative velocity can be derived from measurements of sea surface height on scales of less than about 2000 km where geoid models are believed to be good. Accuracy of better than 5 cm s^{-1} has been claimed for such measurements of variability, resolving scales of 50-80 km along-track (Strub, *et al.*, 1997). The assimilation of altimeter data into ocean circulation models is an active research field (e.g. Wunsch, 1996, Haines, 1991, Haines, *et al.*, 1993). Satellite images of SST and Ocean Colour often have finer resolution (e.g. pixel size of order 1 km for SST data from the AVHRR or ATSR instruments), and so present the possibility of forming more accurate initial velocity fields for models. However, the conversion from measured quantity to velocity is not straightforward and has been an area of much research in recent years. Appendix A of this thesis presents a summary of the status of research into deriving the velocity field from satellite imagery. Generally, a sequence of two or more images over the same area is required to derive the velocity field, and such a sequence is often difficult to obtain due to cloud cover and satellite orbit pattern.

It has been proposed by other researchers (Marshall and Williams, 1989) that velocity could be derived from a single satellite image of a suitable tracer, by using it as a proxy for the potential vorticity (PV) at the base of the oceanic mixed layer. PV is the fluid equivalent of angular momentum, and comprises a planetary component (i.e. due to planetary rotation) and a local component (i.e. due to local forces). Before attempting to implement a scheme to derive velocity from SST treated as a proxy for PV, it is necessary to understand better the relationship between PV and other tracers. Oceanic PV on small scales (order 10 km) has not been studied extensively because of the difficulty of measuring it '*in situ*' and so present understanding is limited. However, it is now possible to study these inter-relationships because methods for mapping oceanic potential vorticity have improved with the increased deployment of undulating towed hydrographic instruments such as SeaSoar (Fischer, *et al.*, 1989, Allen, *et al.*, 1992, Pollard and Regier, 1992).

The main objective of this thesis is to consider the inter-relationships of PV, SST, potential temperature and salinity in three quite different frontal regimes. The areas of study are the North-east Atlantic Ocean, the Sargasso Sea and the Bellingshausen Sea (west of the Antarctic Peninsula). It emerges that these regions show quite different inter-relationships between PV and tracers, and the reasons for this are examined, concentrating on frontal processes and water mass formation. Theories for the setting of PV and tracer values are put forward and investigated, using a 1-dimensional model running at different geographical positions to follow the development of the PV-tracer relationship. This thesis is unique in examining the PV-tracer inter-relationship and in comparing these relationships in such different regions.

It was hoped at the outset that a clear functional relationship between PV and SST would be established, and that this could then be used to derive the velocity field from a single SST image. Some preliminary work was carried out to demonstrate how to implement such a scheme, by inverting the PV field to yield velocity measurements. This work is presented in Appendix B. As it turned out, and will be shown in later chapters, the results of the PV-tracer comparison showed that the relationship is complicated and variable, so the inversion of the PV field was not pursued further in this work.

In the next section of this chapter, the motivation behind the study of the PV-tracer inter-relationship is explained in more detail. Specific objectives for the work are set out in the following section. It is the intention of this thesis to show that these objectives are achieved. In the final section, the layout of this thesis is described.

1.2 WHY STUDY THE RELATIONSHIPS BETWEEN PV AND TRACERS?

Satellite images of SST and ocean colour show strong frontal features, such as the Gulf Stream and its associated eddies and rings (see Figure 1-1).

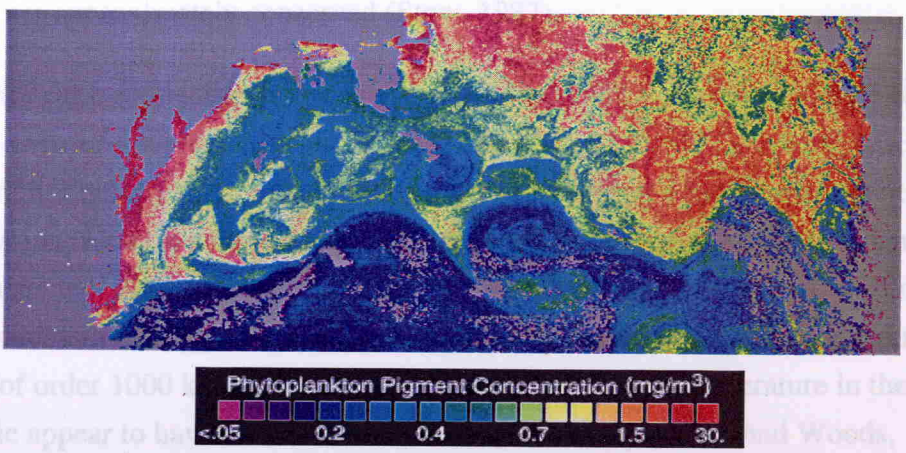

Figure 1-1 Chlorophyll image from the Coastal Zone Color Scanner (CZCS) for 7 May 1979 showing the Gulf Stream and associated rings.

These images are also reminiscent of fields of potential vorticity (PV) from eddy resolving ocean models, an example of which is shown in Figure 1-2 (Holland, *et al.*, 1984, Marshall and Williams, 1989, McDowell, *et al.*, 1982). Potential vorticity can describe the motion of a geophysical fluid such as the ocean, because it is a conserved quantity following a fluid parcel (Hoskins, *et al.*, 1985). Mesoscale features, which have a horizontal length scale of order 100 km, such as eddies and rings, are understood to have strong PV signals associated with them (Apel, 1987).

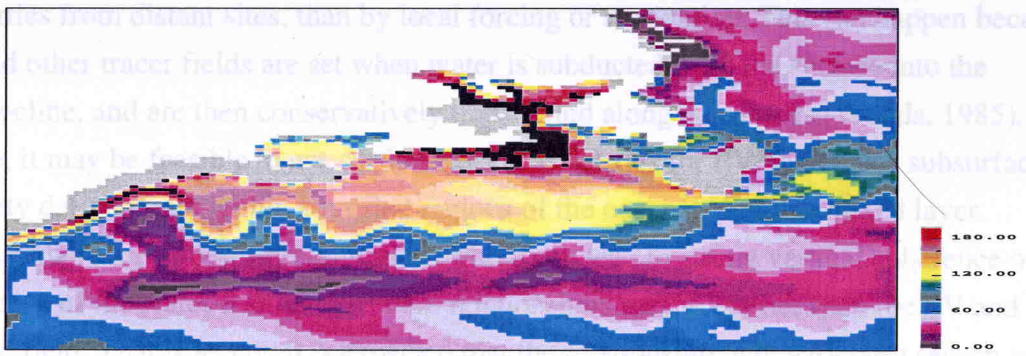

Figure 1-2 Potential vorticity field of the north-west Atlantic Ocean (Gulf Stream area) from layer 5 (102.038 metres) of the Ocean Circulation and Climate Advanced Model (OCCAM). Figure by M.-M. Lee, SOC.

Such observations suggest that a functional relationship may exist between PV and a surface tracer field, such as SST or ocean colour. However, while PV may be considered to be a conserved quantity, SST and ocean colour are better described as quasi-conservative tracers which are advected by the underlying velocity field. Neither SST nor ocean colour is exactly conserved because changes in SST occur when heat is exchanged between the atmosphere, the sea-surface, and the ocean interior, and ocean colour varies as phytoplankton grow and decay with the seasons. Nevertheless, on the length-scales of mesoscale ocean features and over time-scales of the order of a few days, SST and ocean colour are approximately conserved (Stow, 1987).

Evidence for a connection between PV and temperature was presented by Fischer *et al.*, (1989) (henceforth referred to as FLW89). They found that PV and isopycnic potential temperature fields can be functionally related, identifying a near-linear relationship on a shallow isopycnal in a frontal region of the North Atlantic during the summer of 1981. They also demonstrated that when studying mesoscale dynamics, relative vorticity is significant and must be evaluated, although it contributes negligibly to PV on the gyre-scale (of order 1000 km). Climatological values of PV and temperature in the north-east Atlantic appear to have a similar near-linear relationship (Bauer and Woods, 1984, Stammer and Woods, 1987).

Under some circumstances surface fields and sub-surface fields have been shown to be strongly linked. For example, SST and isopycnal potential temperature in the Gulf Stream are strongly correlated in the vertical (Open University, 1991). It may be possible to exploit this to find a functional relationship between a surface tracer field detectable by satellite instruments and sub-surface PV values.

In strong frontal regions, or where there is strong eddy activity, PV and surface tracer fields (such as SST and ocean colour) may be influenced more by horizontal advection of properties from distant sites, than by local forcing or dissipation. This can happen because PV and other tracer fields are set when water is subducted from the surface into the thermocline, and are then conservatively transported along isopycnals (Woods, 1985). Hence, it may be feasible to use surface tracers as proxies for PV, which is a subsurface property defined only within stratified regions of the ocean, below the mixed layer. Because there are various circumstances which can lead to strong vertical coherence of properties of the water column, different relationships may occur between the PV and the surface field. That is to say, it is expected that the relationship may vary with season and geographical region.

The inter-relationships between observed upper ocean PV and other tracers have not been thoroughly examined before, although several researchers have commented that anomalies occur in PV and tracers at the same locations (McDowell, *et al.*, 1982, Voorhis and Bruce, 1982, Arhan and Colin de Verdière, 1985, Marshall, 1995, Talley, 1985). Investigators using models to study frontal processes have also mentioned the relationship between PV and other tracers, but have not studied them closely, e.g. Samelson and Chapman (1995). It is now timely to consider these inter-relationships as they may shed light on the mechanisms of frontal processes and may prove useful in deriving dynamical information from satellites.

1.3. WHAT ARE THE SPECIFIC OBJECTIVES OF THIS THESIS?

Having established that it is worthwhile to examine the relationships between PV and tracer fields, because of their importance in frontal dynamics and ocean modelling, it is necessary to define more detailed and specific objectives to achieve this.

- The first step is to define PV, as its definition depends on the simplifying assumptions which are made in studying ocean dynamics.

- Next, it is necessary to assess what is the best way to derive and map PV from hydrographic data. This leads us to examine the development of PV mapping, the errors involved and the accuracy achieved.

- The next objective is to find out whether FLW89's relationship between PV and isopycnic temperature is found in other data sets from the same region and other regions. In other words, is this a universal relationship? To do this, the data from three frontal surveys are examined.

- Comparisons of the PV fields with temperature, and other measured quantities, show that the inter-relationships are quite complex and different for each data set. From this result emerged the major objective of describing the results and explaining why the data sets show different PV-temperature relationships.

- To explain why the data give different results, it is necessary to examine theories for the setting of PV and temperature in the upper ocean and consider how these can account for the results found in the data.

- It is also desirable to consider whether the data can suggest modifications to the current theories.

- To study the development of the temperature and PV fields, and their inter-relationship, using a one-dimensional mixed layer model which is run using initial fields appropriate to various locations within the Vivaldi '91 region. This allows us to look at whether the resulting PV-temperature relationship is similar to that from the observed data, and to consider why it agrees or disagrees.

The analyses of the data sets show that the relationship between PV and SST at a frontal site are influenced by the conditions and circumstances which have led to the formation of the front. The complexity of these results weakens the possibility of reliably recovering PV from SST, but at the same time provides new insights into the frontal processes which produced them. Some preliminary work was carried out to investigate how to proceed from a PV field through inversion of a model of PV to obtain the velocity field, and this is presented in Appendix B. Plans to take this further, by using the derived PV-temperature relationships in the data sets, were set aside in favour of examining the frontal dynamics that led to these different relationships. However, this could be taken forward at some other time.

This study is unique in looking at three very different regions through high quality surveys. The data sets were from three different regions, where the fronts had different histories and were formed by different mechanisms, and the surveys had been carried out on different spatial and temporal scales.

1.4 HOW IS THIS THESIS LAID OUT?

In the next chapter, various terms are defined. Ways to derive and map PV are examined, and the most appropriate methods selected for the chosen data sets.

Three hydrographic survey data sets were examined in this work, and the results of these investigations are presented in Chapters 3 to 5. Each survey collected measurements of temperature, salinity and pressure, and independent measures of current. These measurements should be sufficient to estimate the PV fields according to the methods established in Chapter 2. The three data sets examined are Vivaldi '91, FASINEX and Sterna '92. These were selected for study because they were readily available locally and are surveys of quite different frontal systems. Additionally, Vivaldi '91 data come from a similar location to the survey examined in FLW89. It should be noted that the author participated in the Sterna '92 cruise, and was involved in the initial collection, processing and calibration of these data.

The Vivaldi '91 data, presented in Chapter 3, were collected during April to June 1991 and comprise a hydrographic survey of the top 450 m of the ocean spanning part of the Azores Current in the north-east Atlantic Ocean. The survey was of six north-south sections between 39°N and 54°N separated by approximately 300 km zonally. In this chapter, the Vivaldi '91 data set is described, and the analysis of the PV, temperature, salinity and other fields is presented and compared with the results of FLW89.

The FASINEX data, presented in Chapter 4, were collected during February 1986 and comprise a hydrographic survey of the top 300 m of the ocean spanning a front in the Sargasso Sea, south-west of Bermuda, in the north-west Atlantic Ocean. This survey was of eight north-south sections between 27°N and 29°N separated by approximately 16 km zonally. In this chapter, descriptions of the data set and results of the analyses are presented for the FASINEX data set, in a similar layout to the analyses of Vivaldi data in the previous chapter.

The Sterna '92 data, presented in Chapter 5, were collected during November to December 1992 and comprise a hydrographic survey of the top 400 m of the ocean spanning a front in the Bellingshausen Sea, in the Southern Ocean to the west of the Antarctic Peninsula. This survey was of seven north-south sections between 66.5°S and 68°S separated by approximately 15 km zonally. In this chapter, descriptions of the data set and results of the analyses are presented for the STERNA data set, in a similar layout to the analyses of the other data sets.

These are followed, in the sixth chapter, by discussion of the results from the three data sets. This chapter also contains a review of current theories of ocean circulation and frontal dynamics with particular reference to water mass formation and PV. These theories are considered alongside the data results.

To explore how the PV-temperature relationships developed, a simple one-dimensional mixed layer model was used to simulate the circumstances of the Vivaldi data set, and this work is presented in the seventh chapter.

Finally, in the eighth chapter, the overall conclusions are presented.

Three appendices to this work are also attached, describing several pieces of work which were carried out during the course of the thesis, but which do not bear directly on the specific objectives of the thesis. Appendix A contains a review of methods for deriving ocean currents from satellite data. Appendix B illustrates how a PV field can be inverted to yield velocity estimates. Appendix C contains a comparison between PV and temperature for the output from a model called the Atlantic Isopycnic Model, and shows how these results compare with those of the Vivaldi and FLW89 data sets.

Chapter 2. BACKGROUND

2.1 INTRODUCTION

The main objectives of this chapter are to define what is meant by Potential Vorticity (PV) in the context of this thesis, and to assess the best way to derive and map PV from hydrographic data. To do the latter, the development of PV mapping will be examined. Following this, a short review of the main theories of mixed layer processes and thermocline circulation is presented, to set the context within which the relationship between PV and other water mass tracers will be examined. In section 2.5, the characteristics and theories are discussed of what happens in frontal and eddying regions of the ocean with respect to subduction. These are relevant when considering the FASINEX and STERNA data in particular, which are surveys at the mesoscale. Finally, in section 2.6, the motives for studying these particular data sets are explained.

2.2 PHYSICAL TERMS USED IN THIS THESIS

2.2.1 Potential vorticity

Potential Vorticity (PV), which is a measure of a water column's tendency to rotate, is very important to theories of ocean circulation (Holland, *et al.*, 1984, Rhines, 1986, Pedlosky, 1990, Marshall and Nurser, 1992). The definition of PV varies in different dynamical situations. The PV definitions appropriate to mesoscale and submesoscale processes at ocean fronts are described in this section.

The PV of a water column bounded vertically by density surfaces is the isopycnic potential vorticity (IPV). The vertical component of IPV within a region where x, y increase east and northwards, respectively, is defined (Apel, 1987, Pedlosky, 1987) by

$$q = \frac{\zeta + f}{\Delta p} \frac{\Delta \rho}{\rho_0} \tag{2.1}$$

where $\zeta = (\partial v/\partial x - \partial u/\partial y)$ and f are the vertical components of relative and planetary vorticity respectively (u and v are the components of velocity in the x and y directions, respectively), Δp is the vertical spacing defined in terms of the pressure difference between two bounding isopycnals of mean density ρ_0 and $\Delta \rho$ is the density difference between these isopycnals. The planetary vorticity, f, is the component of vorticity contributed by the Earth's rotation and is defined by

$$f = 2\Omega \sin\lambda \tag{2.2}$$

where Ω is the earth's angular speed of rotation of approximately 7.292 x 10^{-5} s^{-1}, and λ is the latitude. The relative vorticity, ζ, is the component of vorticity caused by local forces such as wind stress or frictional forces. The sum of the planetary and relative components ($f + \zeta$) is the total vorticity, which is more usually known as absolute vorticity.

From equation (2.1) it is seen that the IPV is the product of the vertical component of absolute vorticity and the density structure of the water column. It is defined only in the statically stable ocean interior, including the seasonal thermocline, but not in any mixed layer, because the mixed layer has homogeneous vertical density structure.

For gyre- or large-scale motions, $\zeta << f$ (Pedlosky, 1987), and IPV reduces to the Sverdrup isopycnic potential vorticity (Woods, 1985) which contains only the part of the PV due to the planetary vorticity, defined as

$$q_s = \frac{f}{\Delta p}\frac{\Delta\rho}{\rho_0} \tag{2.3}$$

Following Pollard and Regier (1992), an alternate formulation to (2.1) for evaluating PV on isobaric surfaces is (see Appendix D for derivation)

$$q = -fg^{-1}N^2\left(1 + \zeta_p f^{-1} - F\right), \tag{2.4}$$

where N is the Brunt-Väisälä frequency $\left(N^2 = -g\rho^{-1}\rho_z\right)$, $F = \left(u_z^2 + v_z^2\right)/N^2$ is the Froude number and $\zeta_p = \zeta + Ff$ is the relative vorticity calculated on isobaric surfaces. In (2.4), $-F$ is a twisting term, expressing the conversion of horizontal vorticity to vertical vorticity by the vertical shear. The equivalent expression to (2.3) on isobaric surfaces is

$$q_S = fN^2/g \,. \tag{2.5}$$

Both forms of the IPV equations, (2.1) and (2.4), and Sverdrup IPV equations, (2.3) and (2.5), were used in this thesis depending on the data set. The formulation used will be indicated in the text. For ease of reference, the potential vorticity unit (PVU) will be defined throughout this thesis such that 1 PVU is equivalent to 10^{-9} $m^{-1}s^{-1}$ (sometimes written as 1 rad $Gm^{-1}s^{-1}$).

2.2.2 Oceanic scales of motion

There is a continuous spectrum of interacting oceanic motions across different time, space and energy scales. Large-scale or gyre-scale motions have horizontal scales of the order of 1000 km, which includes the general circulation of the sub-polar and sub-tropical ocean gyres. Large-scale motions make up the mean motion of the ocean and are the oceanic equivalent of "climate" (Open University, 1991).

Motions at intermediate scales of the order of 100 km, more commonly called mesoscale, are the oceanic equivalent of "weather". Mesoscale motions are dominated by eddies with length scales of 50–200 km and periods of one to a few months. These eddies are believed to gain their kinetic energy from the relaxation of sloping isopycnals which releases potential energy from the oceanic mean flow. Mesoscale eddies are most commonly generated at density discontinuities where flow perturbations called "baroclinic instabilities" may form and evolve into eddies, although there are other mechanisms which can generate mesoscale eddies (Apel, 1987). Such eddies are an intrinsic part of the oceanic circulation and are found throughout the world's oceans. It is thought that most of the ocean's kinetic energy is contained in these mesoscale motions (Open University, 1991).

Smaller scale motions, known as sub-mesoscale motions, of the order of 10 km also occur in the ocean. Most mid-ocean fronts, which are some few tens of kilometres across, fall within this range (Open University, 1991).

The Rossby radius of deformation, R, is an approximation to the distance that a wave, or other perturbation, can travel before being significantly affected by the Coriolis force, or in other words, the length-scale at which rotation effects balance buoyancy effects. It can be shown (Gill, 1982, Pedlosky, 1987) that in the context of quasigeostrophic motion, the Rossby radius is the scale at which the relative vorticity and the vortex stretching make equal contributions to the potential vorticity. When examining the contribution of relative vorticity to PV, it is useful to examine the Rossby radius of the observed oceanic region. There are definitions of barotropic and baroclinic Rossby radii, and the baroclinic Rossby radii include one for each baroclinic internal mode (Pedlosky, 1987). In this work, the relevant quantity is the baroclinic (or internal) Rossby radius,

$$R_i = \frac{(g'H)^{1/2}}{f} \tag{2.6}$$

where H is a characteristic vertical scale height (thickness) for the motion and g' is the reduced gravity which acts at the interface between two isopycnals, ρ and $\rho+\Delta\rho$, given by

$$g' = g\frac{\Delta\rho}{\rho} \tag{2.7}$$

The three hydrographic data sets which are analysed in this thesis will be described in more detail in later chapters, but the scales resolved by the surveys are considered here. All three data sets have along-track spatial resolution of around 4 km. Two of the surveys, STERNA and FASINEX, had between-track separation of around 15 km, so some sub-mesoscale features will have been resolved by these surveys, though the smallest features may well have been aliased. The Vivaldi survey had a between-track separation of some 300 km. Hence, this survey was almost able to resolve mesoscale features between track, and some sub-mesoscale features may be discernible in the along-track direction.

2.2.3 Ventilation and subduction

In the course of this thesis, the properties of the ocean in the mixed layer and seasonal thermocline are examined. These properties may be set and changed by the transfer of water between the mixed layer and the thermocline below, so it is important to consider the mechanisms by which fluid transfer occurs, and how water properties are affected.

Ventilation is the transfer of water from the mixed layer to the thermocline, while subduction is the motion of fluid along an isopycnal from the mixed layer into the thermocline, which means the terms are often interchangeable (Udall, 1993). Fluid from the mixed layer ventilates the thermocline temporarily in the seasonal thermocline, from where it is later re-entrained into the mixed layer, or is permanently subducted beyond the maximum mixed layer depth into the permanent thermocline (Woods, 1985).

2.3 HISTORY OF PV MAPPING

Fluid circulation and vorticity have been recognised as important concepts in meteorology and oceanography since the end of the 19th century, but the theories were so complex that it was difficult to make use of them in studies of the environment (Hoskins, *et al.*, 1985). This was the situation until Rossby made advances in the late 1930s, by recognising that the vertical component of absolute vorticity is the most significant for large-scale atmospheric flow, and that it could be assumed to be conserved in horizontal motion. Rossby developed this notion further by using the concept of PV to describe the interaction of vortex stretching and horizontal advection of absolute vorticity, and extended it to surfaces of constant potential temperature (isentropes). From this time onwards, atmospheric researchers embraced the use of isentropic charts to look at atmospheric motion, and started to see the importance of PV as an air-mass tracer. In a

paper published in 1942, Ertel independently extended Rossby's results to full hydrodynamical generality.

Over the following decades the utility of atmospheric PV has been gradually exploited (Hoskins, *et al.*, 1985). In the late 1940s, PV was used to study the Lagrangian behaviour of the atmosphere. In the 1950s, the idea of PV anomalies was used to explain events in the upper troposphere. Around this time, researchers also began to map out atmospheric PV structures in more detail, and looked at its adequacy as an air-mass tracer. In the 1960s mapping of PV was made easier with the advent of computers, and the 1970s saw these maps being used more routinely to diagnose atmospheric behaviour. By the 1980s PV had taken a leading role in the diagnostics of atmospheric models.

Meanwhile, similar developments were taking place in oceanographic studies, but at a slower place, because of the difficulty of obtaining data sets with sufficient resolution to produce maps. Parr (1938) and Montgomery (1938) were the first to publish plots of large-scale scalar properties on isopycnic surfaces. It took a long time for the utility of this concept to catch on! In the 1960s, several atlases were published of gyre-scale distribution of pressure, temperature, salinity and other properties on selected isopycnals in the Pacific Ocean (e.g. Reid, 1965) and since then it has been accepted that isopycnic maps are valuable in the discussion of the oceanic general circulation. Motion is expected to be approximately in the plane of isopycnals on both the gyre-scale and the mesoscale (McDowell, *et al.*, 1982). However, it was considered difficult to map mesoscale hydrographic data because traditional hydrocast CTD data are widely spaced geographically and temporally. However, in the 1970s and 1980s instruments (e.g. Batfish, SeaSoar) were designed to be towed behind ships, and these could carry CTD equipment from near surface to 400 metres depths and more. The first recorded attempt to map mesoscale scalar properties on isopycnals away from ocean fronts appears to be Woods and Minnett (1979), who used data gathered with a Batfish system. Their aim was to deduce the circulation pattern indirectly rather than using direct measurements from current meters which would be swamped by other motions. The data from such systems is then vertically linearly interpolated onto isopycnals, and some error fields may be estimated during this process to give an idea of confidence in the interpolated values. Horizontally, "radiator" surveys are often used, consisting of parallel survey sections, which are more easily interpolated on to a regular horizontal grid.

At large (gyre) scales the PV can be represented by the Sverdrup PV, as relative vorticity is negligible at these scales, and can be calculated from hydrographic measurements without knowledge of the local velocity field. The first recorded maps of PV on isopycnals are those in Behringer (1972), which used data collected in the South Atlantic in 1927! There appears to be no reason why such maps could not have been constructed

sooner, other than that no one thought to do so. During the 1980s, there was quite a flurry of papers containing isopycnic maps of PV. McDowell *et al.* (1982) produced PV maps of the North Atlantic using data from 1957-58 and 1962, and these were used to validate theories put forward for the general circulation (Rhines and Young, 1982b). Meanwhile others used Levitus climatological data (Levitus, 1982) to produce maps of PV in their areas of interest (e.g. Sarmiento, *et al.*, 1982, Holland, *et al.*, 1984). As the usefulness of such maps was becoming more evident, Stammer and Woods (1987) mapped the seasonal cycle of the Sverdrup PV in the North Atlantic using climatological data, for use in studies of the general circulation and its links with atmospheric fields.

All of these maps were for Sverdrup PV only. McWilliams (1976) also calculated the relative vorticity component of PV, and produced maps of this, along with an analysis of the complex error statistics of the mapping method used, in order to study the conservation of PV. This study used float trajectories and vertical density profiles to generate the PV field. More frequently, in the 1980s, maps began to appear of full PV calculated using measurements of the velocity field independent of the hydrographic data (e.g. Arhan and Colin de Verdière, 1985, Hua, *et al.*, 1986, Fischer, *et al.*, 1989, Pollard and Regier, 1992). Few of these studies explicitly state the estimated errors in the PV field, although they describe measures to use only data within confidence constraints. As an example of the level of accuracy which has been achieved, the PV fields presented by Fischer *et al.* (1989) have mean values around 1.04 PVU, with standard deviation of 0.45 PVU and a range of 2.33 PVU. A confidence level of 0.4 PVU was used to select which data were included in the analysis. Errors (both over- and under-estimates) in PV values of the order of 8% were introduced when relative vorticity was excluded.

These developments in the mapping of PV on isopycnals has led to an increasingly clear picture of the gyre-scale PV field, which is important as the interaction of PV dynamics and thermodynamics is largely unsolved. Theoretical and modelling work suggest that mapping the PV field should be of high priority (Rhines, 1986). The picture is certainly not yet clear at smaller scales.

2.4 MIXED LAYER AND THERMOCLINE THEORIES

2.4.1 Mixed layer processes

The surface layer of the ocean has low vertical gradients of temperature, salinity and momentum as a result of turbulent mixing generated by mechanical and buoyancy forcing, and for this reason is referred to as the "mixed layer"(Niiler and Kraus, 1977). This thesis concentrates on examining hydrographic data gathered from the mixed layer and seasonal thermocline. Mixed layer processes have contributed towards setting the

properties of data gathered, and for this reason it is relevant to this thesis to consider what factors may have influenced the properties of the mixed layer in the data sets. However, it is not the intention here to investigate mixed layer dynamical processes themselves.

The mixed layer can be defined in various ways, but is most commonly defined by requiring that the vertical gradient of temperature or density should be less than a threshold value. However, such definitions of mixed layer do not always yield the same depths for the extent of the mixed layer, especially in regions where the salinity makes a more significant contribution to the density value (Lukas and Lindstrom, 1991). It is usual for a researcher to select the method which most suits their purpose.

The energy flux between the mixed layer and the atmosphere is balanced by viscous dissipation and by changes in the depth of the mixed layer. For example, increased energy in the mixed layer lifts denser water from below and mixes it, deepening the mixed layer as water is entrained into it (Kraus and Turner, 1967, Udall, 1993). Mixed layer deepening, and the corresponding shoaling which occurs when energy is reduced in the mixed layer, follows a diurnal cycle and a seasonal cycle. These variations depend in turn on the cycles of the forcing fields which affect the mixed layer kinetic energy. In more strongly stratified fluids, the entrainment rate is reduced by internal waves and by eddies inhibiting the advance of the boundary between the mixed layer and the stratified fluid. Detrainment is governed by the influences of the surface wind stress, which enables mixing, and the buoyancy flux, which enables restratification, on the mixed layer. Water which is detrained from the mixed layer into the denser layers below will retain the temperature, salinity and potential vorticity values of the mixed layer at the time of detrainment.

Wind stress acts across the mixed layer to transfer momentum and energy into the ocean and varies with the wind speed, swell and wave field (Kraus and Turner, 1967). Wind stress induces waves on the sea surface, which break and introduce turbulence into the mixed layer. This is the mechanism by which wind stress contributes to the total kinetic energy of the water column, and can overcome buoyancy effects during daylight hours (Woods, 1980). This direct influence of the wind penetrates to the depth of the Ekman layer, generating an Ekman drift current (Pedlosky, 1987).

Other mechanisms which alter the buoyancy of the mixed layer include evaporation and precipitation, which lead to fresh water fluxes (Niiler and Kraus, 1977). Buoyancy is also forced by heat fluxes which may result from latent heat of evaporation, sensible heat transfer due to air-sea temperature difference, and solar and terrestrial penetrative radiant heat fluxes. Throughout the day, solar radiation adds heat into the mixed layer while it is simultaneously being lost by latent heat, sensible heat and longwave radiation. This

causes convective overturning in just the top few millimetres of the mixed layer. In contrast, at night convection dominates the total kinetic energy production, and penetrates to much greater depths (Woods, 1980). Studies of the sensitivity of mixed layer models to surface fluxes have suggested that models are more sensitive to buoyancy fluxes than to wind stress (Woods, *et al.*, 1984).

Internal processes such as the production of internal waves and shear-induced instabilities are generally considered to have little effect on the mixed layer (Niiler and Kraus, 1977), but some research suggests that such processes may be important on certain time-scales (Oakey and Elliott, 1982). Some modelling results indicate that only a small proportion (10%) of mixed layer kinetic energy contributes to mixed layer deepening, with the majority being used in the production of internal waves and dissipation, so these mechanisms should therefore be included in mixed layer models (Denman and Miyake, 1973, Kraus and Turner, 1967).

2.4.2 Thermocline circulation

Below the mixed layer and to about 1000 metres depth in the ocean there are strong vertical gradients of temperature and density. This region is labelled the thermocline, or the pycnocline. In many parts of the world's ocean the temperature dominates the density value, and so the terms "thermocline" and "pycnocline" are often interchanged. The data sets which are examined in this thesis are surveys of the top 300 to 400 metres of the ocean, which encompasses the top part of the thermocline. For this reason it is relevant to consider here the processes which determine the properties of the water within this part of the ocean. The thermocline consists of two parts. There is the seasonal upper part which is re-entrained into the mixed layer each winter, where its properties (temperature, salinity, potential vorticity, oxygen content, etc.) are reset to the mixed layer values. And there is the permanent deeper part which is deeper than the annual maximum mixed layer depth and, therefore, is not directly influenced by the mixed layer. The data sets examined here were all gathered in springtime and so the thermocline which is examined is likely to be that part known as the seasonal thermocline. There is little diabatic forcing in the thermocline, so flow there is near geostrophic. Various theories have been proposed for circulation through the thermocline, but in recent years most interest has rested on the theories of "homogenisation of the thermocline" (Rhines and Young, 1982a) and "the ventilated thermocline" (Luyten, *et al.*, 1983).

Rhines and Young put forward the theory of the wind-driven ocean circulation known as the "homogenisation of the thermocline" theory in Rhines and Young (1982a) which is hereafter referred to as RY82. In this theory, the mean circulation tends to distort the potential vorticity isolines to such an extent that they form closed loops within

unventilated isopycnals and within these loops the potential vorticity is homogenised. At the edge of the closed region, there is a concentrated region of high gradients of potential vorticity. Beyond this transition zone lies motionless fluid, or a different flow regime in which the planetary gradient of potential vorticity may be dominant. Potential vorticity is homogenised within the closed geostrophic contours in subsurface isopycnals if the dominant dissipative mechanism is lateral diffusivity of potential vorticity, perhaps due to mesoscale eddies, and direct forcing by external stress or heating is negligible. This homogenisation of potential vorticity has been supported by ocean observations (McDowell, *et al.*, 1982).

Luyten *et al.* (1983) (henceforth LPS83) described a theoretical model for the thermocline which addressed the problem of the ocean conserving its density and potential vorticity fields far from the regions in which they were set. This model is known as the "Ventilated Thermocline". The model consists of an arbitrarily large number of inviscid, homogeneous fluid layers each with a different density. Sverdrupian dynamical balances are assumed throughout, and the surface density is specified in regions where the Ekman pumping is negative (downward). This means that some isopycnals outcrop in certain regions and water pumps down to the thermocline stirring up deep motion even in locations far from the outcrop where the layer is shielded from the direct influence of the wind. A major difference between this approach and that of RY82 is that the ventilated thermocline model allows significant deep flows on open potential vorticity contours that return to the ocean surface rather than the eastern boundary. It also means that distinct flow regimes can be identified. In downwelling areas there are ventilated regions in which all isopycnals are in motion, while at the edge of this there are shadow zones where potential vorticity contours meet meridional boundaries and these shadow zones may bound uniform potential vorticity or stagnant areas. Meanwhile, in upwelling areas isopycnals will outcrop.

Processes which take place above the permanent pycnocline are not considered explicitly by either the RY82 "homogenisation of the thermocline" model or the LPS83 "ventilation of the thermocline" model. In these models, the density and vertical velocity are specified at the top of the permanent pycnocline which is assumed to be at the base of the Ekman layer. This, according to Woods (1985), is unsatisfactory because this treatment of the surface layer is wrong, and the models cannot be used in regions where the surface density distribution is unknown and changing. The problem is that pycnocline depth, which is defined as the annual maximum depth of the mixed layer, does not coincide in the real ocean with the base of the Ekman layer. Between the Ekman layer and the permanent pycnocline lies the seasonal pycnocline, within which water flows geostrophically, then passes near-horizontally into the permanent pycnocline, rather than

being pumped down vertically from the mixed layer as most models prescribe (Lukas and Lindstrom, 1991).

Woods (1985) offers an alternative model of the pycnocline which is ventilated from the seasonal boundary layer in response to the surface fluxes. The theoretical form of the near-surface layers of the ocean is summarised by Figure 2-1, which shows a mixed layer consisting of a statically unstable convection layer overlying the weakly stable part of the mixed layer. Daily variation in the penetration of the convective layer, and daily variation in the depth and temperature of the mixed layer occurs in response to the daily pattern of solar heating which causes convection to be quenched during the day, and to recur just before sunset and through the night. This variation leads to the layer defined as the diurnal pycnocline. Seasonal variations in the length of day, maximum solar elevation, cloud cover and surface fluxes leads to variations in the extent of the mixed layer, and the layer which is defined by this variation is known as the seasonal pycnocline. The annual maximum depth of the mixed layer is where the permanent pycnocline begins.

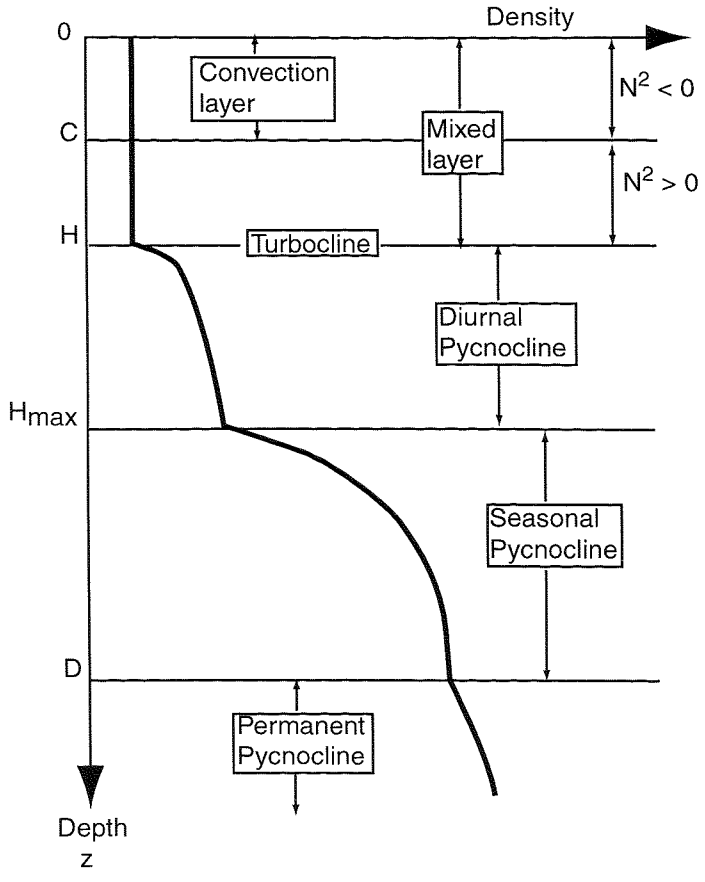

Fig. 2-1 Model of layers in the upper ocean. The convection layer is statically unstable, while the remainder of the mixed layer is weakly stable. The flow is predominantly laminar in the seasonal and permanent pycnocline. (After Woods (1985))

Woods' (1985) model was used to demonstrate the role of advection in the upper ocean. In winter, the mixed layer is deeper than the Ekman layer, and convection controls the mixed layer depth. Increases in the depth of the diurnal pycnocline depend on the daily mean surface buoyancy flux and the density gradient at the top of the seasonal pycnocline. The depth of the diurnal pycnocline reaches to the top of the permanent pycnocline when the daily buoyancy flux changes sign at the start of spring, when warming occurs. If there is no advection in the model, the annual maximum depth of the mixed layer will increase each year. However, this depth is approximately constant in nature. This means that the net annual buoyancy flux due to heating must be balanced by a divergence of advective buoyancy flux, which is to say, advection is necessary to predict the annual maximum mixed layer depth. Most one-dimensional models have neglected advection (Woods, 1985).

Isopycnic potential vorticity is not defined in the mixed layer and so this layer acts as a source (sink) of potential vorticity for water flowing out (in). The mechanism for the input of potential vorticity into the seasonal pycnocline suggested by Woods (1985) is that the top of the diurnal pycnocline rises rapidly in spring leaving behind it a water column with a density profile that sets its potential vorticity profile. The potential vorticity "sinks" to the seasonal pycnocline during the autumn and winter when the mixed layer deepens, entraining water from the underlying pycnocline. In this way, changes in the mixed layer affect the source of potential vorticity in the seasonal pycnocline and in turn this affects the flux of potential vorticity into the permanent pycnocline. Woods (1985) found that potential vorticity therefore flows from the seasonal pycnocline into the permanent pycnocline at places where the annual maximum mixed layer depth decreases downstream, and vice versa.

LPS82, RY83 and Woods (1985) agree in that the properties of the permanent thermocline are set to some extent when the fluid was last in contact with the atmosphere. Potential vorticity, density and temperature are all important elements in controlling the gyre-scale circulation and stratification of the ocean interior. From the literature, it is clear that the physics of the subduction of the mixed layer and the ventilation of the pycnocline are not well known, but are crucial to an understanding of the oceanic circulation. In this thesis, these processes are examined by looking at observations of temperature and PV in the top 300-400 metres of the ocean in late winter/early spring.

More recently, many researchers have carried out modelling studies to investigate subduction, its influence on thermocline circulation, and the factors which moderate subduction (e.g. Nurser and Marshall, 1991, Marshall and Marshall, 1995, Williams, *et al.*, 1995, Csanady and Vittal, 1996, Marshall, 1997). Clearly, this is still an area of active

research, and generally the drive behind these studies is to improve knowledge of subduction rates in order to improve numerical models of the ocean.

2.5 FRONTS, EDDIES AND SUBDUCTION

2.5.1 Definition of ocean fronts

The physical nature and scales of ocean fronts are extremely diverse, which has led to much debate about the definition of "a front". In an extensive review of fronts, Fedorov (1986) offers these strict definitions. An oceanic "frontal zone" is a region of high spatial gradient of the main thermodynamic characteristics (temperature, salinity, density and/or velocity) relative to the mean background gradient. A "frontal interface" is a surface within a frontal zone which has the maximum gradient of one or several characteristics. A "front" is the intersection of a frontal interface with any surface, such as the sea surface or an isopycnal. However, most oceanographers use "front" to describe all of these phenomena and this thesis will adhere to this convention, although "frontal zone" will also be used with Fedorov's meaning.

Researchers have tended to split ocean fronts into four classes when considering frontal dynamics, although the class definitions vary somewhat. There is general agreement that one class contains fronts which occur as the result of large-scale convergence (Rudnick and Davis, 1988, Linden, 1991), although some researchers split this class further into fronts due to convergent surface energy fluxes and fronts due to convergent Ekman Transports (Roden, 1976). A second class of fronts are coastal fronts which arise because of coastal upwelling, and are deemed to include fronts occurring because of western boundary currents (Roden, 1976, Rudnick and Davis, 1988, Linden, 1991). Further class definitions vary, but include shallow sea fronts due to tidal mixing (Rudnick and Davis, 1988, Linden, 1991), double-diffusive fronts where the temperature and salinity field gradients compensate for each other giving no density signature (Linden, 1991), and multiple fronts due to baroclinic Rossby waves (Roden, 1976). In contrast, Fedorov classified fronts according to their scale as large-scale quasi-stationary fronts of climatic origin, mesoscale fronts or small-scale fronts of local origin (Fedorov and Kuz'mina, 1977). Later, this classification was modified to include sub-classification according to whether the frontogenetic mechanism was climatic or synoptic, and whether the front is associated with "geostrophic and semigeostrophic" or "ageostrophic" dynamics (Fedorov, 1986). These classifications give some idea of the superposition of different motions which may be occurring at fronts and within frontal zones. It also makes it clear that in order to understand what is happening at a front, it is necessary to understand the underlying dynamics of the region.

Salinity fronts do not necessarily coincide with thermal fronts (Roden, 1975) but often when there are parallel sources of spatial variability in temperature and salinity, thermohaline frontal zones occur in which the temperature and salinity gradient are coincident (Fedorov, 1986). Where coincident temperature and salinity fronts occur, there may not be a corresponding density front, if there is a positive temperature-salinity correlation (Roden, 1975, Fedorov, 1986). For this reason, it may be unrealistic to identify fronts by density discontinuity. It is more usual in the open ocean to encounter thermal fronts and temperature-dominated thermohaline fronts rather than pure saline fronts or salinity-dominated thermohaline fronts (Fedorov, 1986). It should be noted that while many fronts occur at the boundary between two different water masses, some fronts occur within a single water mass and therefore have the same potential temperature-salinity (also written as θ-S) properties on either side of the front (Fedorov, 1986).

In coastal areas and in the frontal zones of the major boundary currents, thermal fronts may be closely packed, with separations of several tens of kilometres (Fedorov, 1986). In frontal zones in the open ocean, such as that of the Subtropical Convergence Zone in the Sargasso Sea, the mean distance separating thermal fronts is of the order of 100 km, although smaller scales due to mesoscale eddies may be seen too. In other parts of the open ocean, the mean separation of thermal fronts is about 500–1000 km. Thermal fronts are encountered more frequently in the west of ocean basins than in the east.

2.5.2 Frontogenesis

"Frontogenesis" is the rapid development of strong horizontal density gradients in a region of underlying weak density gradients (Hoskins, 1982). "Frontolysis" is the mechanism by which a front is dissipated. Fronts occur both in the atmosphere and the ocean, and while there are major differences between these two systems (for example, ocean is heated from above, atmosphere from below), there are also many similarities between atmospheric and ocean fronts and their mode of formation. For example, both systems feel the effects of the Earth's rotation, and "deformation fields" occur in both. A deformation field is a configuration of streamlines which in combination with any other scalar tracer, such as temperature, results in the compression or spreading out of the tracer's concentration isolines (Fedorov, 1986). In both the atmosphere and the ocean, a horizontal deformation field initiates frontogenesis by creating a frontal zone. Fronts are then sharpened and maintained within the frontal zone, but there is much debate about how this occurs. One theory is that transverse motions occur caused by the initial frontogenesis and these sharpen and maintain the front (Newton, 1978). This theory fits with the situation of a front forming within a frontal zone as a result of mesoscale eddies, themselves caused by the instability of the frontal zone, and their associated vertical motions. Other mechanisms include horizontal or vertical shearing, bottom-friction,

turbulence and mixing, radiation, and Ekman drift convergence (Hoskins and Bretherton, 1972, Roden, 1975). Each of these mechanisms represents a type of deformation field, and there is much active research to examine the frontogenesis induced by them.

A characteristic feature of many ocean fronts is that once established they are self-sustaining by means of transverse convergent circulation or by turbulent entrainment (Mooers, 1978). This explains why frontolysis is so rarely discussed in the literature because it only occurs in response to the self-sustaining mechanism failing. Despite this self-sustaining characteristic, fronts are not stable features but are highly variable. One process which causes this is the exposure of fronts to the wind's influence which can at the very least drive horizontal and vertical flows which strengthen or weaken the convergent circulation in the vicinity of the front. Another factor is that seasonal changes in the fluxes of momentum, heat and moisture between ocean and atmosphere affect the intensity and location of frontal zones in the ocean (Roden, 1975, Hanson, *et al.*, 1991). Other processes also contribute to the variable behaviour of a front during its lifetime, and most of the research in this field has been carried out by using numerical models.

2.5.3 Subduction at ocean fronts

Subduction is believed to occur, at least partly, as a result of downwelling and advection induced by large-scale variations in the atmospheric wind stress curl and net buoyancy flux. Subduction may occur at upper ocean fronts where deep isopycnals outcrop into the mixed layer. It is not clear to what extent frontal subduction is driven by internal frontal processes or by external atmospheric forcing, and in an effort to address this matter Spall (1995) investigated subduction at upper ocean fronts driven by internal instabilities. A simple model, which conserves potential density and potential vorticity, was used to follow parcels subducted across a local potential vorticity gradient. Low potential vorticity, anticyclonic parcels were subducted from a deep mixed layer, while high potential vorticity, cyclonic parcels were subducted from a shallow mixed layer. These parcels were forced to subduct below and across the front by frontogenesis resulting from baroclinic instability, which can generate considerable vertical velocities and ageostrophic cross-front flows. Subduction is achieved by deep ageostrophic cross-front flow carrying water from the mixed layer below and across the front. The subducted parcels gain or lose relative vorticity, to conserve potential vorticity. These modelled subducted parcels are similar to submesoscale eddies whose horizontal and vertical scales are set by the frontogenetic mechanism and the depth of the mixed layer. Spall (1995) suggests that the shallow mixed layer scenario is more representative of summer conditions, and that parcels subducted in the summer will probably not be subducted into the permanent thermocline and so, while relevant to the seasonal thermocline, they will have little effect on the general circulation.

Pollard and Regier (1992) look at the structure of a front in the Sargasso Sea, down to 300 m, by combining density and velocity data gathered at 4 km horizontal resolution (N.B. This data set will be examined in Chapter 4 of this thesis). From these, geostrophic velocity was derived and used to consider the sensitivity of the potential vorticity to stratification and relative vorticity. Large variations in potential vorticity were found across horizontal scales as short as 10 km, but only on isopycnals that outcrop from the seasonal thermocline into the mixed layer. The ageostrophic velocity field was deduced and large vertical velocities (up to 40 m day^{-1}) were found. Near-surface eddies of about 20–50 km diameter were figured to be instrumental in transporting and diffusing properties down from the mixed layer into the seasonal thermocline. These findings from observations of the real ocean concur with the mechanism described in Spall (1995), which was a modelling study.

A paper by Allen *et al.* (1991) looks at how eddies modify the stratification of the thermocline using observations of eddies in a range of locations. This study concluded that when water is subducted from the mixed layer (which is weakly stratified) it carries weak stratification with it, and this results in an anticyclonic anomaly in the thermocline. Cyclonic anomalies only form this way if strongly stratified water from the seasonal thermocline advects deeper to a weakly stratified region. It is more common for cyclonic eddies to form by breaking off a major current e.g. Gulf Stream.

2.5.4 At the base of the mixed layer

In order to clarify the extent to which upper ocean variability is influenced by atmospheric variability or induced by ocean mesoscale circulation, various efforts have been made to model the mixed layer's response to wind fields and mesoscale oceanic circulation. Klein and Hua (1988) studied the spatial variability induced in the mixed layer by an underlying quasigeostrophic flow in the presence of uniform atmospheric forcing. Analytical analysis showed that entrainment of fluid into the mixed layer is affected by the gradient of the velocity of the quasigeostrophic flow, especially the vorticity components. When a coupled mixed layer–quasigeostrophic model was implemented, with a tracer field present in the mixed layer, two time scales of response were identified. Initially, the heterogeneity of the mixed layer depth and tracer distribution was characterised by areas of high gradients which occurred anisotropically. The orientation of the anisotropy was dependent on the wind stress direction. Of great interest to this thesis was their further finding that the mixed layer depth and tracer field were highly correlated with the quasigeostrophic vorticity field, acting as "wind-biased vorticity mirrors". Entrainment due to the underlying flow field was the dominant physical process during this initial stage. As the model continued in time, it was found that the anisotropy decreased, although the intermittent pattern of high gradient regions

persisted. The high degree of correlation between the mixed layer depth and vorticity field was also diminished. At this stage Ekman pumping and tracer wind-driven advection were the most significant processes. However, they also found that the wind stress direction can still influence the mixed layer heterogeneity after the initial period if the quasigeostrophic flow contains some degree of anisotropy.

Naturally, this modelled situation is over-simplified, and in the real world we encounter non-uniform initial conditions, pre-existing inertial motions, non-stationary atmospheric forcing and more processes in the deeper layers than are encompassed by quasigeostrophic assumptions. However, it is still of great interest to find that the presence of a quasigeostrophic flow may quickly trigger a mixed layer mesoscale variability whose main features reflect the quasigeostrophic vorticity field. In the real ocean, such intermittent high gradient regions could lead to frontogenesis.

2.6 CHOICE OF DATA FOR THIS STUDY

Three data sets gathered during different oceanic surveys have been examined in this thesis: Vivaldi (Pollard, *et al.*, 1991), STERNA (Turner, 1993) and FASINEX (Pollard, *et al.*, 1986, Stage and Weller, 1986). These data sets were chosen for study because they are of different ocean regions involving different ocean systems and processes, which were anticipated to be interesting to compare and contrast. The author was involved in collecting the STERNA data, having participated in the cruise and the processing of the underway thermosalinograph data (Morrison, 1993), deep CTD data (Pollard, *et al.*, 1993) and SeaSoar data (Read, *et al.*, 1993). All three data sets were available locally and so they were accessible.

The Vivaldi data set was collected over 6 weeks, and at spatial scales of 4 km along-track, and 300 km between track, which means that this data set resolves synoptic-scale, and some mesoscale features. The Vivaldi data set was located in a similar part of the North Atlantic to the FLW89 data set, which was a survey which resolved the mesoscale and sub-mesoscale, having track separation of 10 km. It was thought that it would be interesting to compare the Vivaldi results with FLW89 to see whether the same relationship was encountered at larger scales, and in a different year. Both the FASINEX and STERNA data sets were surveys at fine-scale, resolving the mesoscale and sub-mesoscale, as in the case of FLW89.

In this study, water properties were examined primarily on isopycnic surfaces, because water particles in the ocean tend to move on surfaces of constant density and so properties are near-conservative on isopycnals. The density, ρ, of seawater is a function of salinity, s, temperature, t, and pressure, p. By convention, oceanographers denote the pressure, p,

to be the hydrostatic pressure, so that $p = 0$ is atmospheric pressure (Pond and Pickard, 1983). Isopycnals are described here by their potential density value referenced to the sea surface, σ_0, where $\sigma_0 = \rho(s,t,0) - 1000$ and is, by convention, written without units. It should also be noted that the approximation of 1 m $\cong$ 1 dbar is widely used, and is used in this study, but can give rise to large errors at greater depths (Open University, 1991). Analyses were also carried out on isobaric surfaces. This was done because it was clear from the FASINEX data that more significant relationships were evident on isobarics than on isopycnals. Also, if the base of the mixed layer were defined as a particular depth, rather than an isopycnal, then it may be more relevant to attempt to connect PV and temperature on an isobaric surface, if one were trying to use satellite data to extrapolate down from surface values to "base of mixed layer" values.

The vertical coherence of the potential temperature and potential vorticity fields of each data set were examined, to see how well correlated the values on isopycnals are as their separation increases. The reason for doing this is that it gives an indication of how closely tied are deeper parts of the ocean to surface influences. If the correlation between near-surface and deeper isopycnals is poor, it indicates that recent surface heating and mixing are unlikely to have influenced the temperature and potential vorticity at depth.

In this study, the relationship between potential vorticity and near-surface temperature were of primary interest. For this reason, it is desirable to study the properties on isopycnals that lie just below the mixed layer, in the main thermocline, since potential vorticity is not defined in the mixed layer. Preferably these isopycnals would lie just below the mixed layer across the whole study area. The mixed layer is defined as the region below the surface, in which the water has a vertically homogenous structure, but its identification is dependent on the precision to which the density is measured, and its vertical extent varies across each data set. Many isopycnals outcrop into the mixed layer at some location within the survey areas, most usually in the vicinity of a front. Isopycnals that lie just below the mixed layer in some areas may also deepen to below the maximum survey depth in other areas.

The results from the Vivaldi data set, which is from part of the north-east Atlantic Ocean, were compared with similar analyses of the potential vorticity and temperature fields of the Atlantic Isopycnal Model (AIM). AIM is a simulation of the North Atlantic Ocean based on a coordinate system of a set of isopycnic layers whose thickness can vary in space and time (New, *et al.*, 1993). The model and the comparison of the results are described in Appendix C.

The next three chapters describe in detail each hydrographic data set and its analysis.

Chapter 3. VIVALDI '91

3.1 INTRODUCTION

The Vivaldi cruises were part of the UK contribution to the World Ocean Circulation Experiment (WOCE), and were planned to be a series of seasonal hydrographic surveys of the north-east Atlantic (Fig. 3-1). The Vivaldi '91 trial cruises took place during 25 April–16 May and 18 May–10 June 1991, aboard the RRS *Charles Darwin* (Pollard, *et al.*, 1991). The cruises combined fine-scale surveys, using the towed undulating SeaSoar, with deep CTD stations at intervals of 3 degrees of latitude along tracks 300 km apart. The SeaSoar carried CTD (Conductivity-Temperature-Depth) instrumentation, and can reach 450 metres depth. A thermosalinograph (TSG), Acoustic Doppler Current Profiler (ADCP) and GPS navigation system were operating throughout the cruises. These instruments, along with the SeaSoar and CTD, collected data from which temperature and potential vorticity can be calculated and compared.

The survey tracks lay close to north-south, as shown in Figure 3-1, which indicates their definition as sections W, X, Y, Z, A and B, going from west to east, and shows the near-surface temperature as measured during the cruises. This illustrates the surface position of the temperature front passing through the region. The southern parts of the tracks were surveyed first, from east to west, with an inter-cruise break after section X. Then, section W was surveyed, followed by the northern ends of the other sections from west to east. This meant that the northern end of section A, for example, was surveyed almost 6 weeks after the southern end, which accounts for the temperature discontinuity at 48°N between sections X and A.

In this chapter, an overview is presented of what is known about the background oceanography of the survey region and the conditions encountered during the cruises. Then, the hydrographic data gathered during the survey are studied, and the Sverdrup IPV field derived. The inter-relationships of the Sverdrup IPV field and other quantities is examined, and compared with the results from FLW89. Finally, the results are discussed with particular regard given to how the IPV and tracer fields came to be set.

3.2 BACKGROUND

Two major gyres contribute to the circulation of the North Atlantic: the cyclonic subpolar gyre circulates north of about 48°N; and the anticyclonic subtropical gyre circulates south of about 45°N. The North Atlantic Current (NAC) flows eastwards in several branches at the southern edge of the subpolar gyre, and the Azores Current flows eastwards at the

northern edge of the subtropical gyre. The area between the two gyres is complex and poorly understood, and has a weak mean circulation.

Pollard and Pu's review of past work (Pollard and Pu, 1985) concluded that a surface anticyclonic wedge of saline water (shallower to the north) over much of the region was the northern outcrop of the subtropical gyre with a weak eastward/south-eastward circulation. However, when Pollard *et al* re-examined the circulation of this region by looking at the Vivaldi data set, they reached quite different conclusions (Pollard, *et al.*, 1996).

The top 500 metres of water between the two gyres were entirely North Atlantic Central Water (NACW). Central Water has a well defined θ/S relationship, formed by air-sea interactions over a large range of latitudes (Iselin, 1939). However, it has long been recognised that waters in the western North Atlantic are fresher than in the eastern North Atlantic at lower densities (Harvey, 1982). Hence, the term NACW encompasses the three sub-divisions of Western North Atlantic Water (WNAW), Eastern North Atlantic Water (ENAW) and freshened WNAW, using the terminology suggested by Pollard *et al.* (1996). These sub-divisions may not always be distinguishable because their θ/S characteristics can vary from year to year, depending on the extent of deep winter mixing.

During the Vivaldi survey, freshened WNAW entered the region from the west, mainly between the northern and southern branches of the NAC, and recirculated northwards at 20°W. South of the NAC, there was evidence of weak westward recirculation of salty ENAW from east of 20°W, interspersed meridionally with fresher WNAW moving slowly eastward. There has been evidence that ENAW has two sources (Ríos, *et al.*, 1992): colder $ENAW_P$ from the subpolar gyre moves southwards; warmer $ENAW_T$ from the subtropical gyre moves northwards. Both these types of ENAW recirculate westwards and are modified by winter mixing.

Many researchers have sought to explain the mechanism behind the anomalies in salinity which have been recorded in the region, and different hypotheses have been put forward. These hypotheses have included: air-sea interaction in the form of winter mixing and subduction (Pollard and Pu, 1985, Pollard, *et al.*, 1996); advection of water round the subpolar gyre (Dickson, *et al.*, 1988); downward pumping of salt beneath the NAC (Arhan, 1990); mixing with Mediterranean Water (MW) (Harvey, 1982, Ellett, *et al.*, 1986, Pollard, *et al.*, 1996). Pollard *et al.* (1996) conclude that these various theories are not contradictory, but that they all contribute, but with different balances at different locations in different years.

3.3 DATA COLLECTION AND PROCESSING

SeaSoar, ADCP and thermosalinograph data were collected during both Vivaldi '91 cruises, and combined into one data set consisting of six meridional sections. These data were manipulated to achieve the three-dimensional density field, the near-surface temperature and salinity fields, the three-dimensional velocity field and the three-dimensional vorticity field. The processing of these data is described in detail in this section.

3.3.1 Three-dimensional density field

The SeaSoar is an instrument platform which is towed behind a ship in an undulating pattern. It follows a vertical saw-tooth path through the water, from the sea-surface down to about 500 metres depth (maximum depth attained depends on various factors such as ship speed and length of towing cable). With the operational set-up used for Vivaldi, it took approximately 3 km in the horizontal direction to complete each undulation. The instruments deployed on SeaSoar were a Neil Brown CTD (measures Conductivity, Temperature and Depth), a Chelsea Instruments Fluorometer and a Chelsea Instruments Irradiance Sensor. After acquisition, the data from these instruments were processed in batches of 4 hours of data to convert them from engineering units to calibrated measurements (Cunningham, *et al.*, 1992). These data were then interpolated into 4 km bins along-track, so that each bin contains at least one undulation, with each bin containing an average of data over 12 km, to smooth out noise somewhat. Finally, the data were vertically interpolated by the author in three different ways: onto pressure surfaces of 8 metres thickness; density surfaces (isopycnals) spaced at intervals of 0.02 kg m^{-3}; thicker density surfaces spaced at 0.15 kg m^{-3}. The data values on each surface were calculated as the average value of all the measurements within the pressure or density range represented by that layer. One might expect the thicker isopycnic layers to be less susceptible to noise bias and the effects of internal waves, because their values are the average of more data, and that the thinner layers may contain more spiky data. This expectation is examined later in this chapter.

3.3.2 Surface temperature and salinity fields

Seabird TSG data were logged every 30 seconds, and calibrated against the SeaSoar data, being the most accurate absolute measurement of temperature and salinity (Pollard, *et al.*, 1991). Temperature data were reckoned to be generally within 0.01°C (standard deviation 0.009°C) of the SeaSoar measurements, with larger errors where the temperature changed rapidly, and the salinity data were found to be around 0.03 (standard deviation 0.02) above the SeaSoar values throughout. The TSG data were sorted by the author into the

same sections as the SeaSoar data, and then merged by matching the closest TSG data to the SeaSoar data. This merging was done by latitude for the north-south tracks and by longitude for the short east-west connecting tracks. The water intake for the TSG was at a depth of about 5 m below the sea surface, so the TSG temperature corresponds to the temperature at about 5 m depth. The TSG near-surface temperature field is shown in Figure 3-1.

3.3.3 Three-dimensional velocity field

The data from the RD Instruments 150kHz ADCP were averaged and logged every two minutes, with vertical binning into 8 metre cells down to 512 metres while in water-tracking mode (Pollard, *et al.*, 1991). Bottom-tracking mode was used while over the shallow shelf, and calibration manoeuvres were carried out, but water-tracking mode was used during SeaSoar runs. The vertical range achieved varied from 400 metres in areas where the spring bloom was active, reducing to 100 metres in southern areas where the bloom had ceased. Velocity measurements showed less scatter while on station as compared with underway measurements, so the data were processed and calibrated as two series: "on station" when ship speed was minimal; and "underway" during SeaSoar runs. The along-track resolution depends on ship speed because the data were recorded at regular time intervals. The data were interpolated into 12km bins at 4km separation, to match the gridding of the SeaSoar data. The ADCP velocities were then merged with the SeaSoar data by matching up the time fields of the data.

3.3.4 Vorticity

The Sverdrup IPV, q_S, as given by equation (2.3) was calculated for both density-gridded data sets, which were gridded on 0.02 and 0.15 kg m^{-3} isopycnal spacing. First differences were used for the density gradient with respect to depth. For analyses on isobaric surfaces, Sverdrup IPV was interpolated along with the other properties to give Sverdrup PV. The full IPV as given by equation (2.1) was not calculated for the Vivaldi data because the zonal spacing of the survey sections was too coarse to resolve the relative vorticity adequately. It would require the calculation of the across-track derivatives of the along-track component of velocity.

3.4 RESULTS

3.4.1 Water mass analysis

The Vivaldi survey was made over two months, working westwards on the southern part of each north-south section, then eastwards on the northern parts. Thus, the eastern-most sections consist of two parts separated by some time and frontal features or positions may

have changed meanwhile. Analysis of potential temperature and salinity using "θ-S" plots may help highlight such changes by identifying water masses, while sectional plots of potential temperature, salinity and potential density may be used to locate these water masses and trace their paths.

Plots of potential temperature (θ) against salinity (S), known as θ-S plots, were produced for each section of the survey, and are presented for both the 0.02 kg m^{-3} gridded data set (Fig. 3-2) and the 0.15 kg m^{-3} gridded data set (Fig. 3-3). Sectional plots of density (Fig. 3-4), potential temperature (Fig. 3-5) and PV (Fig. 3-6) against depth were constructed using the data gridded on isopycnals separated by 0.15 kg m^{-3}. These figures show some of the major features of the data set which are described here, and are discussed in greater detail in Pollard *et al.* (1996).

The θ-S plots illustrate that there is a range of near-surface (mixed layer) water characteristics within each section, but the majority of data points lie on a curve corresponding with the Central Waters which dominate the upper 500 – 1000 m of the North Atlantic (Pollard, *et al.*, 1996). The northern parts of the survey sections, which were completed during the second half of the cruise, show well-stratified surface waters caused by increased warming and lighter surface winds, while the earlier southern sections show a well-mixed layer at the surface (Fig. 3-5). Deeper waters, known as "intermediate waters", are evident as "tails" at low temperatures on sections W, X and Y. Comparing Figures 3-2 and 3-3 shows that coarser gridding of the data retains most of the features of the finely gridded data, but some features are obscured particularly in the mixed layer and in the coldest, deepest regions. These plots give us reason to believe that the coarsely gridded data will contain adequate representation of the Central Waters for comparison of the derived PV field with tracer quantities. The potential temperature structure (Fig. 3-5) shows that temperature is well correlated with density (Fig. 3-4) in the Vivaldi region, and is the dominating factor in setting the density.

The low temperature tails in the θ-S curves of sections W, X and Y correspond with the characteristics of Sub-Arctic Intermediate Water (SAIW), and these waters are evident north of the northern branch of the NAC (Fig. 3-5). From west to east (section W through to section B), the main part of the θ-S plots (Figs. 3-2 and 3-3) becomes slightly more saline for a given temperature (above 10°C), by about 0.08 by section B. This main part of the curve is identified by Pollard *et al.* (1996) as Western North Atlantic Water (WNAW) in the western sections and Eastern North Atlantic Water (ENAW) in the eastern sections. Below 10°C, Pollard *et al.* (1996) identified "freshened WNAW" in the NAC, which is WNAW freshened by mixing with SAIW from the north-west. WNAW flows eastward in the North Atlantic Current (NAC) and consists of a northern and southern branch. These branches of the NAC are evident in the profiles of density

structure (Fig. 3-4) as strong fronts corresponding to the northern branch at about 51°N in section W, and the southern branch at 48.5°N. These fronts can be traced as continuing eastward through subsequent sections, then turn northwards between 25°W (section Y) and 20°W (section Z) at 54°N. South of the NAC, freshened WNAW penetrates slowly eastwards interspersed with ENAW flowing weakly westwards.

The Sverdrup IPV, q_S, structure is shown in Figure 3-6. The 0.2 PVU isoline lies at a depth of about 80–130 metres throughout the Vivaldi region, with occasional excursions to shallower depths. Deeper than this, there is very little IPV structure with values reaching negligible levels by 500 metres, because the vertical density gradient is weak at these depths. At shallower depths, and particularly north of 48°N and west of section A (16.5°W), IPV values are higher, up to 1.4 PVU, and demonstrate greater variability.

3.4.2 Correlation of properties on different surfaces

In trying to establish the relationship between SST and IPV at the base of the mixed layer, it is relevant to consider the extent to which physical properties are correlated with depth or density.

The potential temperature fields of several isopycnals in the 0.02 kg m^{-3} and 0.15 kg m^{-3} density-gridded data sets were plotted (Fig. 3-7) against the values for the 27.00 kg m^{-3} isopycnal which acts as a reference layer for these plots. The 27.00 kg m^{-3} isopycnal was selected as the reference layer because it lies within the surveyed depths throughout most of the survey, whereas many other surfaces outcrop or deepen beyond 400 m in some locations. Figure 3-7a shows that the 0.02 kg m^{-3} layers are well correlated between closely neighbouring layers, with tightly defined curves of similar slope. Correlation is slightly poorer at higher temperatures, shown by increased scatter. As the separation between layers increases, correlation reduces as scatter increases and the curves have shallower gradient. This good degree of vertical coherence shows up in the 0.15 kg m^{-3} thick layers also (Fig. 3-7c), although the scatter is slightly greater than for the thinner layers. However, the gradient does not decrease with increased separation of layers. As in the case of 0.02 kg m^{-3} layers, there is poorer correlation at higher temperatures, which occur at depths greater than 100 m, as shown by Figures 3-7b and 3-7d, where only data deeper than 100 m on a given layer have been plotted. This indicates that the best vertical temperature correlation occurs within the mixed layer, while stratified waters have reduced correlation.

The correlation of Sverdrup IPV between isopycnals in the 0.02 kg m^{-3} and 0.15 kg m^{-3} data sets was also examined (Fig.3-8). The 0.02 kg m^{-3} layers show very little correlation between layers, while the 0.15 kg m^{-3} layers are somewhat better correlated between

neighbouring layers. This may reflect that the 0.02 kg m^{-3} layers contain errors due to such things as internal waves and the influence of outlying data points which are averaged out in the 0.15 kg m^{-3} layers. Shallower isopycnals (e.g. 26.85 kg m^{-3}) span a greater range of IPV values than deeper levels (e.g. 27.30 kg m^{-3}). The correlation of the 0.15 kg m^{-3} layers is poorer at higher values of IPV, which occur where the layers are thinnest (in terms of the pressure difference across the layer). Figures 3-8b and 3-8d show the IPV relationship after the removal of points shallower than 100 dbar, which may lie within the mixed layer where IPV is not really defined. These plots are very similar to those for the complete data set, so the spread is not explained by the inclusion of mixed-layer values. The gradient of the best-fit line varies greatly, suggesting that there is really very little vertical coherence of IPV, unlike the potential temperature field.

The correlation of properties between pressure surfaces was considered by creating plots of potential temperature, salinity and IPV regridded onto isobaric surfaces (40, 80, 120, 160 and 200 dbar) against the same property on a reference level of 120 dbar (Fig. 3-9). These showed very similar results to the correlation between isopycnals. Temperature and salinity correlate well between layers, with increased scatter for increased separation. The PV curves swing round from high PV range for shallower surface to small PV range at greater depth, much as for isopycnals, suggesting that PV does not show significant vertical coherence.

3.4.3 Comparison of PV with temperature and salinity measurements

Isopycnic comparison of Sverdrup PV with temperature and salinity

Isopycnic Sverdrup PV, q_S, was compared with the isopycnic potential temperature, θ, and with the thermosalinograph (TSG) near-surface temperature, over the complete survey data set. The plots for five isopycnals from 26.85 kg m^{-3} through to 27.45 kg m^{-3} are shown in Figure 3-10, with different colours assigned for latitude as a geographical locator.

The relationship between q_S and isopycnic θ varies considerably with the density, tending from a well-spread cluster at cooler temperatures/higher q_S and tighter relationship at warmer temperature/lower q_S at 26.85 kg m^{-3} through quite a tight near-linear relationship on 27.15 kg m^{-3}, to near constant q_S on 27.45 kg m^{-3}. Let us consider the curve corresponding to isopycnal 27.00 kg m^{-3} (Fig. 3-10b) which shows a near-linear relationship at higher temperatures and greater spread at lower temperatures. The gradient of the best-fit line to this curve is -0.29 PVU K^{-1}, with a correlation coefficient r of -0.80. The more scattered data points occur at northerly latitudes, where the temperature is lower and the IPV is higher. Denser (deeper) isopycnals have best-fit lines which are less

steep (the magnitude of the gradient is less), but have less scatter. FLW89 found that for their data the slope of the variation of q_s with θ on the isopycnal 26.9 kg m^{-3} (0.1 kg m^{-3} thick) was -0.31 PVU K^{-1}, with a correlation coefficient r of -0.79. Hence, the results for the Vivaldi data on a similar isopycnal are in good agreement with FLW89.

The correlation between q_s and the TSG surface temperature (also Fig.3-10) is not as good, showing more scatter in all geographical regions than for the isopycnic θ because the near-surface temperature shows greater variability than isopycnic θ. The gradient of the best-fit line for isopycnal 27.00 kg m^{-3} is -0.12 PVU K^{-1}, with a correlation coefficient r of -0.57.

Similar plots were produced showing the variation of Sverdrup IPV with salinity on isopycnals (Fig. 3-11). These show relationships which are very similar to those between Sverdrup IPV and temperature. The gradient of the relationship between Sverdrup IPV and salinity on 27.15 kg m^{-3} is -1.22 PVU PSU^{-1} with a correlation coefficient r of 0.81. The gradient of the relationship between Sverdrup IPV and near-surface salinity from the thermosalinograph is -0.82 PVU PSU^{-1}, with a correlation coefficient r of 0.74. The near-surface salinity relationship has much better correlation than the near-surface temperature relationship.

Figures 3-10 and 3-11 were produced using the 0.15 kg m^{-3} gridded data. Similar comparisons were made using the 0.02 kg m^{-3} gridded data, particularly the isopycnals 26.9, 27.0, 27.1 and 27.4 kg m^{-3}, but the resulting plots are not shown here. These comparisons were very similar to the 0.15 kg m^{-3} thick comparisons, with even more pronounced scattering at the higher temperature/salinity values. The scatter of data values at lower temperature/salinity is much greater in the 0.02 kg m^{-3} thick layers, and is probably due to variations caused by internal waves, and other effects, which are smoothed when the data are interpolated on to 0.15 kg m^{-3} thick layers.

Isobaric comparison of Sverdrup PV with temperature and salinity

The inter-relationships of Sverdrup IPV and water mass properties were examined regridded onto constant pressure surfaces (40, 80, 120, 160, 200 dbar) as well as isopycnals. The plots of Sverdrup PV against potential temperature are presented in Figure 3-12 and Sverdrup PV against salinity in Figure 3-13. These plots show both the relationship between Sverdrup PV and temperature/salinity on the pressure surface and the relationship with near-surface (40 dbar) temperature/salinity. These plots show that deeper than 120 dbar Sverdrup PV is nearly constant, and very small, on isobaric surfaces, so there is no functional relationship with Sverdrup PV. Shallower than this, the Sverdrup PV range increases, but no functional relationship is seen.

Relative vorticity

To evaluate the relative vorticity the along- and across-track gradients of velocity components must be measured. Given that the Vivaldi north-south sections were spaced about 300 km apart, and the scales of interest are of order 100 km (see section 2.1.1), it is not possible to calculate across-track gradients over the scales of interest. Nevertheless, the along-track gradients alone may give some insight into the relative vorticity's contribution to the full PV at these scales. ADCP measurements are not generally used directly as absolute velocity measurements, but are used to calibrate geostrophic velocity calculations (from density data) by referencing them to a "level of known motion" (Pollard and Regier, 1992, Allen and Smeed, 1996) This technique will be explained in greater detail in Chapter 4. However, ADCP measured velocities are adequate for making "order of magnitude" estimates as is required here.

The along-track gradients of the cross-track ADCP surface velocity component were calculated. Most values fell within a range of $\pm 0.35 \times 10^{-4}$ s^{-1}. Over the Vivaldi region, the planetary vorticity (f) ranges from 0.9×10^{-4} s^{-1} at 39°N to 1.2×10^{-4} s^{-1} at 55°N. Hence, if the along-track flow is negligible and the cross-track component of velocity represents the total velocity, the relative vorticity at the sea surface may contribute more than 30% of f to the absolute vorticity ($f+\zeta$). This suggests that relative vorticity should not be neglected in estimates of PV on scales of the order of 100 km.

3.5 DISCUSSION

Vivaldi data from isopycnal 27.00 kg m^{-3} showed a strong functional relationship between Sverdrup IPV and isopycnic potential temperature/salinity, and a more scattered relationship between Sverdrup IPV and near-surface (TSG) temperature/salinity. The isopycnic relationship is in good agreement with FLW89's findings in a similar region in the summer of 1981. FLW89 proposed the following mechanism to explain this relationship.

The correlation between Sverdrup IPV and water mass characteristics is set during the formation of the seasonal pycnocline in the spring (Woods, 1985). The θ-S characteristics of an isopycnal will be determined by its location at the time of subduction of that layer, setting the θ-S values to those of the surface water of the region. The IPV of an isopycnal will depend on the time of subduction because northward migration of the surface outcrop is faster at the beginning of the heating season, leading to thinner spacing of isopycnals and larger IPV, and slows as the spring goes on. If adiabatic advection is assumed, then these properties will be conserved on the isopycnal, and will be advected by the gyre-scale circulation, perhaps being drawn together in confluent regions, which would lead to

synoptic-scale variability in θ-S and IPV values on an isopycnal. This mechanism could explain the Vivaldi results too. The northernmost points have the highest IPV values, corresponding with thin isopycnals resulting from later subduction than those in the south.

Appendix C shows that the Atlantic Isopycnal Model (AIM) produces similar results to both sets of observations, Vivaldi and FLW89, from the region. This is true both for the magnitude of the physical properties and their inter-relationships. This is indicative of the model representing the physics that led to these results, so they are not the result of some hitherto unexplained process.

FLW89 identify that a similar correlation can be found between climatological isopycnic temperature and IPV (gradient of about –0.25 PVU K^{-1}) on isopycnal 27.00 kg m^{-3} for their region of interest in August. The climatological data were not available to the author, but on looking at the published maps, reproduced in Figure 3-14, showing isopycnic temperature, salinity (Bauer and Woods, 1984) and IPV (Stammer and Woods, 1987) on isopycnal 27.00 kg m^{-3} in May (because Vivaldi took place during April through to June), it is possible to pick out any similarities within the Vivaldi region. There is little variability evident in temperature and salinity. The contouring of the IPV shows more variability, but the broad pattern of the contours is similar to the temperature/salinity. The correlation is not nearly as obvious as for the FLW89 case, but this may be an artefact of the contouring.

The effect of averaging within isopycnals is still unclear, in that there are differences between the results from the Vivaldi data gridded on to isopycnals of different thickness. Other researchers make no comment on why they chose the isopycnal thickness that they have (Fischer, *et al.*, 1989, Pollard and Regier, 1992), and it seems that this is selected in a subjective fashion "to be large enough to suppress noise in the data, yet small enough to cover a single flow regime" (McDowell, *et al.*, 1982).

Many researchers have carried out analysis of water masses and circulation in this part of the North Atlantic, and it seems clear that it is a complex, and possibly unstable, region (Harvey, 1982, McCartney, 1982, McCartney and Talley, 1982, Pollard and Pu, 1985, Dickson, *et al.*, 1988, Ríos, *et al.*, 1992, Pollard, *et al.*, 1996). However, the Vivaldi results when compared with the FLW89 and AIM results show that the Sverdrup IPV and temperature relationships have been steady and are predictable to some extent.

Fig. 3-1 Sea surface temperature during Vivaldi '91 with cruise tracks overlaid.

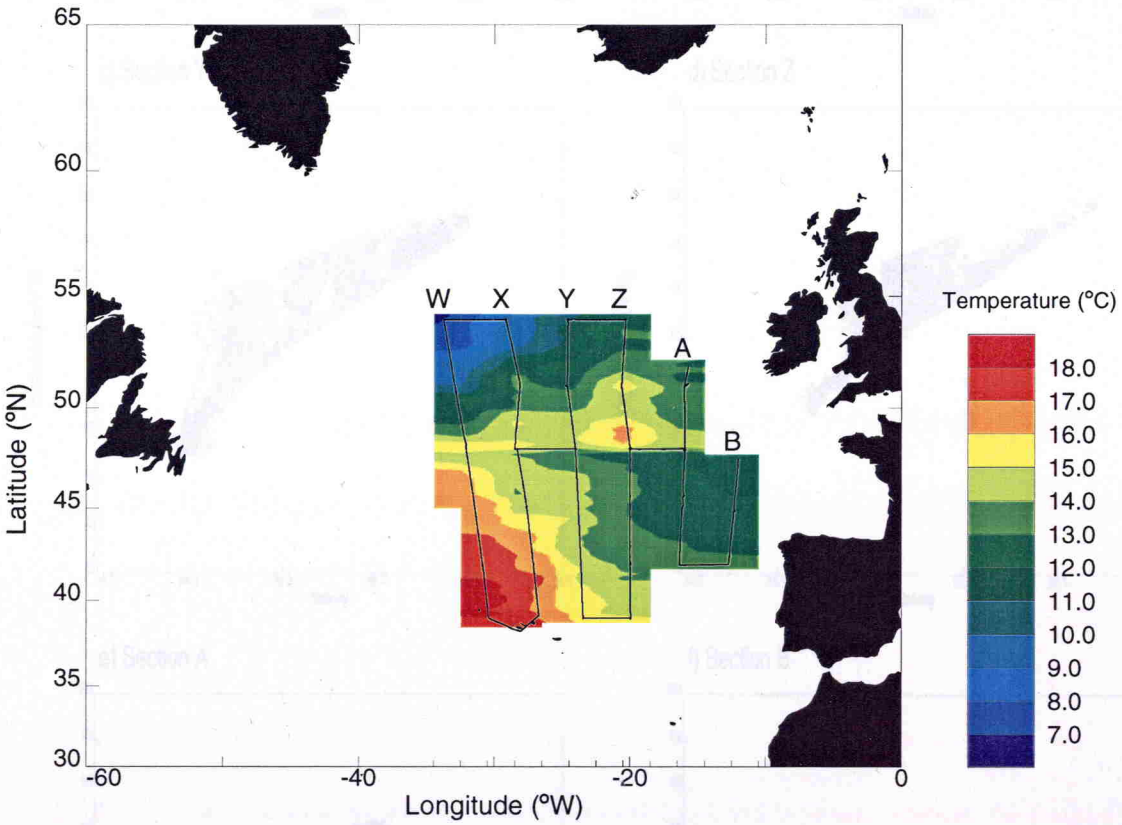

Fig. 3-2 Theta-S plots for 0.02 kg/m^3 isopycnal data.

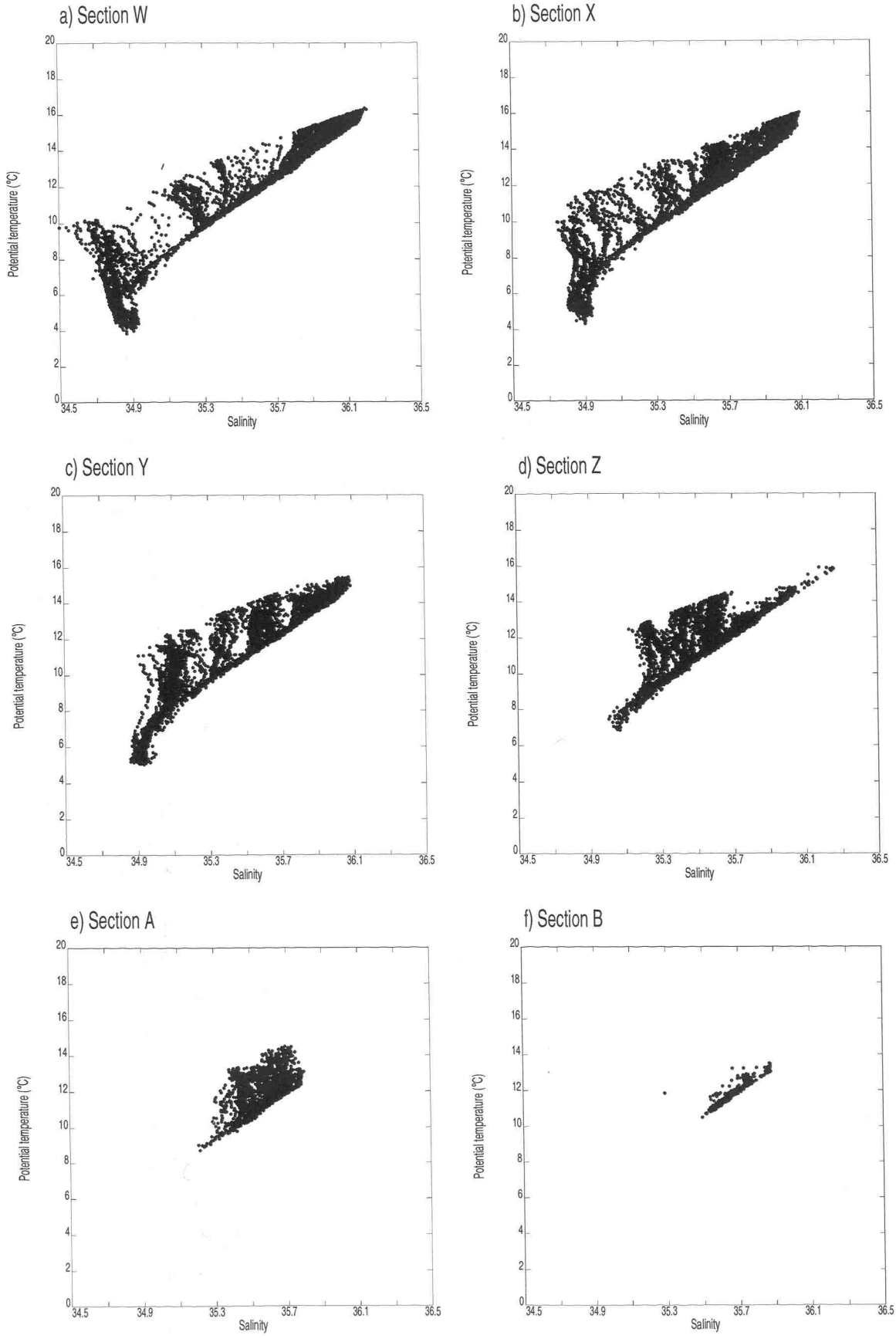

Fig. 3-3 Theta-S plots for 0.15 kg/m^3 isopycnal data.

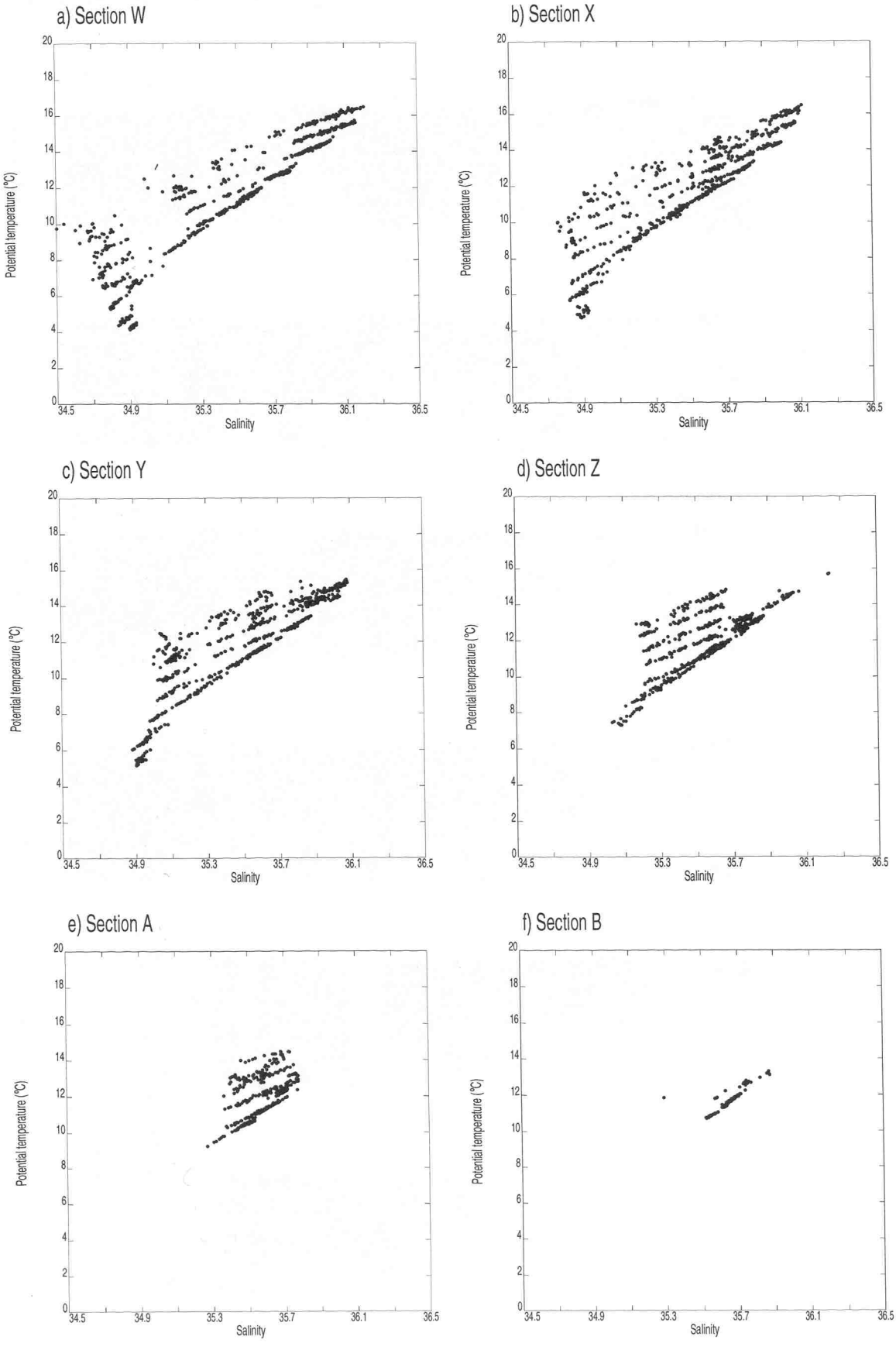

Fig. 3-4 Potential density vertical sections.

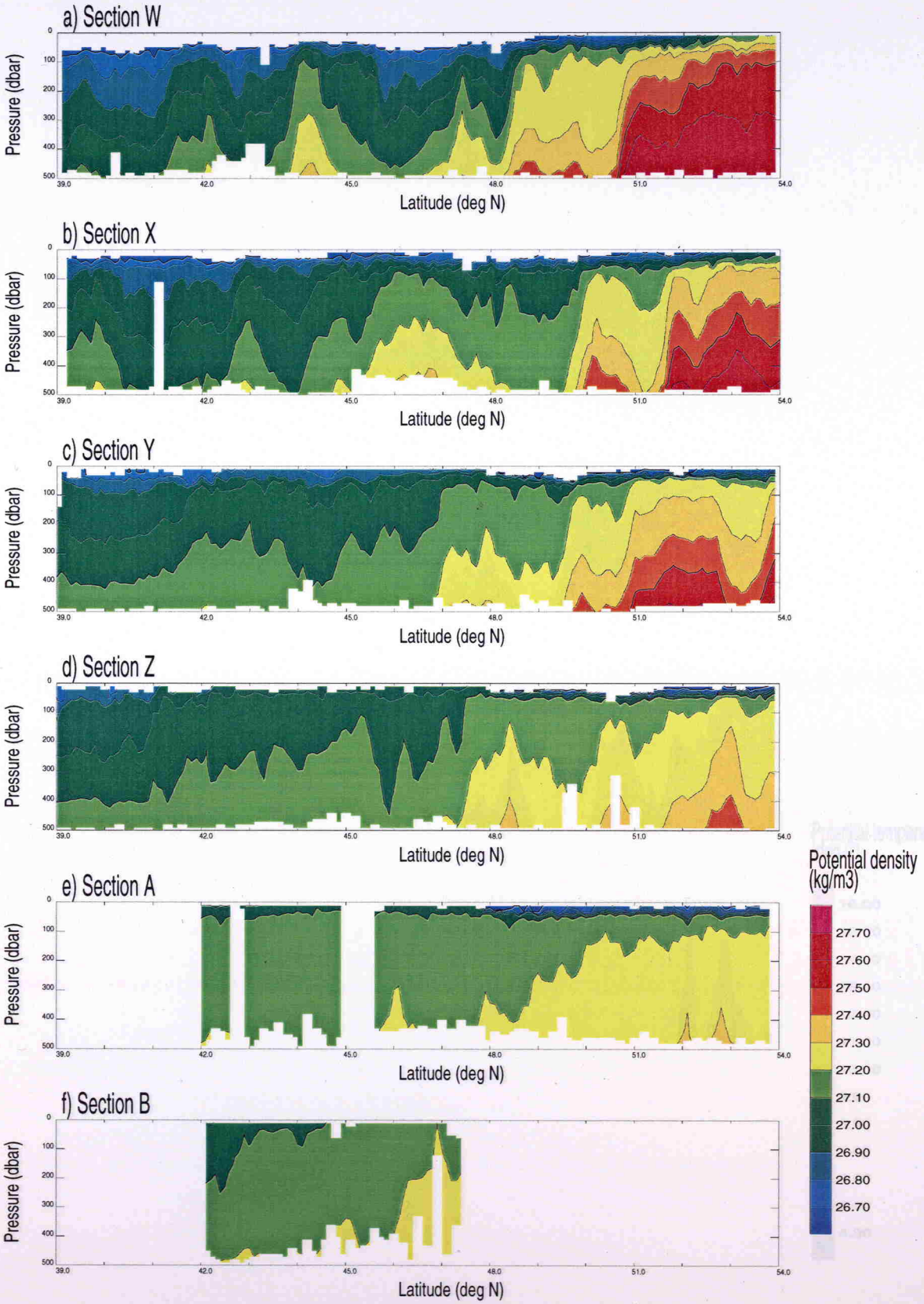

Fig. 3-5 Potential temperature vertical sections.

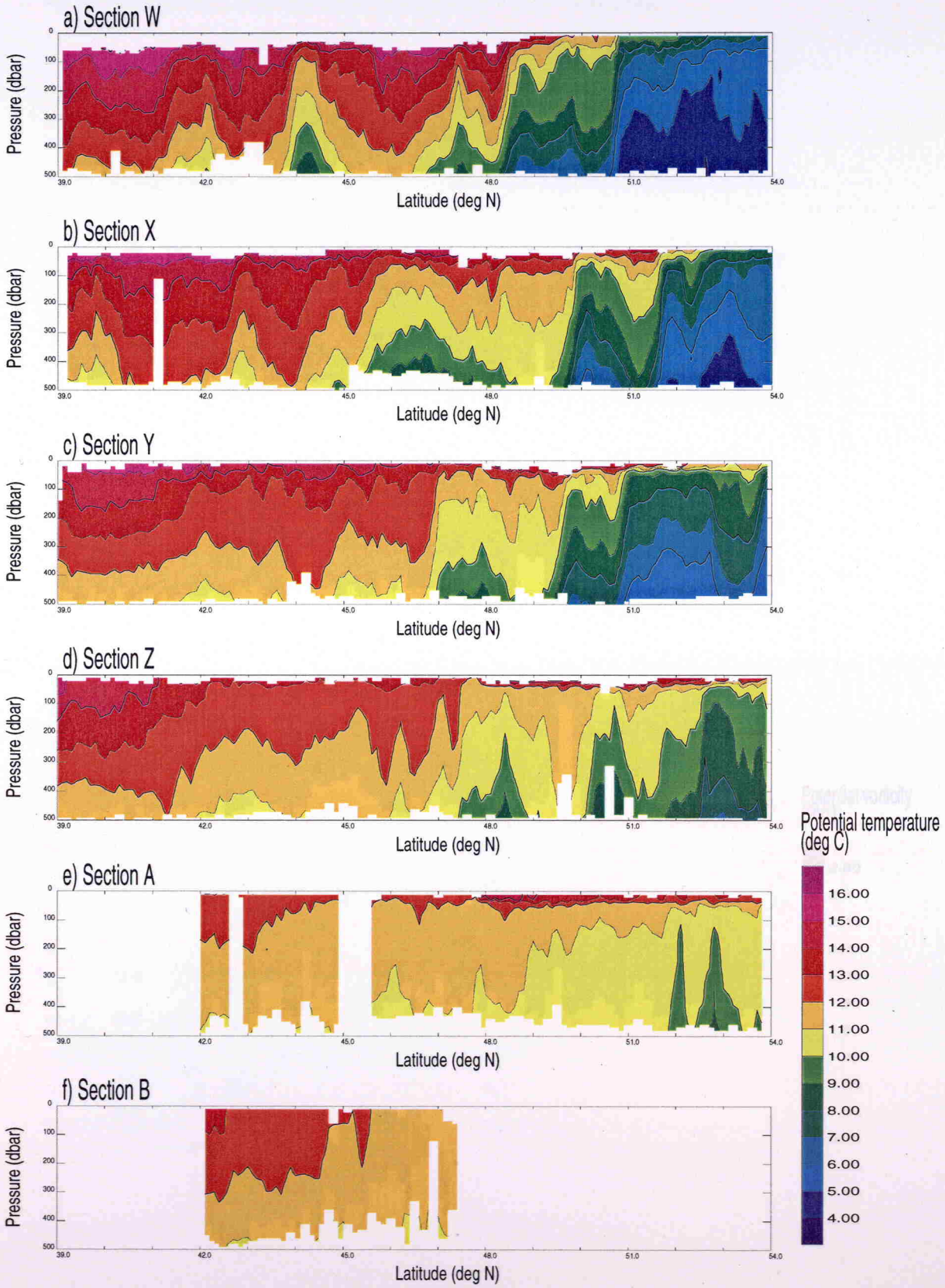

Fig. 3-6 Potential vorticity vertical sections.

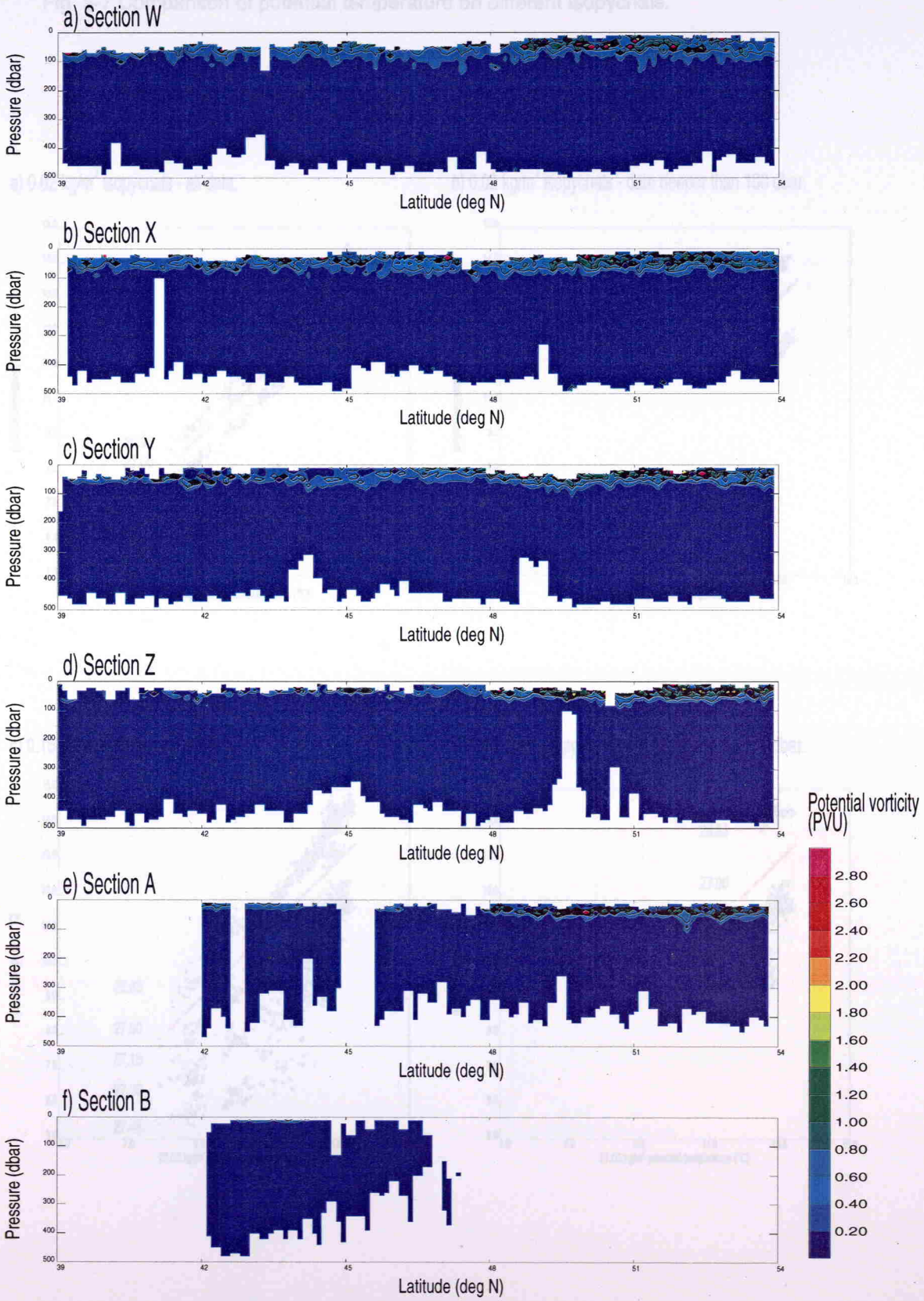

Fig. 3-7 Comparison of potential temperature on different isopycnals.

a) 0.02 kg/m^3 isopycnals - all data.

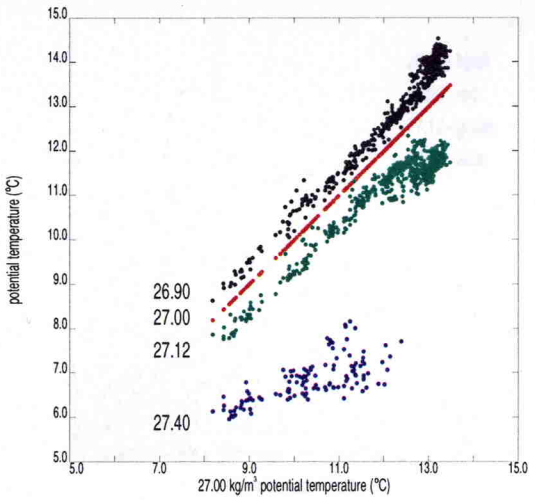

b) 0.02 kg/m^3 isopycnals - data deeper than 100 dbar.

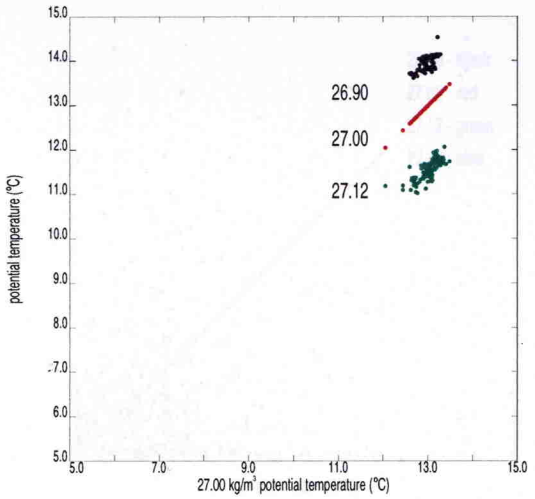

c) 0.15 kg/m^3 isopycnals - all data.

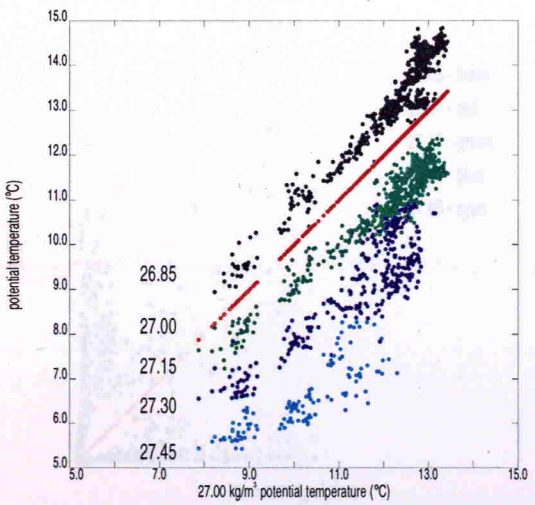

d) 0.15 kg/m^3 isopycnals - data deeper than 100 dbar.

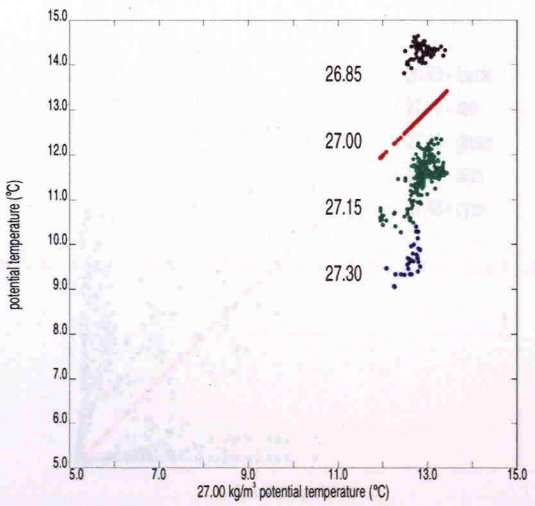

Fig. 3-8 Comparison of IPV on different isopycnals.

a) 0.02 kg/m^3 isopycnals - all data.

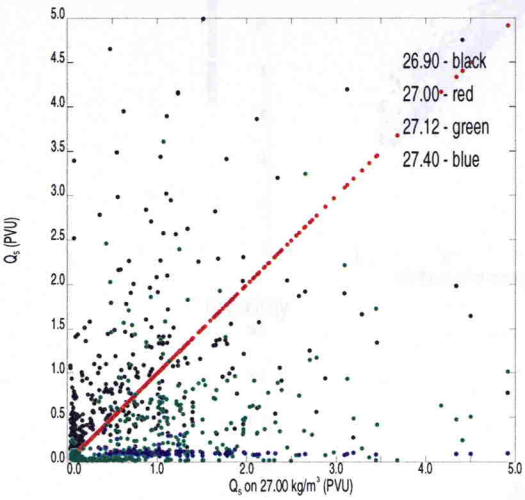

b) 0.02 kg/m^3 isopycnals - data deeper than 100 dbar.

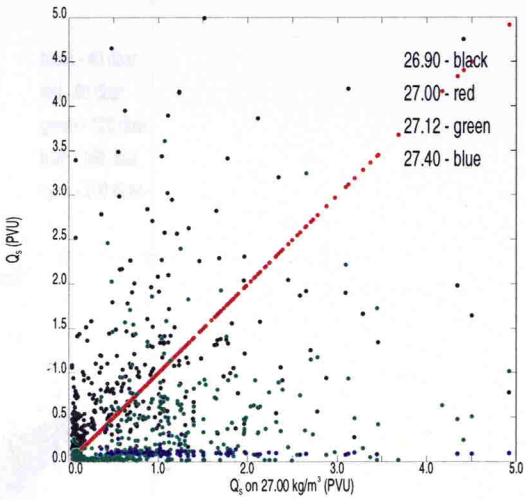

c) 0.15 kg/m^3 isopycnals - all data.

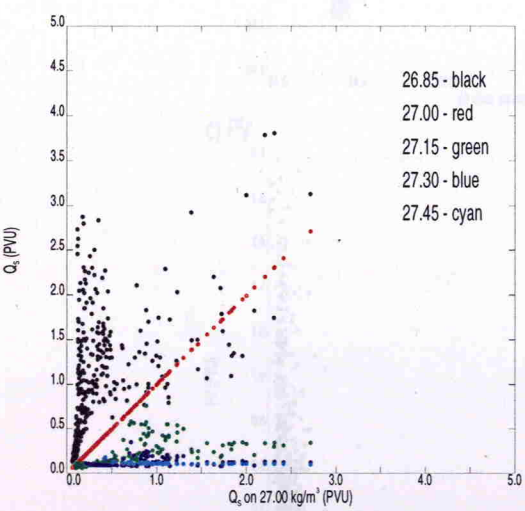

d) 0.15 kg/m^3 isopycnals - data deeper than 100 dbar.

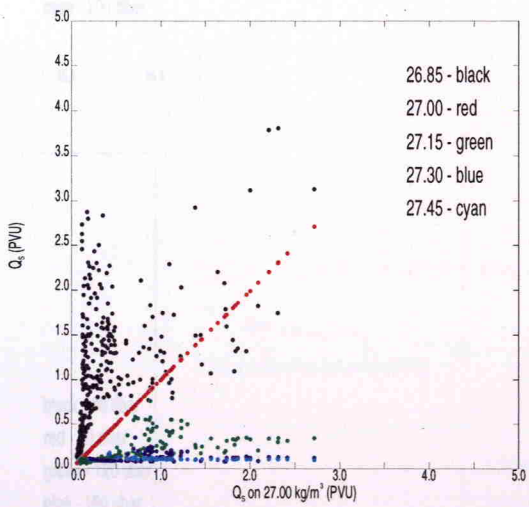

Fig. 3-9 Comparison of properties on different isobaric surfaces.

a) Potential temperature

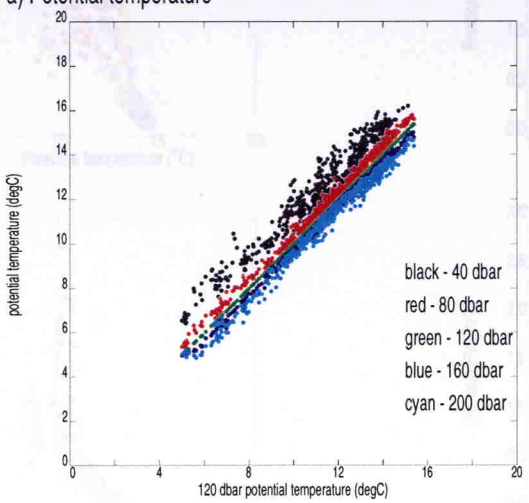

b) Salinity

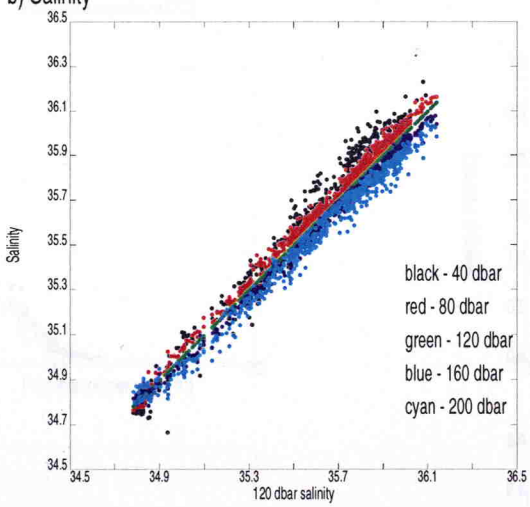

c) PV

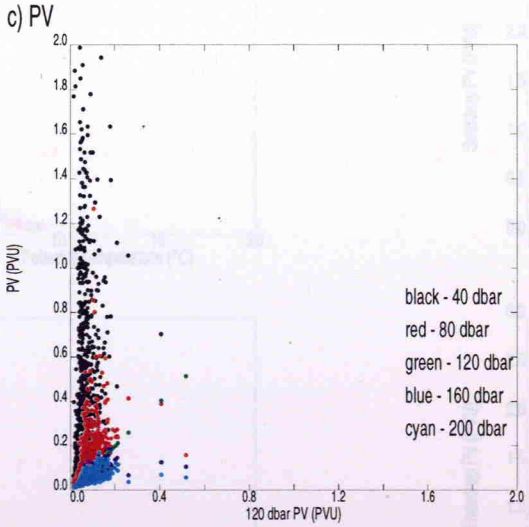

Fig. 3-10 Relationship between Sverdrup IPV and temperature on isopycnals of 0.15kg m^{-3} gridded data.

a) 26.85 kg/m^3

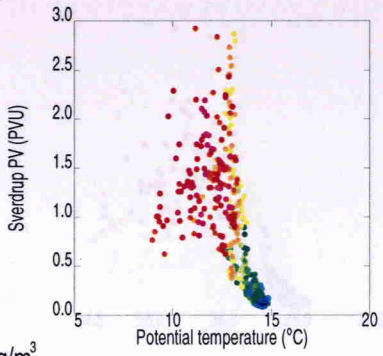

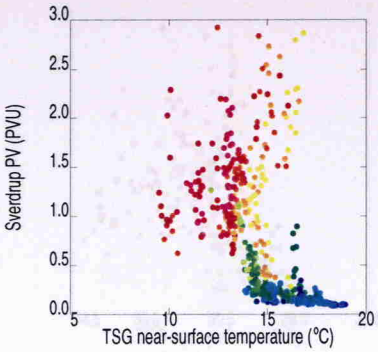

b) 27.00 kg/m^3

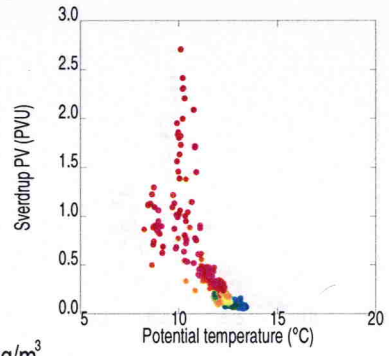

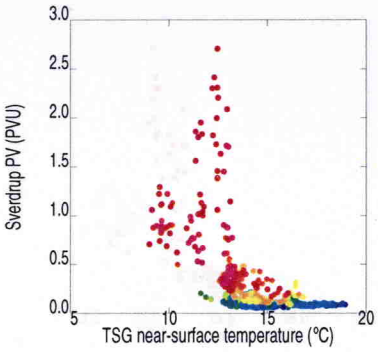

c) 27.15 kg/m^3

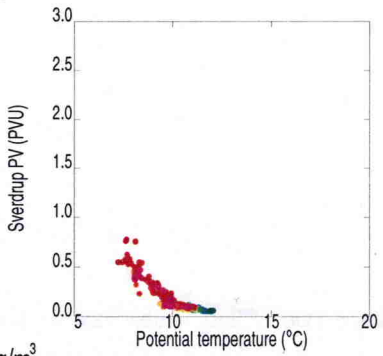

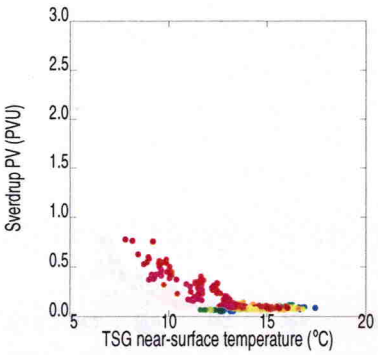

d) 27.30 kg/m^3

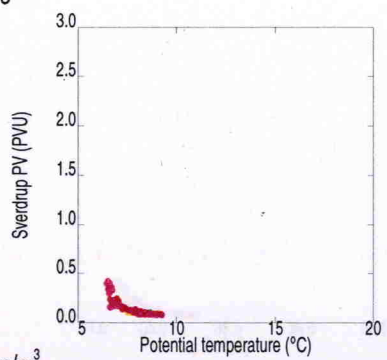

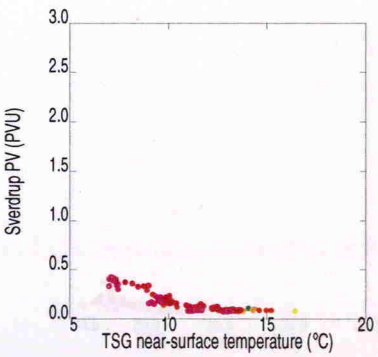

e) 27.45 kg/m^3

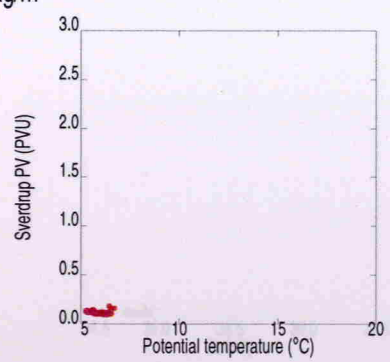

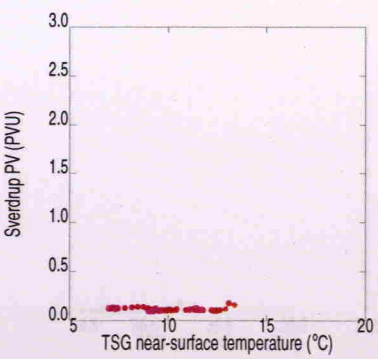

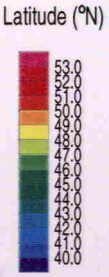

Fig. 3-11 Relationship between Sverdrup IPV and salinity on isopycnals of 0.15kg m^{-3} gridded data.

a) 26.85 kg/m^3

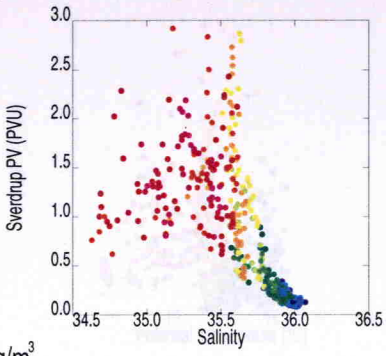

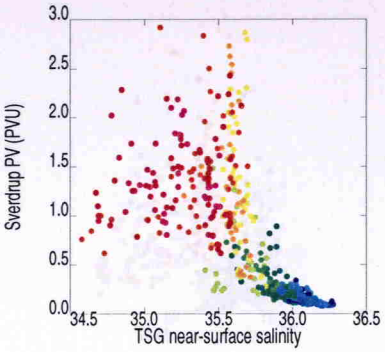

b) 27.00 kg/m^3

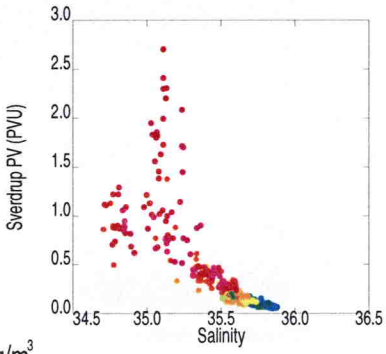

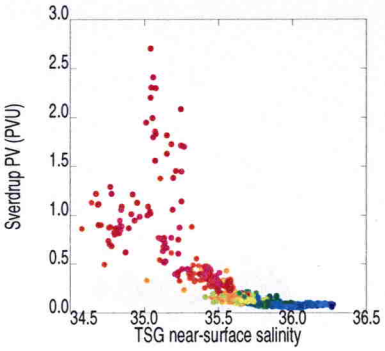

c) 27.15 kg/m^3

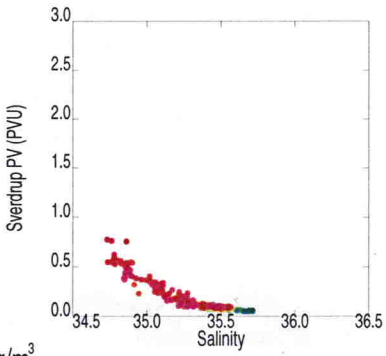

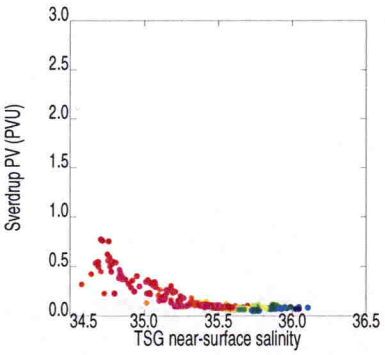

d) 27.30 kg/m^3

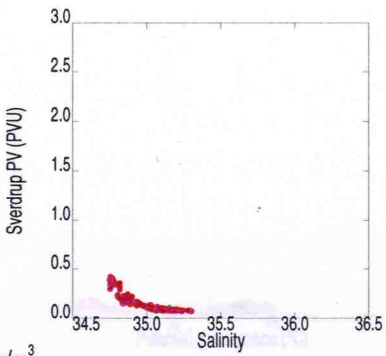

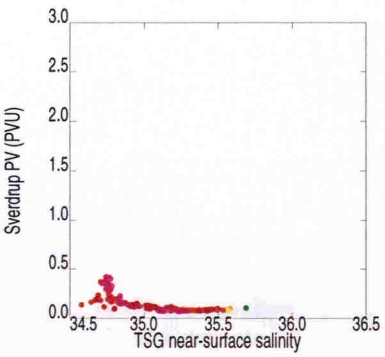

e) 27.45 kg/m^3

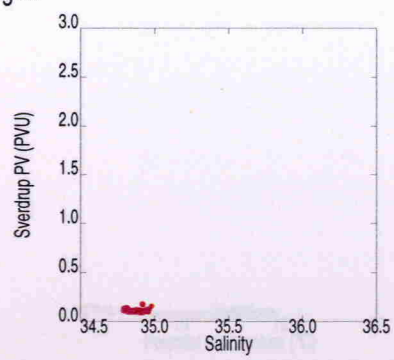

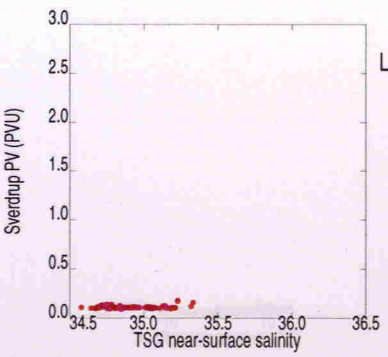

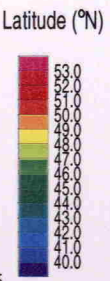

Fig. 3-12 Relationship between Sverdrup IPV and temperature on isobaric surfaces.

a) 40 dbar

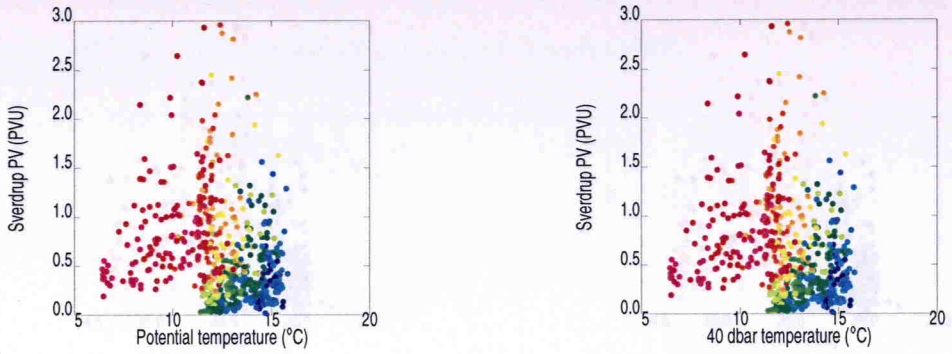

b) 80 dbar

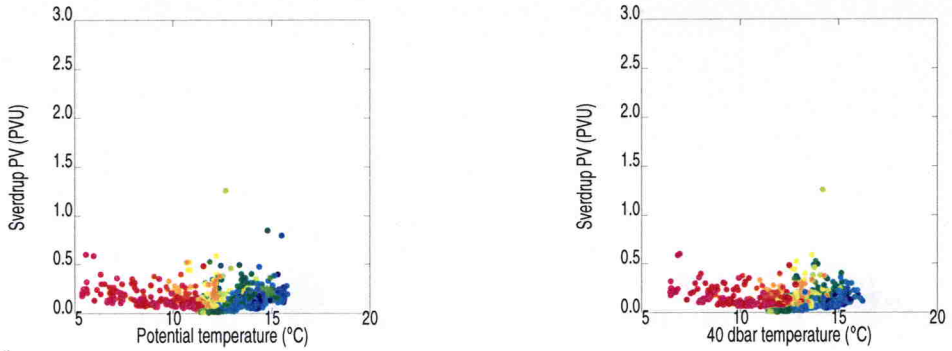

c) 120 dbar

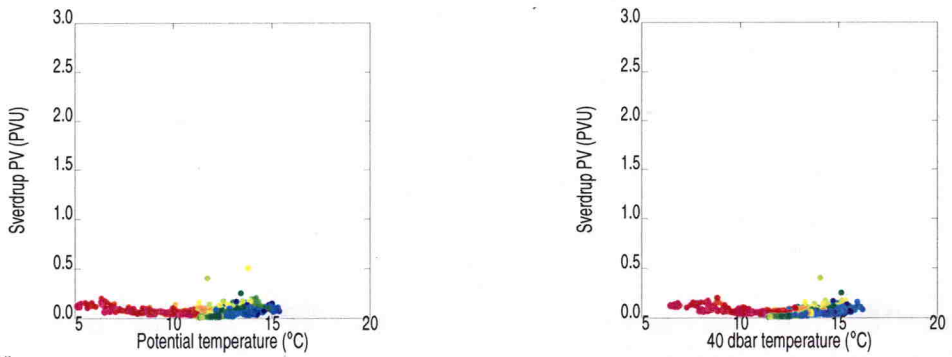

d) 160 dbar

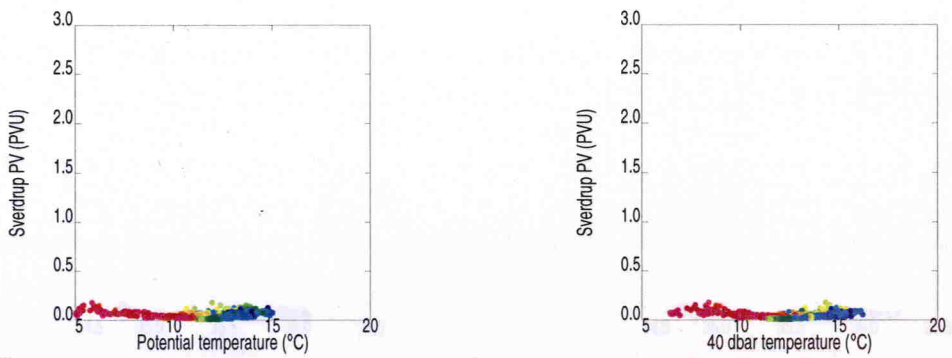

e) 200 dbar

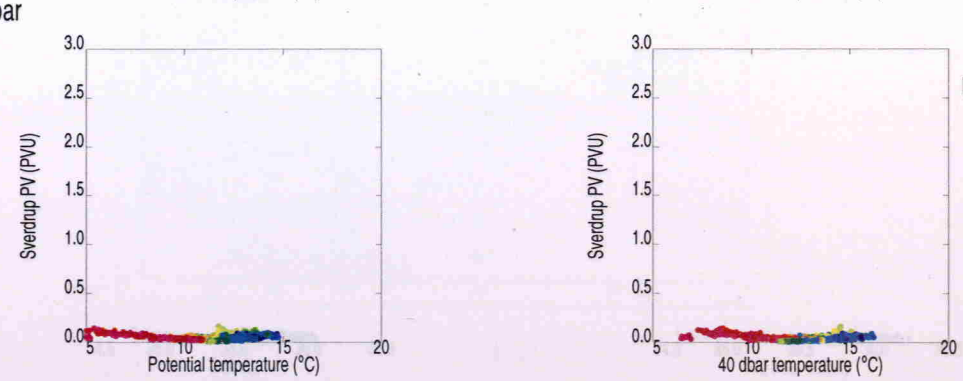

Fig. 3-13 Relationship between Sverdrup IPV and salinity on isobaric surfaces.

a) 40 dbar

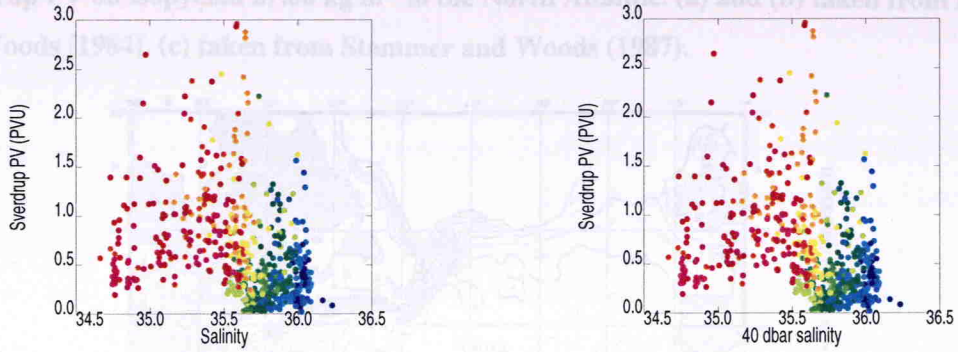

b) 80 dbar

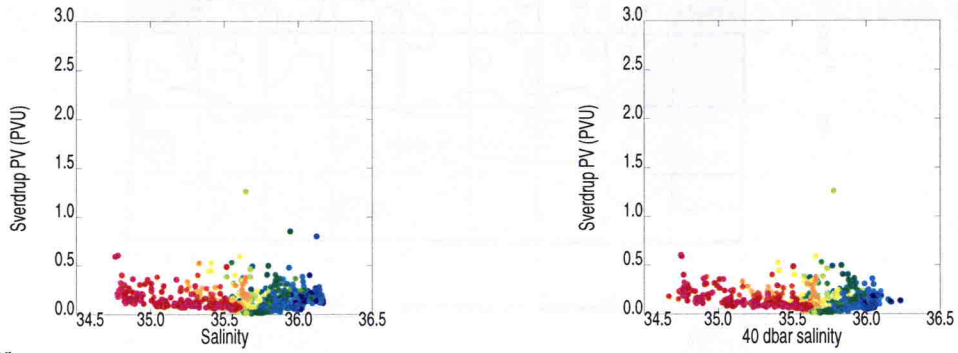

c) 120 dbar

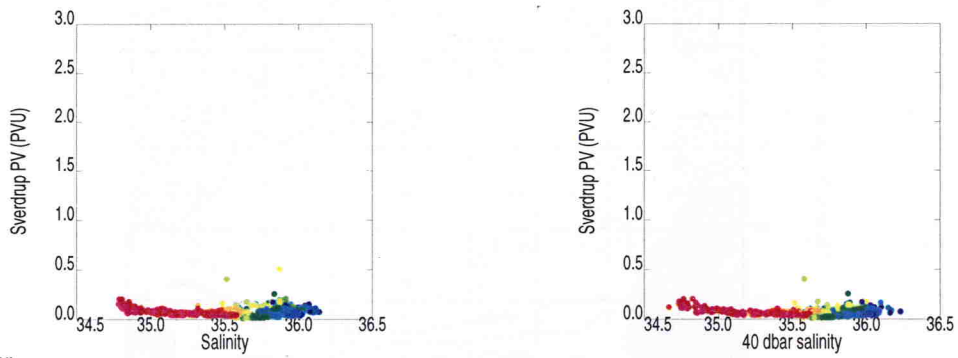

d) 160 dbar

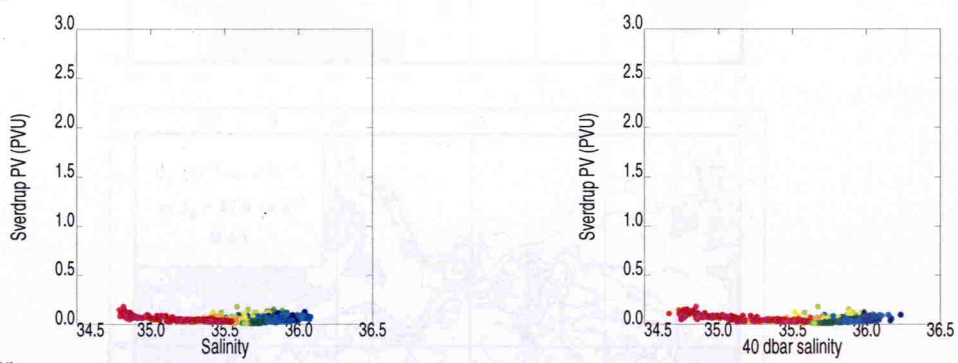

e) 200 dbar

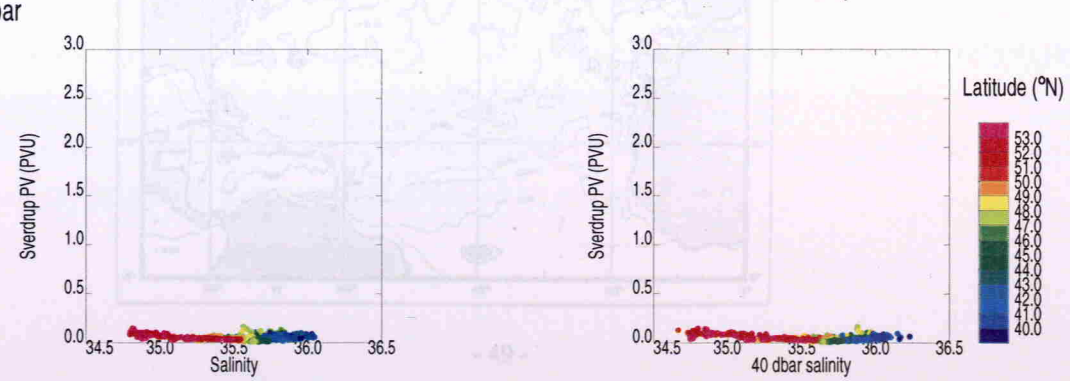

Fig. 3-14 Maps showing climatological values for May of (a) temperature, (b) salinity and (c) Sverdrup PV on isopycnal 27.00 kg m^{-3} in the North Atlantic. (a) and (b) taken from Bauer and Woods (1984). (c) taken from Stammer and Woods (1987).

(a)

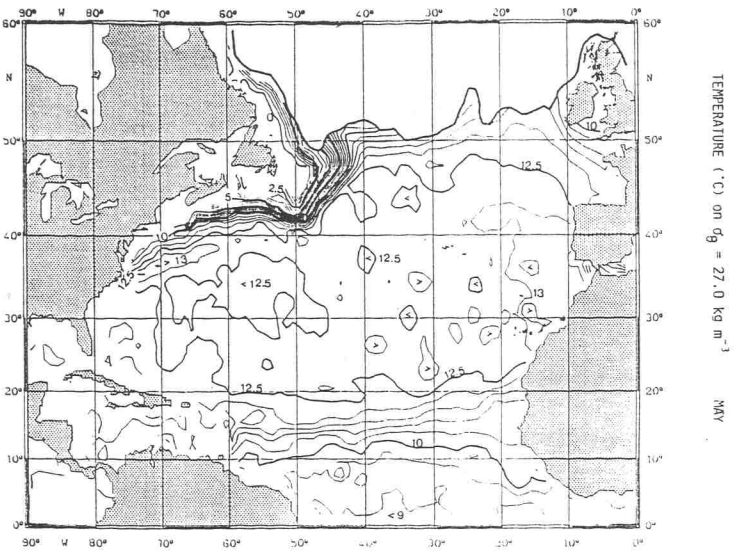

(b)

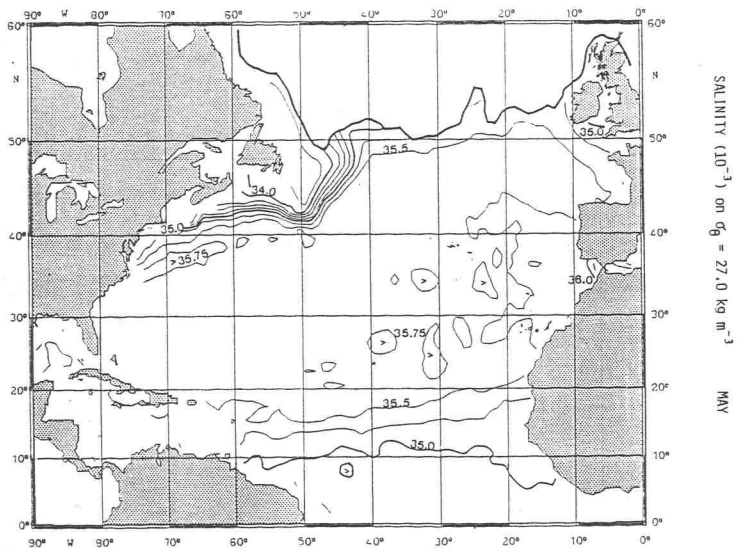

(c)

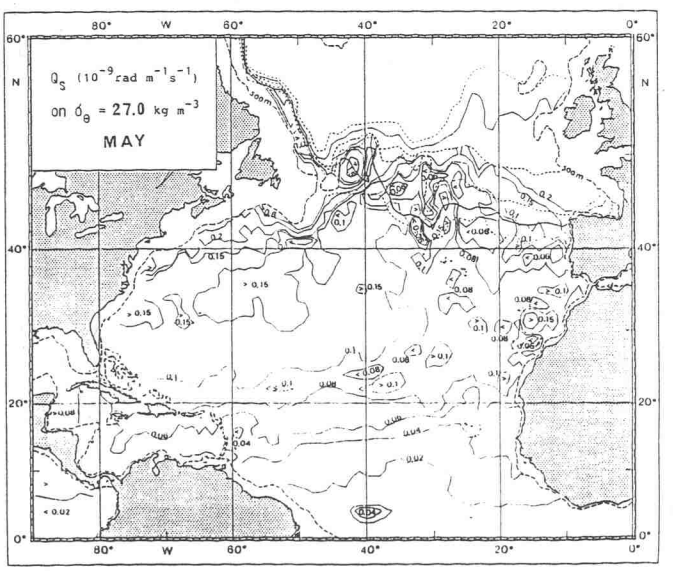

Chapter 4. FASINEX

4.1 INTRODUCTION

The Frontal Air-Sea INteraction EXperiment (FASINEX) was a co-operative air-sea interaction experiment which was conducted in the subtropical convergence zone (STCZ) south-west of Bermuda (see Figure 4-1) from 1984 to 1986 (Weller, 1991). The overall objective was to study air-sea interaction on 1 to 100 km horizontal scales in a region characterised by strong horizontal gradients in upper ocean and sea surface properties, especially temperature. Open ocean was observed, rather than coastal, to isolate the response of the atmospheric boundary layer to sea surface temperature (SST) gradients from the effects of the transition from land to sea. It also avoided observing strong boundary currents, such as the Gulf Stream, which would dominate oceanographic variability and complicate observation strategies. Historical collections of satellite SST imagery of the North Atlantic Ocean were used to select regions where sharp SST gradients regularly occurred, and then logistical constraints led to the choice of an area south-west of Bermuda. Ocean fronts were readily visible in images of this area from autumn through to spring.

During February and March 1986, 2 ships and 6 aircraft worked in the area of a front as it moved slowly to the north-west. During this time, five SeaSoar surveys were carried out to map the structure of the oceanic front. The location and pattern of the survey is shown in Figure 4-1, indicating the labelling used for each of the 8 legs of the survey.

In this chapter, an overview is presented of the climatic conditions in the survey region, the existing larger-scale oceanography during the surveys and some of the dynamical processes believed to be taking place. Then, the data gathered during the second of these SeaSoar surveys is studied, and the inter-relationships of the PV field and other properties are considered. Finally, these results are discussed in terms of how the PV and tracer fields were set.

4.2 BACKGROUND

The fronts of interest in FASINEX are the results of large-scale and mesoscale processes that produce SST gradients of up to 0.3°C km^{-1}. These fronts are not observed everywhere in the oceans, but are often observed in the Sargasso Sea south-west of Bermuda during winter months. The fronts are less visible to satellite sensors during summer months when the surface temperature signature is obscured by surface heating.

The large-scale climatological setting for FASINEX was examined by Hanson *et al.* (1991), using a 40-year climatology of the area compiled from the Comprehensive Ocean-Atmosphere Data Set (COADS) and higher resolution, shorter-term climatologies constructed from the US National Ocean Data Centre (NODC) archive.

Between about 15° and 45°N in the central North Atlantic, the mean large-scale circulation comprises a basin-scale anticyclonic gyre. The Sargasso Sea is a region where meridional convergence occurs due to the pattern of large-scale mean wind velocities, and is often referred to as the Sub-Tropical Convergence Zone (STCZ). The convergence is near-normal to the mean surface isotherms, and acts to increase the magnitude of the SST gradients within a zonally oriented band several degrees wide, often between 25° and 32°N in the Sargasso Sea. This band is known as the Sub-tropical Frontal Zone (SFZ). Smaller-scale non-linear dynamical processes then act to form the strong fronts found there.

Long-term average SST maps within the FASINEX region show an annual cycle consisting of a zonally symmetric north-south movement of isotherms (Hanson, *et al.*, 1991). Also, the large-scale north-south SST gradient decreases during the summer and increases during the winter, being maximum in late February. The area of maximum SST gradient lies within the FASINEX area during February and March, making this a near-optimal time and position for observing intense SST fronts. With a range of SST between about 21° and 24°C in the region, the February 1986 conditions were unusual in being about 1°C warmer than average for that time of year.

Having considered the large-scale climatology of this region, medium- to large-scale variability of the FASINEX region during the SeaSoar surveys was examined by Halliwell *et al.* (1991), by looking at monthly averaged SST fields and 5-day SST composites derived from AVHRR images.

Monthly averaged SST fields are too smooth to resolve individual fronts, but the SFZ shows up as the dominant feature meandering across the domain. The meander pattern in the SFZ moved to the south-west during January to May 1986. Convoluted fronts were observed throughout the domain except in May and June, when strong solar heating of the surface makes them more difficult to detect. The strength and location of individual fronts often changed dramatically within a period of one to several days. Fleet Numerical Oceanography Centre (FNOC) monthly-averaged wind stress fields changed dramatically each month because of strong synoptic-scale variability (2 days to 2 weeks). This means that to show the large-scale wind stress pattern responsible for Ekman frontogenesis, the wind stress field must be observed over periods of much longer than one month

(Halliwell, *et al.*, 1991). Longer time averages suggest that Ekman frontogenesis does contribute to the generation of the SFZ, but this relationship was not evident by eye.

Halliwell *et al.* (1991) created six gap-free 5-day infrared composite images of 4 km resolution, which show up the unusually warm feature that was passing through the region at the time of FASINEX. These also show that frontal variability was very small between February 25 and March 1, with a long single coherent front generally present within each band which migrated no more than 20–30 km. In contrast, there was large variability between March 7 and 11, with paths migrating over cross-band distances up to 100 km, and with broken or multiple fronts present in some segments of the frontal bands. The second SeaSoar survey, which is analysed in this chapter, took place during 16 to 20 February, so these composites show the changing situation shortly afterwards.

In summary, the formation of subtropical fronts in the FASINEX region takes place when an enhanced background SST gradient is modulated by baroclinic eddies at medium and large scales (Halliwell, *et al.*, 1991). The enhancement of meridional SST gradients between about 25° and 32°N is due, at least in part, to Ekman frontogenesis caused by the large-scale "mean" wind stress field. Eddies of wavelength ~800 km and period of ~200 days force the SST variability within the STCZ by generating bands of enhanced SST gradient that are ~200 km wide and separated by up to several hundred kilometres. The mechanism for this is believed to be through deformation in the horizontal current field. Smaller-scale eddies then exert a dominant influence on frontogenesis and frontolysis within these bands. At the medium- to large-scales resolved in Halliwell's analysis, frontogenesis involved complex interactions among the large-scale Ekman transport pattern, the mean current pattern, the oceanic baroclinic eddy field, and the mixed layer.

4.3 DATA COLLECTION AND PROCESSING

Density and velocity data were collected from five surveys during a cruise on *R.V. Oceanus* that took place in February 1986 in the Sargasso Sea south-west of Bermuda, as part of FASINEX. In this chapter, the data from the second of these surveys is examined. The other surveys were short surveys across fronts in a box pattern, and are not suitable for resolving mesoscale patterns and PV. In contrast, the second survey data consist of eight meridional sections across a near-zonal front collected during the 3.5-day survey, from 16 to 20 February 1986, using a SeaSoar and a ship-mounted ADCP.

4.3.1. Three-dimensional density field

Pressure, temperature and conductivity were sampled by a Neil Brown CTD towed behind the ship mounted on a SeaSoar following a sawtooth path between the surface and

about 300 m, completing a full cycle every 3 km. The SeaSoar was not usually allowed within about 30 m of the surface to avoid fouling of the sensors by the seaweed which is prevalent in this part of the Sargasso Sea. The sections of the survey were spaced about 16 km apart. Derived fields such as salinity and density were calculated, and initial reduction, calibration and editing were performed (Pollard and Regier, 1992). The data (pressure, density, potential temperature and salinity) were then interpolated onto a 10 m (vertical) by 4 km (along-track) grid by averaging all values within ±5 m and ±5 km of each grid point. Bécause of this, horizontally adjacent grid points are not independent, but the 10 km averaging is necessary to smooth the internal wave field. The averaged data are sufficiently smooth to allow calculation of dynamic height and hence geostrophic shear between adjacent columns along-track.

4.3.2. Three-dimensional velocity field

R.V. Oceanus was equipped with two positioning systems —Loran C and GPS (Global Positioning System)— and a 150 kHz RDI ADCP. Loran and GPS positions were logged once per minute. In 1986, GPS positions were not available at all times, but whenever they were, they were used in preference to Loran positions (Pollard and Regier, 1992). ADCP data were initially logged over 30 second intervals, and binned into 4.1 m depth intervals. Subsequently, the ADCP corrected velocities of the water relative to the ship were averaged to 5 minutes and combined with the ship's velocity (from GPS or Loran fixes) to obtain a time series of absolute water velocity, which was further averaged over the entire ADCP profiles.

Next, the vertical profile of geostrophic velocity (from SeaSoar) at each grid point was compared with the ADCP profile at that grid point. The ADCP velocity deviates from the geostrophic velocities near the surface due to ageostrophic features, such as inertial oscillation. This means that the ADCP velocities themselves are not suitable for calculating the relative vorticity straight from the divergence of the velocity. However, at some depth, the ADCP shear should be very close to the geostrophic shear, because the ageostrophic features do not penetrate to great depth. Hence, the ADCP velocity at this depth may be used to "correct" the geostrophic velocity calculated from the SeaSoar, by providing a "level of known motion" (as opposed to a "level of no motion" which has often been guessed at in the past) where the known velocity may be different at each data point, and the geostrophic velocity may be integrated from this level. By comparing plots of the ADCP and geostrophic shear profiles by eye, a level is chosen where the ADCP is believed to represent the actual geostrophic velocity. A streamfunction is fitted to the ADCP velocity at this depth, to give the dynamic height field. The geostrophic velocities at other levels are then integrated from this dynamic height field and should contain little or no baroclinic tidal/inertial contamination.

For the FASINEX data, the shears compare well in the depth range 100–150 m. Below 150 m, quite unrealistic shears were apparent in the ADCP data, due to a fault in the instrument and so all ADCP data below 150 dbar were discarded. Near surface, there was significant ageostrophic ADCP shear caused by strong wind-driven inertial oscillations (Pollard and Regier, 1992). Hence, the data at 150 dbar were used to provide the "level of known motion". A streamfunction (dynamic height field) was fitted to the ADCP data at 150 dbar to approximate a geostrophic (non-divergent) velocity field. The dynamic height fields at all other levels between 50 dbar and 250 dbar were then obtained from the SeaSoar density data by adding the dynamic heights relative to 150 dbar at each grid point. The non-divergent velocity fields were then recovered by taking central differences on the boundaries.

The resulting smooth velocity field (Pollard and Regier, 1992) shows a tendency for the velocity to oscillate from track to track, which is most probably due to the residual inertial oscillation at 150 dbar, because the time taken for *R.V. Oceanus* to traverse each track was approximately half an inertial period.

It is important to derive the velocity field as accurately as possible because the vorticity calculation depends on horizontal gradients of the velocity field. The ADCP data could not be directly used for this, as they contained inertial motions that would severely bias gradients between adjacent tracks. The errors were significantly reduced by the use of the non-divergent velocity field at 150 dbar and calculating the dynamic heights relative to that level. Errors in the gradients of the velocity field were further reduced by calculating these between alternate tracks surveyed approximately an inertial period apart (Pollard and Regier, 1992).

4.3.3. Vorticity

For the FASINEX data, the full PV, q, was calculated on isobaric surfaces according to equation (2.4), then re-gridded on to isopycnic surfaces. The isopycnic PV, IPV, in which the relative vorticity is calculated on density surfaces rather than pressure surfaces, was calculated also, according to equation (2.1).

4.4 RESULTS

4.4.1. Water mass analysis

The θ-S relationship for each section is shown in Figure 4-2. These highlight a number of features of the water properties. First, there is a salinity maximum at the base of the mixed layer, and this is more saline on the warm side of the front. The curves also show that there is little change in water type across the front at depth, where Subtropical Mode

Water is present (Erikson, *et al.*, 1991). However, in the mixed layer, the θ-S relationship varies sharply across the front as a result of confluent flow sharpening the background gradient of θ -S values into a front, bringing together water properties that were not set locally (Pollard, 1986). Ocean fronts often occur as the result of convergent flow bringing together distinct water masses, but this is not indicated here because at depth the θ-S curves from each side of the front overlap (Charnock and Businger, 1991).

Density sections for the eight legs of the survey are shown in Figure 4-3. These show that several isopycnals outcrop at the surface front and slope downward to the south to 100–150 m in the seasonal thermocline. The mixed layer is about 100 m deep on both sides of the front. The thickness between any pair of isopycnals 0.1 kg m^{-3} apart varies along and between sections, leading to variations in IPV (Fig. 4-5). Several areas of weakly stratified water can be seen corresponding with regions of low IPV. These weakly stratified patches stretching across several legs and up to 50 m in height are caused by shallow anti-cyclonic eddies of about 40 km diameter. These eddies carry frontal water over the top of the mixed layer to the north and trap less stratified water in the thermocline. The potential temperature, θ, sections (Fig. 4-4) have patterns almost identical to the density sections, with isotherms outcropping and separating at the same locations. This is an indication that the density is controlled mostly by temperature.

Dynamic height fields derived from ADCP and SeaSoar data were derived by Pollard and Regier (1992) and show that, in the western half of the survey area, a warm mesoscale feature is moving to the north-northwest, while in the eastern half the flow is turning eastward at 28.4°N along the line of the front.

The IPV sections (Fig. 4-5) show that its values are very small, less than 0.2 PVU, in the mixed layer and below 200 m. In the seasonal thermocline, just below the base of the mixed layer, it reaches over 1.4 PVU. These values reflect the degree of density stratification in those areas, with the strongest stratification occurring just below the base of the mixed layer. The isopycnic surfaces deeper than 26.2 kg m^{-3} nearly follow q contours (compare Fig. 4-5 with Fig. 4-3), showing that q is near-constant on isopycnals at these depths. Where isopycnals outcrop into the mixed layer at the front, wind mixing decreases the stratification in the mixed layer and IPV gradients are intensified as the stratification increases just below the base of the mixed layer.

The greatest values of IPV lie in several elongated east-west tongues up to 100 km long, 10–30 km wide, and 20–40 m high. Comparison with plots of the isopycnic relative vorticity, IV (Fig. 4-6) shows that these high IPV bands correspond with regions of anomalous cyclonic vorticity. Between these lie tongues of minimum IPV, which are in regions of anti-cyclonic relative vorticity and weak stratification. Hence, the eddies act to

strain isopycnic potential vorticity variations into bands of alternately high and low values, which will induce vertical velocities along the front, in accord with frontal theory (Hoskins, *et al.*, 1985, Woods, 1985). Such ageostrophic vertical motions are induced as the fluid column adjusts to conserve IPV. A closed ageostrophic circulation results, in which water from the anticyclonic side of the front crosses toward the cyclonic side near the surface, with a deeper return flow. The details of the ageostrophic circulation depend critically on the initial distribution of potential vorticity. Most studies of frontal ageostrophic circulations have been made using computer models (e.g. Bleck, *et al.*, 1988). Real data are much more complex!

4.4.2 Correlation of properties on different surfaces

Figure 4-7 shows plots of potential temperature, salinity and IPV referenced to one surface for the data gridded on to isopycnic surfaces and on to isobaric surfaces. Isopycnal 25.70 kg m^{-3} was used as the reference layer to look at the correlation of properties with increasing density, and the 120 dbar surface was chosen as the reference layer to look at the correlation with increasing pressure. These surfaces were chosen because they lie at the base of the mixed layer over most of the survey region.

First, we consider the isopycnic correlation. The potential temperature (Fig. 4-7a) curves show very little scatter and are nearly linear, with a shift to lower values on denser surfaces. This indicates good correlation with density. However, the salinity (Fig. 4-7c) and IPV (Fig 4-7e) plots show much more scattered relationships, with very little correlation evident. This situation is quite different to that of the Vivaldi data (Chapter 3), and is probably as a result of the salinity maximum which occurs at the base of the mixed layer in the FASINEX data set.

Looking at the isobaric correlation, where good vertical coherence would be expected when geostrophic dynamics prevail, we see quite different results. The potential temperature (Fig. 4-7b) curves display a step in values across the front at all levels, but more pronounced within the mixed layer (40 and 80 dbar curves). As in the isopycnic case, some vertical coherence can be seen. However, the salinity (Fig. 4-7d) and IPV (Fig. 4-7f) curves show much greater scatter, and less vertical coherence, although the frontal step is still evident in salinity.

These plots are further indicators that the prevailing dynamics are quite different in the FASINEX survey and the Vivaldi survey. Vertical coherence is reduced in the FASINEX data partly as a result of the presence of eddies in the thermocline, and not deeper, which "interrupt" the background vertical coherence.

4.4.3. Comparison of PV with temperature and salinity measurements

Isopycnic comparison of PV with temperature and salinity

Isopycnic layers were studied and were centred on densities from 25.05 kg m^{-3} through to 26.45 kg m^{-3} in steps of 0.05 kg m^{-3}.

Isopycnic PV (IPV), as given by equation (2.1), was plotted against the potential temperature and salinity on each isopycnal. Plots from a selection of isopycnals are shown in the left hand columns of Figure 4-8 (potential temperature) and Figure 4-9 (salinity). IPV is calculable at very few locations on the shallowest surfaces, so these have not been plotted. On each isopycnal deeper than 25.15 kg m^{-3}, the potential temperature and salinity fall within very narrow ranges, and IPV lies within a range of 0 to 1.6 PVU. From 25.25 to about 25.70 kg m^{-3}, there appears to be a strong indication that high IPV corresponds with the larger temperatures and salinities on that isopycnal, although the plots show quite scattered data. The relationship between IPV and temperature appears to be linear with a positive gradient of order 5 PVU K^{-1}. For example, for the 25.70 kg m^{-3} surface, the gradient is 2.95 PVU K^{-1} with a correlation coefficient, r, of 0.68. This is quite different to the -0.31 PVU K^{-1} gradient of the FLW89 report and the –0.29 PVU K^{-1} gradient of the Vivaldi data. By 25.75 kg m^{-3} the warm end of the IPV-temperature plot is more scattered, while the cool end of the plot bends back on itself, i.e. there are two PV-θ relationship regimes. At this density, the IPV-salinity plot is also more scattered at higher salinities. On yet deeper isopycnals, the plots become more scattered and a cluster of data is seen, rather than a line. It can also be seen from Figure 4-8 and Figure 4-9 that deeper isopycnals include data from further north in the survey, while shallower isopycnals are only present in the south of the survey, outcropping towards the north.

IPV was compared with near-surface values of potential temperature and salinity. Data gathered at 30 m were used, because SeaSoar did not surface to avoid fouling by seaweed, and 30 m values should be similar to the surface values because the mixed layer extended to a greater depth than this over most of the survey region. However, these comparisons (right hand columns of Figures 4-8 and 4-9) did not indicate any functional relationship between IPV and surface temperature or salinity.

Isobaric comparison of PV with temperature and salinity

The IPV values, calculated according to equation (2.1), were interpolated onto pressure surfaces. The full PV was calculated on pressure surfaces according to equation (2.4) including the Froude term. Then IPV and PV were each plotted against potential temperature and salinity, for pressure levels from 30 dbar to 250 dbar, in steps of 10 dbar.

The results for IPV and PV were very similar, but IPV was calculable at more locations (the calculation involves fewer differencing operations so more data are retained at the top and bottom of each water column), so additional data were available and so IPV is used throughout this chapter. The results for IPV against potential temperature and salinity on five different pressure levels are shown in the left hand columns of Figures 4-10 and 4-11.

There are very few data shallower than 80 dbar. At 80 dbar, as can be seen in Figures 4-10 and 4-11, there are no relationships between IPV or PV and potential temperature or salinity. There is a two-temperature, two-salinity regime, reflecting that some of the water is north of a front, and some south of it, giving a jump in the temperatures and salinities measured. This structure, with no functional relationships, continues down to 120 dbar. Deeper than this, some positive-gradient relationship starts to become apparent in the data, particularly at lower temperatures and salinities. This is much clearer at 160 dbar where there is still significant scatter at the higher temperatures and salinities, but a quite tight line at the lower values. By 200 dbar, there are very few outliers from the main line of gradient 0.29 PVU K^{-1} (correlation coefficient, r = 0.92) for the potential temperature plots, and 4.48 PVU PSU^{-1} (r = 0.86) for salinity. These lines are very tightly correlated, especially for the IPV-θ case. This situation persists down to about 240 dbar, after which there are very few data (because SeaSoar did not go any deeper!). At depths of greater than 150 dbar, the pressure surfaces are quite coincident with isopycnals, and stratification is more uniform throughout the survey region, leading to a simpler IPV and PV structure.

At the "base of the mixed layer"

Given that the mixed layer should be vertically homogeneous by definition, then the temperature, salinity and density at the base of the mixed layer should be the same as at the sea-surface, at each geographical position. Water just below the mixed layer has the IPV value which was set when the water was subducted, and temperature just about the same as the mixed layer, if it is assumed that there is no sharp vertical discontinuity. Because of this, it was decided to compare IPV at the base of the mixed layer with the near-surface/mixed layer temperature, looking for a functional relationship. But how is the depth of the base of the mixed layer defined? Different definitions of mixed layer use temperature, salinity or density and lead to quite different results depending on the region (Lukas and Lindstrom, 1991). Three different definitions were tried on the FASINEX data, depending on the vertical structure of density or buoyancy frequency (N). Some definitions depend on a threshold value, which was varied and the "best" value selected empirically. Values of IPV at the "base of the mixed layer" were compared with near-surface values, for each of the following definitions of "base of the mixed layer".

The first method to identify the mixed layer depth was to look at the rate of change of density with depth down through each water column in the gridded survey region. Where this rate of change of density exceeds a selected threshold, that depth is considered to be at the base of the mixed layer, and is defined as the mixed layer depth. Several different values for the threshold were tried and the value and variability of the mixed layer depth was examined. With a threshold value of 0.1 kg m^{-3} density change between isobars, the mixed layer depth over most of the survey region was very shallow in the range of 10–20 metres. Thís depth was not very sensitive to the magnitude of the threshold value. Comparisons of IPV and absolute vorticity at the mixed layer depth with temperature and salinity at the mixed layer depth showed no relationship. Further comparisons of IPV and absolute vorticity at the mixed layer depth with temperature and salinity near the sea-surface also showed no relationship.

The second method used to identify the mixed layer depth was to look down each vertical water column and compare the density with the 30 metre (shallowest) value of density for that column. The mixed layer depth is selected as the depth where the difference from the surface value exceeds a certain threshold. Two different values for the threshold were used: 0.05 and 0.1 kg m^{-3}. The mixed layer depths for each threshold were in the ranges of 10–120 and 20–140 metres, respectively, and tended to be shallowest near the surface expression of the density front. Again, there was no evidence of a relationship between mixed layer depth IPV or absolute vorticity, and temperature or salinity at the mixed layer depth, or near-surface.

The third method for identifying the mixed layer depth was to look down through each water column, and pick out as the mixed layer depth the level where the square of the buoyancy frequency, N^2, achieved its maximum value. The mixed layer depth values found in this way were mostly in the range 100–150 metres. This method gave the result that corresponded most closely with the "by eye" estimate of MLD from plots of the density structure (Fig. 4-3). However, once again, no relationships were evident between mixed layer depth PV or absolute vorticity, and temperature or salinity at the mixed layer depth, or near-surface.

Relative vorticity - isopycnals and isobarics

Papers by Klein and Hua (Klein and Hua, 1988, Klein and Hua, 1990), and the PhD thesis by Claire Burren (Burren, 1993) indicate that in modelling studies SST variability has been linked to the subsurface temperature and relative vorticity fields, showing similar variability, although the sense of the relationship depended on the mixed layer deepening circumstances. Following this idea, relative vorticity, on the same isopycnals as before, was compared with isopycnic potential temperature, salinity, depth (pressure), and 5 dbar

potential temperature, salinity and their gradients. None showed any functional relationship whatsoever!

Similar results were also obtained looking at relative vorticity on pressure surfaces.

4.5 DISCUSSION

The FASINEX survey of an ocean front in the STCZ yielded a rich data set from which it was possible to dérive IPV and compare it with other ocean properties. This was one of the first such detailed studies to be carried out (Pollard, *et al.*, 1986). The surveyed front is believed to have been created as a result of Ekman frontogenesis acting on the background SST gradient and subsequent modulation by large-scale and mesoscale eddies.

Water mass analysis confirms that the front is the result of such confluence rather than the convergence of different water masses. Anti-cyclonic eddies were distinguishable, which strained the frontal water across to the north of the front, and trapped less stratified water in the thermocline. Salinity reached a maximum at the base of the mixed layer, where IPV also peaked.

These features of the survey show that the region is subject to quite different dynamics from the Vivaldi region. However, it should also be borne in mind that the FASINEX survey is a much finer-scale survey than Vivaldi, both spatially and temporally.

On isopycnals, the relationship between IPV and temperature and salinity is considerably weaker than in the Vivaldi region. The curves display more scatter, and the gradient is positive and an order of magnitude greater. There was no functional relationship between IPV and near-surface temperature or salinity.

On pressure surfaces, at depths of 200 dbar and beyond, strong correlation is found between PV and temperature or salinity, of the same order of magnitude as the Vivaldi isopycnic relationship, but still of a positive gradient. By this depth, there are very few ageostrophic motions, so the isopycnals and isobars are nearly parallel. Values of water properties at these depths are not the result of local effects, but are the result of air-sea interaction at remote locations at the time of subduction.

On the basis of these results, it appears that IPV and temperature or salinity are not related in a straightforward manner in the FASINEX region in late winter. Clearly, these results show that the relationship between IPV and other water mass properties depends on the history of the region and how the IPV, temperature and salinity were set. The results most likely vary throughout the heating/cooling seasons as subduction/entrainment occurs.

Fig. 4-1 30dbar potential temperature during FASINEX SeaSoar Run 2 with cruise tracks overlaid.

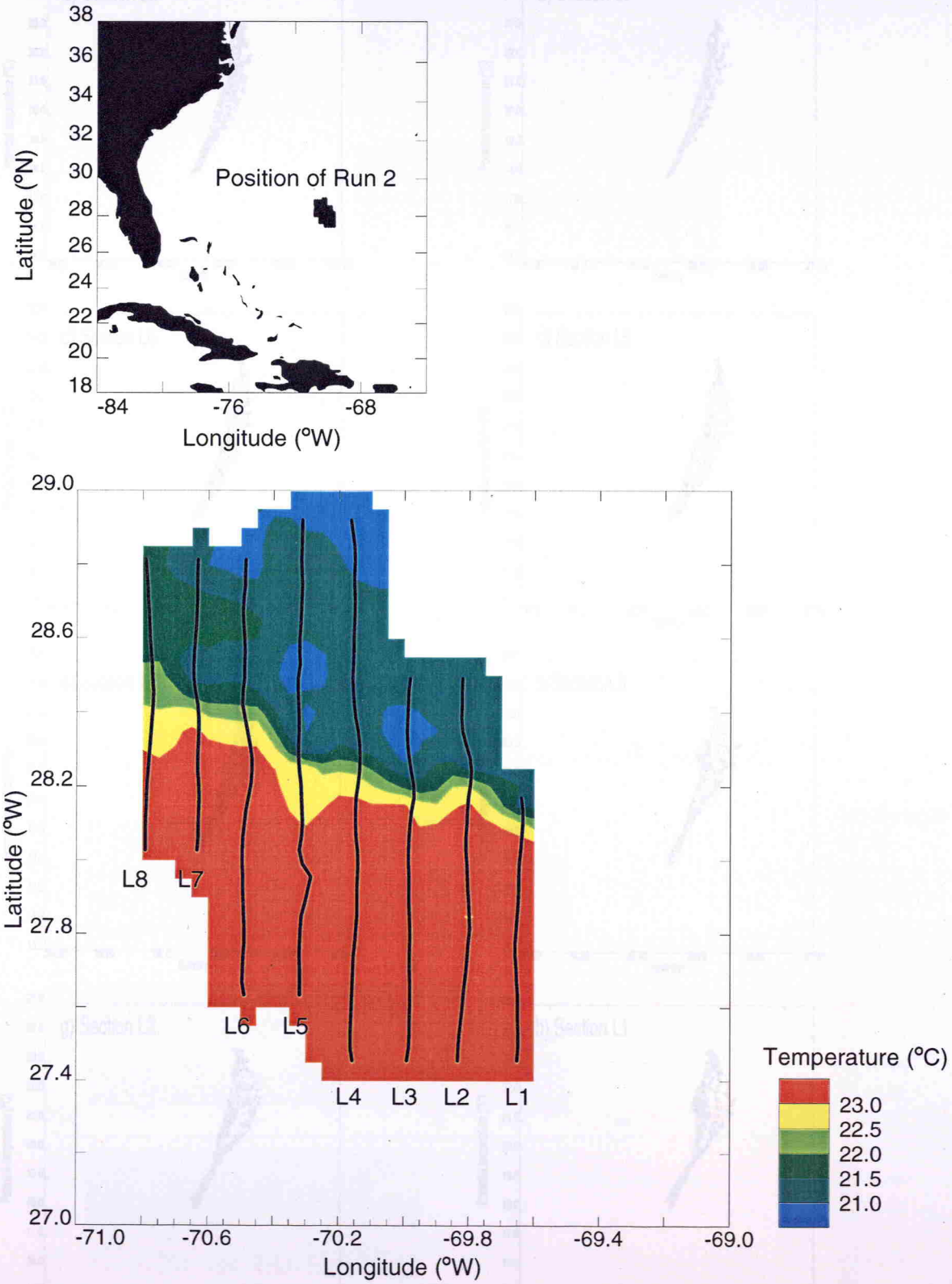

Fig. 4-2 Theta-S plots.

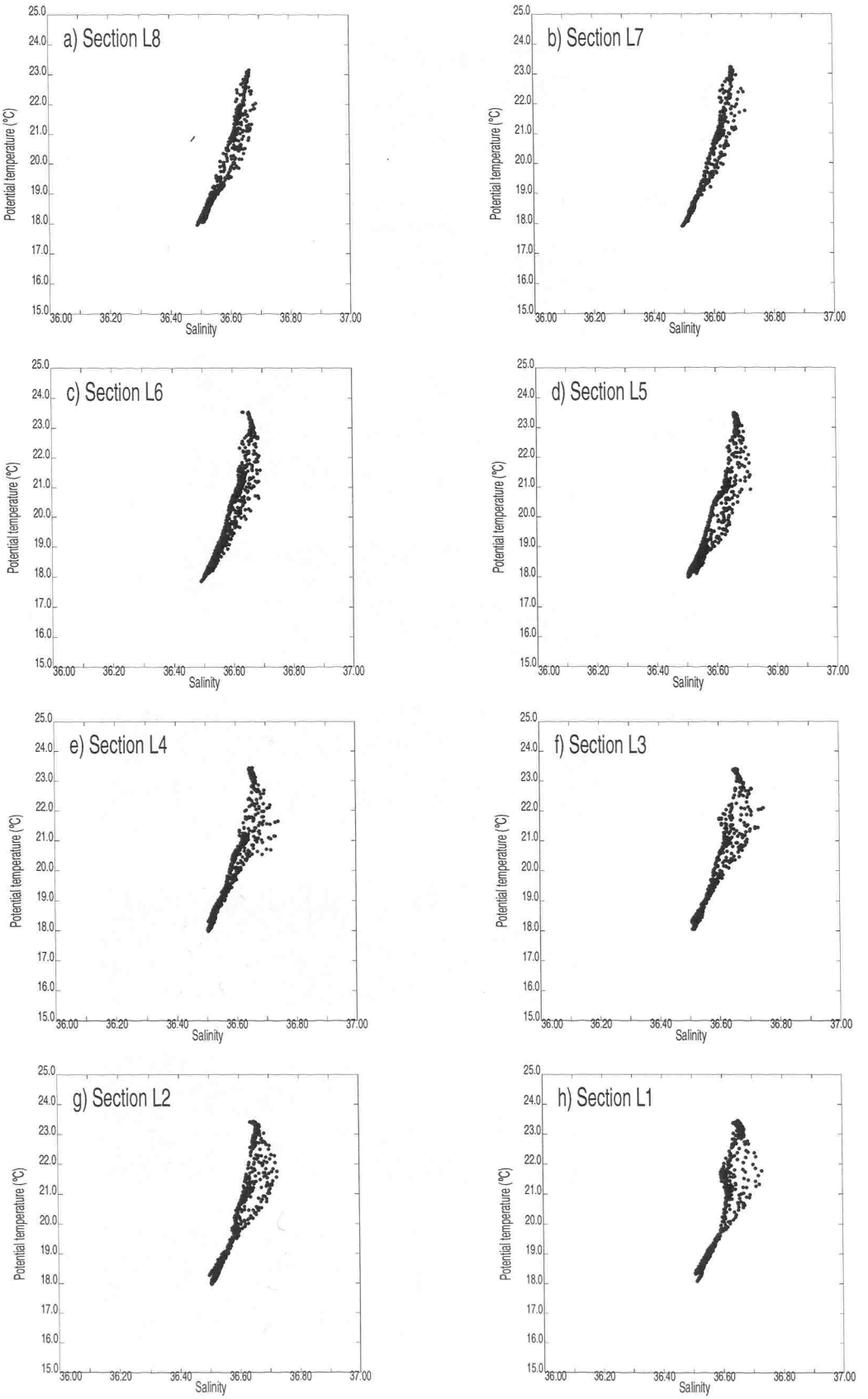

Fig. 4-3 Potential density vertical sections.

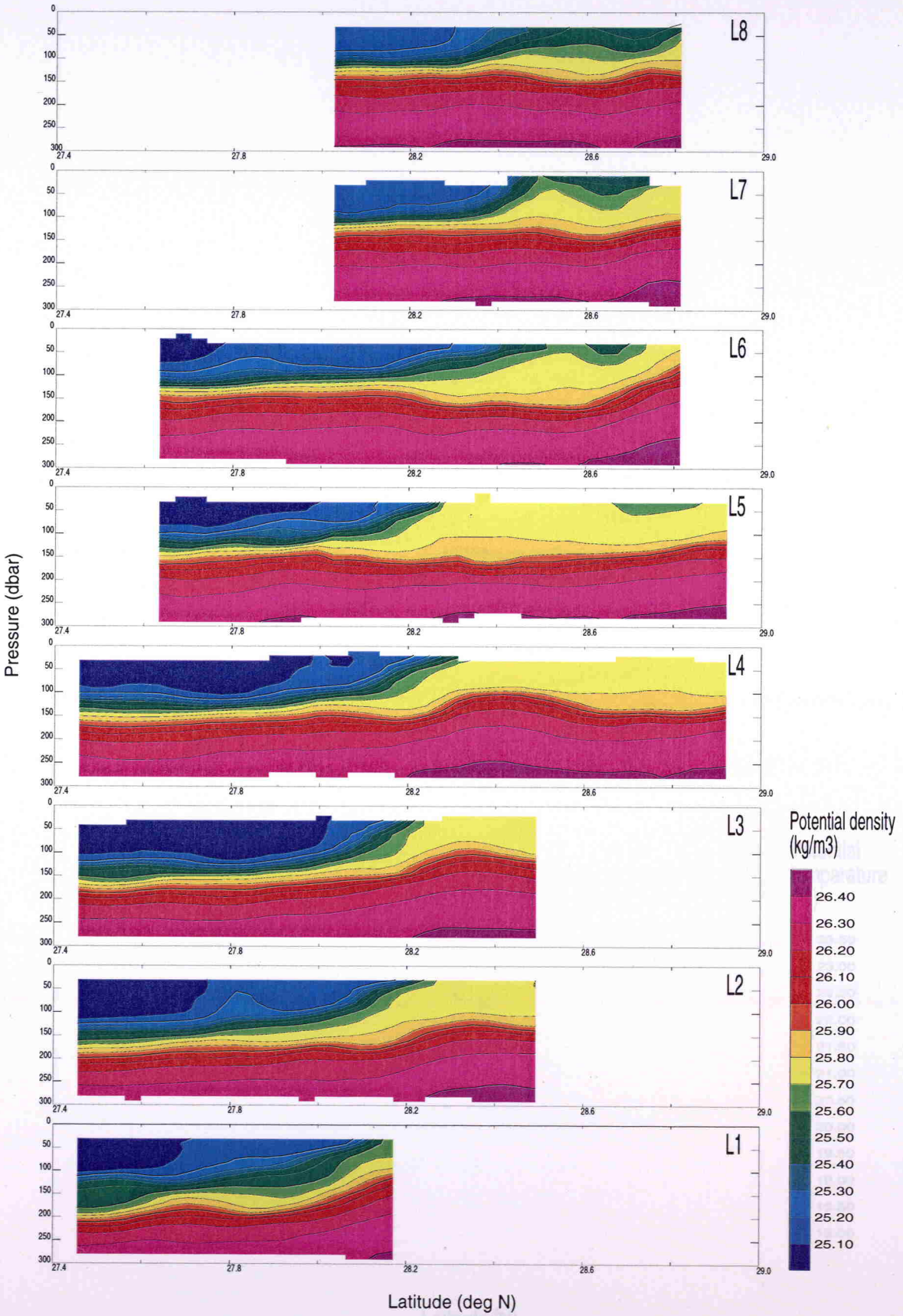

Fig. 4-4 Potential temperature vertical sections.

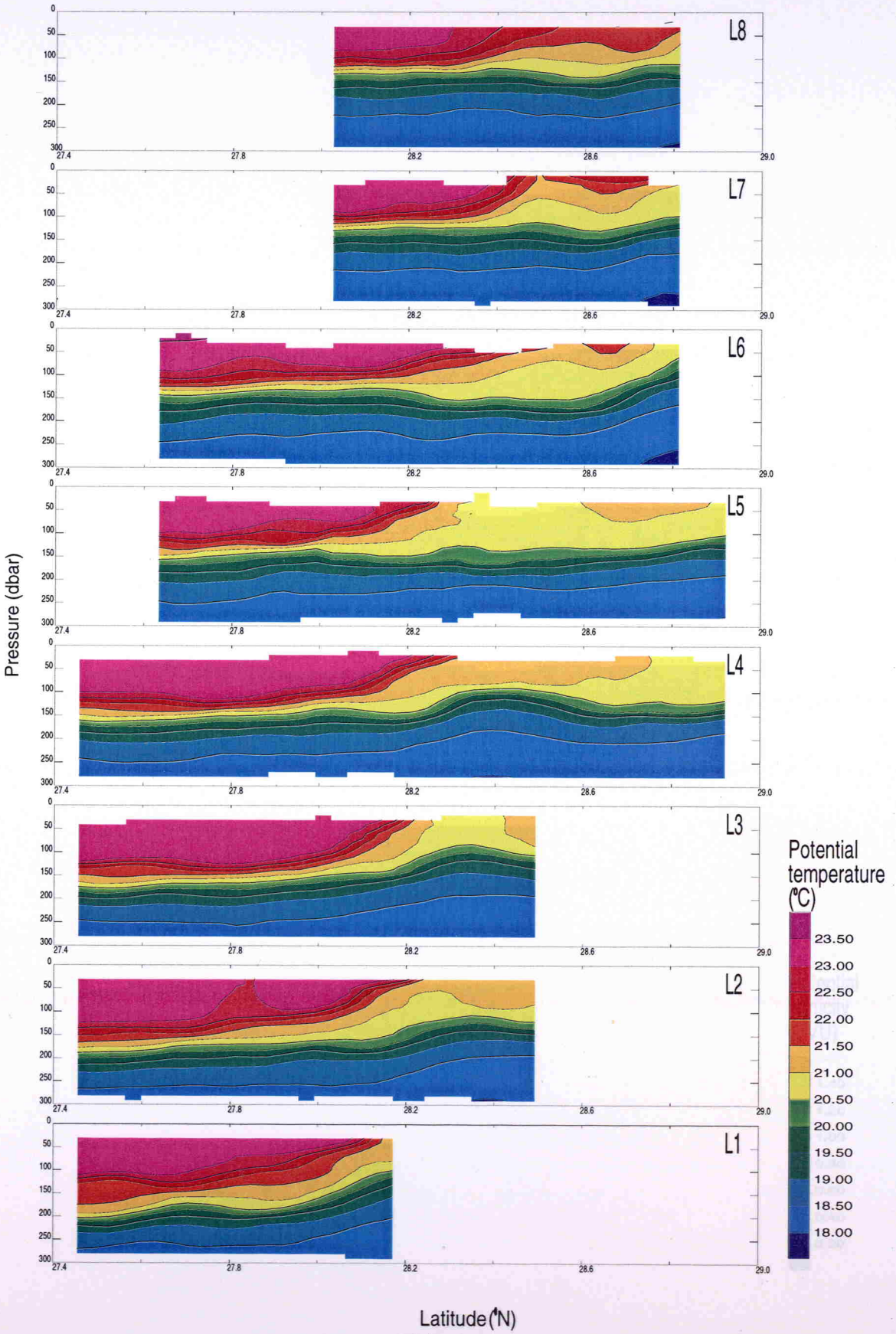

Fig. 4-5 Potential vorticity vertical sections.

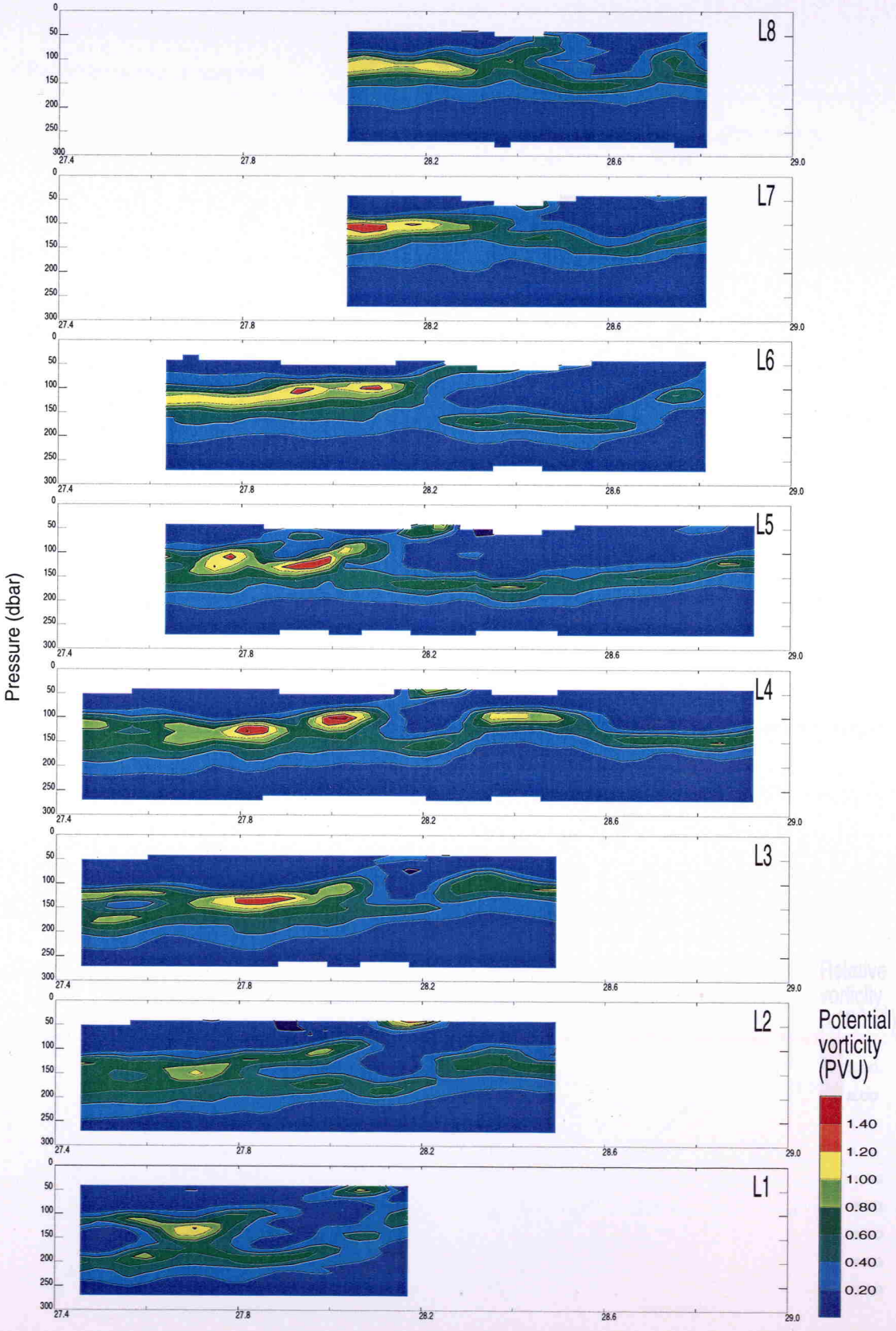

Fig. 4-6 Relative vorticity vertical sections.

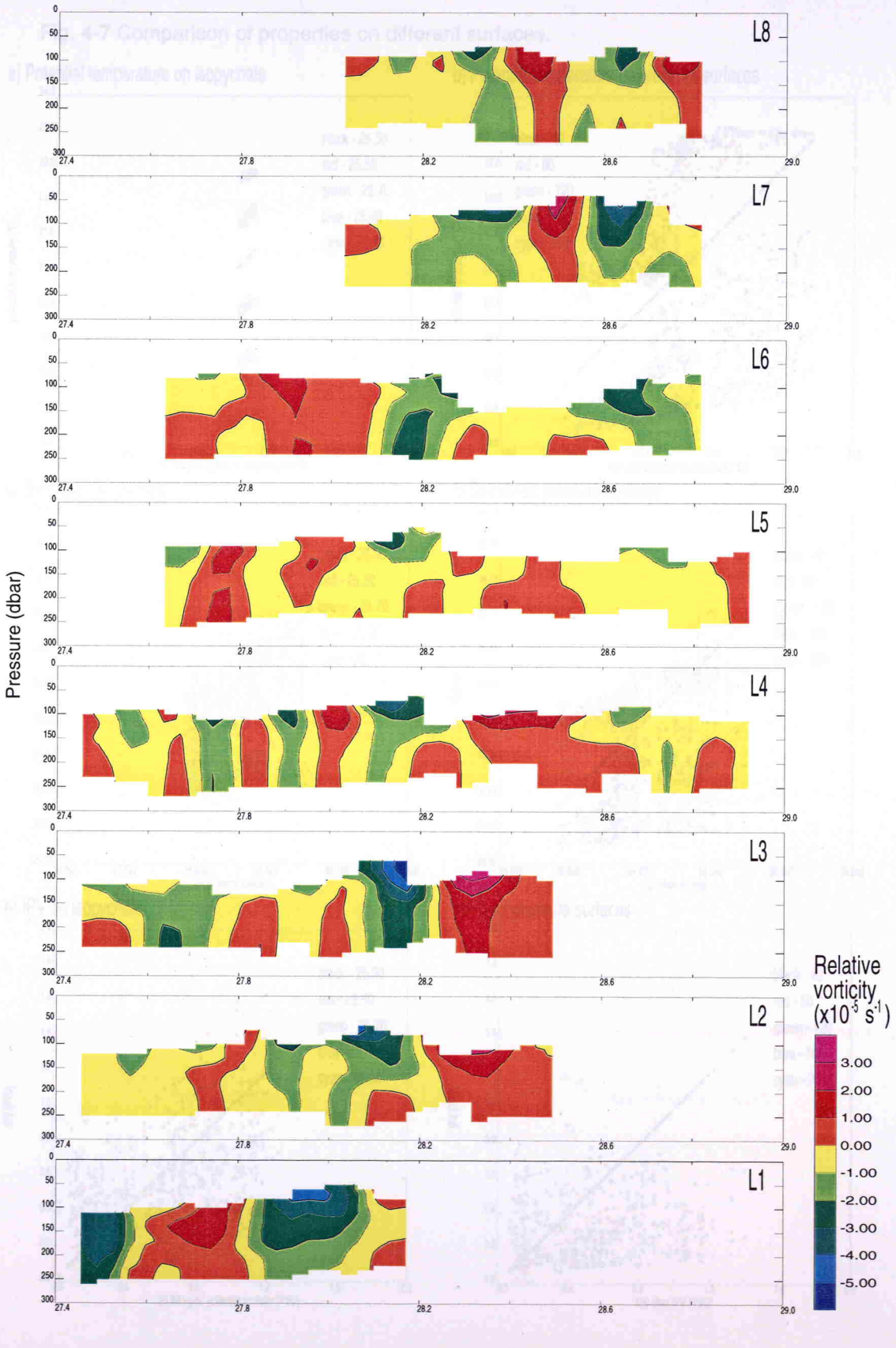

Fig. 4-7 Comparison of properties on different surfaces.

a) Potential temperature on isopycnals

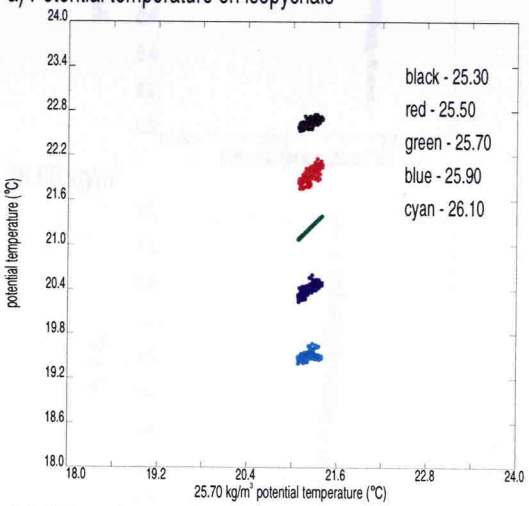

b) Potential temperature on pressure surfaces

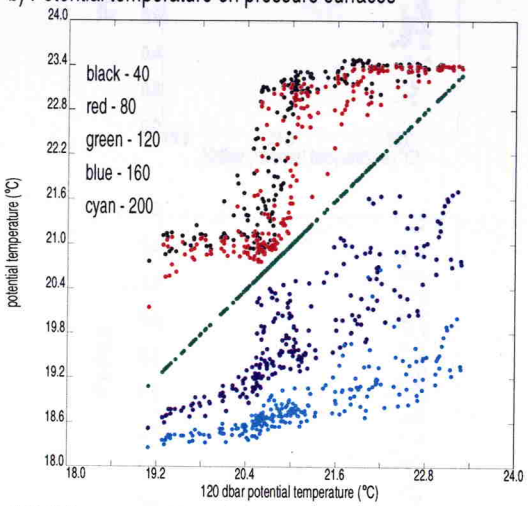

c) Salinity on isopycnals

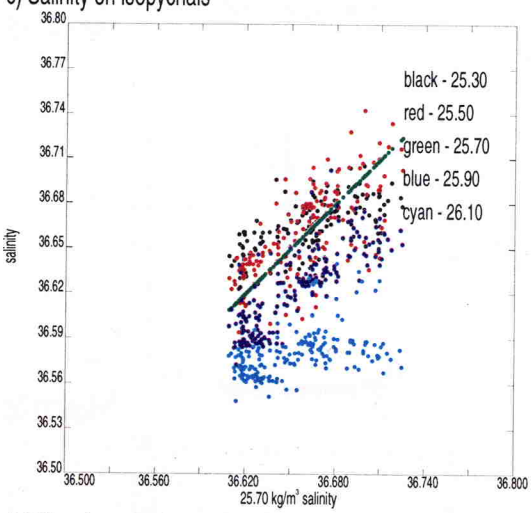

d) Salinity on pressure surfaces

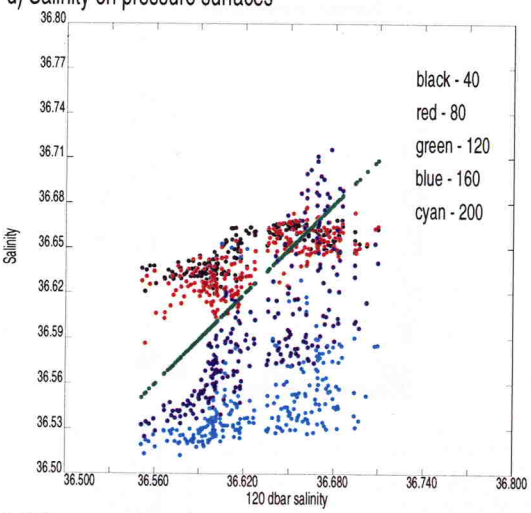

e) IPV on isopycnals

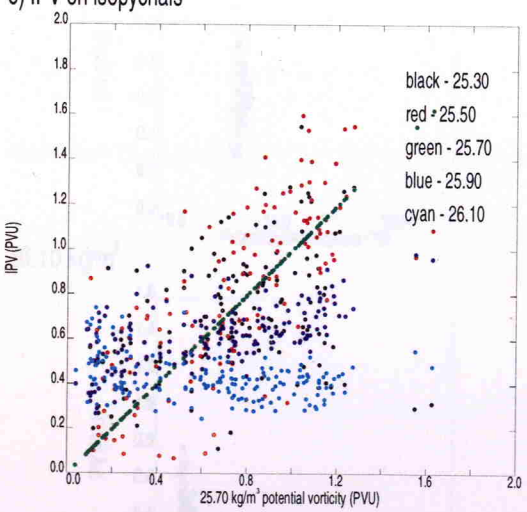

f) IPV on pressure surfaces

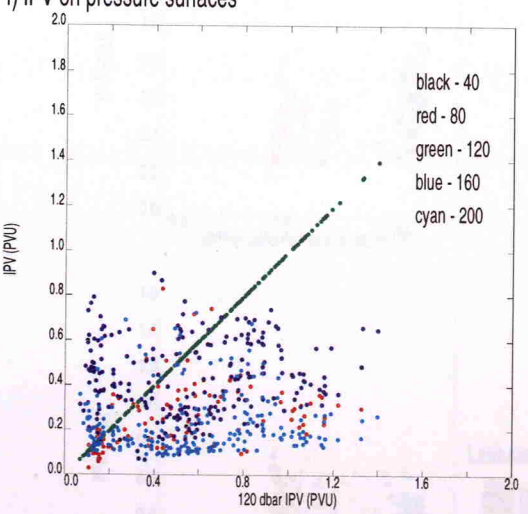

Fig. 4-8 Relationship between IPV and temperature on various isopycnals.

a) 25.30 kg/m^3

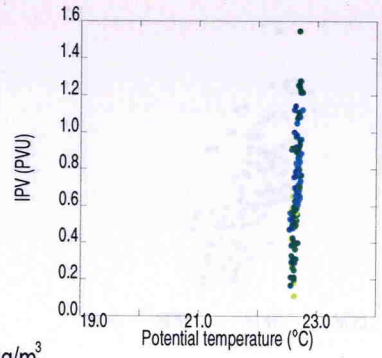

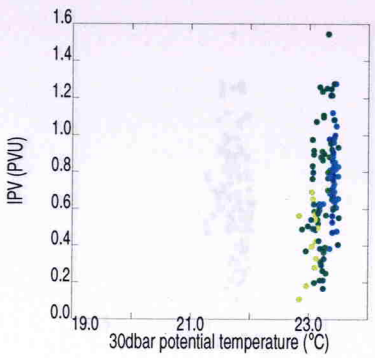

b) 25.50 kg/m^3

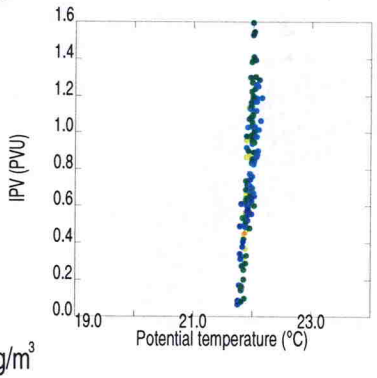

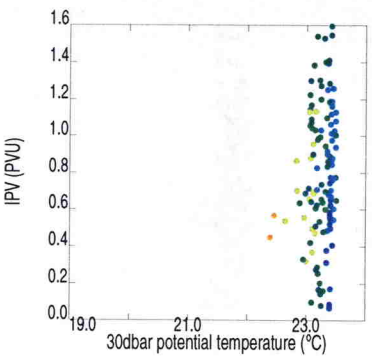

c) 25.70 kg/m^3

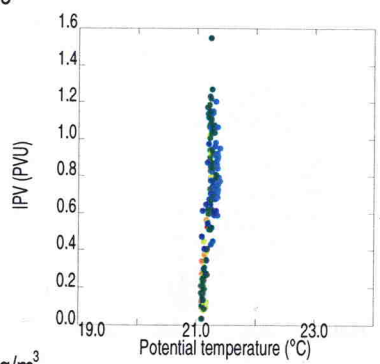

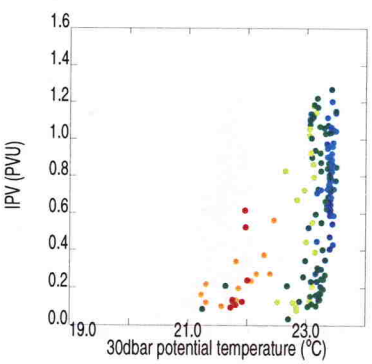

d) 25.90 kg/m^3

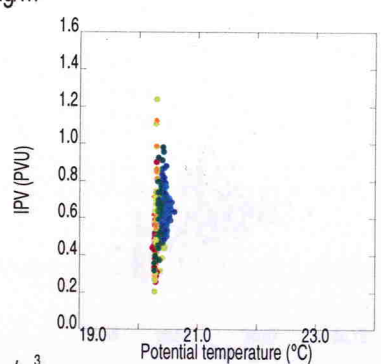

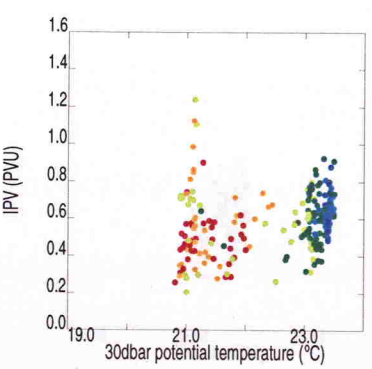

e) 26.10 kg/m^3

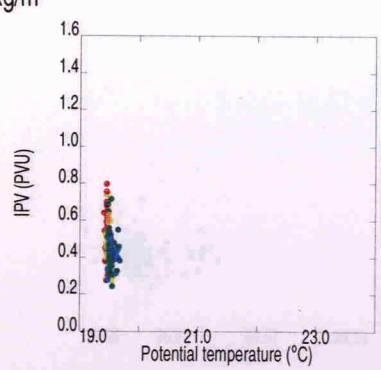

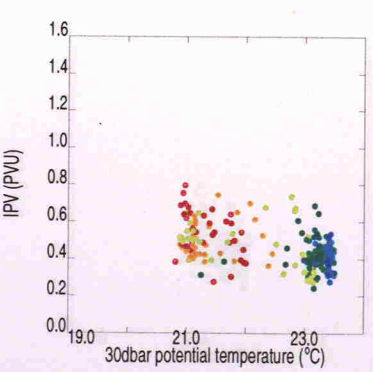

Fig. 4-9 Relationship between IPV and salinity on various isopycnals.

a) 25.30 kg/m^3

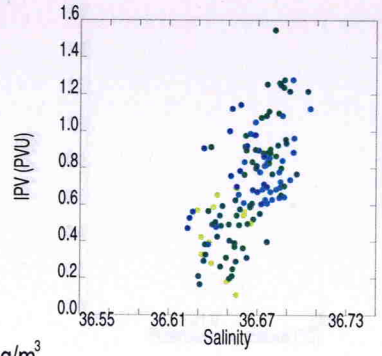

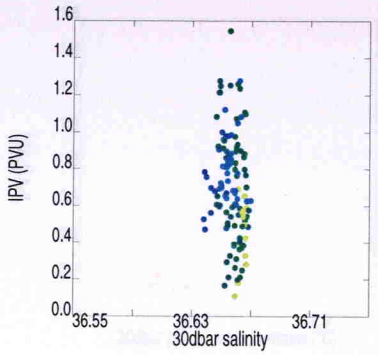

b) 25.50 kg/m^3

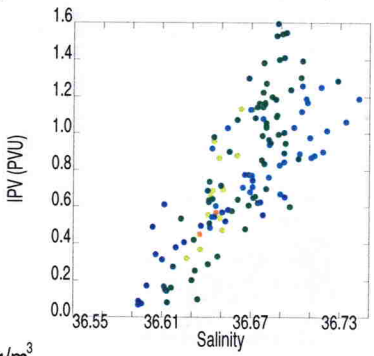

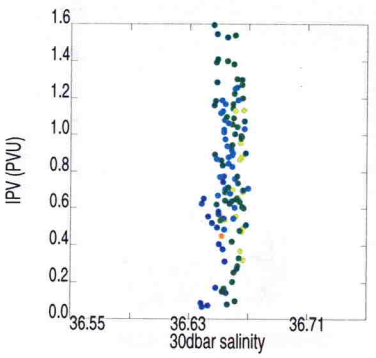

c) 25.70 kg/m^3

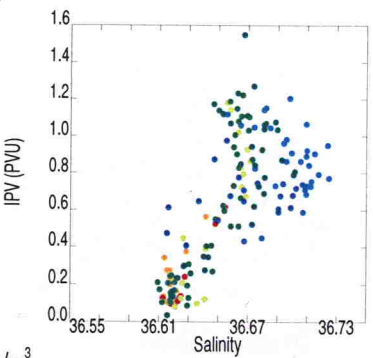

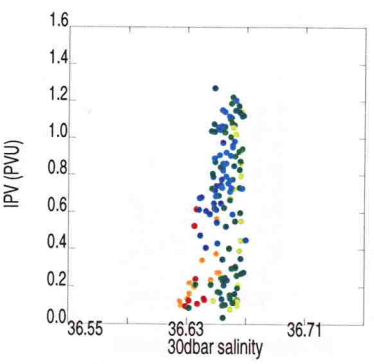

d) 25.90 kg/m^3

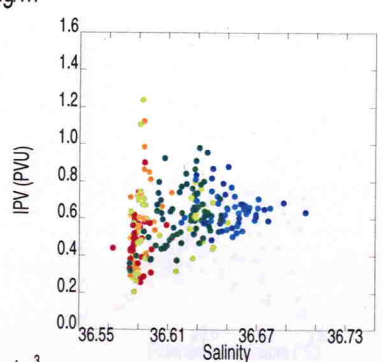

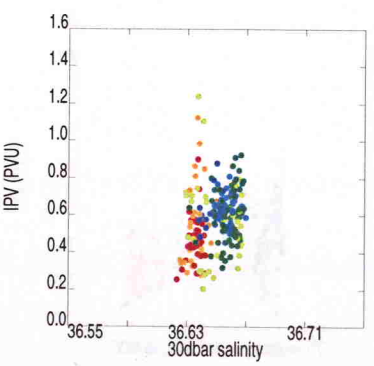

e) 26.10 kg/m^3

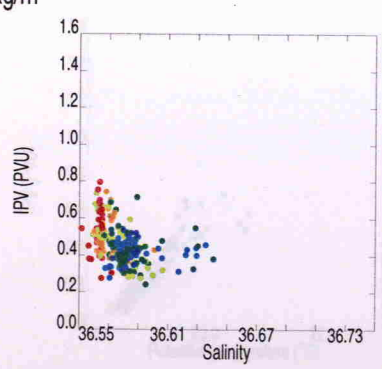

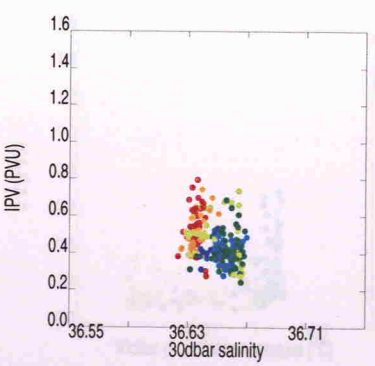

Fig. 4-10 Relationship between IPV and temperature on various pressure surfaces.

a) 40 dbar

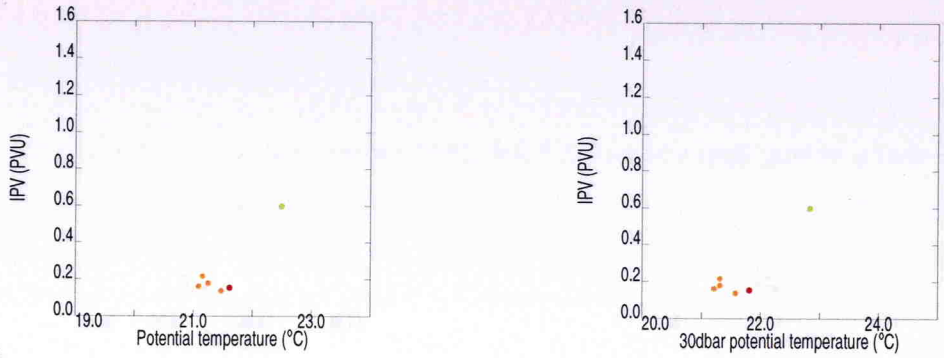

b) 80 dbar

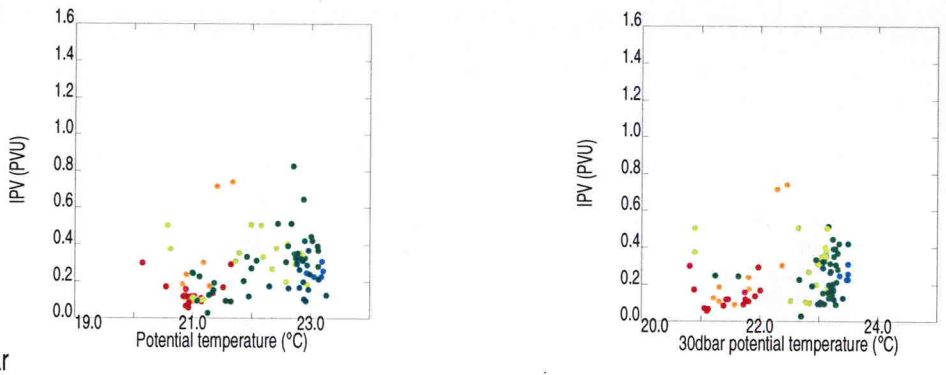

c) 120 dbar

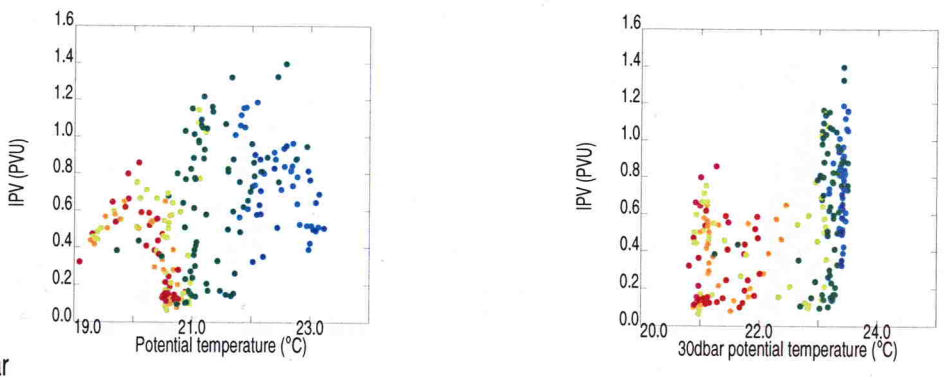

d) 160 dbar

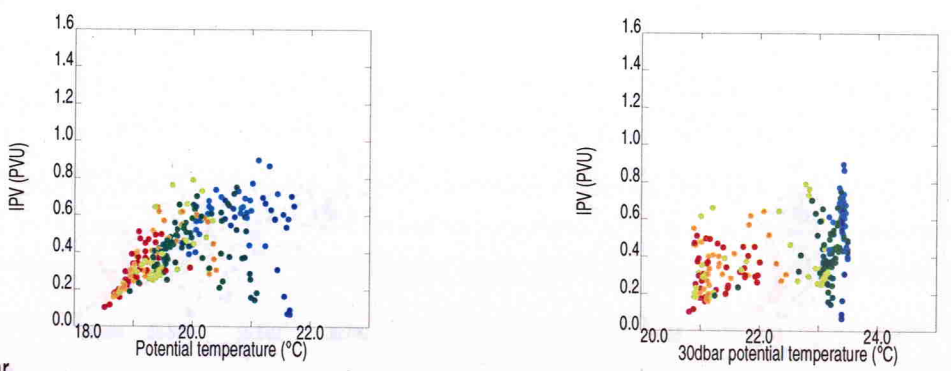

e) 200 dbar

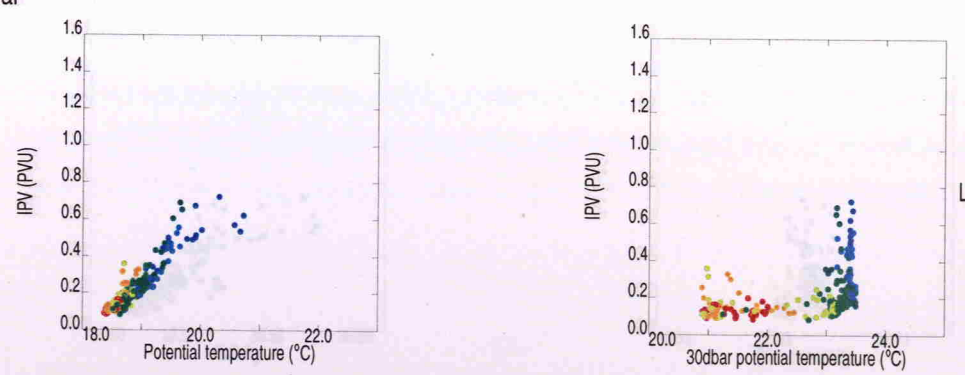

Fig. 4-11 Relationship between IPV and salinity on various pressure surfaces.

a) 40 dbar

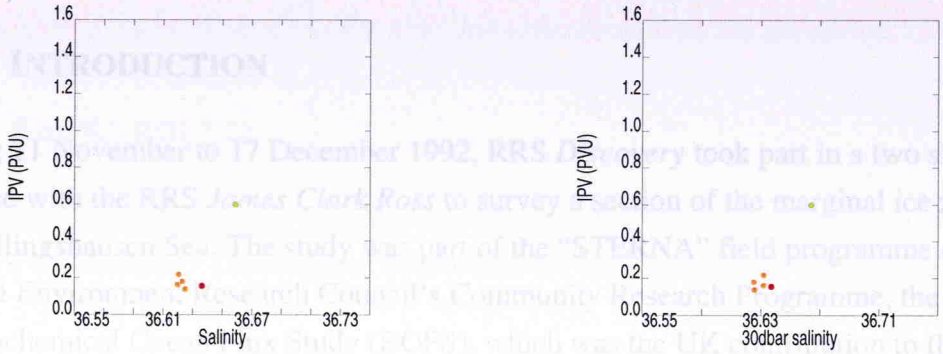

b) 80 dbar

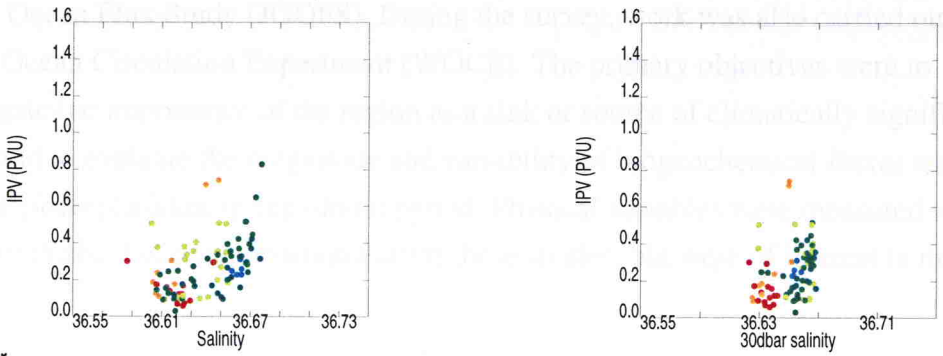

c) 120 dbar

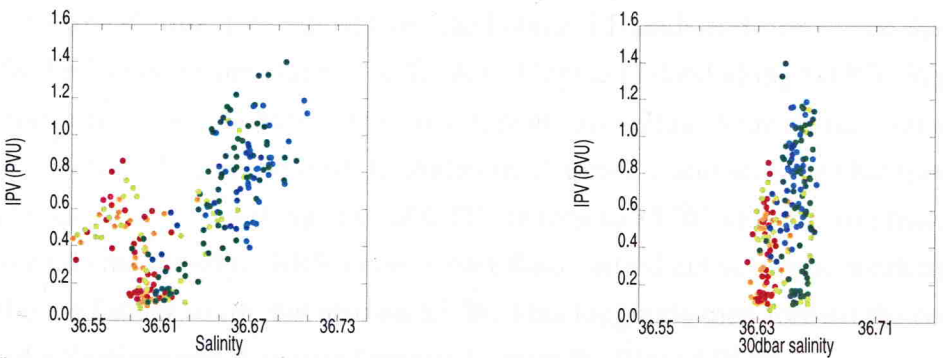

d) 160 dbar

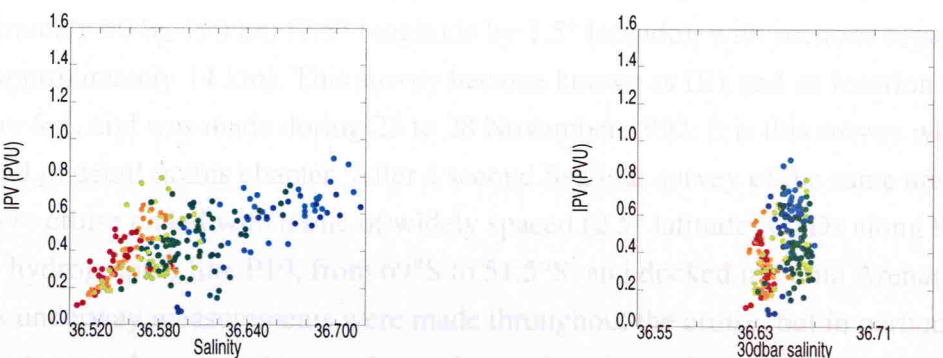

e) 200 dbar

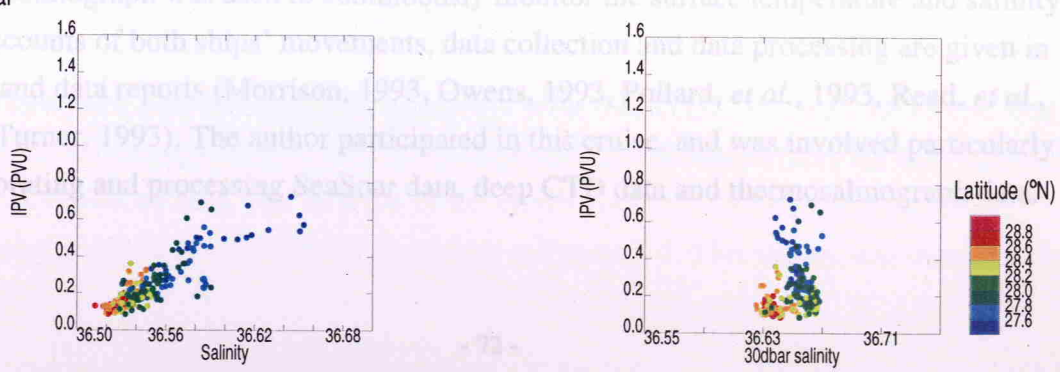

Chapter 5. STERNA '92

5.1 INTRODUCTION

During 11 November to 17 December 1992, RRS *Discovery* took part in a two ship exercise with the RRS *James Clark Ross* to survey a section of the marginal ice zone in the Bellingshausen Sea. The study was part of the "STERNA" field programme of the Natural Environment Research Council's Community Research Programme, the Biogeochemical Ocean Flux Study (BOFS), which was the UK contribution to the Joint Global Ocean Flux Study (JGOFS). During the survey, work was also carried out for the World Ocean Circulation Experiment (WOCE). The primary objectives were to investigate the importance of the region as a sink or source of climatically significant gases, and to evaluate the magnitude and variability of biogeochemical fluxes associated with the phytoplankton spring bloom period. Physical variables were measured to establish the background environment for these studies, but were of interest in their own right.

RRS *Discovery* (Cruise 198) sailed from the Falkland Islands and first towed the SeaSoar across Drake Passage from Burdwood Bank to Elephant Island along WOCE Repeat Hydrography line SR1 (Turner, 1993). Instrument calibrations were carried out among the South Shetland Islands west of the Antarctic Peninsula, and then the ship travelled westwards along 65°S, working several CTD stations to 85°W and then southwards down 85°W towards the ice edge. RRS *James Clark Ross* carried out scientific work near to and within the ice farther south, but also on 85°W. This longitude then formed the central section of a SeaSoar and Acoustic Doppler Current Profiler (ADCP) survey covering approximately 90 by 150 km (2.5° longitude by 1.5° latitude), with sections separated by 8 nm (approximately 14 km). This survey became known as IE1 and its location is shown in Figure 5-1, and was made during 23 to 28 November 1992. It is this survey which is examined in detail in this chapter. After a second SeaSoar survey of the same area, the *Discovery* cruise ended with a line of widely spaced (2.5° latitude) CTDs along 88°W, WOCE hydrographic line P19, from 69°S to 51.5°S, and docked in Punta Arenas, Chile. Various underway measurements were made throughout the cruise, but in particular a thermosalinograph was used to continuously monitor the surface temperature and salinity. Full accounts of both ships' movements, data collection and data processing are given in cruise and data reports (Morrison, 1993, Owens, 1993, Pollard, *et al.*, 1993, Read, *et al.*, 1993, Turner, 1993). The author participated in this cruise, and was involved particularly in calibrating and processing SeaSoar data, deep CTD data and thermosalinograph data.

In this chapter, an overview is presented of what is known about the background dynamics of the survey region. Then, the data gathered during the IE1 survey is studied, and the inter-relationships of the PV field and other properties are examined.

5.2 BACKGROUND

Read *et al.* (1995) considered the physical data from this cruise in the wider context of the extent of the Antarctic Circumpolar Current (ACC) in the south-east Pacific, between 145°W and the Drake Passage at 55°W. In that paper, we concentrated on data from the deep CTDs and surface temperature and salinity. The study was extended westwards by using historical data from the *Eltanin* surveys of 1962-1972 (Gordon, 1967) and model output from the Fine Resolution Antarctic Model (FRAM) (Webb, *et al.*, 1991). The Antarctic circumpolar current is taken to refer to the eastward water flow round the Southern Ocean, not including the eastward flowing southern parts of the subtropical gyres.

The literature generally identifies three major fronts within the ACC, namely the Subantarctic Front (SAF), the Polar Front (PF) and the Continental Water Boundary (CWB). Some researchers have also observed another front in the Drake Passage, believed to be a second southern branch of the PF. This was identified in the Sterna 85°W CTD line (Read, *et al.*, 1995), and has been labelled the southern Polar Front (SPF). The SPF was also identified on the 85°W section, and the 88°W section, with an associated baroclinic geostrophic transport of 15Sv (1Sv = 10^6 m^3 s^{-1}). The ice conditions before and during the survey are described by Turner and Owens (1995), and establish that the SPF was present at 85°W, 67°S before the ice cover retreated.

The SPF was also traced in the *Eltanin* data (Gordon, 1967) and in atlases of observations (Olbers, *et al.*, 1993) and model data (Webb, *et al.*, 1991), suggesting the front is a permanent feature and extends as far west as 145°W. Strong currents are associated with the PF and SPF (Read, *et al.*, 1995), so care must be taken in identifying these fronts by temperature and/or salinity features. It is better to use the slope of isopycnals, or where sharp changes occur in the deep θ-S properties, indicating a water mass transition.

5.3 DATA COLLECTION AND PROCESSING

As stated before, two detailed SeaSoar surveys were conducted, although the second was only partially completed due to the loss of the SeaSoar. The results from the first survey, IE1, are considered here. The location of the survey, and the labelling used for the meridional sections (W through C) are shown in Figure 5-1. This survey was intended to

consist of eight legs, with parallel north-south tracks surrounding the 85°W section and crossing the SPF as already detected by the CTD survey. Kinks at the southern ends of Legs Y, Z and B (Fig. 5-1) show where course was altered to avoid icebergs. During the survey, the wind freshened from the north-west, and so time was lost on the north-going legs and leg Z was ended further south than intended. By the time Leg C was begun, the southward course could not be maintained, and the ship hove to into wind at the southern end of Leg C. The data collected during this survey are described in this section.

5.3.1. Three-dimensional density field

Pressure, temperature and conductivity were sampled by a Neil Brown Mark 3 CTD towed behind the ship mounted on a SeaSoar profiling between the surface and 400 m, completing a full cycle in less than 4 km. After initial reduction and editing, the 1 second averaged SeaSoar data (temperature, salinity and oxygen measurements) were interpolated in the horizontal to intervals of 3 km with a search radius of 4.5 km. Thus horizontally adjacent grid points are not independent, but the 9 km averaging is necessary to smooth the internal wave field. In the vertical these data were interpolated in two ways:

a) over pressure: 5–453 dbar, at 8 dbar intervals

b) over σ_0: 26.8–27.8 kg m^{-3} at 0.02 intervals.

The data were then interpolated on to a regular latitude/longitude grid with latitude intervals of 0.0268° (approximately 3 km) and longitude intervals of 0.3333°. As with the FASINEX data, the averaged STERNA data are sufficiently smooth to allow calculation of dynamic height and hence geostrophic shear between adjacent columns.

5.3.2. Three-dimensional velocity field

The 30 second ADCP data (consisting of amplitude, percent goodness, absolute and relative east and north velocities) were vertically interpolated from 13 to 517 metres in 8 metre intervals, and averaged to 3 km horizontal resolution.

The ADCP data are contaminated by near-surface inertial oscillations and tides, and so cannot be used directly in the calculation of relative vorticity. A more accurate velocity field was calculated in the same way as with the FASINEX data (see Section 4.3.2), by using the ADCP data to provide a level of known velocity from which to integrate the geostrophic velocity. The chosen level for the STERNA data was 149 m, at which depth the ADCP velocity was believed to be free of ageostrophic contamination.

5.3.3. Vorticity

For the STERNA data, the full isopycnic IPV, q, in which the relative vorticity is calculated on density surfaces rather than pressure surfaces, was calculated according to equation (2.1). For analyses on isobaric surfaces, the IPV is interpolated along with the other properties to give the quantity called PV here.

5.4 RESULTS

5.4.1. Water mass analysis

This survey was carried out where it was because a significant front was found at about 67.5°S, transporting 15 Sv (1 Sv = 10^6 m^3 s^{-1}) of water eastwards (Read, *et al.*, 1995), and high productivity seemed to be associated with the boundary of the front rather than the ice edge (Pollard, *et al.*, 1995). Here we consider the water mass properties of the survey area. Plots of potential temperature against salinity ("θ-S plots") are shown for each leg of the survey in Figure 5-2. The front is the boundary between two distinct water masses, which shows up as distinct curves in the θ-S plots. Intermediate θ/S relationships occur because of mixing across the boundary. The curves also highlight the near-surface salinity minimum. It should be noted (particularly by those more familiar with mid-latitude θ-S plots) that the lowest temperature waters lie in the mixed layer, where the ice has recently melted, and becomes warmer with depth. The temperature and salinity minima and other features can be seen more clearly in the sectional plots of each leg, W through C. Plots of potential density (Fig. 5-3), potential temperature (Fig. 5-4), salinity (Fig. 5-5), chlorophyll *a* (Fig. 5-6), oxygen (not shown), PV (Fig. 5-7), and relative vorticity (Fig. 5-8), were examined.

The features of these section plots are very similar, indicating that there is little zonal variability. Isopycnals rise towards the south, and stratification increases below the mixed layer, which reaches to about 60 metres across the whole region (Fig. 5-3). The 27.2 kg m^{-3} isopycnal outcrops at about 67.5°S in the west, and slightly further north towards the east. There is a small lower density patch near the surface at 67°S. The salinity plots (Fig. 5-5) have similar structure to the density plots, unlike the potential temperature sections (Fig. 5-4), which show a minimum just below the mixed layer. Clearly the salinity, rather than the temperature, sets the density in this region, where the sea is close to its freezing point. The 33.85 isohaline outcrops at about 67.5°S, like the 27.2 kg m^{-3} isopycnal. The potential temperature sections show a mixed layer to about 100 metres depth, and a very shallow gradient horizontal front at about 67°S, with changes of less than 0.2°C across it at the surface. This mixed layer is deeper than the

density/salinity mixed layer. There is an indication to the north of the front that the density/salinity mixed layer was deeper previously, because of a region of reduced stratification between 80 and 170 metres depth. This is believed to be the remains of the winter mixed layer. The most rapid changes are seen between 120 and 220 metres depth and there is very little structure below 250 metres. Chlorophyll *a* measurements (Fig. 5-6) are negligible below 80 metres, but show a high at 67.5°S and 30 metres depth, decreasing gradually to the south, but decreasing sharply to a negligible value to the north. This band is south of the density/salinity front. Oxygen measurements (not shown) were well correlated with the density and salinity plots, reaching a maximum just below the surface and decreasing with depth.

The IPV sections (Fig. 5-7) show that it is negligible within the mixed layer, from near surface down to about 70 metres. Values as high as 0.8 PVU occur immediately below this in a thin layer (~10 metres), reaching its highest value in a band around 67.4°S, but also high around 67°S. The IPV gradually decreases to negligible values from 85 to 250 metres. Below 250 metres, it decreases towards zero. The relative vorticity structure (Fig. 5-8) again shows little zonal structure, while meridionally alternating bands of cyclonic (positive) and anti-cyclonic (negative) relative vorticity are evident. North of about 67.1°S the relative vorticity is predominantly cyclonic, and again south of about 67.6°S. Between these latitudes, mainly anticyclonic relative vorticity occurs, with just two or three narrow streaks of cyclonic relative vorticity.

In the paper Pollard *et al.* (1995) we considered these θ-S plots, section plots and other biological data from the cruise all together. We concluded that while the front is a boundary between different water masses, there is also strong advection into the area from the west. This advection varies across the front leading to strengthening of cross-frontal gradients of properties. For example, a band of high chlorophyll, which is confined to the mixed layer, extends across the region just to the south of the main frontal jet. These chlorophyll levels could only be achieved by advection into the area rather than growth at that location. The frontal zone itself is very narrow (70-80 km longitudinally), and outside of this jet only weak velocities are recorded.

5.4.2. Correlation of properties on different surfaces

Figure 5-9 contains plots of potential temperature, salinity and PV referenced to one surface for the data gridded on to isopycnic and isobaric surfaces. Isopycnal 27.40 kg m^{-3} was used as the reference layer to look at the coherence of properties with increasing density, and 101 dbar was used as the reference layer for the coherence of properties with

increasing pressure. These reference surfaces were chosen because they lie just below the mixed layer over most of the survey region.

Coherence was examined between potential temperature on isopycnals from 27.1 kg m^{-3} through to 27.6 kg m^{-3} at 0.1 kg m^{-3} intervals and each 0.02 kg m^{-3} "thick" (Fig. 5-9a). Generally the coherence was good, although somewhat non-linear. Between pressure surfaces, the coherence seems worse (Fig. 5-9b). However, on closer examination it is seen that between the 101 dbar and 149 dbar levels, there is a sharp discontinuity. Below and above these levels, the potential temperatures on surfaces are coherent with each other, but not across this boundary. This level corresponds approximately with the depth of the base of the temperature mixed layer, as seen in section plots (Fig. 5-4). The salinity mixed layer only reaches to about 80 dbar depth. This discontinuity indicates that the mixed layer is decoupled from the thermocline.

Salinity coherence (Fig. 5-9c&d) is very much like that of potential temperature, although the decoupling between 101 dbar and 149 dbar is less well-defined.

IPV is not at all coherent between isopycnals nor pressure surfaces (Fig. 5-9e&f). This probably reflects that IPV values are very low except within a narrow band just below the mixed layer where stratification is enhanced.

Having looked at the coherence of these data on isopycnals of 0.02 kg m^{-3} thickness, the data were averaged down to fewer density levels which were each 0.1 kg m^{-3} thick, and the coherence of properties on different density levels was re-examined. Mostly the results were very similar to those for the 0.02 kg m^{-3} thick surfaces, with the potential temperature and PV results being almost identical. The differences which occurred were that in the salinity comparisons, the 27.2 kg m^{-3} surface values spanned a wider range, corresponding to the low salinity points of the 27.3 kg m^{-3} surface, and vertical coherence between these surfaces was improved. These small differences can be explained as follows. The 27.2 kg m^{-3} and 27.3 kg m^{-3} surfaces straddle the base of the mixed layer, and so have the largest changes of values here, and so averaging across these surfaces may be unreliable. As the thicker and thinner surfaces showed such small differences, the 0.02 kg m^{-3} thick surfaces were used throughout the rest of the analysis.

5.4.3. Comparison of PV with temperature, salinity and chlorophyll *a* measurements

Isopycnic comparison of PV with temperature, salinity and chlorophyll a

Each comparison was carried out on five isopycnals between 27.2 kg m^{-3} and 27.6 kg m^{-3} at 0.1 kg m^{-3} intervals, with each isopycnal of 0.02 kg m^{-3} "thickness".

Comparing IPV with potential temperature on these isopycnals (Fig. 5-10), the deepest isopycnals studied, 27.6 kg m^{-3} and 27.5 kg m^{-3}, show near linear, negative gradient relationships in which the gradient is -0.08 and –0.11 PVU K^{-1}, respectively, with correlation coefficients of -0.87 and -0.97, respectively. For all isopycnals most data are clustered at the high and low temperature values, with a few forming a line between the two clusters. These clusters correspond with the distinct water masses on either side of the front, and the points between are due to some mixing across the front. On the shallower 27.4 isopycnal, the low temperature end of the curve bends down to lower IPV values. The latitudes of these data points indicate that they correspond to the part of the 27.4 kg m^{-3} isopycnal which outcrops into the mixed layer. The higher temperature end of this curve also contains some low PV values. In contrast, the 27.3 kg m^{-3} curve consists of a very steep, near vertical line of points at the lowest temperatures with a large PV range. These data originate in the mixed layer. At the highest temperatures, there is another cluster of fairly low (for this isopycnal) PV. Between these clusters, the data follow a smooth gentle curve of negative gradient at top temperatures and positive gradient at cooler temperatures. In the case of the 27.2 kg m^{-3} surface which only exists in the northern half of the survey region, the data are well dispersed, showing no functional relationship.

The right hand column of Figure 5-10 also shows IPV on these same isopycnals compared with the 5 dbar temperature. The 27.6 kg m^{-3} surface results have a single near-spherical cluster of data centred at about -1.45°C and 0.1 PVU, with a diameter of about 0.45°C and 0.1 PVU. Above this, on the 27.5 kg m^{-3} surface, at low temperatures corresponding with those of the 27.6 kg m^{-3} surface, the IPV appears to be independent of the temperature in the range 0.1 to 0.45 PVU. Above a particular temperature, around –1.2°C, the IPV is fairly constant at around 0.1 PVU. This gives the plot an L-shape. For the 27.4 kg m^{-3} surface, the curve is very similar, though the transition temperature is lower, around -1.35°C. The 27.3 kg m^{-3} surface data again maps out an L-shape, but the range of IPV values at the lowest temperatures is now much higher, in the range 0.2 to 0.8 PVU. The 27.2 kg m^{-3} surface data show there is no functional relationship between IPV and 5 dbar potential temperature, with IPV ranging from 0 to 0.8 PVU. All the

surfaces display high and low temperature clusters with few data in-between, except for the 27.6 kg m^{-3} surface with its single cluster.

IPV against salinity comparisons (Fig. 5-11) are very like those for temperature. Near-surface and on the 27.6 kg m^{-3} isopycnal, the range of salinity values is very small. The gradients (and correlation coefficients, r) of the 27.6 and 27.5 kg m^{-3} plots are -1.36 PVU PSU^{-1} (0.84) and -1.45 PVU PSU^{-1} (0.97), respectively.

The IPV fields were also compared with 5 dbar salinity (right hand column of Fig. 5-11). These show that on the 27.6 kg m^{-3} surface with its small range of IPV values and larger range of near-surface salinity, there is a reasonably well-correlated line of small positive gradient. On the 27.5 kg m^{-3} surface, the line bends back on itself at lower IPV, at the low salinities, making an elongated tilted C-shape. By 27.4, it is clearer that there are two salinity regimes, within each of which IPV is not related to salinity, and a few data points lie in-between. This is the case for the 27.3 kg m^{-3} surface also, and on the 27.2 kg m^{-3} surface the saltier cluster is almost absent, showing no functional relationship.

Chlorophyll *a* measurements were also available from this survey. These were also compared with IPV values to see if any functional relationship were evident (Fig. 5-12). These plots show that no such relationship was found, for chlorophyll *a* was negligible on all but the 27.2 and 27.3 kg m^{-3} isopycnals. Within these layers, and south of the front, the IPV varied greatly but without apparent correlation with the chlorophyll value. No relationship was to be found with 5 dbar chlorophyll *a* either.

In summary, these comparisons show that there are generally two clusters of data corresponding to conditions on either side of the density front, and sometimes a few points lie between. Functional relationships between potential temperature or salinity and IPV were observed only on isopycnals lying deep in the pycnocline. No relationship was observed between IPV and chlorophyll *a*.

Isobaric comparison of PV with temperature, salinity and chlorophyll a

No notable relationship was observed between PV and temperature (Fig. 5-13), salinity (Fig. 5-14) or chlorophyll *a* (Fig. 5-15) on pressure surfaces. On most isobars, there exist two clusters corresponding with each side of the front and a few points falling in between where mixing has occurred. In the cases of temperature and salinity, deeper than about 150 dbar, the data appear to form a negative-gradient line (Fig. 5-13e & Fig. 5-14e). At these depths, isobars are more coincident with isopycnals as ageostrophic near-surface motions become less significant.

No coherent relationship was observed with near-surface values either. And once again, there was no functional relationship between PV and chlorophyll *a*.

At the "base of the mixed layer"

In the same way as with the FASINEX data, IPV at the base of the mixed layer was compared with the near-surface/mixed layer temperature and salinity, using three different definitions of mixed layer depth based on either density or buoyancy frequency, N.

The first method is to find the difference between density value at each level and the previous level. When this difference exceeds a selected threshold that level is defined as the base of the mixed layer for that water column. This is repeated for each column of water at each point on the latitude-longitude grid. This method was implemented both looking from the surface downwards, and from the bottom upwards, which do not always give the same results. Comparison of IPV at these "base of mixed layer" depths with near-surface parameters showed no functional relationships.

The second method used is to look down each vertical water column, comparing the density with the 5 dbar value of density for that column. When the difference from the surface value exceeds a certain threshold, that level is selected as the mixed layer depth. Several different values for the threshold were tried: 0.01, 0.05, 0.1, 0.2, 0.3, 0.4 kg m^{-3}. The "base of mixed layer" IPV fields, by each of these threshold values, were compared with near-surface parameters and show no functional relationships, except possibly when the threshold was 0.3 kg m^{-3}. In this case, the comparison with 5 dbar potential temperature shows a quite coherent line, with approximate gradient of -0.25 PVU K^{-1}, and correlation coefficient (r) of 0.72. However, it is felt that this is coincidental rather than causal, as the relationship does not hold with larger threshold values. The two temperature clusters regime, with a few data falling between is evident here as it was in the isopycnic and isobaric comparisons.

The third method is to look down through each column, and pick out as the mixed layer depth the level where the buoyancy frequency (N^2) achieves its maximum value. However, once again, the "base of the mixed layer" IPV compared with the near-surface parameters shows no functional relationships.

Relative vorticity - isopycnals and isobarics

As explained in Chapter 4, in certain modelling studies SST variability has been linked to the subsurface temperature and relative vorticity fields, showing similar variability, although the sense of the relationship depended on the mixed layer deepening circumstances. Relative vorticity, on the same isopycnals as before, was compared with isopycnic potential temperature, salinity, depth (pressure), and 5 dbar potential temperature, salinity and their gradients. As with the FASINEX data, no functional relationships were found at all. In general, the familiar two temperature clusters occurred, corresponding with the water masses on either side of the front. This was also the case for data on pressure surfaces.

5.5 DISCUSSION

The STERNA survey IE1 of a front in the Antarctic Circumpolar Current produced a high-quality set of hydrographic, current and biological data. The survey was carried out during the austral spring, less than a week after the retreat of the ice edge. The front, which marked the boundary between two distinct water masses, was dominated by changes in salinity rather than temperature. Evidence was presented of some mixing across the front, but the major transport was along the front, with differential advection from the west leading to strengthened cross-front gradients.

Very good correlation was observed between IPV and potential temperature, and between IPV and salinity, on isopycnals which lie deep in the pycnocline. These isopycnals are located below both the salinity/density mixed layer and the temperature mixed layer which indicates the greater depth of the winter mixed layer. The relationship gradients observed on these isopycnals were of the same order of magnitude, and of the same sign as those of the Vivaldi data. On shallower isopycnals, the data separated into two clusters showing the sharpness of the front and how little mixing was occurring across-front at these depths. No relationship was seen between near-surface tracer values and IPV, nor was any relationship demonstrated between IPV and chlorophyll *a*. On isobaric surfaces, the data again split into two clusters according to water mass type. These results are much more similar to the Vivaldi data set than the FASINEX data.

As in the Vivaldi data, the results varied with the averaging of data on to thicker isopycnals, and this may be due to amplification of changes as isopycnals rise from depth, through the pycnocline and into the mixed layer, as well as the reduction of noise.

It is somewhat disappointing that no correlation was observed between chlorophyll *a* and IPV, as one might expect that variations in local flows (leading to variations in IPV) might affect the growth and demise of phytoplankton. Had such a correlation existed it

could have been exploited by using satellite ocean colour measurements. Alas, from these results this seems as unlikely as the possibility of using SST measurements to derive PV fields.

The STERNA IE1 front occurred as the result of differential advection from the west of waters of two different water masses. This is similar to the Vivaldi situation of the confluence of different water masses from the subtropic and subpolar gyres, coupled with springtime restratification. The FASINEX front occurred in a late winter situation in a region of convergence of water due to the wind field, with no water mass change across the front. The STERNA results add to the impression gained in earlier chapters that the relationship between IPV and tracer fields depends on the dynamics of the front and its history. These matters will be considered in greater detail in the next chapter.

Fig. 5-1 5 dbar potential temperature during STERNA SeaSoar Run IE1 with cruise tracks overlaid.

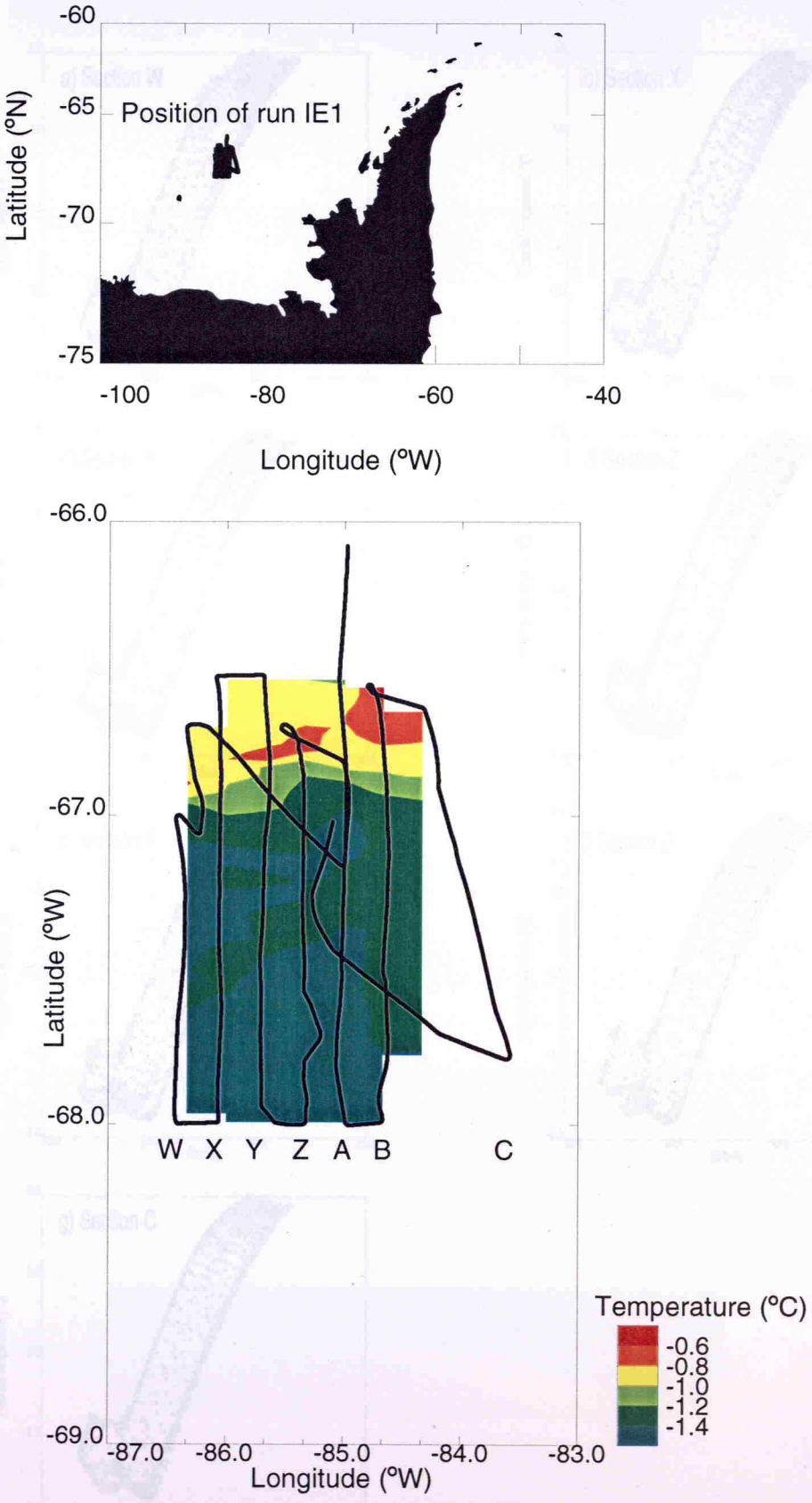

Fig. 5-2 Theta-S plots.

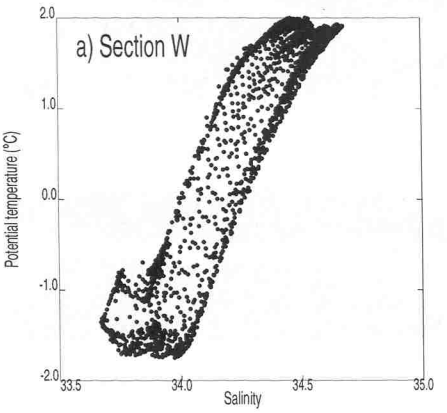

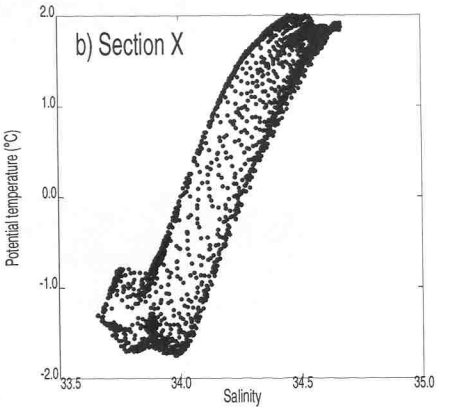

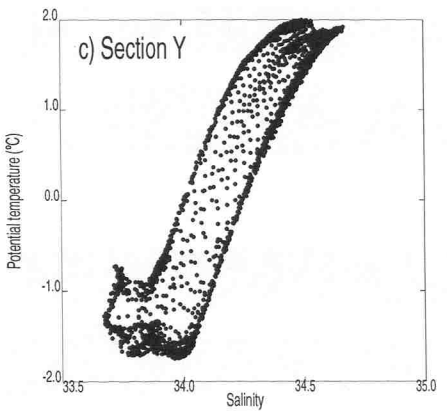

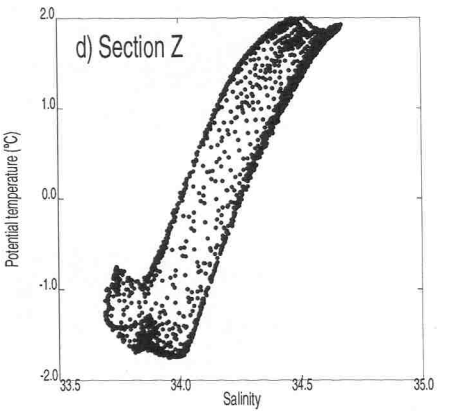

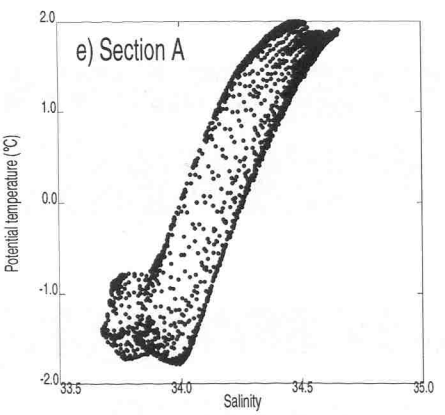

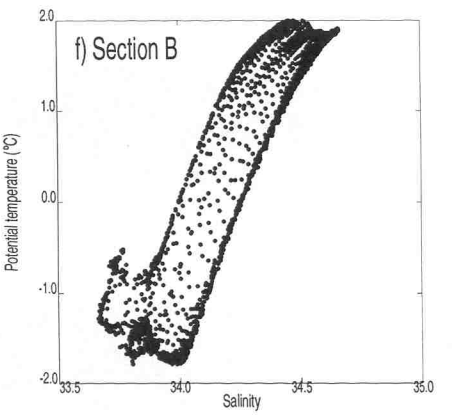

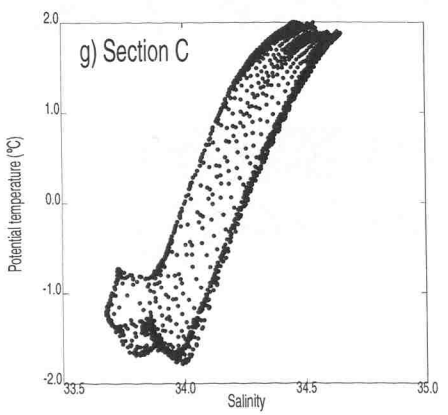

Fig. 5-3 Potential density vertical sections.

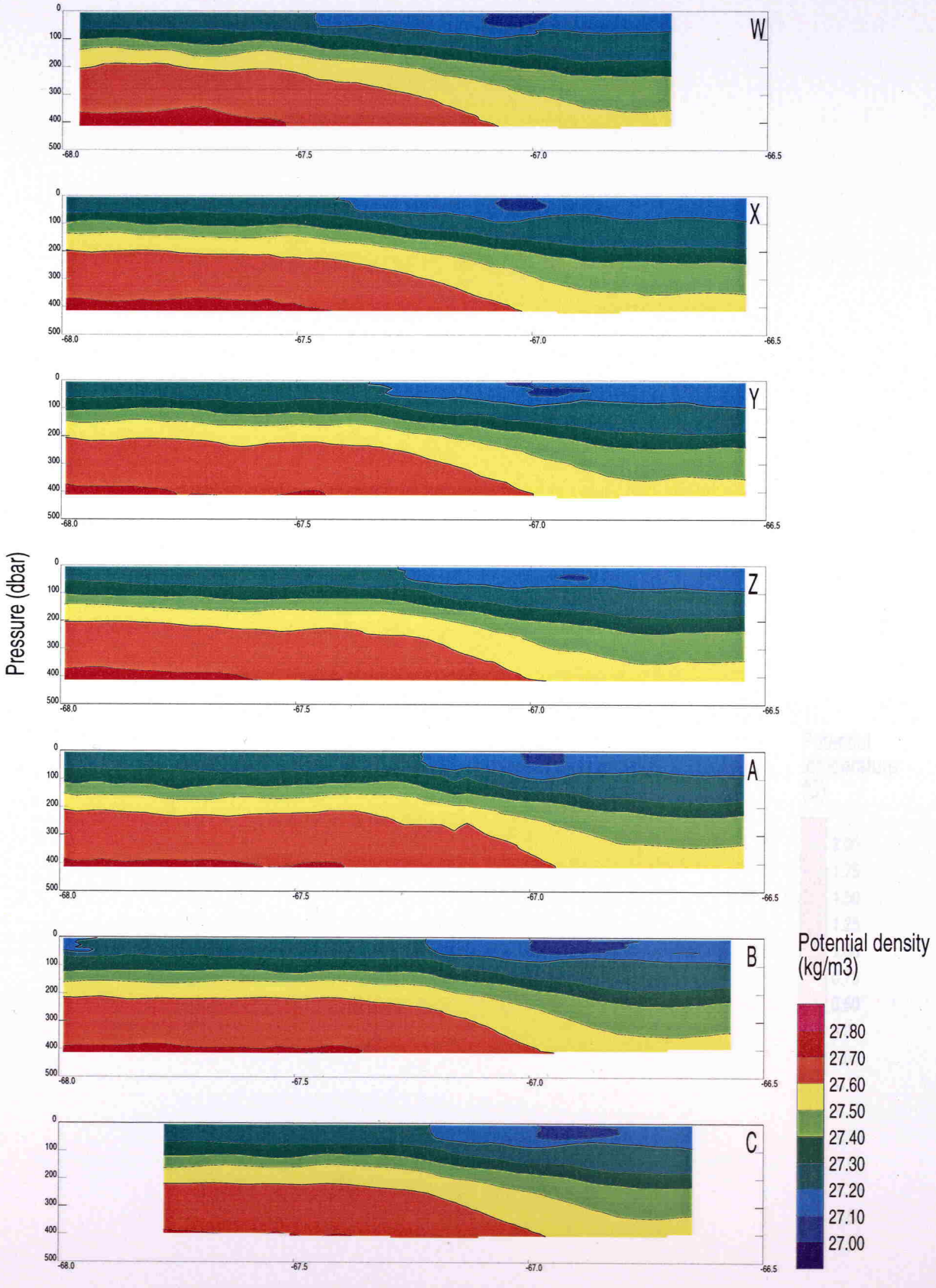

Fig. 5-4 Potential temperature vertical sections.

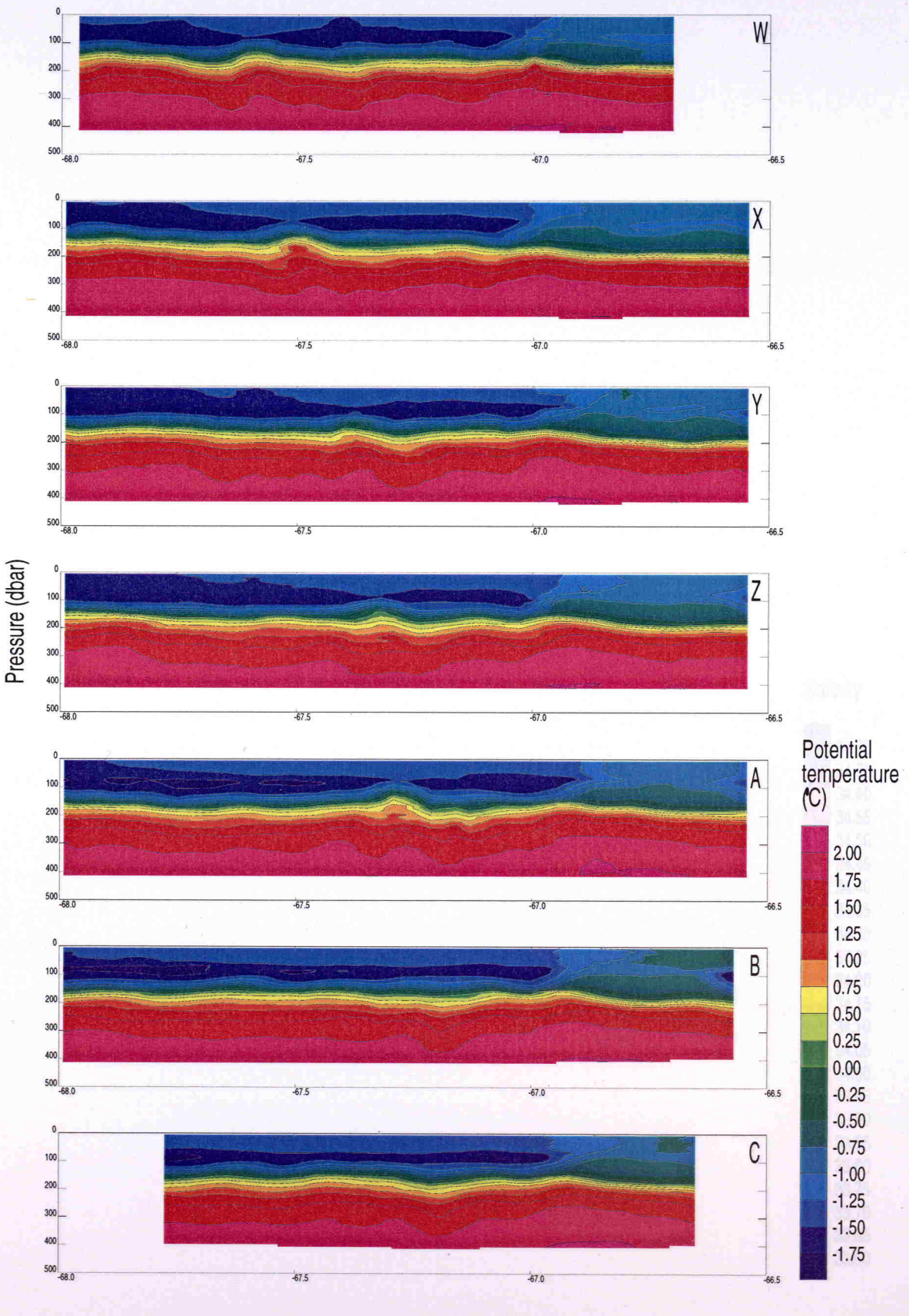

Fig. 5-5 Salinity vertical sections.

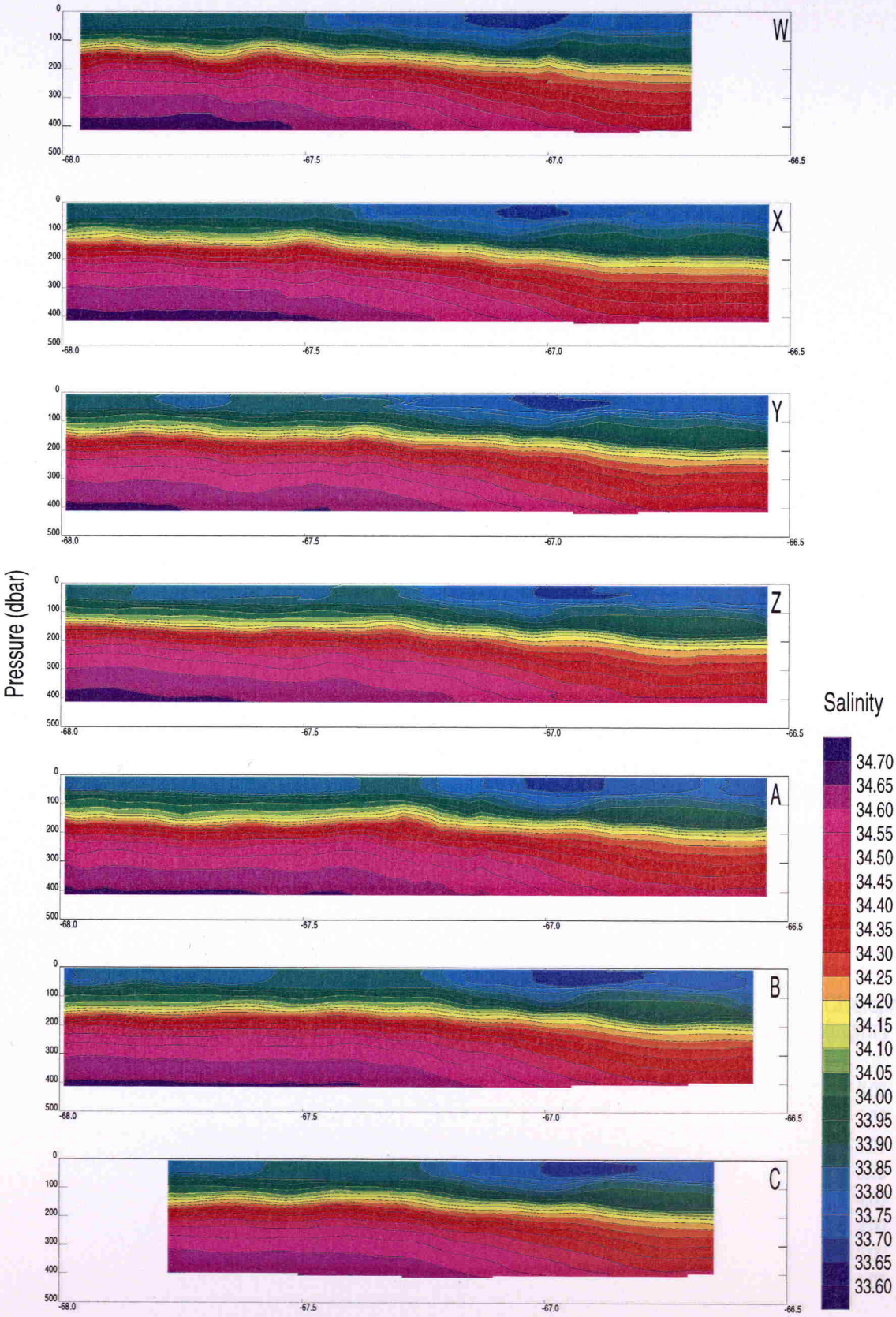

Fig. 5-6 Chlorophyll vertical sections.

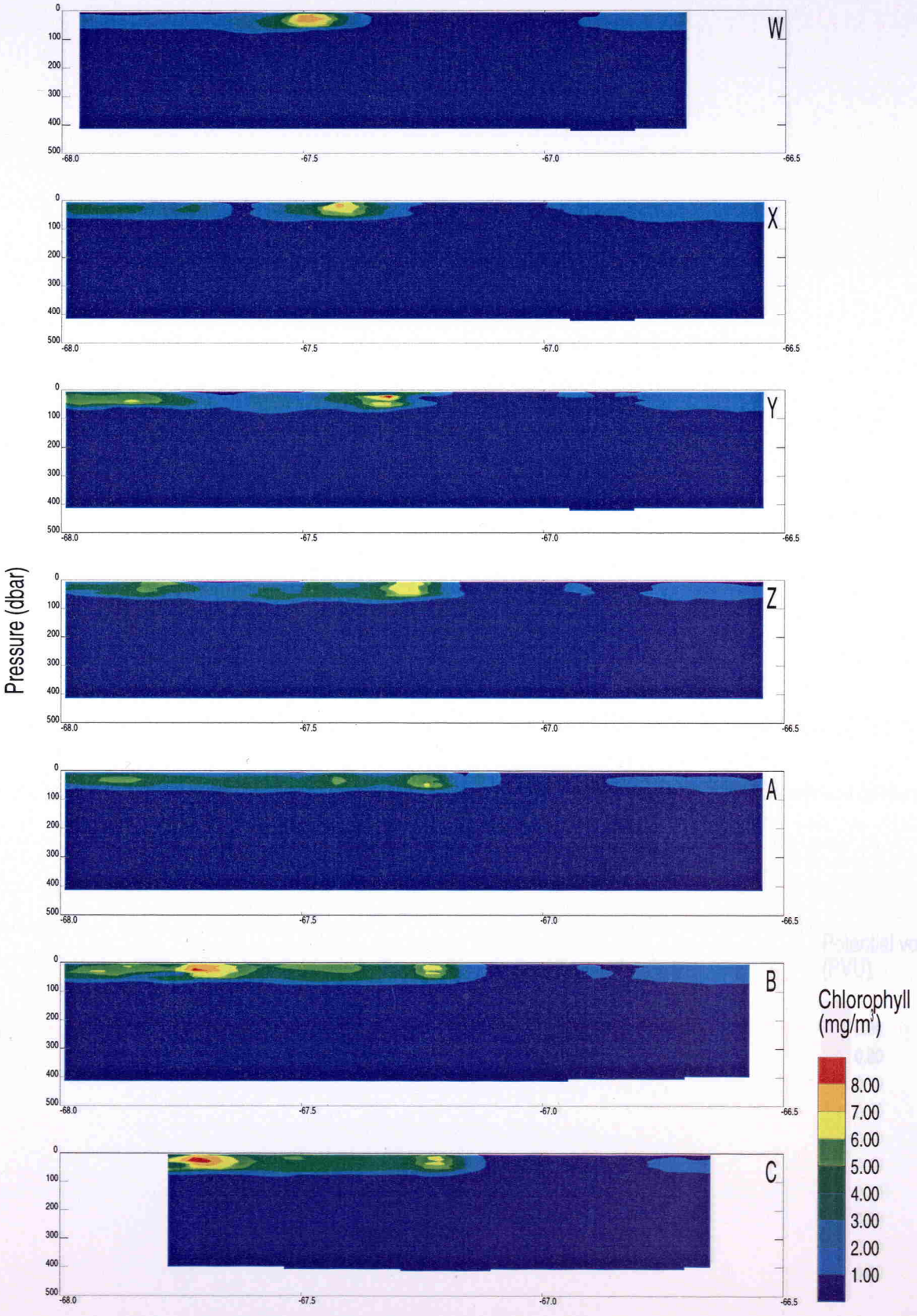

Fig. 5-7 Potential vorticity vertical sections.

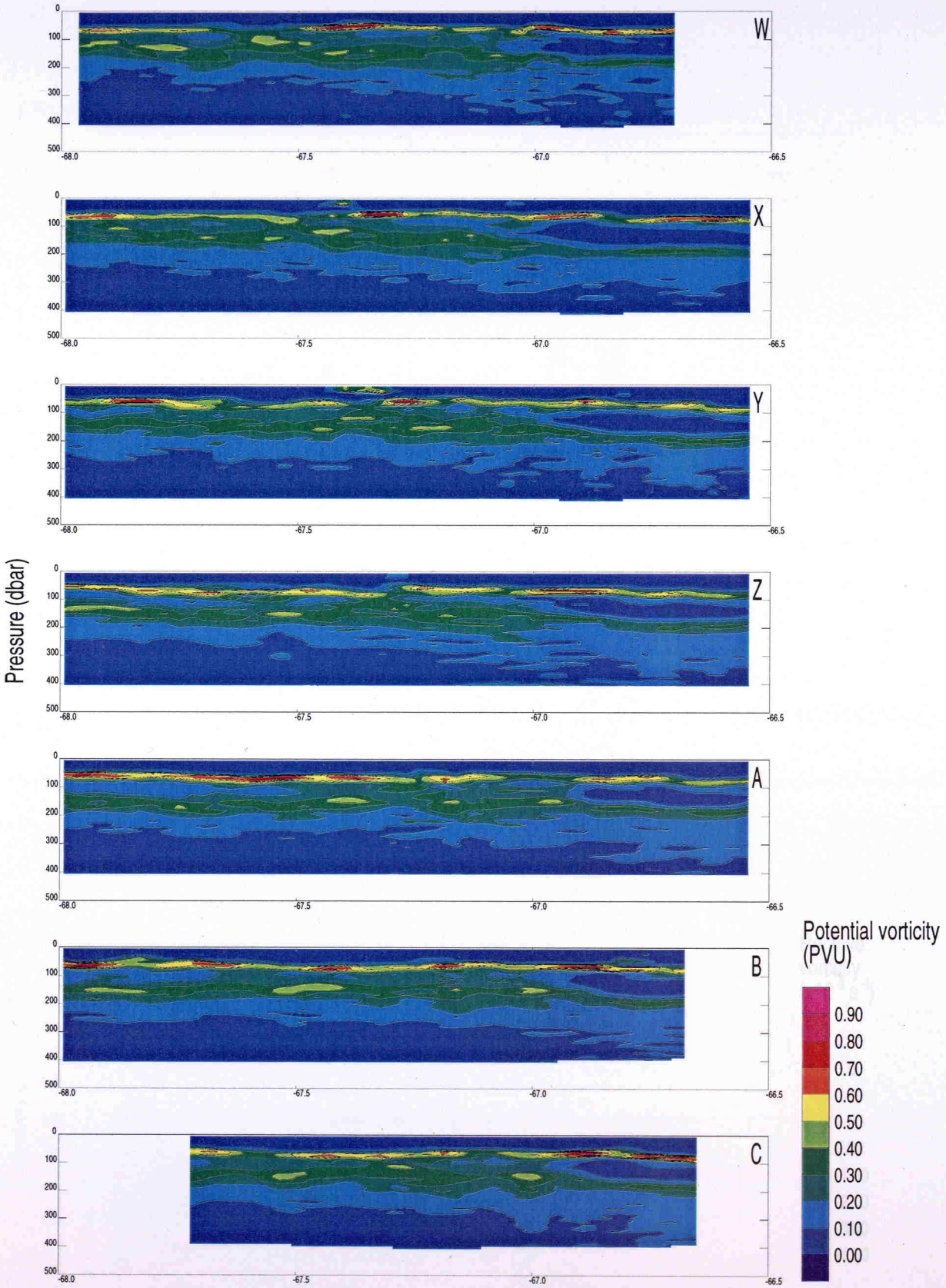

Fig. 5-8 Relative vorticity vertical sections.

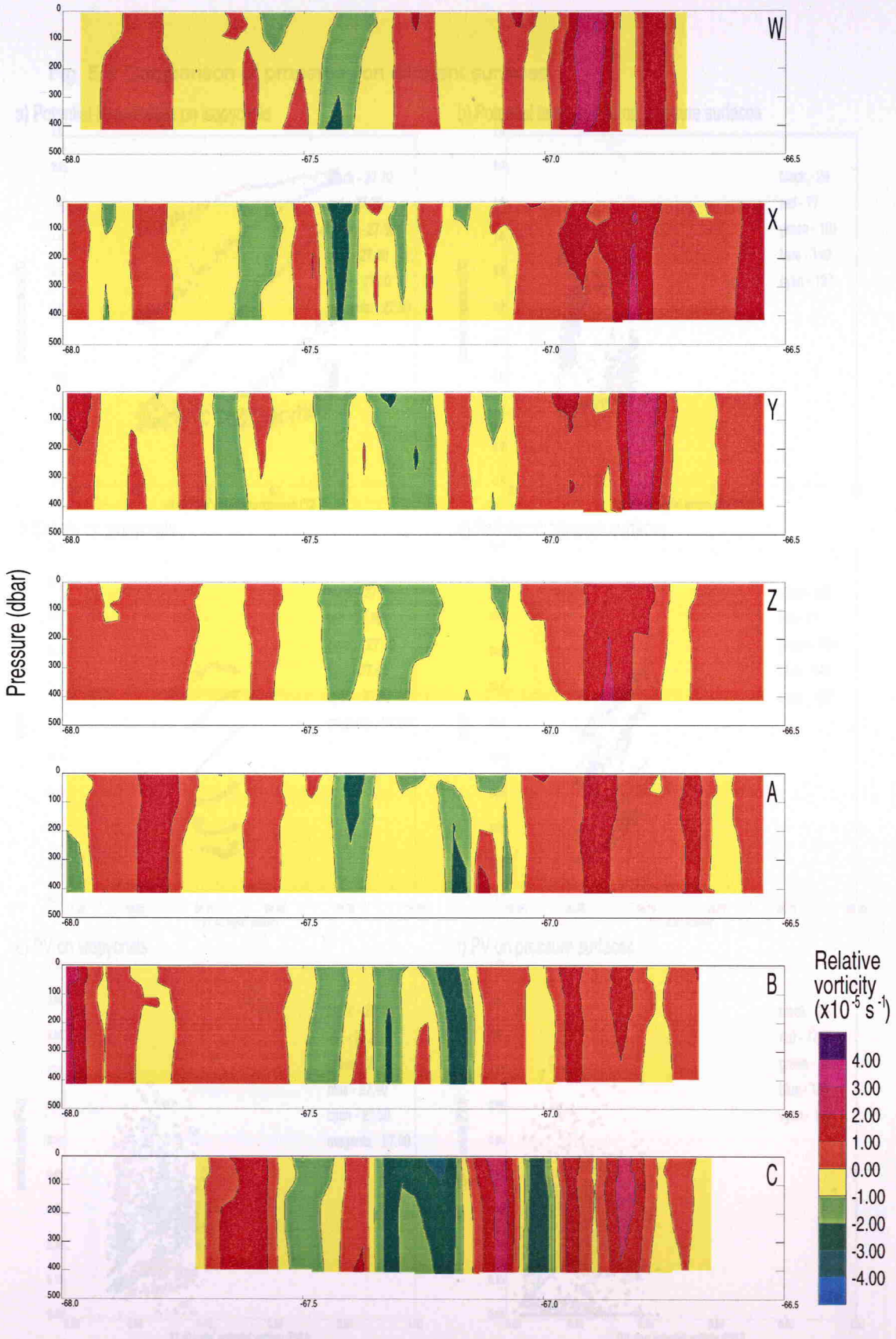

Fig. 5-9 Comparison of properties on different surfaces.

a) Potential temperature on isopycnals

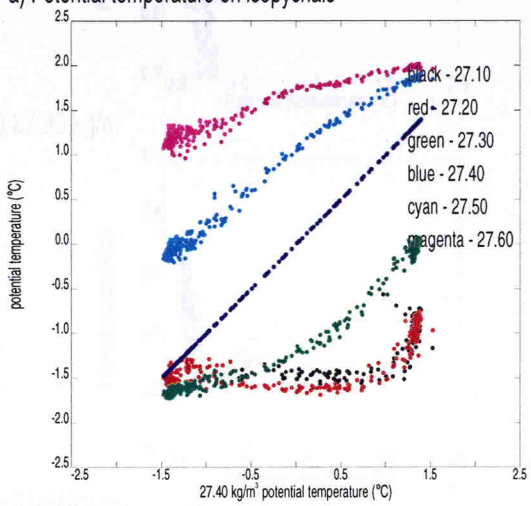

b) Potential temperature on pressure surfaces

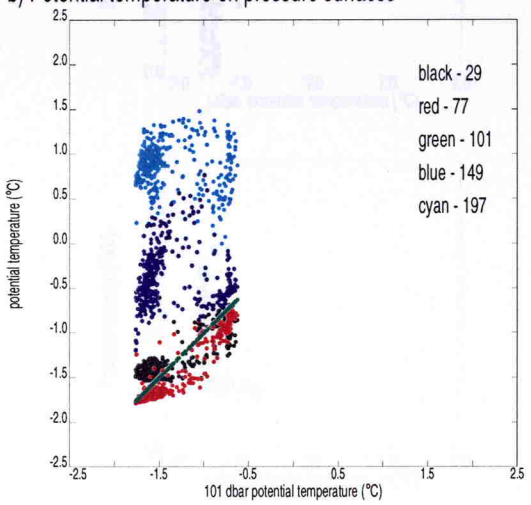

c) Salinity on isopycnals

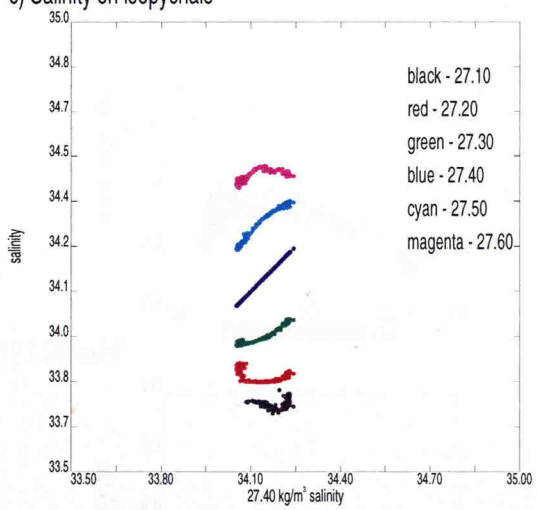

d) Salinity on pressure surfaces

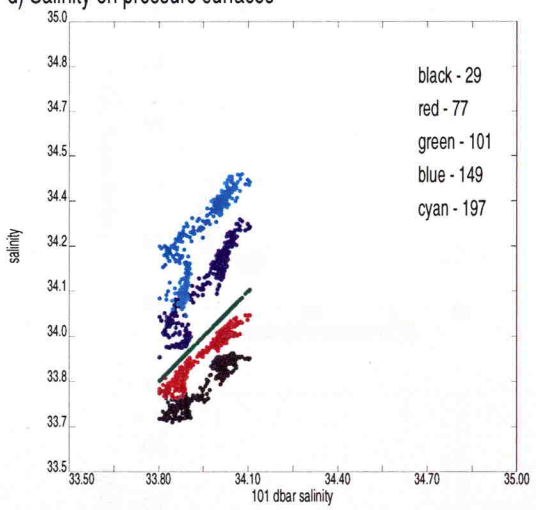

e) PV on isopycnals

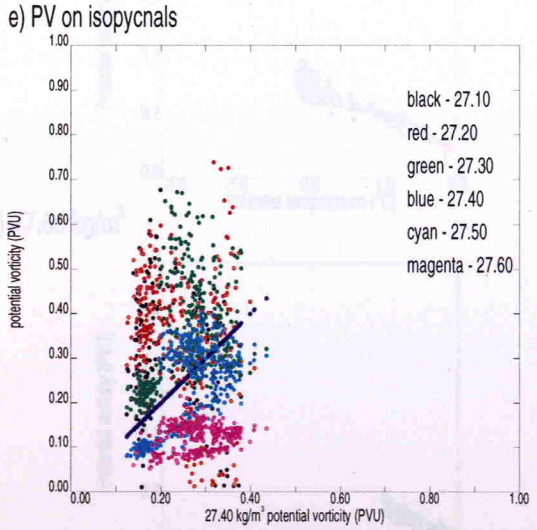

f) PV on pressure surfaces

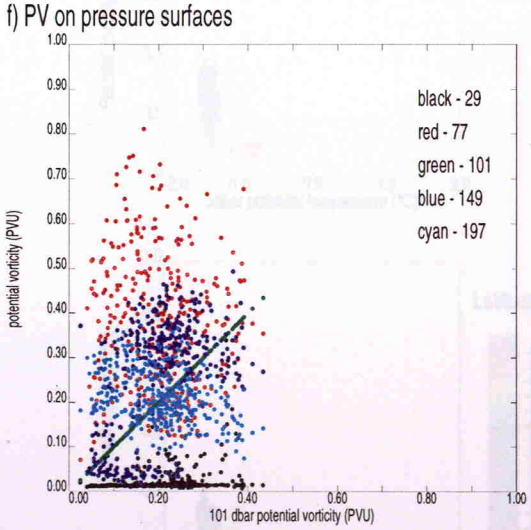

Fig. 5-10 Relationship between IPV and temperature on various isopycnals.

a) 27.20 kg/m^3

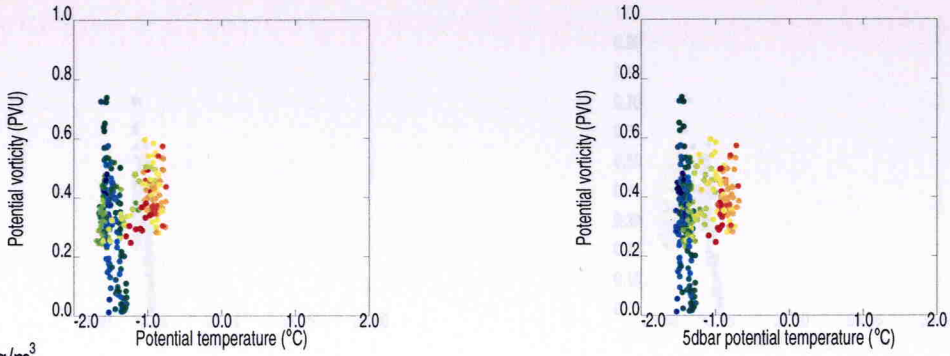

b) 27.30 kg/m^3

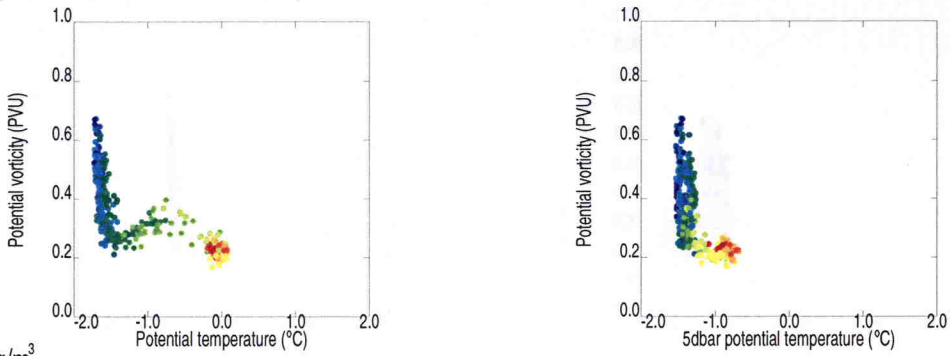

c) 27.40 kg/m^3

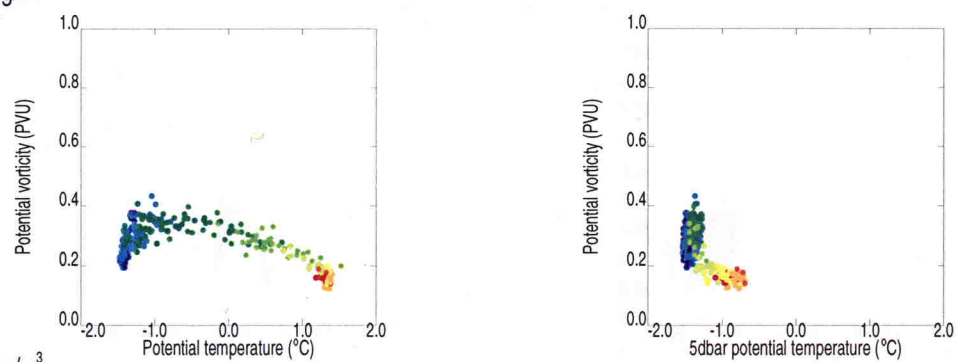

d) 27.50 kg/m^3

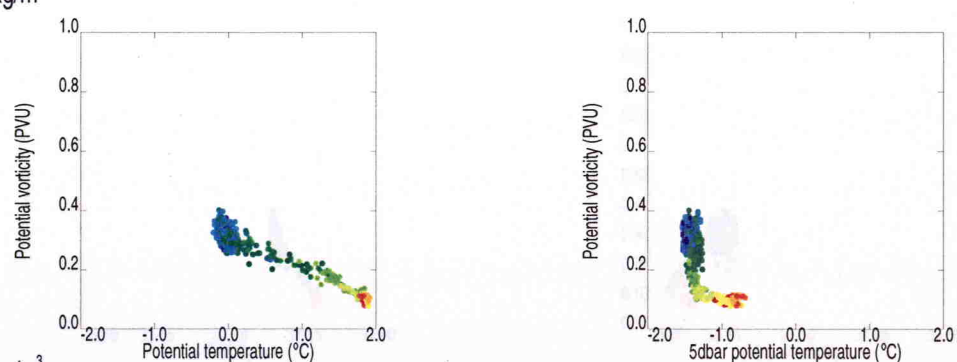

e) 27.60 kg/m^3

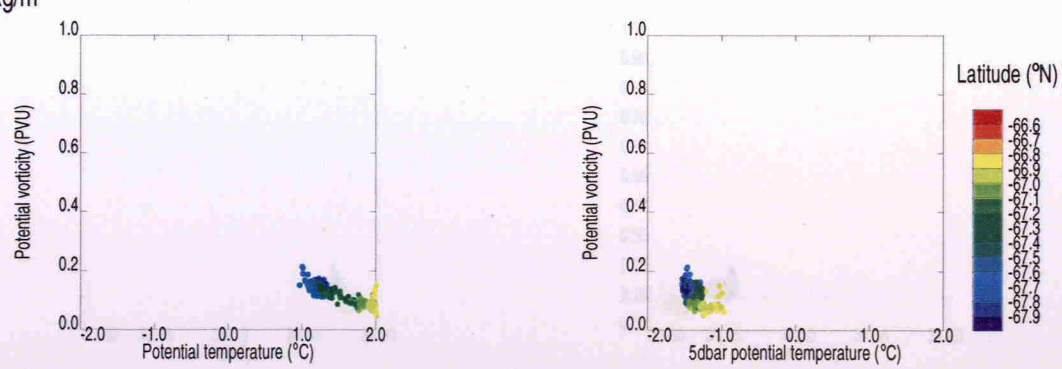

Fig. 5-11 Relationship between IPV and salinity on various isopycnals.

a) 27.20 kg/m^3

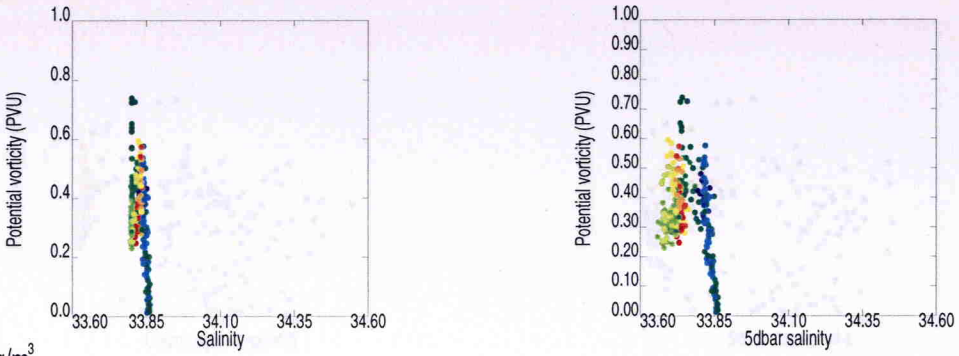

b) 27.30 kg/m^3

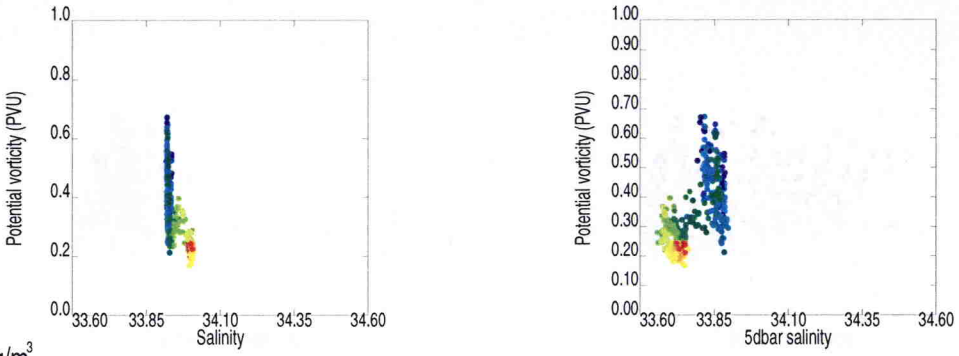

c) 27.40 kg/m^3

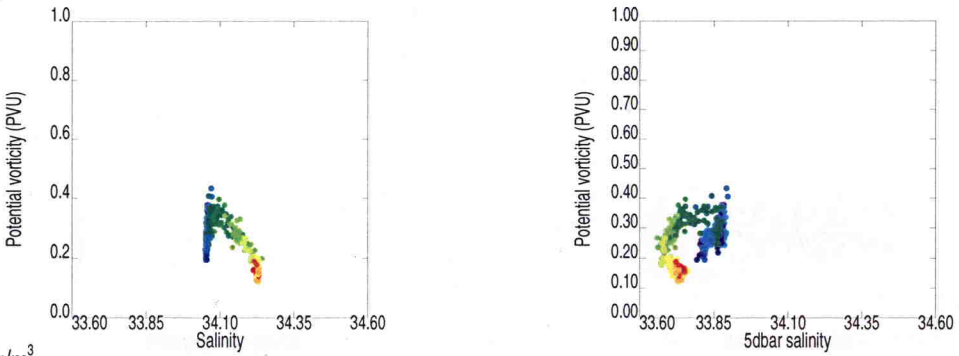

d) 27.50 kg/m^3

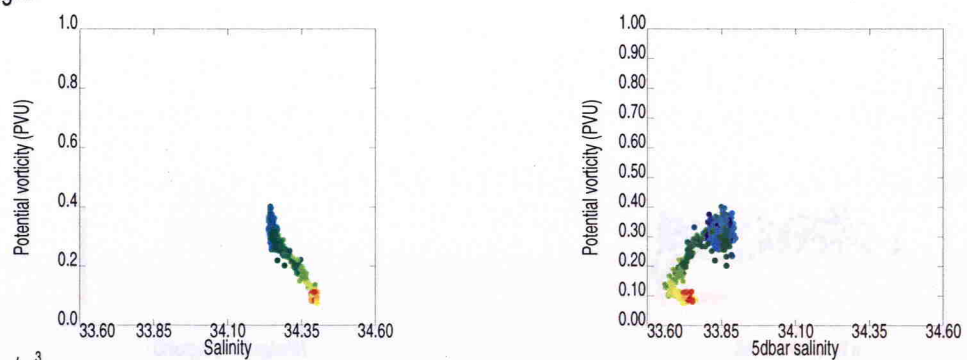

e) 27.60 kg/m^3

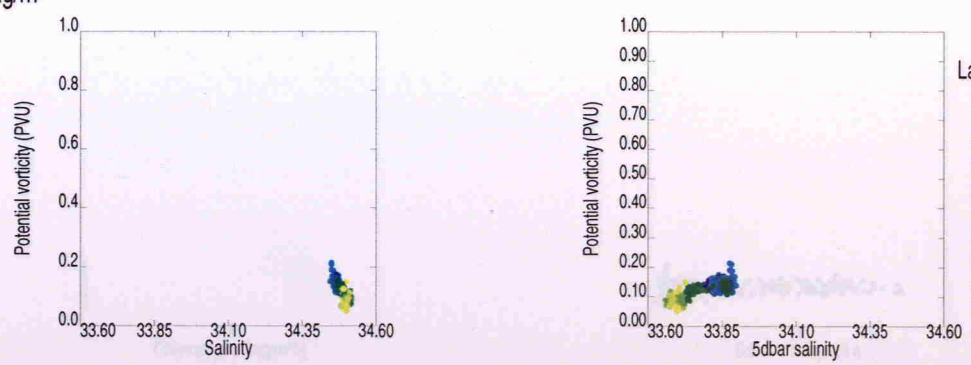

Fig. 5-12 Relationship between IPV and chlorophyll a on various isopycnals.

a) 27.20 kg/m^3

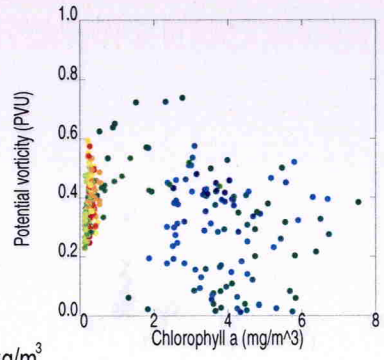

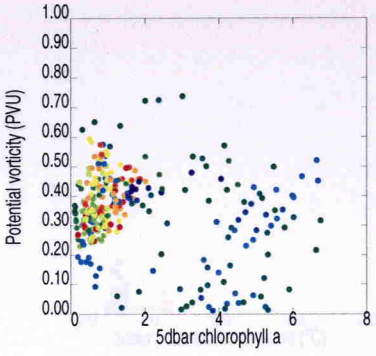

b) 27.30 kg/m^3

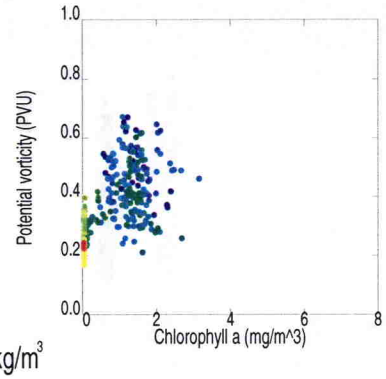

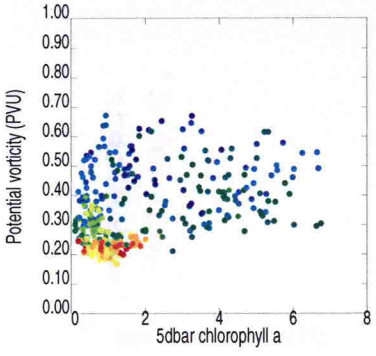

c) 27.40 kg/m^3

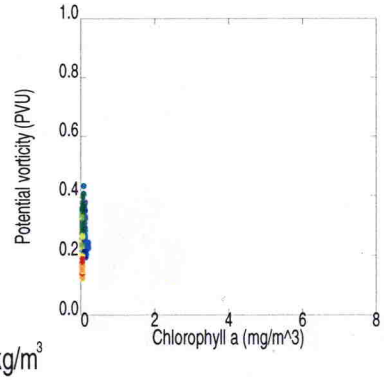

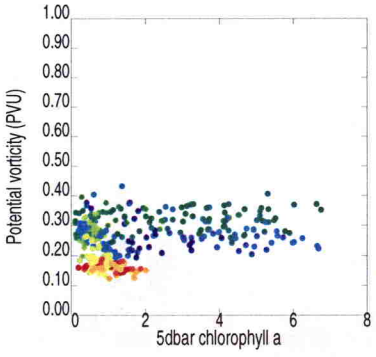

d) 27.50 kg/m^3

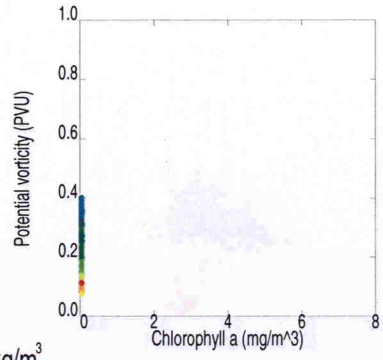

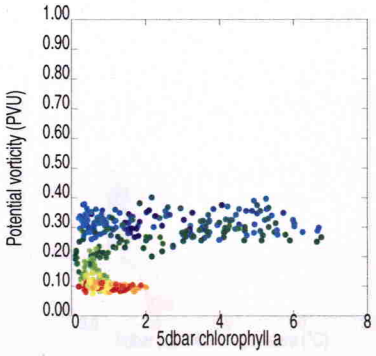

e) 27.60 kg/m^3

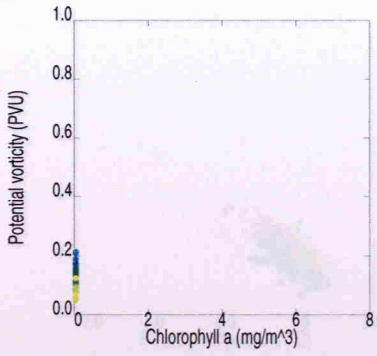

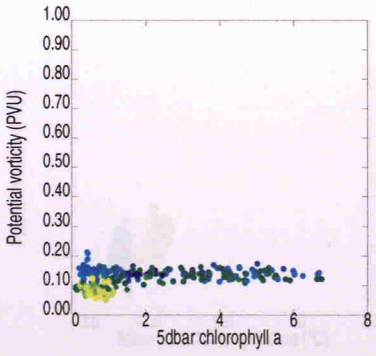

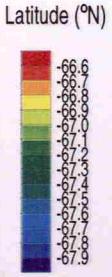

Fig. 5-13 Relationship between PV and temperature on various pressure surfaces.

a) 29 dbar

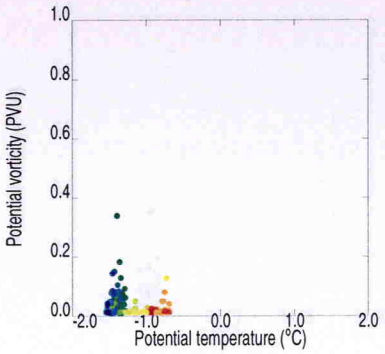

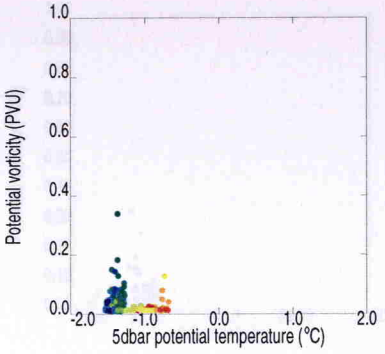

b) 77 dbar

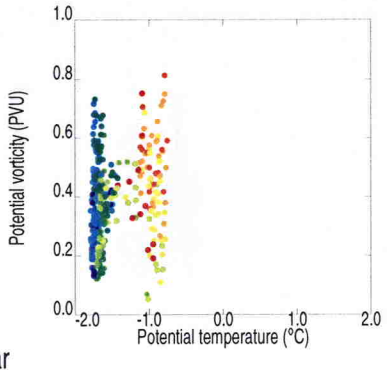

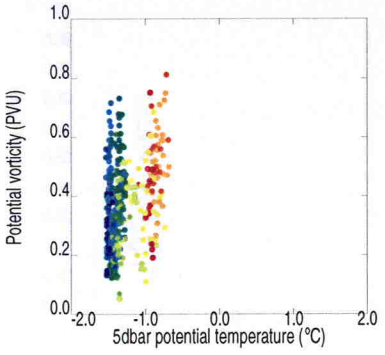

c) 101 dbar

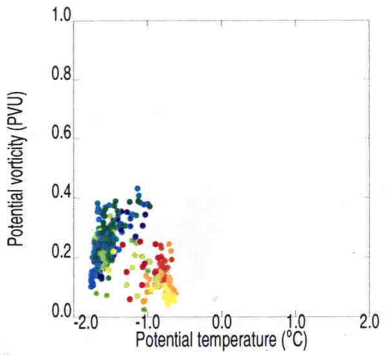

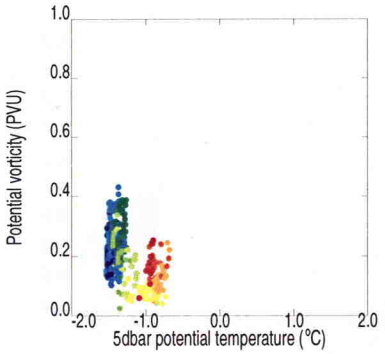

d) 149 dbar

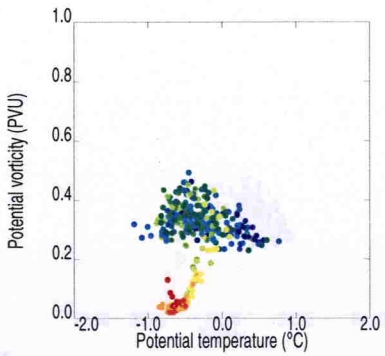

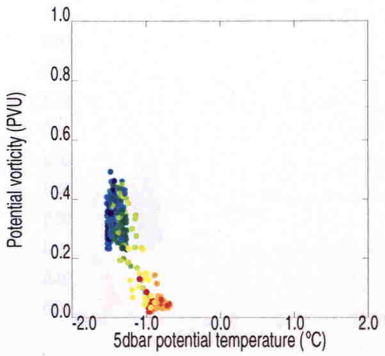

e) 197 dbar

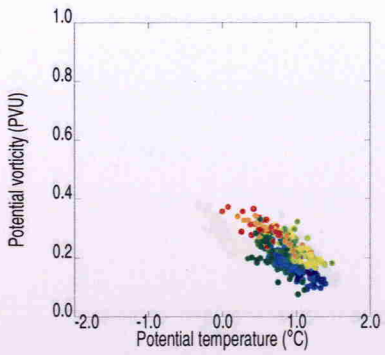

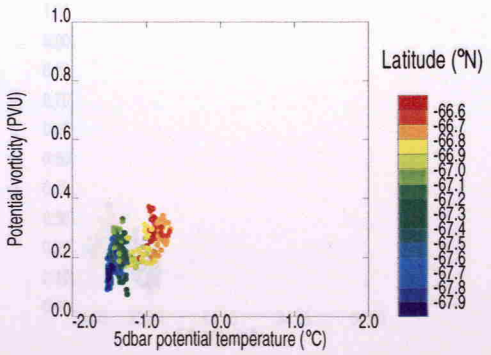

Fig. 5-14 Relationship between PV and salinity on various pressure surfaces.

a) 29 dbar

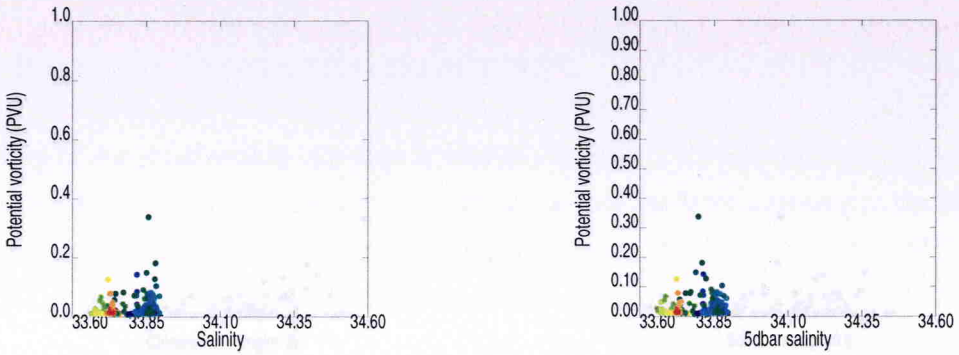

b) 77 dbar

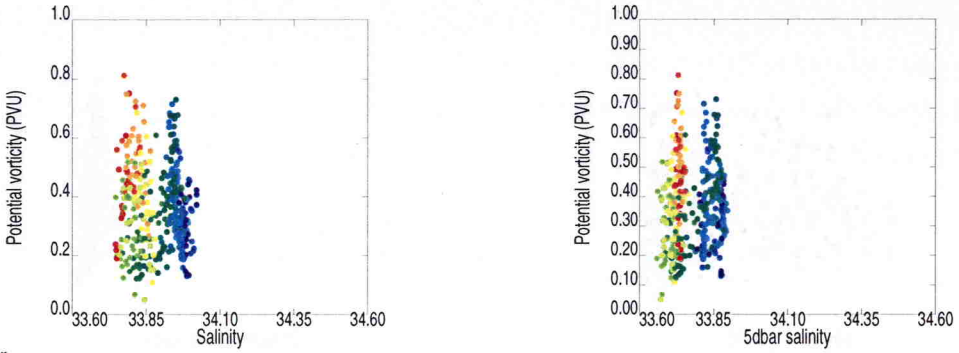

c) 101 dbar

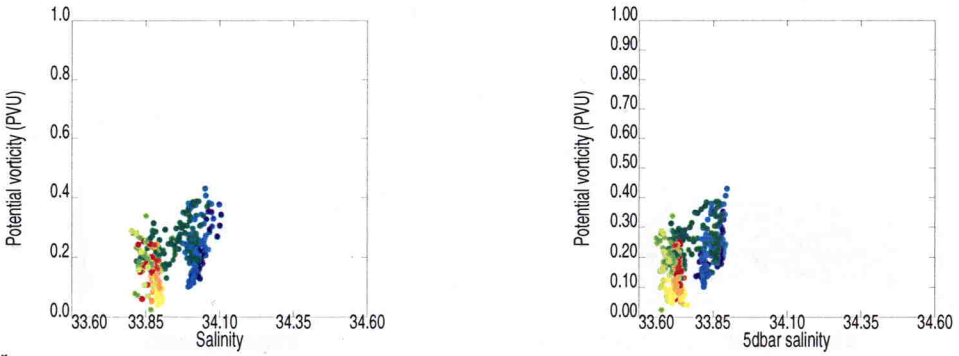

d) 149 dbar

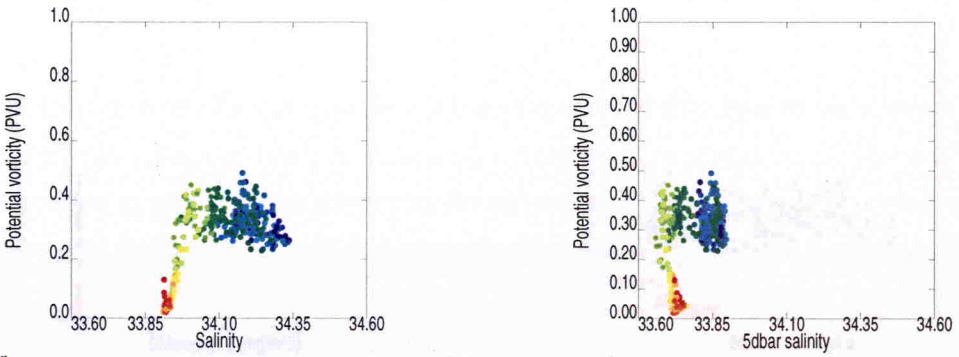

e) 197 dbar

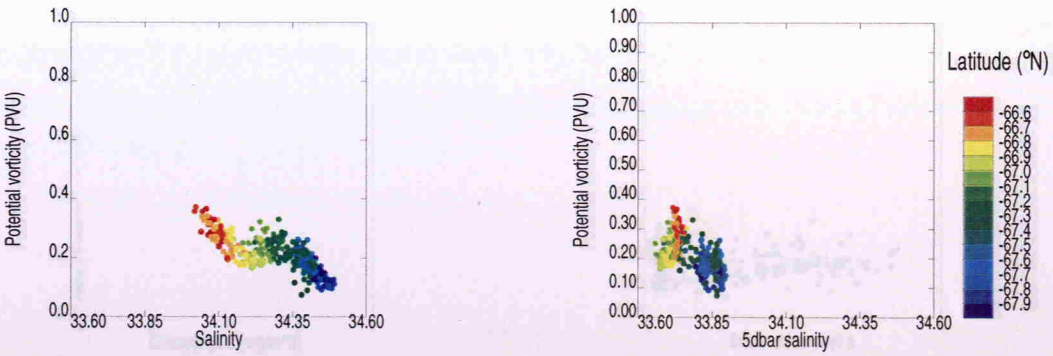

Fig. 5-15 Relationship between PV and chlorophyll a on pressure surfaces.

a) 29 dbar

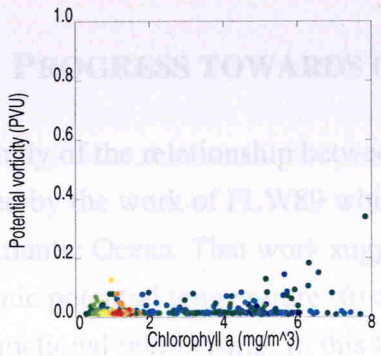

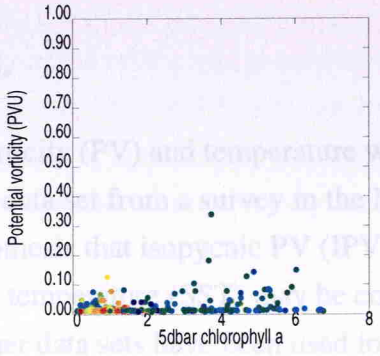

b) 77 dbar

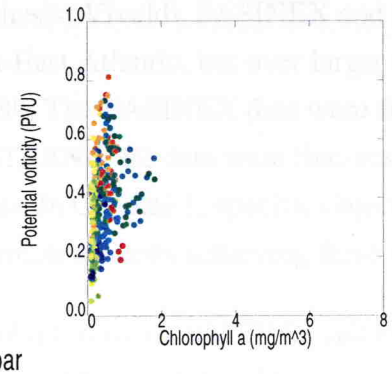

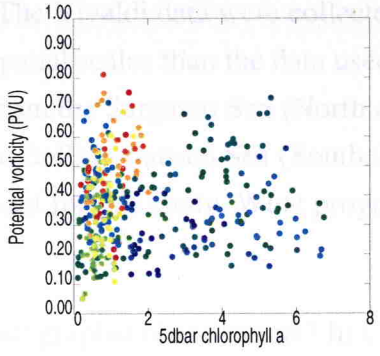

c) 101 dbar

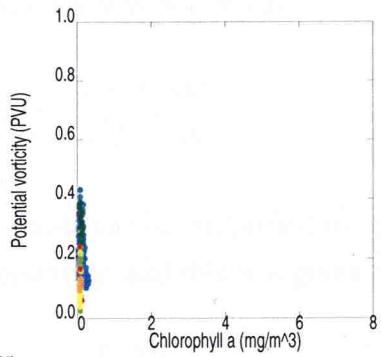

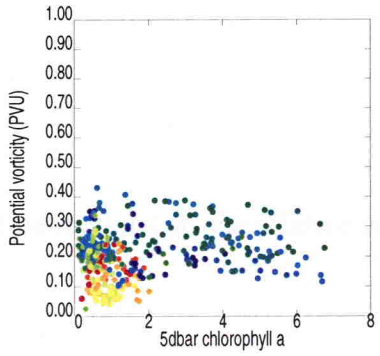

d) 149 dbar

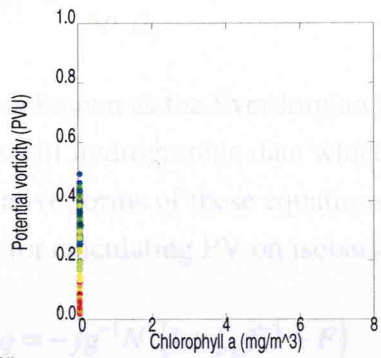

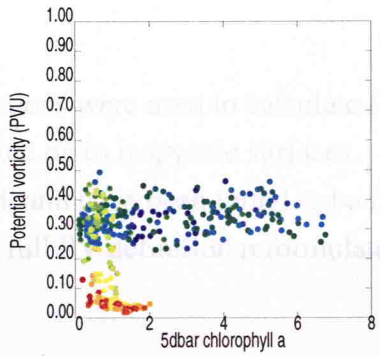

e) 197 dbar

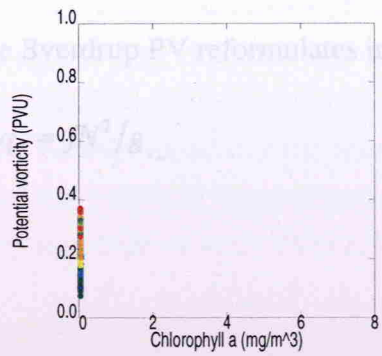

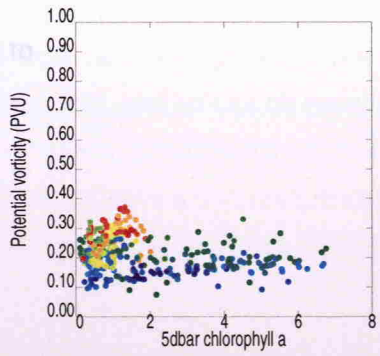

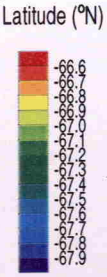

Chapter 6. DISCUSSION

6.1 PROGRESS TOWARDS OBJECTIVES.

This study of the relationship between potential vorticity (PV) and temperature was initiated by the work of FLW89 which examined a data set from a survey in the North-East Atlantic Ocean. That work suggested the hypothesis that isopycnic PV (IPV) and isopycnic potential temperature (θ) and sea-surface temperature (SST) may be connected by a functional relationship. In this thesis, three other data sets have been used to test this hypothesis: Vivaldi, FASINEX and STERNA '92. The Vivaldi data were collected in the North-East Atlantic, but over larger temporal and spatial scales than the data used in FLW89. The FASINEX data were fine-scale data from the Sargasso Sea (North Atlantic) and STERNA '92 data were fine-scale data from the Bellingshausen Sea (Southern Ocean). In Chapter 1, specific objectives were laid out for this study. What progress has been made towards achieving these objectives?

First of all, how should PV be calculated from oceanographic observations? In Chapter 2, isopycnic PV was defined as

$$q = \frac{\zeta + f}{\Delta p} \frac{\Delta \rho}{\rho_0} .$$

This formula can be simplified for gyre- or meso-scale motions, as the relative vorticity is then negligible, and this was given as

$$q_s = \frac{f}{\Delta p} \frac{\Delta \rho}{\rho_0}$$

which is known as the Sverdrupian PV. These equations were used to calculate PV from data sets of hydrographic data which was interpolated on to isopycnic surfaces. Alternative forms of these equations can be derived, and have been found to be more robust for calculating PV on isobaric surfaces. The full PV definition reformulates to

$$q = -fg^{-1}N^2\left(1 + \zeta_p f^{-1} - F\right)$$

and the Sverdrup PV reformulates in the same way to

$$q_S = fN^2/g .$$

The history of PV mapping was also described in Chapter 2, and there was mention of the level of accuracy achieved in calculating PV.

The remaining objectives defined in Chapter 1 concern the relationships between PV and other water mass tracers, which were analysed in Chapters 3, 4 and 5. The results of these analyses are summarised in the next section, and the rest of this chapter considers why the relationships are not similar, and how this fits in with, or modifies, currently accepted theory.

6.2 HOW WELL DO THE RESULTS SUPPORT THE HYPOTHESIS OF A LINEAR RELATIONSHIP BETWEEN PV AND WATER MASS TRACERS?

The original hypothesis, from the results of FLW89, was that a correlation exists between IPV and water mass characteristic (potential temperature, in their study, but here we also consider salinity and chlorophyll *a*). In this study, it is considered to what extent three different sets of observations of IPV and other tracers support this hypothesis. The best correlations of IPV and isopycnic potential temperature from each data set are summarised in Table 1, below.

Table 1. Summary of best correlation results from the data sets studied.

Data Set	Isopycnal (kg m^{-3})	Gradient (PVU K^{-1})	Correlation Coefficient, r
FLW89	26.90	-0.31	-0.79
North Atlantic Climatology	27.00	-0.25	N/K
Vivaldi '91	27.00	-0.29	-0.80
FASINEX	25.70	2.95	0.68
STERNA '92	27.50	-0.11	-0.97

Vivaldi data, like the FLW89 data, strongly support the idea of IPV and θ being functionally related such that high IPV and low θ correspond. In fact, the Vivaldi IPV-θ relationship is very similar to that of FLW89. Both these data sets consist of the Sverdrupian IPV only with no relative vorticity component, and so can be compared directly. FLW89 found that the relationship had a correlation coefficient of -0.79 and slope of -0.31 PVU K^{-1}. In comparison, the Vivaldi results have a correlation coefficient of -0.80 and slope of -0.29 PVU K^{-1}. Perhaps this strong agreement is not surprising,

given that the data were collected in the same part of the North-east Atlantic, in late spring. However, the data were collected 10 years apart, with different instrumentation and different time and space scales, so the similarity should not be taken for granted. Very similar results were also achieved for the relationship between IPV and salinity, i.e. there was a strong linear relationship.

The FASINEX data may support the idea of IPV and water mass characteristic being related in some way, but this is less clear than in the Vivaldi data. The range of temperature and salinity values represented across the FASINEX survey region is very narrow, because only one water mass is present. The fronts in the region surveyed occurred because of wind-induced convergence, rather than the confluence of different water masses. The observed IPV-θ relationship for FASINEX data tends towards a positive steep gradient at depths deeper than the surface mixed layer. For example, on isopycnal 25.70 kg m^{-3} for the relationship between IPV and potential temperature the correlation coefficient is 0.68, and the gradient is 2.95 PVU K^{-1}. This is a little weaker correlation than in the FLW89 and Vivaldi data sets, and a completely different relationship. However, on isobaric surfaces deeper than about 150 metres there was very good correlation between PV and potential temperature or salinity. For example, on 200 dbar the PV-potential temperature relationship has a correlation coefficient of 0.92 and gradient of 0.29 PVU K^{-1}. The magnitude of this gradient is similar to that in the FLW89 and Vivaldi data sets, but the sign is opposite. This sort of relationship on isobaric surfaces is not seen in the other data sets in this study. This result disagrees with the hypothetical relationship. However, there are significant differences between the FASINEX and Vivaldi regions, including different sources of frontogenesis, and the results may have occurred as a consequence of these factors. The relationship differences may be an indicator of the dynamical history of an area of the ocean.

The STERNA '92 data support the hypothesis of IPV and water mass characteristic being linearly related, at least on isopycnals which are below the near-surface mixed layer. The relationship between IPV and potential temperature has a shallower gradient than that found in FLW89 and the Vivaldi data, with the gradient on isopycnal 27.5 kg m^{-3} being -0.11 PVU K^{-1} and a very strong correlation coefficient of 0.97. The IPV and isopycnic salinity shows just as strong a correlation. In the STERNA '92 case, the front contains water which has been advected in from west of the region, and different water masses occur to the north and south of the region. Once again, these background circumstances leading to the existence of the front in the STERNA survey are different to those of Vivaldi and FASINEX. These may contribute to the different results obtained.

As an extension to the main hypothesis, relationships between other quantities were also examined in each data set. For example, the variation of relative vorticity with potential

temperature or salinity was considered, and the variation of IPV with surface temperature and salinity. In the case of the STERNA data, the variation of IPV with chlorophyll *a* was also examined. None of these comparisons displayed a functional relationship.

The hypothesis that IPV and SST may be clearly functionally related, as suggested by Marshall and Williams (1989), is not supported by the three data sets considered. However, two of the data sets support the hypothesis that IPV and isopycnic temperature or salinity are functionally related. And even the FASINEX data agree with this hypothesis to some extent, but display a quite different relationship. The differences between the results must be a reflection of how the IPV and other water mass characteristics were set at the time of subduction, and be dependent on the frontal dynamics which occur in the survey regions. These aspects of the data sets are considered in the rest of this chapter, in the context of thermocline theory.

As was stated in Chapter 1, it was hoped that a clear functional relationship between SST and IPV would have been established, and used to derive flow fields from single satellite images. The lack of this relationship between surface fields and sub-surface IPV led to that plan being abandoned in favour of investigating the inter-relationships and their dependence on the circumstances of the front. The reasons for the failure to establish a relationship between SST and IPV are also considered in the following sections.

6.3 WHY DO THE RESULTS VARY FROM THAT OF FLW89?

In looking at the relationship between IPV and θ below the mixed layer, the effects seen are primarily the results of fluid exchange between the near-surface mixed layer and the ocean interior. The temperature and stratification of the near-surface layers of the ocean are determined by interactions with the atmosphere (momentum, heat and fresh water fluxes). After fluid has transferred from the mixed layer to the ocean interior, it is decoupled from the influences that can change it, and so its properties are essentially fixed. Hence, if geostrophic flow is assumed to be along isopycnals in the ocean interior, then the fluid's characteristic temperature, salinity and IPV signals are conserved on isopycnals. So how does transfer from the mixed layer to the ocean interior (subduction) take place? The principal processes which are believed to be responsible for these transfers are Ekman pumping, isopycnal eddy mixing and wintertime convection. Let us consider now what has occurred in the data sets being studied here.

FLW89 attribute their observed correlation between IPV and water mass characteristic to the dynamics occurring at the time of spring subduction of mixed layer fluid into the seasonal thermocline (Woods, 1985). This can be understood by considering two water columns representative of the subtropical and subpolar gyres (see Figure 6-1).

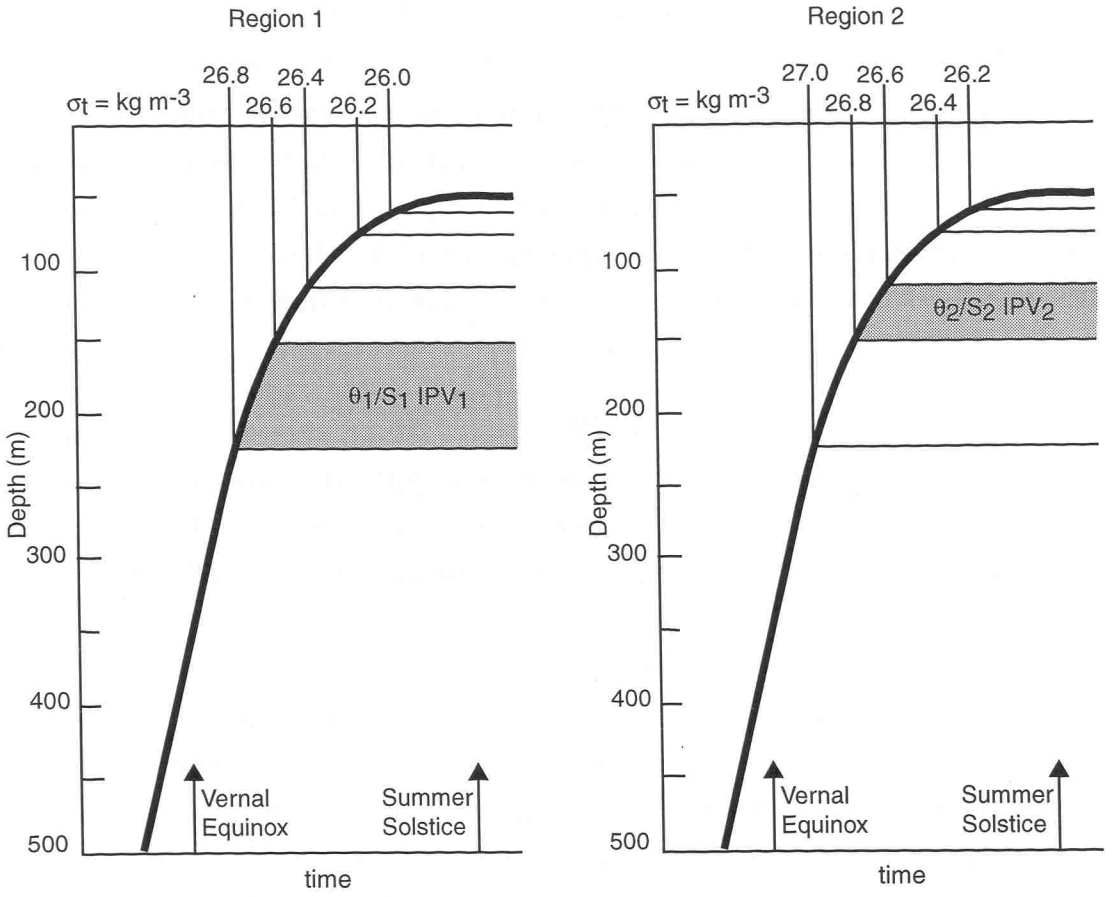

Fig. 6-1 Schematic diagram of IPV generation and the establishment of IPV-water mass correlation. The spring rise of the mixed layer depth (heavy line) and the subduction of isopycnals into the seasonal thermocline are shown. Region 1 is representative of the subtropical gyre, and region 2 of the subpolar gyre. For a pair of isopycnals the θ-S relationship is determined by the region, while the spacing is determined by the time of subduction. (After Fischer *et al.* (1989))

During the spring heating season, the mixed layer shoals and the thermocline sharpens as fluid is subducted from the mixed layer down along isopycnals. This means that the water mass characteristics (θ-S) on an isopycnal are determined by the geographical position of the fluid at subduction. That is to say, for a particular isopycnal, water subducted in the subtropical gyre will be warmer and saltier than water subducted in the subpolar gyre. However, the IPV on an isopycnal is determined by the vertical separation of the bounding isopycnals on subduction, which in turn is determined by the horizontal separation of these isopycnals in the mixed layer. During spring, the surface outcrops of isopycnals migrate northwards in the North Atlantic, moving more quickly at the start of the heating season and slowing later (Stammer and Woods, 1987). This means that the isopycnal thickness is determined by the time of subduction. For example, early subduction in the subtropical gyre gives thicker isopycnals, and consequently lower IPV, than later subduction in the subpolar gyre where thinner isopycnals give rise to higher

IPV values. At gyre-scale the IPV is dominated by the thickness rather than the relative vorticity, so it is reasonable to neglect the effects of relative vorticity on the values of IPV at subduction. For adiabatic advection on an isopycnic surface, these quantities are conserved and can be drawn together by confluent gyre-scale circulation. This results in large-scale gradients which are further enhanced into mesoscale fronts, where synoptic-scale confluence occurs due to the meandering flow field. This confluence brings about the situation of inverse correlation of θ and IPV on an isopycnal, as in the FLW89 and Vivaldi data.

This proposed mechanism for the setting of IPV and θ values in the North East Atlantic data sets, is essentially a description of the consequences of wintertime convection. On the large spatial and temporal scales of Vivaldi, the effects of mesoscale eddies on the subduction of fluid has not really been considered. Mesoscale eddies are of the order of 100 km horizontal scale, which is too small to be adequately resolved in the Vivaldi data set where the tracks are separated by 300 km. FLW89, with a data set of tracks at 10 km separation, do consider the effects of mesoscale eddies by making their calculations for both Sverdrup IPV and full IPV, which includes the local flow fields via the relative vorticity. In fact, given the large difference in horizontal scale of the FLW89 and Vivaldi data, it is remarkable how similar their results are. This lends credence to FLW89's theory. Vivaldi took place early in the heating season (April to June), while FLW89's data was collected later in the summer (late July to early August), but this seems to have had little effect on the results.

The FLW89 mechanism is a particular subduction model for how IPV and θ are set in the context of large-scale circulation, across a fairly stable large-scale front. We have seen that this model holds well for the Vivaldi data in a nearby part of the North Atlantic subtropical gyre, at a slightly earlier time in the heating season. How relevant is this model to the FASINEX data set?

FASINEX data give quite different results to those from the north-east Atlantic. These data were collected in a region of quite different dynamics, and earlier in the year (late February) before the heating season was under way. The survey was carried out within the Subtropical Convergence Zone (STCZ) at the southern edge of the subtropical gyre, which is a region of large-scale convergence within which fronts often form due to smaller scale dynamics. There is no surface water mass change, as occurs in the north-east Atlantic, but mesoscale eddies appear to be very important to the local dynamics. Indeed, Pollard and Regier (1992) show evidence from FASINEX that mesoscale eddies may be responsible for mixing surface waters down along isopycnals.

In FASINEX data there is a smooth background field of IPV, θ and potential density, with several anomalous bands of reduced stratification on the southern side of the front. The bands are caused by small (40 km diameter) shallow anticyclonic eddies carrying surface frontal water northwards over the weakly stratified mixed layer water and trapping it in the thermocline. The lower stratification water is pulled down by 50 m or more, and the parcel increases its anticyclonic relative vorticity to conserve IPV. Where fluid parcels have been strained across the front, low stratification parcels (low IPV) with low θ (from north of front) end up located within a region of higher stratification (higher IPV) and higher θ. This accounts for the relationships found within the FASINEX data in Chapter 4. The range of values of a property on an isopycnal is small because there is no water mass change across the front, whereas these variations were bigger for the Vivaldi data set where different water masses were flowing together into the region.

The transference of fluid across the front is in accord with thermocline ventilation theory (Hoskins, *et al.*, 1985, Woods, 1985). Pollard and Regier (1992) illustrated this ageostrophic circulation as shown in Figure 6-2. Consider a front which is maintained by large-scale confluence (as in FASINEX). Fluid travelling towards this front on the southern anticyclonic side reduces its absolute vorticity, and must compress vertically to conserve PV. The sea surface is fixed, so an upward vertical velocity is induced. A corresponding downward velocity takes place on the cyclonic side of the front as fluid moving towards the front gains absolute vorticity and stretches to conserve PV. These vertical velocities decrease in magnitude with depth as the influence of the surface confluence is reduced. This results in a closed ageostrophic circulation where water crosses the front northwards near the sea surface, and then returns southwards at a deeper level. In reality, as distinct from a model prediction, the ageostrophic circulation will be greatly affected by the initial distribution of potential vorticity. Furthermore, over the course of several weeks the varying wind field over the ocean will mix or re-stratify the top 50-100 metres and disrupt the front, which will then sharpen up again and the vertical motions will restart. In fact, it would be expected that this mechanism would affect the circulation alongside the straining due to mesoscale eddies, and this interplay could lead to diffusion of properties across the thermocline.

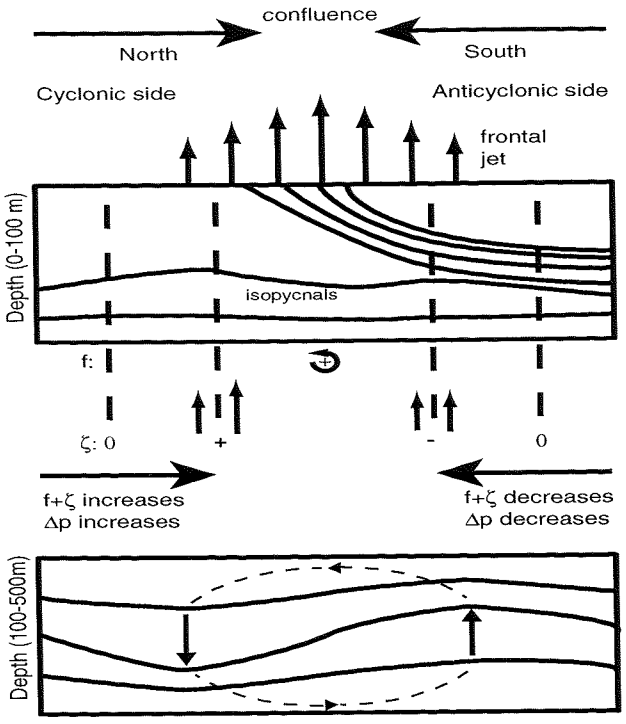

Fig. 6-2 Schematic diagram showing a confluence moving water into an area of increasing (decreasing) absolute vorticity on the cyclonic (anticyclonic) side of a front, causing the separation of isopycnals to increase (decrease). Since the surface is fixed, a vertical circulation is set up as shown. (After Pollard and Regier (1992))

The inference that an ageostrophic circulation takes place in the FASINEX data was further confirmed by calculation of the vertical velocity according to the ω-equation (Pollard and Regier, 1992). Vertical velocities of the order of 10^{-4} m s^{-1} were inferred, with maxima of 4 x 10^{-4} m s^{-1}, or 40 m day^{-1}. These velocities are in good agreement with other estimates for the same region (Voorhis and Bruce, 1982). However, these velocities are an order of magnitude larger than those estimated for the FLW89 data set by Leach (1987). This is further confirmation that the front which was studied in FLW89 is the result of quite different ocean dynamics to that in FASINEX, and shows that cross-frontal circulation is not a major contributor to the IPV-θ relationships of the FLW89 data sets.

Now, consider the STERNA results. The IPV-θ relationship proved to be similar to the Vivaldi data on denser isopycnals, with gradients of the same order of magnitude, but smaller. The IPV-S relationship was similar to the Vivaldi data, and of similar gradient. In this region, salinity has more influence on the density field than temperature does, and the temperature varies little across the front. On shallower isopycnals, the relationships are more complex, taking the form of tight but non-linear curves. Like the Vivaldi data, the STERNA data were collected at a front which forms the boundary between two distinct water masses. This can be seen clearly in θ-S plots of the deep CTD data (not shown) as well as the SeaSoar data (Figure 5-2), and show that the water mass transition

is not confined to the near-surface isopycnals. Some mixing of water masses would also occur at the front, which accounts for the water of intermediate θ-S properties. Although Vivaldi and FASINEX data had strong jets associated with those fronts, the STERNA data records strong advection of water into the frontal region. This led to differential advection of water properties on either side of the front, which sharpened up the cross-front gradients, and introduced water with different θ-S properties from the surrounding water. Evidence of this is seen in the temperature anomalies which lie south of the main front. These surface-trapped anomalies also account for the more complex IPV-θ and IPV-S curves on the lighter isopycnals. Apart from the temperature anomalies which were advected in from upstream, there is no evidence of eddies breaking off from the front, nor transference of fluid across the front by eddy motion.

In the STERNA data, the survey had much the same time and space scales as the FLW89 and FASINEX data, which were much shorter than those of the Vivaldi data. The survey was also carried out early in the heating season. On certain isopycnals the results were similar, but on others, where advected water masses were present, the results were quite different. Certainly, the gradients of relationships were different from those in Vivaldi and FLW89. These comparisons of the different data sets indicate that IPV and water mass characteristics are related in frontal regions, but that the relationship varies critically with the dynamics which are active in the area. These results indicate that winter convection followed by springtime subduction are important mechanisms in setting the relationship, but that mesoscale eddy mixing may also play a role. It is now worth considering these mechanisms in the context of theories of thermocline ventilation.

6.4 HOW DO THE RESULTS FIT WITH THEORIES OF THERMOCLINE VENTILATION?

In Chapter 2, several theories of thermocline circulation were introduced. These theories did not consider what dynamics were occurring above the permanent pycnocline in the seasonal or diurnal pycnocline. Woods' (1985) analytical model of thermocline ventilation was developed to study the dynamics of this part of the water column. To recap on the main features, according to Woods (1985) Ekman pumping does not force water directly from the surface down to the permanent pycnocline, as is assumed by many models. Instead, a stratified layer forms below the base of the Ekman layer and is known as the seasonal pycnocline. The vertical extent of the seasonal pycnocline is limited to that part of the water column that is changed at least once a year by direct interaction with the surface fluxes. Within the seasonal pycnocline fluid flows geostrophically until it passes nearly horizontally through the sloping surface into the permanent pycnocline. The near-surface convection layer acts as a source (sink) of PV for water transferring into (out

of) the seasonal pycnocline. Any vertical motion in the seasonal pycnocline is due to vortex stretching to conserve PV as the circulation moves the water column to different latitudes, rather than a direct response to Ekman pumping which drives the geostrophic flow. While upwelling or downwelling does not affect the spacing between isopycnals at the time of subduction, more fluid is transferred to the permanent pycnocline in downwelling areas. In Woods' model, the maximum mixed layer depth is achieved near the end of March, and shoals rapidly until mid-July. This rise of the mixed layer base leaves behind a stratified water column with calculable PV, which is consumed during the autumn entrainment of the seasonal pycnocline.

The model proposed by FLW89 to explain the setting of the water mass characteristics (θ, S and PV) fits well with Woods' (1985) analytical model, to describe what happens at the time of subduction during the heating season. The observations of the IPV-θ relationships in FLW89 and Vivaldi are in keeping with what would be predicted to occur in the seasonal pycnocline. The values would be set at the time of subduction in late winter, and remain until the following autumn when entrainment may be expected of those shallow isopycnals. The front in the Vivaldi data is of a fairly permanent nature, lying at the boundary between the subtropical and subpolar gyres which contain different water masses. However, it is quite a weak front, and little active frontogenesis has been detected (Leach, 1987). Other modelling work (Williams, *et al.*, 1995) suggests that the mixed layer and permanent thermocline are only coupled in late winter and this bias is maintained even when eddy stirring takes place, which would appear to be confirmed by the Vivaldi data. The Vivaldi data do not resolve mesoscale motions so the influence of eddies on the subduction cannot be evaluated.

For a parcel of fluid in the mixed layer to pass into the stratified thermocline in the way suggested by FLW89, it must be stratified by buoyancy input which can be supplied by local air-sea exchange and/or by lateral advective processes. Marshall and Marshall (1995) demonstrated stratification of the mixed layer by modelling a mixed layer over a thermocline under various seasonal cycles. In keeping with the modelling work already considered, they found that the annual subduction rate depends to first order on late winter mixed layer properties. However the annual-mean air-sea buoyancy exchange is sensitive to the seasonal cycle pattern and decreases as the effective subduction period shortens. At this limit, buoyancy changes are controlled by advective processes acting in the Ekman layer, and this could be the case for the Vivaldi data.

If we look next at the FASINEX data set, we find that its IPV-θ relationship is quite different. Clearly, the values of IPV and water mass characteristic are not the result of spring stratification as seen in the Vivaldi data set. The FASINEX survey was taken from a transient front at the end of winter, before spring heating was under way, and in a

strongly advective region within the Subtropical Convergence Zone. Rudnick and Weller (1993) analysed the velocity and temperature fields derived from an array of moorings across the entire FASINEX region. They concluded that in the top 160 metres the low frequency heat budget is dominated by horizontal advection, caused by the mean northward advection of a series of fronts, and surface heating has very little effect. Surface heating effects become significant only in the top 40 metres, and particularly at diurnal frequency.

Pollard and Regier (1992) found that ageostrophic circulation patterns were evident in the SeaSoar data, and these are believed to be responsible for subducting water parcels across the front from the mixed layer into the seasonal or permanent pycnocline. In some areas of the ocean, it may be that subduction driven by frontal processes may be as significant as that due to interaction with the large-scale wind field, and this has been confirmed by the results from various modelling efforts (Follows and Marshall, 1994, Spall, 1995, Marshall, 1997). In particular, Spall (1995) modelled a front very similar to that in FASINEX to investigate this by looking at subduction at fronts in the absence of surface forcing. Spall's model demonstrates how baroclinic instability and resulting frontogenesis drives subduction of parcels below and across the front. The frontogenesis drives a deep ageostrophic flow which carries mixed layer water below and across the front, where it gains relative vorticity as the parcel compresses to match the surrounding PV. Anticyclonic parcels with anomalously low PV, are subducted from a deep mixed layer situation like FASINEX, whereas cyclonic parcels with anomalously high PV, are subducted from a shallow mixed layer. The horizontal and vertical scales of these eddies are found to be set by the frontogenesis mechanism and the mixed layer depth. A shallower mixed layer leads to shorter time scales and shorter horizontal scales, and the parcels are more likely to be only temporarily subducted. The subduction achieved by frontogenesis may be local and temporary in some situations, and permanent in others, such as that occurring at the end of winter when the mixed layer is at its deepest. In discussing the subduction mechanism, Spall (1995) goes as far as stating that "one may think of layer thickness as a proxy for potential temperature", which matches with the findings of Chapter 4, in that on isobaric surfaces, potential temperature and PV are positively correlated for the FASINEX survey.

In the case of the STERNA data set, the front studied is believed to be permanent and marks the boundary between two different water masses (Read, *et al.*, 1995). The front is more apparent in the density and salinity fields than in the temperature field. It is also a region with strong advection, bringing in water with characteristics set much further west. The survey was made in early spring, so the heating season was already underway, as seen by the fact that the ice had retreated from the frontal region in the previous week.

There was also evidence of the deep winter mixed layer in the temperature field, but not in the salinity and density fields.

These features of the STERNA front suggest that a restratification following the end of winter has taken place and that the water mass characteristics of the seasonal thermocline will have been set in a manner similar to the Vivaldi data from the North Atlantic. That is to say, the model of Woods (1985) may be said to hold for this region, and it is this mechanism which sets the PV and water mass characteristics in the seasonal thermocline on either side of the front. However, some cross-frontal motions were evident in the data, leading to the anomalous band of warmer water south of the main front, possibly due to eddies breaking off the southern side of the front (Pollard, *et al.*, 1995). It is this mixing across the front which leads to there being a range of IPV, temperature and salinity values, rather than clusters corresponding with the conditions on either side of the front.

The STERNA data show that more than one mechanism may be involved in setting the IPV in the seasonal thermocline of a region. The interplay between various mechanisms of frontal dynamics has been the subject of several investigations using frontal models, which consider the effects on PV and other tracers. In this way, Follows and Marshall (1994) looked at the exchange of mass and properties between the mixed layer and thermocline at ocean fronts, and while they found strong vertical circulations could occur, such as those in the FASINEX data set, there was no evidence of irreversible subduction of fluid at fronts. Likewise, while the FASINEX and STERNA data suggest that fluid has transferred into the seasonal thermocline, it is by no means evident that this exchange is permanent. It would need longer time series of data in these regions to look at this.

In his study of subduction of water masses in an eddying ocean model, Marshall (1997) showed that mesoscale eddies can affect the rate of transfer of fluid from the mixed layer to the thermocline, especially where there is strong baroclinic instability, e.g. at fronts. In fact, it was demonstrated that the part of the subduction rate due to eddies can swamp the mean part, and vice versa. The observational data presented in this study do not give the subduction rate, but they do indicate what degree of subduction has taken place, and it has been seen that while the Vivaldi front shows little evidence of eddy transfer of fluid to the seasonal thermocline, the other data sets do show transfer of fluid. It should also be remembered that the Vivaldi data were spatially larger-scale than the others, and mesoscale motions were not resolved.

A further interesting modelling study is that of Csanady and Vittal (1996), which analyses the flux of PV into the thermocline for the case where isopycnal outcrops migrate with the seasonal surface heating. They find that most of the PV flux due to seasonal heating is used up to stratify the ocean as the outcrops move northwards (in the northern

hemisphere). This means that in fairly quiescent regions very little PV remains to be injected into the thermocline, but in regions of vigorous geostrophic turbulence, PV transport is greater. This mechanism is an extension of the ideas in Woods (1985), where the PV is created as isopycnal outcrops migrate in spring. However, the observational data sets which fit this mechanism (Vivaldi, STERNA) neither prove nor disprove this theory, and further data sets would be necessary, perhaps including surveys taken before restratification began.

6.5 MODIFICATIONS TO THEORY SUGGESTED BY THE RESULTS

Woods' (1985) theory explains the IPV-θ relationship found in the FLW89 and Vivaldi data sets, while Spall's (1995) theory explains the FASINEX results. However, neither theory properly explains the STERNA results. If we think of the Woods (1985) model as the mechanism for the large- and mesoscale, and Spall (1995) as what occurs at submesoscale, such that the effects of their PV-setting mechanisms are superimposed on each other, then the STERNA results are better explained.

This concept of the two models combining at different scales is not in contradiction to the results of Vivaldi or FASINEX, because those data were collected on different scales, and different dynamics were occurring at those fronts. For example, the Vivaldi data showed little evidence of active frontogenesis and vertical movement of fluid across the front, while this was quite significant in the FASINEX data. Also, the Vivaldi front is permanent, lying between different water masses, while the FASINEX front is temporary and moving, although occurring in a region prone to the frequent formation of such fronts. And the third major difference between these fronts is that the FASINEX frontal zone is a result of convergent flow fields caused by the wind field, while the Vivaldi front occurs because of confluent flow between the subpolar and subtropical gyres. STERNA appears to have elements of both theories present. That is to say, background IPV levels have been set on the larger scale by outcrops retreating as the spring restratification takes place, while superimposed on this is a submesoscale re-setting of IPV on some isopycnals due to transfer of fluid across the front in response to ageostrophic circulation. This combination of the two theories appears to adequately explain the STERNA results, so it seems that it is not necessary to look for explanations through other theories.

The real question which arises in merging the two analytical models is at what point does one mechanism dominate the other, and under what circumstances? Comparisons of the Vivaldi data with output from the Atlantic Isopycnal Model (AIM), as presented in Appendix C, shows a poorer correlation between the Sverdrup IPV and isopycnic potential temperature. This is most probably due to the coarser resolution of the model output, but there is general agreement with the sense of the relationship between Sverdrup

IPV and isopycnic potential temperature. As that run of the AIM had horizontal resolution of 0.5–1°, it was unable to resolve the mesoscale and submesoscale motions. It may be that the Vivaldi region and FLW89 region produce IPV-θ relationships which are affected by these smaller scale motions, and so the combined model may be more accurate even for these eastern North Atlantic data sets, if applied at appropriate scales.

6.6 WAYS TO TEST THESE IDEAS

More information is needed to be able to draw firm conclusions about how the IPV and water-mass tracer fields are determined in the frontal regions studied. In particular, very little is known about the STERNA region of the Bellingshausen Sea, as there are very few historical data sets. There are data from a second survey of the ice edge region, across the front, which was collected a few days after the first one. This survey was not completed because of the complete loss of the SeaSoar instrument, but may still have sufficient information to shed some light on the stability and endurance of the front and velocity field associated with it. Several Southern Ocean models cover this region, but these are usually too coarse in resolution to be of use, and they often perform more poorly close to the shelf and ice edges.

While it might seem appropriate to analyse many more observational data sets in various frontal regions, on different scales, this may just add to the complexity of phenomena to be explained, while not clarifying the situations already explored. This could also be an expensive route to follow, in terms of ship-time costs, manpower, time and effort. Better returns may be achieved by using numerical models to simulate the frontal regions. With this in mind, it was decided to try to simulate one of the frontal regions using an array of one-dimensional models. This would then allow the IPV-θ relationship to be estimated and compared with the observational results. The rationale and analysis of this modelling effort is described in Chapter 7, where such an array of models is used to simulate the Vivaldi region. The models can only simulate some of the dynamics encountered in the region, for example advection is excluded, and so they are not expected to give exactly the same IPV-θ relationship as the data. However, modelling may help to confirm the dynamics that go into producing the results, and may highlight any deficiencies of Woods' (1985) model. If the modelling proves useful, it may be worth carrying out a similar exercise for each of the regions studied, providing suitable flux fields can be derived to drive the model. The Vivaldi region was selected as being the simplest of the three regions to start with.

Chapter 7. MIXED LAYER MODELLING

7.1 INTRODUCTION

Comparison of PV and water mass characteristics in earlier chapters showed results which comply with the mechanisms of two analytical models of PV-setting at the base of the mixed layer. To look at these mechanisms more closely, it was decided to model the development of the IPV and water mass characteristics at one of the regions of interest. The Vivaldi region was chosen as the most straightforward to implement, with the intention of extending the modelling effort to the FASINEX and STERNA regions during future work beyond the scope of this thesis. More climatological data (air-sea fluxes, etc.) are easily accessible for the Vivaldi region, while for other regions data might need to be collected to derive these fields.

The specific aim of this modelling work is to study the development of the temperature and IPV fields, and their inter-relationship. The chosen way to do this is to use a one-dimensional mixed layer model run with initial fields and forcing appropriate to various locations within the Vivaldi '91 region. From the output of these model runs, a simulation of results from a survey can be created, and the Sverdrup IPV-temperature relationship across the region can be studied. This allows us to look at whether the resulting Sverdrup IPV-temperature relationship is similar to that from the observed data, and to consider why it agrees or differs, within an environment where all the forcing fields are known.

In section 7.2, a short review is made of the history and concepts behind the use of one-dimensional mixed layer models. The particular UK Meteorological Office mixed layer model which is used in this study is described in section 7.3. Next, section 7.4 describes the way the model is integrated and is used to study the Vivaldi region and its Sverdrup IPV-θ relationship, while the results are presented in section 7.5. These results and their implications are discussed in section 7.6. Finally, in section 7.7, conclusions are presented along with some thoughts on extension of this modelling work to the FASINEX and STERNA cases.

7.2 HISTORY AND CONCEPT OF MIXED LAYER MODELLING

Upper ocean temperature and salinity show greater variability over shorter time and space scales in the vertical than the horizontal in many oceanic regions. In these places, vertical air-sea exchange processes and vertical mixing dominate horizontal advection and horizontal mixing in determining local conditions. This means that the upper ocean may often be treated as homogeneous along the horizontal, with change occurring in the

vertical only, and so it is feasible to use one-dimensional models to examine the processes and development of the upper ocean.

Oceanic temperature, velocity and density fields interact with each other. In a one-dimensional model of the upper ocean, the evolution of all these properties must be evaluated using a set of one-dimensional conservation equations. To solve these equations, explicit expressions are required for the turbulent fluxes. There are four techniques which have generally been used to do this (Niiler and Kraus, 1977). First, "deterministic solutions" have been used, where the initial conditions are specified on a fine spatial scale and the model is integrated forward on a fine time scale. This method is too slow and expensive for most oceanographic applications. Second, "turbulence closure models" involve Reynolds flux equations which require the calculation of higher order moments. In parameterising these calculations, extra uncertainties are introduced and it is a cumbersome process. Third, "the eddy coefficient and mixing length hypothesis" is the classical method, based on an analogy with molecular transports. This method assumes that turbulent fluxes can be expressed by the gradient of the transported quantity multiplied by an appropriate eddy diffusion coefficient. The physical basis of this method is dubious and will break down in certain circumstances. The fourth method, "mixed layer modelling" assumes a vertically homogeneous surface layer, in terms of temperature, salinity and horizontal velocity, which is a concept in agreement with observations from many parts of the world's oceans showing that the surface layer is well mixed. The existence of a mixed layer allows the vertical integration of the system of one-dimensional conservation equations, which gives expressions for the turbulent fluxes in terms of mean quantities and external inputs. This method is the easiest and most useful to implement in order to examine the development of the mixed layer during the annual heating cycle.

In mixed layer models, a flux of turbulent energy is necessary to entrain denser water through the base of the mixed layer. This energy flux is provided by heat, buoyancy and momentum fluxes through the ocean surface, along with small-scale dissipative effects. The original mixed layer model by Keith Ball (1960) did not include any mean horizontal motion. Kraus and Turner extended and modified this model for oceanic use to produce the "standard" Kraus-Turner mixed layer model (Kraus and Turner, 1967). Other recent models have been based on the same principles. Mixed layer models invariably assume that the mean temperature, salinity and horizontal velocity are fairly uniform in the mixed layer. It is also assumed that on the depth and time scales of the model, these fields are near discontinuous across the atmosphere-ocean boundary, and the lower mixed layer boundary with the ocean interior. Most models, but not all, additionally assume that the local rate of change of the turbulent velocity variance is much smaller than the generation

and dissipation effects of turbulence, and they neglect temperature changes associated with frictional dissipation and with changes in salinity. There are other assumptions in any model, including those which enable estimation of the flux boundary conditions at the sea surface and at the base of the mixed layer, and dissipative effects. The particular model to be used in this work is described in the next section.

7.3 DESCRIPTION OF UK METEOROLOGICAL OFFICE MIXED LAYER MODEL

The UK Meteorological Office Unified Model is based on the Kraus-Turner (1967) bulk mixed layer approach, which balances the energy available for mixing the water column with the buoyancy variations at the sea surface, such that water is mixed down from the surface until no mixing energy remains. This description of the implementation of the model is based on the thorough description in a UK Meteorological Office internal document (Foreman, 1990).

The model is based on the principles of energy conservation, and three major assumptions are made in formulating the model. The first is that all surface fluxes are used up. That is, heat flux is used to heat the column, all fresh water flux modifies salinity, and all other tracer fluxes modify the corresponding tracer values. Second, all the kinetic energy available for mixing is used to increase the potential energy of the water column. Third, mixing is instantaneous.

The heat content of the mixed layer, of depth d, is defined as

$$H = \rho_0 c_p \int_0^d \theta(z)\, dz \tag{7.1}$$

and the potential energy is defined as

$$P = -g \int_0^d \rho(z)\, z\, dz \tag{7.2}$$

where z is the vertical coordinate, ρ_0 is a reference density, θ is the potential temperature, c_p is the specific heat capacity of sea water at the surface, $\rho(z)$ is the depth profile of the potential density with reference to the sea surface and g is the acceleration due to gravity. The equations (7.1) and (7.2) are discretised for model implementation, as summations over N layers at depths h_n for n=1 to N. The base of the mixed layer is calculated by the energy balance and does not need to coincide with an interface between model layers.

Several basic quantities are used in calculating the energy balance. These are: the non-penetrative heat flux (Q_N); the change in density at the surface due to non-penetrative heating and fresh water exchange with the atmosphere ($\Delta\rho_N$); the penetrative component of the surface heat flux ($Q_S(z)$); the density change due to the penetrative heat flux ($\Delta\rho_S(z)$); and the mechanical energy which is available for mixing water in a stably stratified column (M_0). A few other coefficients are set within the model and held constant. These are: the proportion of surface mechanical mixing which is available for mixing the ocean interior (λ set to 0.7); the rate of decay of mechanical energy with depth (δ set to 100 m); and the proportion of potential energy released by the overturning of unstable layers which is available for mixing lower in the water column allowing convection to penetrate into stable layers (ε set to 0.15).

There are three basic stages to the mixed layer model. The first is to increment the tracer values with the profile derived from surface fluxes and to deplete the mechanical energy. This is a straightforward procedure where temperature changes in each layer are calculated by

$$\Delta\theta = \Delta Q(z)\Delta t \Big/ \left(\Delta z c_p \rho_0\right) \tag{7.3}$$

where $\Delta Q(z)$ is the heat flux absorbed in the layer of thickness Δz, and Δt is the time step. Similar calculations are performed for salinity and other tracers. The mechanical energy is depleted simply by multiplying the incoming energy, M_0, by the scaling factor, λ.

The second stage is to calculate the energy required to mix each layer internally and to calculate density changes arising from the changed tracer profiles. While these calculations are described here, the equations have been omitted. Assuming that the non-penetrative fluxes are absorbed at the ocean surface, energy is required to mix the layer if the fluxes make the water less dense, or energy will be released by convection if the water becomes denser. Following this, if convection occurs the mixing energy is increased and it is depleted if the column stabilises.

Below the surface, the density is changed by the penetrative solar heat flux, which has a known vertical profile $Q_S(z)$. This cannot be converted directly to a profile of density changes because density is nonlinearly dependent on pressure, temperature and salinity. Instead, a simplification is made in the calculation of the change in potential energy with depth for the solar heat flux, by calculating the density change at layer n from the change in temperature of the layer.

More heat is absorbed in the top part of each layer than in the bottom part, and energy is used to mix within the layers. This means that the profile stabilises within the layer, and

potential energy increases due to solar heating to a level above the mixed state energy, so energy is used in mixing the layer wherever there is surface heating. This further reduces the energy left for mixing between layers.

The density change at the surface is calculated using the full density calculation, but to reduce computation, density in each lower layer is assumed to depend linearly on temperature, and vertical variations in the coefficient of proportionality are ignored. Therefore, at each level the density change due to the penetrative heat flux is in proportion to the surface density change.

The third stage of the model works downwards from the sea surface, examining each layer in turn. The tracers are mixed between the mixed layer and the new layer if the two layers are unstable or if there is mechanical energy available to mix between stable layers. Then, starting at the second layer (as long as ocean exists at that depth), a sequence of calculations is performed for layer n, representing mixing between the mixed layer and layer n.

First, the mechanical mixing is decayed. Then, the energy needed to mix the water in the lower layer with that in the mixed layer is calculated (neglecting the non-linear dependency of density on temperature and salinity) by summing the potential energy of the two layers and subtracting the final potential energy state. The density which occurs from the complete mixing of the water in the mixed layer with the layer below is then easily calculated. However, a decision must be made as to whether full or partial mixing occurs, according to how much energy is available. The energy required for full mixing is compared with the mechanical energy available for mixing to level n. If there is not enough mechanical energy available then partial mixing is performed, which is more complex than full mixing.

If there is enough mechanical mixing energy available to fully mix the water in the mixed layer with that in the layer below, then all tracer values, Θ, are set in the new mixed layer (from surface to layer n) according to the assignment statement:

$$\Theta_{new} = \left(\Theta_{mix} h_{n-1} + \Theta_n \left(h_n - h_{n-1}\right)\right) / h_n \tag{7.4}$$

The mixed layer density is reset and the mixing energy modified. Where the stratification is initially stable the energy required for mixing is subtracted from the available mechanical energy, but if the layers were convectively unstable, the mechanical energy is increased by a proportion of the potential energy released by convection. The calculated mixed layer depth is taken as the base of the layer to which mixing has taken place.

However, if there is not enough mechanical mixing energy available to mix a complete layer into the mixed layer, as will often be the case, then partial mixing is allowed by the model in such a way that energy and tracers are conserved. This is much more convoluted than the full mixing case, and will not be described fully here. Although the mixed layer depth is not part of the energy balance calculations, a level may be defined to which mixing would have occurred in a continuous model with identical density and tracer profiles. This diagnostic calculation assumes that heat and potential energy are conserved and that mixing occurs to a depth $h_{n-1}+d$, which lies between layers in the finite difference model. Conservation of heat yields a new tracer concentration equation

$$\Theta_{new} = \frac{h_{n-1}\Theta_{mix} + d\Theta_n}{h_{n-1} + d} \tag{7.5}$$

and conservation of potential energy gives a modified mechanical energy for mixing which is dependent on d. This can then be solved for, and, after some further complicated algebra to correct for distorted physics due to different time steps in each layer (except where rapid changes occur such as in the mixed layer), the system of equations can be closed, and the values of tracers and density can be calculated for the partial mixing case.

7.4 IMPLEMENTATION OF MODEL

7.4.1 Initialisation and control of the model

Initial temperature and salinity profiles may be fed into the model to start it off. For this implementation, it was decided to use the Levitus 1994 climatology (Levitus and Boyer, 1994, Levitus, *et al.*, 1994). These data are built up from hydrographic data over many years and are provided on CD-ROM. They consist of profiles vertically gridded on 33 standard (unevenly spaced) levels from the surface to the ocean bottom or 5500 metres, and on a 1° latitude-longitude grid. The profiles are available as annual, seasonal and monthly analyses of the source data to give climatological values. The monthly analyses often suffer from a lack of data within 1° boxes, and so the seasonal and annual data were used to initialise the mixed layer model. Profiles were extracted from the climatology at the correct latitude and longitude, and then interpolated on to regular levels from 0 to 400 metres at 10 metre intervals.

The model relies on heat and freshwater fluxes, and wind fields to provide forcing. It was decided to use climatological fluxes, as contained in the COADS climatology, and extracted for the north-east Atlantic (pers. comm. John Hemmings and Simon Josey, Southampton Oceanography Centre). These fluxes are monthly averages and gridded to a 1° latitude-longitude grid. The annual cycle of fluxes was extracted at each grid point

where the model was to be implemented, and stored in a data file to be read by the model. The data contained in this file were the sensible heat, latent heat, long wave, short wave and freshwater fluxes and the wind speed and standard deviation. In fact, the freshwater flux was set to zero throughout this region because of lack of observations. However, this is not an unreasonable approximation, as shown by Schmitt *et al.* (1989). These fluxes could perhaps be replaced by more accurate observations made during cruises such as Vivaldi, but at the time of carrying out this work, these were not available. At some locations, the climatological heat fluxes do not balance completely. This would lead to excessive and unrealistic deepening of the mixed layer during model runs of many years, without advection to balance the energy. Instead, the model makes an adjustment, within the mixed layer, for any flux imbalance so that they are, in effect, balanced.

7.4.2 Running the model for this application and analysis techniques

As it is the aim of this modelling work to study the development of the temperature and PV fields, and their inter-relationship within a simulated "Vivaldi '91 region", the model was run a number of times. Each run was to simulate the development of the temperature and salinity fields at a specific location, and when the output from all the runs were considered together a survey was simulated. The model does not calculate IPV, so this was carried out for the model output and the Sverdrup IPV-θ relationship studied and compared with the observed Vivaldi results.

As the variations in the Vivaldi data set were principally meridional, it was decided to use the model to look at the variation along one latitude section at 20°W, corresponding with survey section Z. The model was to be run at latitudes from 38 to 54°N, at separations of 1° of latitude.

The fluxes and initial temperature and salinity profiles were extracted from the larger source files for each latitude-longitude point at which the model was to be run. Then the model was run on a UNIX workstation, using a UNIX script to control the procedure. This procedure included converting the Levitus temperature from '*in situ*' to potential temperature, which is used in the model. The model itself was run using a "switches" data file to control it. This switches file sets the file names for the initial temperature and salinity profiles, the flux file and output files. It also contains values for the start day and year, end day and year and the vertical extent of the profiles. Day 0 corresponds with January 1st. A two hour time-step was used over a 365-day year during all runs of the model. Temperature and salinity profiles corresponding to each day of the final year of the model run were then stored and '*in situ*' temperatures calculated. The Sverdrup PV was then calculated according to equation 2.3. This procedure was followed at all the latitudes along the 20°W "section".

The array processing package MATLAB was used to examine the output files from the model, and to produce plots of various quantities. In particular, a movie sequence of the temperature and salinity profiles was used to check that the model was running correctly at single locations, using output from different implementations of the model. For example, with initial profiles from different seasons, and using model runs of various lengths. The results of this examination are presented in the next section which looks at the stability of the model. Plots were also produced for the simulated "section" of model output.

7.4.3 Stability of the model

To look at the stability of the model, it was run for various lengths of years from the same initial conditions, and the resulting temperature and salinity profiles were examined. Model runs were used from 2 to 10 years, from initial conditions corresponding to winter Levitus values at 20°W 38°N and 20°W 54°N. Conclusions from these were that the model is fairly stable for runs of 4 years or more, as the mixed layer depth ceases to vary much for longer runs. The maximum mixed layer depth occurs at different dates for the two locations, being about 150 metres on day 55 (25 February) at 38°N and about 350 metres on day 92 (3 April) at 54°N, which dates correspond with the beginning of the heating season. The temperature jump at the base of the mixed layer is very small (~0.1°C) at this time. The shallowest mixed layer depth occurs round about day 240-246 (end of August, beginning of September) for both locations at depths of 20–40 metres, and this corresponds with the end of the heating season. The temperature jump at the base of the mixed layer is quite large (~6–8°C) at this time. A deeper thermocline is maintained at 150–350 metres which corresponds with the maximum extent of the mixed layer, and never quite disappears even when the seasonal thermocline has shoaled to near-surface. The temperature values themselves are steady over the years, further indicating stability of the model. Very little happens with the salinity profile because of the assumed zero freshwater flux. The cycle of the changes in the profiles is quite consistent over the years. All in all, these features give confidence that the model is behaving in a stable manner for these forcing fields and initial conditions.

The model results were also compared with the results from section Z of the Vivaldi data. While the temperature and salinity values gave good matches, peak Sverdrup IPV values were often larger by a factor of 10. However, the patterns of the isolines were similar, so this was accepted as being due to the model allowing very small values of isopycnic thickness which would not be resolved in observed data. The model isotherms tend to deepen more quickly than the Vivaldi isotherms, but the match is better for models initialised with the summer and autumn Levitus values, rather than annual, spring or

winter. The depths of isopycnals correspond well between model and data, although the surface densities are larger for the model.

These stability investigations established that the main model run should be carried out using summer Levitus values to initialise the temperature and salinity fields, and that the model should be run from that date on year 0 to the end of year 5. Day 228 (17 August) was used as the date corresponding to the summer Levitus data, which is a 3 month average over July, August and September, and the model was integrated forward from this date.

7.5 MODEL OUTPUT FOR VIVALDI REGION

The main model runs for locations along 20°W were carried out at intervals of 1° of latitude, and the output analysed. Day 137 (18 May) corresponds with the middle of the period during which section Z of the Vivaldi survey was carried out, and so the output for this day was closely examined. Sectional plots of potential temperature, salinity, Sverdrup IPV and isopycnal depth are shown in Figure 7-1. The potential temperature plot shows there are two thermoclinic regions, with a lesser one on surfaces lighter than 27.5 kg m^{-3} corresponding to the seasonal thermocline, and a deeper one with higher Sverdrup IPV values corresponding to the maximum mixed layer depth at the end of winter. It is this shallower thermocline that is reckoned to be similar to the Vivaldi seasonal thermocline because of the density values. Indeed, the Sverdrup IPV values shown in Figure 7-1 are similar in magnitude to those in the Vivaldi data of Chapter 3, reaching maxima of O(5 PVU). Isopycnals within this region (26.85 through to 27.30) are considered in more detail below.

Figure 7-2 shows time series of the potential temperature and Sverdrup IPV on isopycnals 26.85, 27.00, 27.15 and 27.30 for each day of the final year of the model, at 3° latitude separation along 20°W. These show that at all latitudes, the temperature varies slightly throughout the year, oscillating slightly as it rises in the autumn and early winter, and that most of these surfaces outcrop into the mixed layer at the end of winter, and are maintained there at the same temperature until the heating season starts to wane. At the most southerly latitudes, the denser isopycnals are free of the mixed layer throughout the year. During times when the isopycnals are stratified and free of the mixed layer, the Sverdrup IPV is seen to rise from negligible levels to large levels which oscillate in the autumn. Day 137 (15 May) is seen to correspond with a time when most isopycnals have recently restratified, and Sverdrup IPV levels are beginning to rise.

Sverdrup IPV against potential temperature plots were prepared for the same four isopycnals, and examined at weekly intervals, from day 1 to 364 at 7 day intervals. The

plot for day 140, which lies within the dates of the Vivaldi survey, is shown in Figure 7-3. In itself, this plot says very little, except that different relationships are observed on different isopycnals, with the lighter isopycnals showing evidence (negligible Sverdrup IPV levels) of still being outcropped at some latitudes. However, as the year goes on, these plots change considerably, and often quite quickly. By day 161 (11 June), which is towards the end of the Vivaldi survey time, the results are as shown in Figure 7-4. On isopycnal 27.15, a curve similar to that of the Vivaldi survey is seen, showing a high Sverdrup IPV-low temperature correspondence over most of the temperature range. By day 203 (23 July), as shown in Figure 7-5, this is the situation on all four isopycnals. Throughout the rest of the year, the relationships continue to evolve. At most times, the curves take the form of a peak with lower regions either side. This peak moves across the range of temperatures present on that isopycnal, and its position influences whether most of the curve has a positive or negative gradient.

7.6 DISCUSSION

Although this model has some serious discrepancies in modelling the Vivaldi region, it nonetheless recreates some similar features in the horizontal temperature and Sverdrup IPV structure. The disagreements are seen in the density structure, the model being denser than reality at similar locations and times of year. It was pleasing to find that the Sverdrup IPV-θ relationship is similar in late spring to the Vivaldi relationship, although the values of Sverdrup IPV are much higher in the model, along with the gradients. The relationship varies with the density, so it is clearly important to establish a better simulation of the density structure when trying to model this part of the North Atlantic.

The oscillation of the Sverdrup IPV values in the autumn, and the high values of Sverdrup IPV need further investigation. These may be due to problems with the forcing fields used in the model, and it would be a good next step to look at the effects of varying the forcing fields of the model, both in their magnitude and their timing.

7.7 CONCLUSIONS

This has been a very brief look into what can be learnt by using an array of mixed layer models to study the formation of IPV and potential temperature structure in the ocean. Clearly, this area of work can be continued much further. It seems that the annual heating cycle may indeed be the primary factor in determining the IPV and potential temperature structure on isopycnals just below the mixed layer in the spring, but more investigation would be necessary to demonstrate this thoroughly.

On certain isopycnals at certain times of year, a similar Sverdrup IPV-θ relationship to the Vivaldi observations was seen, which suggests that the physics within the model are sufficient to explain it. That is to say, no further processes are responsible for the relationship developing in this way, although they may modify it. There is a suggestion in Figures 7-3, 7-4 and 7-5 that at some times and on some isopycnals, the Sverdrup IPV-θ relationship may have a positive correlation, and this may be relevant to why the FASINEX data showed such a relationship.

This first attempt at modelling the Sverdrup IPV-θ relationship has shown that modelling could prove to be a useful tool in looking at how these relationships are formed. More sophisticated efforts would also have to make some allowance for advective fields, which are important in frontal regions in particular.

Fig. 7-1 Section plots from model, day 137 year 5.

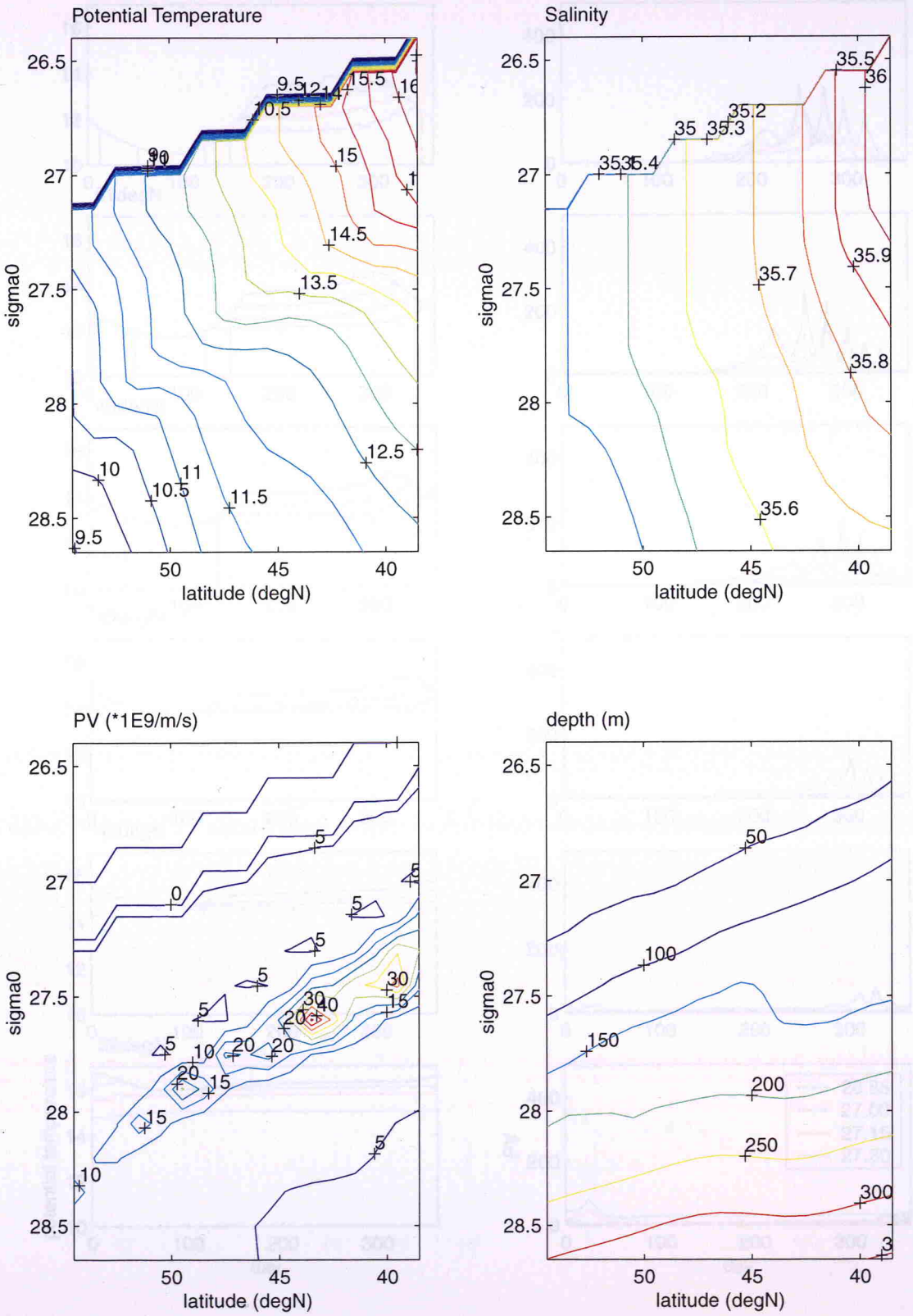

Fig. 7-2 Time series of potential temperature and PV from model at selected latitudes.

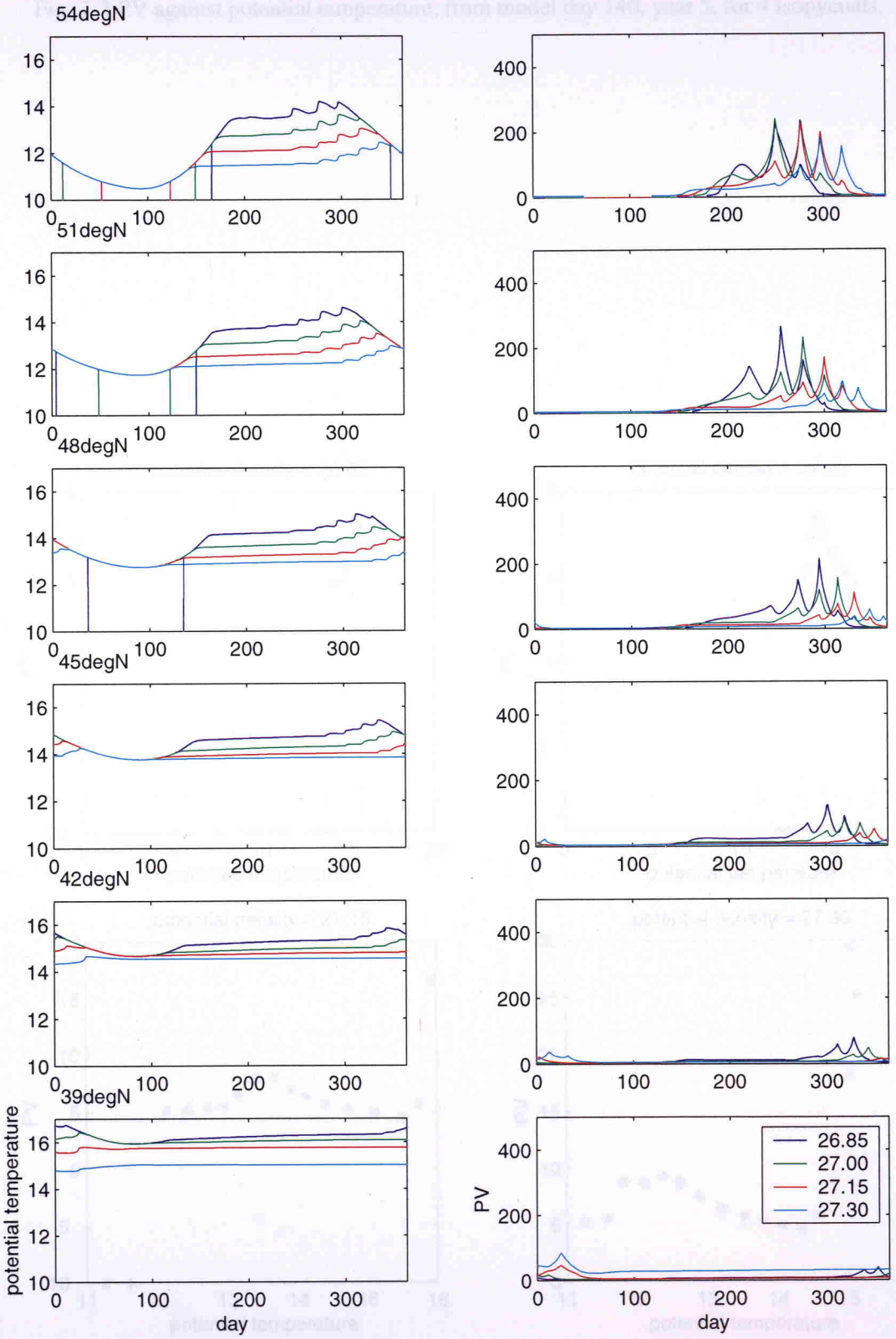

Fig. 7-3 PV against potential temperature, from model day 140, year 5, for 4 isopycnals.

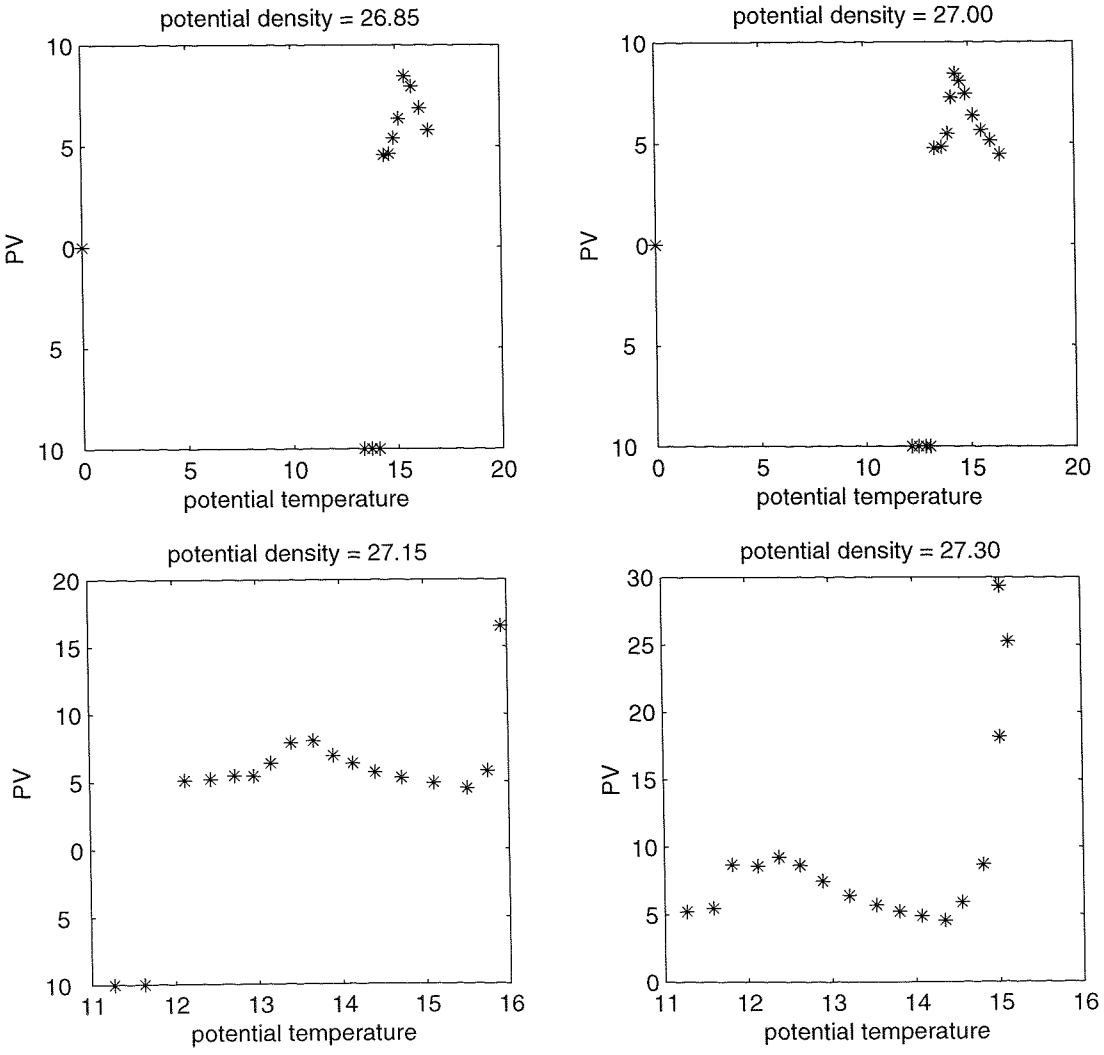

Fig. 7-4 PV against potential temperature, from model day 161, year 5, for 4 isopycnals.

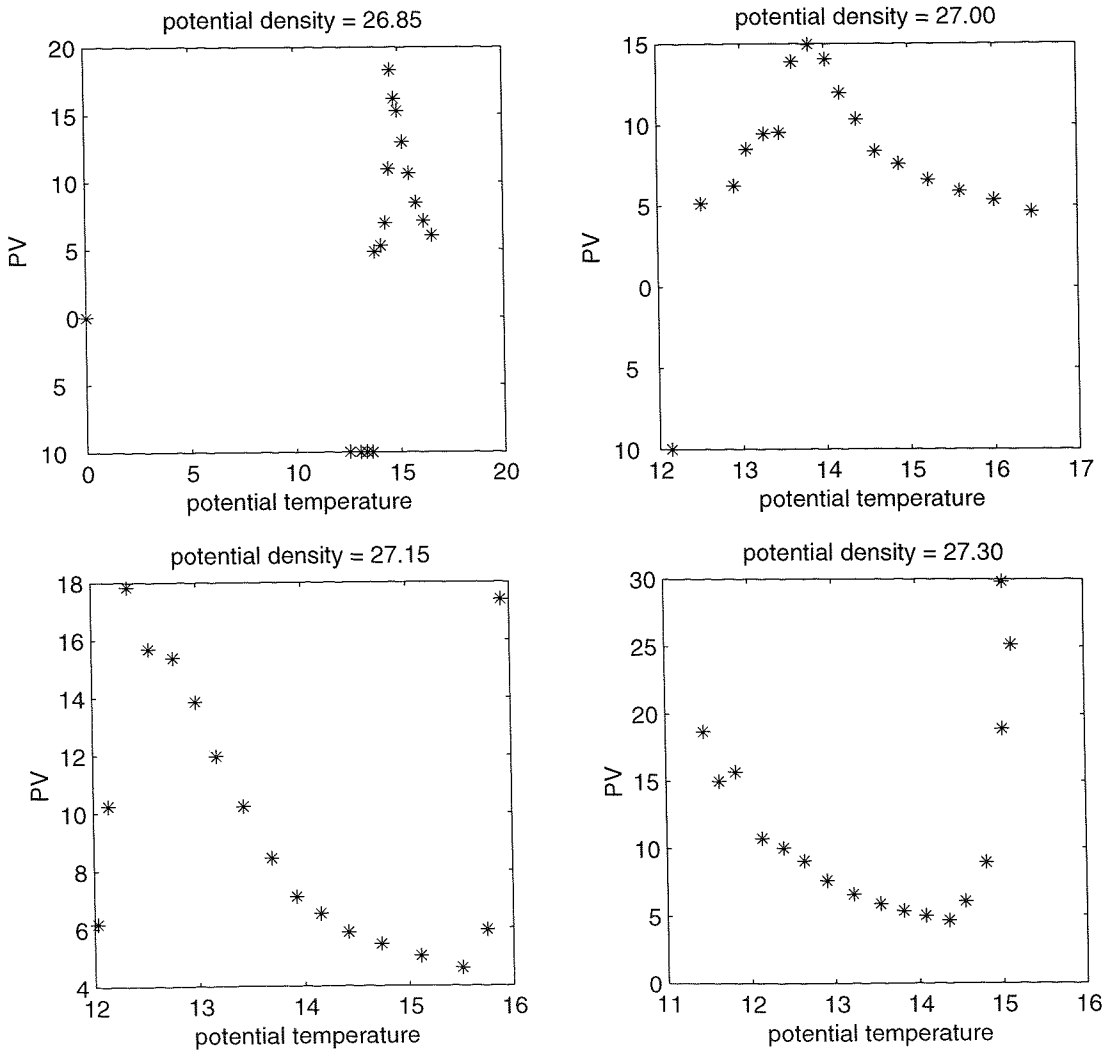

Fig. 7-5 PV against potential temperature, from model day 203, year 5, for 4 isopycnals.

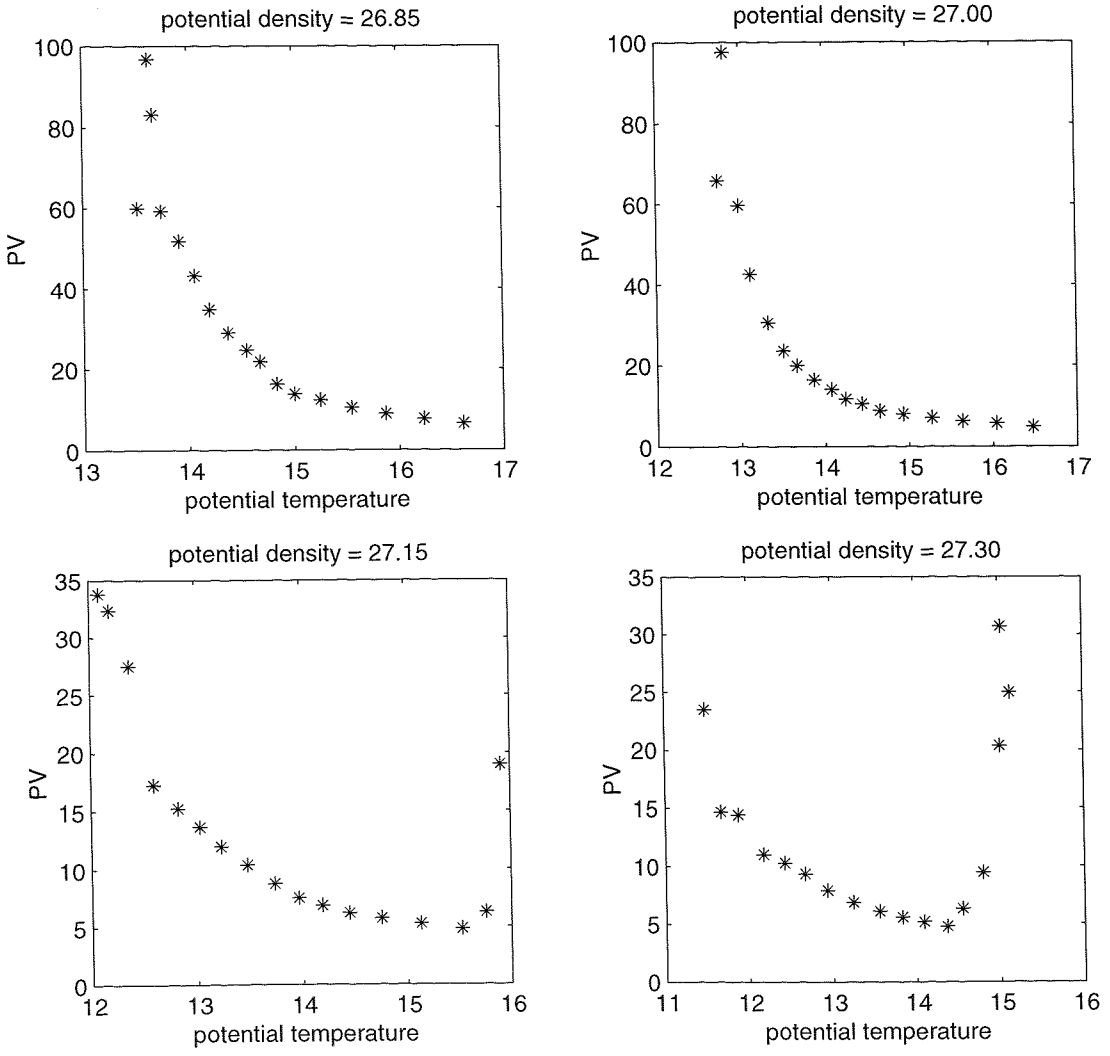

Chapter 8. CONCLUSIONS

8.1 ACHIEVEMENTS

Fischer *et al* (FLW89) found a near-linear relationship between IPV and isopycnic potential temperature on a shallow isopycnal in the North Atlantic during the summer of 1981, and showed that relative vorticity made a significant contribution to IPV on small scales. This relationship was also evident in climatological values of Sverdrup IPV and temperature in the north-east Atlantic. Lack of published results indicates that these inter-relationships have not been thoroughly examined, although some researchers have made assumptions about them, or noted perceived correlations. In Chapter 1, a number of specific objectives were laid out with the overall aim of investigating the inter-relationships between PV and water-mass characteristics. These objectives have been achieved, and they are reviewed here.

The first objective was to define PV, and this was carried out in Chapter 2. Full PV includes a relative vorticity term which may be neglected on the gyre-scale. This form of PV is called Sverdrup PV. On shorter scales, relative vorticity is significant and so the full PV should be used. Formulations were given for calculation of isopycnic PV from data gridded on isobaric surfaces.

The second objective was to assess the best way to derive and map PV from hydrographic survey data. The history of mapping hydrographic quantities on isopycnals and the more recent mapping of PV was described in Chapter 2. The convention has been established of calculating PV from hydrographic data and then interpolating these onto isopycnal surfaces for mapping. The PV patterns may then be used to infer the oceanic circulation. This review of PV mapping in the literature illustrated that the accuracy and errors are complex to quantify, but that established procedures exist to reduce the errors, and these were implemented where possible in the data analyses.

The next objective was to find out whether the relationship found in FLW89 is universal, and this was achieved by examining three data sets from different frontal regions.

The first data set examined was from the Vivaldi '91 cruises in the north-east Atlantic, between 39–54°N and 12–32°W, during 25 April to 10 June 1991. The survey consisted of north-south sections at 300 km separation. This region lies between the subpolar and subtropical gyres where there is a weak mean circulation, and the dynamics are complex and ill-understood. Different water mass types were identified on either side of the front through the survey region. This occurred because of the confluence of water from the two

gyre systems. The Vivaldi data on isopycnal 27.00 kg m^{-3} showed a well-correlated relationship between Sverdrup IPV and isopycnic potential temperature θ (gradient = -0.29 PVU K^{-1}, correlation coefficient r = -0.80), and a more scattered relationship between Sverdrup IPV and near-surface temperature (-0.12 PVU K^{-1}, r = -0.57). Similar relationships were found between Sverdrup IPV and salinity. These results were in close agreement with the IPV-θ relationships found by FLW89 in a similar region (-0.31 PVU K^{-1}, r = -0.79), and with the relationship found using climatological values for the North Atlantic (-0.25 PVU K^{-1}).

The second data set was a fine scale survey from the FASINEX campaign carried out south-west of Bermuda within 27–29°N and 69–71°W, during 16 to 20 February 1986. The survey sections lie north-south and at 16 km separation, which is much finer scale than the Vivaldi data. This survey measured hydrography in the vicinity of an ocean front within the subtropical convergence zone (STCZ). No water mass change was identified across the front, which lies in a region of confluent flow due to the mean wind field. Anticyclonic eddies were observed in the data set, which were held responsible for the transfer of fluid across the front. On isopycnals, only weak relationships were observed between full IPV and potential temperature, and these had positive gradient of an order of magnitude greater than those already found in the north-east Atlantic. For example, for the isopycnal 25.70 kg m^{-3}, the gradient is 2.95 PVU K^{-1} and the correlation coefficient, r, is 0.68.

The third data set was a fine scale survey of an ice-edge front in the Bellingshausen Sea which lies to the west of the Antarctic Peninsula. The survey was carried out within 68–69°S and 83–87°W during 23 to 28 November 1992. The north-south sections were separated by 8 nm (approximately 14 km). The front was discovered to be quite stable and at the boundary between different water masses which were advected in from the west. Salinity changes were more significant across this front than temperature changes. An extremely well-correlated relationship was recorded between full IPV and potential temperature (for 27.5 kg m^{-3}: -0.11 PVU K^{-1}, r = -0.97), and similarly between IPV and salinity, on isopycnals which lie clearly in the pycnocline below the remains of a temperature mixed layer which reaches deeper than the density/salinity mixed layer. These relationships are similar in sign and magnitude to those in the north-east Atlantic where conditions are quite different. However, on shallower isopycnals, the relationship breaks up rapidly and there was no evidence of a relationship between IPV and near-surface tracer values.

These results show that the relationship found by FLW89 is not restricted purely to the north-east Atlantic, because a similar result is seen in the STERNA data. However, they also show that the same relationship does not hold everywhere, as is seen by the

FASINEX results. The Vivaldi results also show that the north-east Atlantic relationship holds on different scales to the FLW89 survey, and that they endure in different years.

The next objective was to explain the reasons why the three data sets show different IPV-θ relationships. This was carried out in Chapter 6. The Vivaldi Sverdrup IPV and θ values are believed to have been set at the time of the restratification of the seasonal thermocline at the end of winter. The variation in values occurs because of the different sources of water from the two gyre systems, and the change in the rate of migration of the isopycnal surface outcrops, which determines the IPV. This may also be the case for the STERNA data, although the restratification process almost certainly occurred upstream of the survey region. The FASINEX data were from a transient front in a convergent region of only one water mass, and the variation in its IPV-θ values is held to be due to frontal ageostrophic motions. Anticyclonic eddies transfer fluid across the front, with IPV and θ already set. This leads to a different relationship to that found in the permanent confluent frontal situations of Vivaldi and STERNA.

The next objective identified was to examine theories for the setting of IPV and temperature in the upper ocean, and to consider how these may account for the results obtained. This was also carried out in Chapter 6, where Woods' (1985) analytical model was described, which accommodates the mechanism suggested by FLW89 as responsible for the results in the north-east Atlantic. Woods' model is believed to account for the Vivaldi results, and partially accounts for the STERNA results. Spall's (1995) model explains the FASINEX data.

A further objective of this work was to consider what modifications to current theories are suggested by the data, if any. In Chapter 6 again, it was noted that neither Woods' nor Spall's model properly accounted for the STERNA results. A combination of these two models was suggested, with frontal processes occurring on different spatial scales to the restratification processes.

Finally, there was an aim to follow the development of the temperature and IPV fields, and their inter-relationship, using a one-dimensional mixed layer model to simulate various locations within the Vivaldi '91 region. This was done in Chapter 7, and allowed comparison of the modelled Sverdrup IPV-temperature relationship with the observed data from Vivaldi. The UK Meteorological Office mixed layer model was run for 5 years with initialisation corresponding to locations at 1° intervals from 38–54°N along 20°W, and the output temperature and salinity fields were analysed. Sverdrup IPV was calculated from these values, and the Sverdrup IPV-θ relationship investigated. It was found to be similar to the observed relationship on certain isopycnals and at certain times of year. This indicated that the annual heating cycle does indeed play a significant role in

determining Sverdrup IPV-θ values, but more investigation would be necessary to make firmer conclusions. For example, some discrepancies were noted in the model's density field when compared with the observed density, and these should be cleared up.

Having worked through the set objectives, it is clear that the relationship between IPV and water mass tracers is a complicated matter, but very interesting. There are clear benefits to be gained in understanding this relationship, not least to help improve the design of ocean circulation models, but also to confirm or discount some of the assumptions which are made in the literature about the links between PV and other tracers.

8.2 FUTURE WORK

While progress has been made in the quest to understand the relationship between IPV and other water mass tracers, there still remains a lot to explain. In order to achieve this, it would be worthwhile to model the development of the IPV and tracer values throughout the year, at different locations. To improve the results, better surface flux fields would be desirable. However, varying the forcing strength, pattern and cycle would also be interesting, as this would allow the investigation of how these affect the development of the tracer fields (including IPV). It would also be desirable to extend the modelling effort to simulate the other geographical regions studied.

Furthermore, it would be interesting to examine any other suitable hydrographic data sets from other regions. As a first effort, the other ice edge survey made during the STERNA cruise should be examined, to look at the stability of the relationship there just a week later.

Finally, the author would like to investigate the horizontal patterns of PV and other tracers in looking for correlations. Because of the flow of water along isopycnals, the values of IPV, temperature and salinity on isopycnals are displaced horizontally from the place where they were set. It would be interesting to see whether the subsurface fields bear any relationship to the surface values. If so, this could account for the visually good correlation between satellite images and modelled IPV fields as reported at the outset of this work, but the poorer correlation found between surface temperature and subsurface IPV values at the same location.

8.3 FINAL COMMENTS

Driven by interest in measuring the oceanic velocity field from space, sea surface temperature (SST) has been suggested as a proxy for potential vorticity (PV), which may

then be inverted to give the velocity. However, little is known about the relationships between PV and other water mass tracers. It was difficult to map PV until recent years when hydrographic technology improved greatly, but now it can be mapped from scales of a few kilometres up to the gyre-scale. This thesis has considered the inter-relationships between IPV, SST, potential temperature and salinity in three quite different frontal regions of the ocean, and found quite different results. The reasons for this were examined, concentrating on frontal processes and water mass formation. Theories for setting IPV and tracer values were investigated, and a one-dimensional computer model was used to follow the development of the relationship in the north-east Atlantic.

In conclusion, use of sea surface temperature as a proxy for PV, to be inverted to obtain the velocity field, is not recommended in general. In certain locations, under particular dynamical circumstances, this method may prove feasible, but further knowledge of the inter-relationship between PV and temperature is needed before these circumstances can be established.

Appendix A. OCEAN VELOCITY FROM SATELLITES

A.1 REMOTELY-SENSED TRACERS OF SURFACE FLOW

A tracer of surface flow is a material particle or property of the water which varies spatially and temporally and is dependent on the velocity of the flow. To be remotely sensed, a tracer must exhibit a signature that can be detected by a satellite borne instrument (Stow, 1987). This means that the tracer signature needs to be radiated to be measured by a passive instrument, or reflected in the case of active instruments, and the tracer magnitude must vary with variations in the flow. It must also be possible to transform the distribution of the radiated signature into an accurate map of the tracer distribution. To be able to interpret maps obtained in this way, it is necessary to have some knowledge of the sensor's penetration depth at its operating wavelength, that is, whether the radiated signature represents, say, the surface millimetre, or the top ten metres of the ocean. Complementary to this, one also needs to know the tracer's vertical distribution within that penetration depth. A final requirement is that one must know to what degree the tracer is conserved between sequential images: that is, one needs to know how the tracer changes with time, rather than moves with the flow.

How well any tracer is measured depends on several factors. One must have the technical ability to resolve the tracer's features both spatially and temporally. It must also be possible to observe the ocean at the desired positions and times. This is much simpler to achieve using satellites rather than ships or aircraft, although clouds and other atmospheric effects may still interfere with the measurements. Probably the most important factor is how thoroughly understood are the tracer properties, horizontally, vertically and with regard to diffusion.

Remotely sensed tracers of surface flow which have been used include the following: fluorescent dyes and man-induced pollutants; suspended sediment; chlorophyll-a and other chlorophylls in phytoplankton; sea-surface height; sea-surface temperature (SST). The dyes and pollutants have had limited use, and suspended sediment is really only of use in estuarine and coastal waters. Chlorophylls alter the colour of the sea-surface, which can be detected by radiometers operating in the appropriate spectral bands, such as the Coastal Zone Color Scanner (CZCS) which was operational during 1978–1986 and had several visible channels. These data are potentially of great use but CZCS was the only such instrument to have been deployed until recently when the Modular Optoelectronic Scanner (MOS) was deployed aboard the Indian Remote-sensing Satellite P3 (IRS-P3) in March 1996 (Cipollini and Corsini, 1996). A duplicate MOS instrument is aboard a module which docked on the Russian space station MIR in April 1996 and the Ocean

Colour and Temperature Sensor (OCTS) was deployed on the Japanese ADEOS satellite between August 1996 and July 1997, when it ceased to function. The Sea-viewing Wide Field-of-view Sensor (SeaWiFS) was launched in August 1997 aboard the United States' SeaStar spacecraft, and is intended to continue returning high quality ocean colour measurements for 10 years. It is expected that these instruments, and others which are due for deployment in the near future, will lead to greater use of ocean colour in determining surface flow. Sea-surface heights from radar altimetry can be converted to a measure of surface flow if the flow is assumed to be geostrophic (Marshall, 1985). However, the altimeter's measurements are of a single footprint beneath the satellite track rather than scanning over a wide swath to create an image of a large area. This means that the velocity field derived from altimetry is sparser than that derived from an image. To date, the SST has been the most widely used tracer for surface flow, and can be derived from passive measurements of the infrared energy emitted from the sea-surface.

A.2 APPROACHES TO ESTIMATING SURFACE CIRCULATION FROM SATELLITES

There are three basic ways to approach the estimation of surface circulation from satellite data (Stow, 1987):

1) single-date descriptive approach: a qualitative process involving the visual analysis of a single image by a human being, or automated to some extent. An image is examined for tracer patterns following a path from a source, and is described in terms of these patterns.

2) Lagrangian drift: a quantitative analysis of a number of spatially-registered (geolocated) time-sequential images, carried out by tracking tracer features, for example eddies, often by automated techniques. The positions of the features are followed in successive images, and so flow is estimated in the regions around these features.

3) Eulerian modelling methods: also a quantitative analysis of a number of spatially registered time-sequential images. Spatial and temporal gradients are calculated and used to evaluate the flow at each point on the image rather than just where there are distinct features such as a front.

Some examples of the more frequently used quantitative approaches are described and evaluated in the next section.

A.3 EXISTING METHODS FOR EVALUATING SURFACE FLOW FROM SATELLITE IMAGES

To derive velocity fields according to the approaches outlined above, two methods are commonly used. The first method is to follow the motion of small features — hence, this is called "feature-tracking" — which are assumed to be conserved between successive images and to have been advected by the underlying flow. The second method is to require that the velocity field complies with certain physical principles, for example, the conservation of temperature between images, so that any differences are due to the flow. This second method is an inverse modelling technique. Both these methods require that time-sequential, spatially registered images are used, and the spatial registration must be carried out to a high degree of precision. These methods are described next, highlighting their advantages and drawbacks.

One way of carrying out automated feature-tracking is to use Maximum Cross-Correlation (MCC) between successive images, where the dependence on a human operator, which is difficult to evaluate, is removed. This technique was originally suggested for tracking clouds (Leese, *et al.*, 1971) and was first applied to oceanic feature tracking by Emery *et al.* (1986). This technique can be applied to both SST and ocean colour images. The MCC technique (fully explained in Emery *et al.* (1986) and Garcia and Robinson (1989)) is carried out by comparing images which cover the same geographical region at successive times. A two-dimensional cross-correlation matrix is evaluated for small areas within the images, taking a reference area in the first image, and moving the "search" area around the subsequent image. The greatest correlation value is interpreted as occurring at the position on the second image to which the reference area has been displaced. Velocity is then calculated from the displacement of the reference area between the two images and the time separation. The procedure is carried out for reference areas over the whole image. The method has been shown, in the previously mentioned references, to give reasonable agreement with velocities derived from sea-surface drifters and current profilers, with better results achieved when the time lapse between images is shorter. One major disadvantage of the method is that it is insensitive to rotational motion. As satellite configurations usually force the time lapse between subsequent images to be greater than twelve hours, mesoscale oceanic features, of order 100 km, may well have rotated in that time and their advection may be wrongly evaluated. Neither does the method allow for other non-advective mechanisms (Wahl and Simpson, 1990). Also, its accuracy is critically dependent on the geometric correction applied to the images, which is highlighted when an area of land is sometimes evaluated as having a flow field, because successive images do not exactly correspond.

An application of inverse modelling is used by Kelly (1989), in which the two-dimensional non-diffusive heat equation is inverted, assuming simplified surface heat fluxes and vertical entrainment. The inverse problem was formulated to determine the velocity responsible for near-surface horizontal temperature advection. The along-isotherm velocity component is not uniquely defined by solving the inverse problem, so the problem had to be forced to be over-determined by adding weighted constraints on energy, and the divergence and curl of the velocity field (see Kelly (1989) for a more detailed explanation). The horizontal gradients of temperature were calculated from an image, and the temporal gradient was approximated by looking at the rate of change of the temperature at each geographical location in successive images. If horizontal non-divergent flow is assumed, a streamfunction can be defined for the flow. With the inclusion of constraints on the energy, divergence and vorticity of the flow, realistic total velocity solutions were obtained during testing on synthetic images created by imposing synthetic velocities on an initial image, and again with real images and *'in situ'* measurements of velocities. It was found that Kelly's method produced flows that compared well with *'in situ'* data from Doppler Acoustic Log (DAL) measurements of current velocity, in regions of strong temperature gradients. The solution velocities tended towards the same direction as DAL velocities, but were of smaller magnitude, in regions of high temperature gradients. Horizontal advection accounted for about 40% of the variance of the temporal gradient of temperature.

Kelly and Strub (1992) carried out work comparing the MCC and inverse methods for deriving surface velocities from a series of AVHRR images. Although the inversion method uses longer periods between images and can use lower spatial resolution data (4 km instead of 1 km), both methods resolved features of horizontal scale greater than 50km, with the inverse method performing better near the edges of the images, and giving a smoother solution. However, there was strong qualitative agreement between the estimates from the two methods. In comparison with *'in situ'* measurements, both methods underestimated the magnitude of the velocity, being 35% lower than shipborne Acoustic Doppler Current Profiler (ADCP) measurements, and 56% lower than surface drifter data. The root-mean-square differences in the estimated direction were 60°-70°, which is only marginally lower than the difference between ADCP and drifter measurements. These differences are believed to be due to the assumptions made in implementing the methods, and not to inadequacies in the data. Initial experiments into assimilation of altimeter data into these methods did not yield significant improvements.

More recent implementations of feature-tracking techniques (Breaker, *et al.*, 1994) have overcome some of the problems associated with the MCC method. An implementation of a shape-matching method to track eddies (Kuo and Ho, 1996) suggests that it is possible

to measure the rotation and deformation of features in this way. Preliminary experiments to track clouds using neural network methods to minimise a cost function between images (Côté and Tatnall, 1995) indicate that these methods may be more accurate, faster, and better at detecting and measuring rotation and deformation of features. Preliminary experiments with a functional analytic method (Bannehr, *et al.*, 1996) suggest that it too may be a better method than MCC techniques.

Appendix B. INVERTING PV TO VELOCITY

B.1 MODEL TO BE USED FOR PV INVERSION

Hoskins *et al.* (1985) note that PV maps can be helpful in understanding the dynamics of ocean processes for the two reasons that PV is a conserved quantity and it is invertible. This means that the velocity field of a particular ocean model can be derived from the PV distribution. To formulate the inversion problem, some assumptions and approximations must be applied to the PV equation (2.1) defining a model of the ocean (Hoskins, *et al.*, 1985). Adequate boundary conditions must also be imposed on the model, so that a unique solution is determined after inversion. This appendix presents the preliminary work that was carried out to investigate how to proceed from a PV field, derived from a sea surface temperature (SST) image, by inverting a model of PV to obtain the velocity field.

The assumptions and approximations applied must be physically feasible, complying with the spatial and temporal scales of the motions in the model. The simplest set of assumptions are those which apply for geostrophic balance, which assumes that the Coriolis force due to the Earth's rotation balances the pressure gradient force due to differences in the height of the sea surface caused by the velocity field. However, geostrophic balance is valid to first order only, because the ocean is a stratified fluid and deviations occur as a result of buoyancy effects. This is accounted for in quasi-geostrophic (QG) theory, where the buoyancy of the fluid enters into the governing equations of motion. From these can be derived the quasi-geostrophic potential vorticity (QGPV), which is an approximation to the PV and is approximately conserved.

In this appendix, a simple model of the ocean is used to define the QGPV inversion problem. In subsequent work, the model could be developed to be more realistic and, consequently, more complex. An ocean is defined as shallow if the width of the basin is much greater than the depth, as with real oceans, and then shallow-water dynamics govern the motions (Apel, 1987). The vertical component of the geostrophic PV for a homogeneous (constant density), shallow water region which has a perturbed surface can be shown to be (Apel, 1987)

$$Q(x,y) = \frac{\zeta + f_0 + \beta y}{D + \eta} \tag{B.1}$$

where the modelled region is rectangular with x and y increasing to the east and north, respectively; D is the mean depth of the fluid; η is the perturbation depth which is much

smaller than D and varies with x and y; the vertical component of the planetary vorticity is assumed to vary linearly with y such that $f = f_0 + \beta y$; and $\zeta = (\partial v/\partial x - \partial u/\partial y)$ is the vertical component of the relative vorticity. By expanding the denominator, combining the constant terms with Q, and neglecting higher order terms (see Pedlosky (1987)), equation (B.1) reduces to

$$Q_{QG}(x,y) = \zeta + \beta y - \frac{\eta f_0}{D} \tag{B.2}$$

where $Q_{QG}(x,y)$ is the QGPV for inviscid homogenous shallow water at the position given by (x,y).

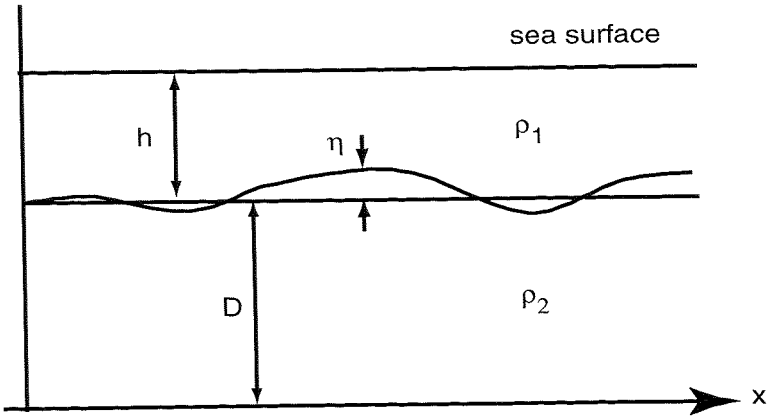

Fig. B-1 Two layer model of different density fluids, top layer much shallower than lower layer, with flow only in top layer.

Now, consider a slightly more constrained model: two layers of water of slightly different density (see Figure B-1). The top flowing layer, of density ρ_1 and variable depth h, is much shallower than the deep quiescent lower layer, of density ρ_2 and depth D. Both surface and bottom boundaries are held fixed, while the interface depth may vary. If the flow in the top layer is represented as (u,v), then we can define a streamfunction, Ψ, according to

$$u = -\frac{\partial \Psi}{\partial y}, \quad v = \frac{\partial \Psi}{\partial x}. \tag{B.3}$$

Differentiating the components of flow in equation (B.3), and taking their difference gives the relative vorticity, ζ, as

$$\zeta = \nabla^2 \Psi. \tag{B.4}$$

The linearised geostrophic equations of motion, taken with the hydrostatic approximation, relate the flow velocity to the perturbation height according to

$$f_0 u = \frac{-1}{\rho_1}\frac{\partial p}{\partial x} = -g'\frac{\partial \eta}{\partial x}$$
$$f_0 v = \frac{1}{\rho_1}\frac{\partial p}{\partial x} = g'\frac{\partial \eta}{\partial x} \qquad \text{(B.5)}$$

where g' is the reduced (or "effective") gravity which is the vertical restoring force due to the density difference at the boundary between the two layers, and is given by

$$g' = \frac{\rho_2 - \rho_1}{\frac{1}{2}(\rho_2 + \rho_1)} g \qquad \text{(B.6)}$$

Now, substituting with the streamfunction derivative (B.3) for u or v in (B.5) yields the relationship

$$\eta = \frac{f_0}{g'}\Psi + \text{constant} \qquad \text{(B.7)}$$

Finally, we substitute (B.4) and (B.7) into (B.2), which represents the more general case (the integration constant of equation (B.7) can be absorbed into the left hand side) to give the QGPV for this model as

$$Q_{QG}(x,y) = \nabla^2\Psi - \frac{1}{L_D^2}\Psi + \beta y \qquad \text{(B.8)}$$

where $L_D^2 = \frac{g'D}{f_0^2}$.

The length L_D is the internal Rossby radius of deformation, which for the open ocean is of order 100 km, and is of the same order as the characteristic length scale of mesoscale motions (Pedlosky, 1987).

Equation (B.8) is the equation for QGPV that will be inverted to give the flow field given Q_{QG}, with L_D selected as an appropriate value for mesoscale motions. Clearly this model is far from representing the ocean realistically. Future developments of the model would include multiple layers of varying density, and varying thickness.

B.2 INVERSION TECHNIQUES AND PRELIMINARY RESULTS

The equation to be solved (B.8) is a two-dimensional second order elliptic partial differential equation. To date, only a few specific elliptic equations, with particular boundary conditions, have been solved analytically. Numerical approximation methods are the only means of solution of many elliptic equations (Smith, 1990), and the most frequently used are finite-difference methods, where the derivative at a point is approximated by a difference over a small interval.

Numerical solution of an equation is carried out in two steps. First, the equation is approximated by a number of algebraic equations. These are set up by overlaying the region of interest with a grid, and at each node of the grid a finite-difference approximation is substituted for each derivative of the elliptic equation. This generates an algebraic equation corresponding to each mesh point, in terms of the values of the unknown field (for equation (B.8) this would be the streamfunction, Ψ) at that point, and neighbouring points. The accuracy of this part of the solution process is influenced by the number of mesh points considered in the finite-difference scheme.

The second step is to solve the system of linear algebraic equations, which is not straightforward because a large number of equations are generally involved. Techniques used are usually direct or iterative methods. Direct methods, such as Gaussian elimination, solve the system of equations in a fixed number of steps, with errors due solely to rounding errors. Iterative methods use a first estimate of the solution to calculate an improved estimate which in turn is used to improve the estimate further, and so on, until the difference between successive iterations is small and the solution is described as having "converged". Direct methods are usually the quickest and most accurate. However, when the system of equations is very large, iterative methods are more useful as they require less computer capacity and are simpler to implement.

The finite-difference scheme selected for use here is a general scheme for discretising any second order elliptic partial differential equation on a rectangular region with given boundary conditions (see NAG FORTRAN Library Manual (1991) , Sub-routine D03EEF). The finite difference scheme discretises the equation on to a rectangular grid by approximating it at each grid point, using six of the neighbouring points. The result of this is a system of linear equations, which are modified according to the boundary conditions.

A "multigrid" iterative method was selected as being the most suitable way to solve the system of equations (NAG FORTRAN Library Manual (1991), Sub-routine D03EDF). Multigrid methods are an improvement over traditional iterative methods because they

are better at removing the low wavenumber components of the error, which can prevent convergence of the solution (Broutman, 1990). The multigrid method used requires an initial estimate of the solution, or can start from a zero guess. The system of equations is "smoothed" to remove high frequency components of the error, and then the system is mapped on to a sequence of coarser grids. The errors are smoothed again, and then mapped on to finer grids. On the finest grid the solution estimate is corrected. This procedure (explained more fully in Wesseling (1982)) is repeated until the solution converges, or for a maximum number of iterations.

Preliminary tests of this inversion procedure for equation (B.8) were carried out. The original premise of this work was that PV and SST were functionally related (FLW89, Marshall and Williams, 1989). Accordingly, a simulated Q_{QG} field was produced from an AVHRR image of the SST of part of the Gulf Stream region. A 200 km by 200 km sub-image was extracted from the full image. The mean value was then subtracted across the sub-image, and the resulting values were negated. This produced a field (Figure B-2) in which the QGPV increases as the SST decreases, which is consistent with the observations of FLW89. It must be stressed that this field is not necessarily a true representation of the QGPV field in that part of the Gulf Stream, but was produced purely to allow the testing of the inversion procedure on a field with some sort of mesoscale structure. This field was then inverted to yield a stream function, which in turn was translated into velocity vectors at each point on the inversion grid. Various values for the scale length, L_D, were used, to test empirically the effect on the results. With smaller values, the solution streamfunction contains more structure. The solution to the Q_{QG} field using $L_D = 10.0$ is shown superimposed on the Q_{QG} field in Figure B-2, for the case of boundary conditions set such that the streamfunction is zero on the boundaries, which means there is no flow through the boundaries. These boundary conditions force the flow to circulate round the outer edges of the region. Apart from this, the flow field estimated is not unrealistic in terms of the direction of flow, though the relative magnitudes are less believable. Some attempts were made to improve the boundary solution. For example, the initial Q_{QG} field was surrounded by an outer frame of values set by linear interpolation from the boundary values of the original region down to zero at the new boundary, and then the solution of this larger Q_{QG} region was computed, and the solution for the frame discarded. However, this showed no significant improvement in the solution field for the original region, nor did other attempts using frames round the initial field of values set in various ways. Other ways could be tried to improve the solution at the boundaries, such as using more feasible boundary conditions. For example, by constraining the solution such that there is no flow through the north and south boundaries, and that flow in through the west boundary is matched by flow out through the east.

Fig. B-2 Simulated QGPV field produced from 200x200km AVHRR SST imagery of a Gulf Stream ring, overlaid with velocity vectors (arbitrary units) derived by inverting the QGPV using scale length 10.0 and boundary conditions of zero streamfunction.

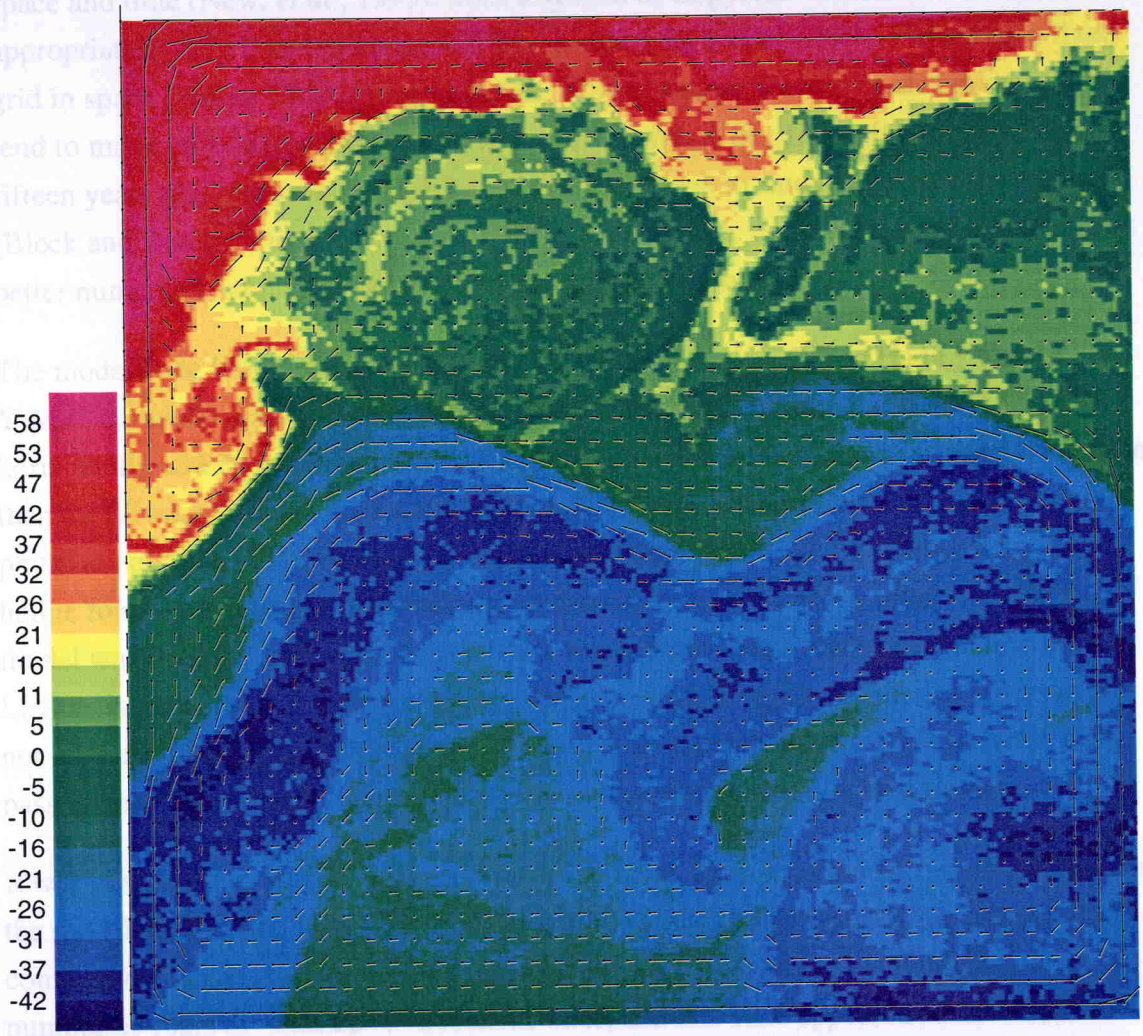

Appendix C. ATLANTIC ISOPYCNIC MODEL (AIM)

C.1 THE MODEL

The Atlantic Isopycnal Model (AIM) is a simulation of the North Atlantic Ocean based on a coordinate system of a set of layers of constant density, whose thickness can vary in space and time (New, *et al.*, 1993). Such a system of isopycnic coordinates is a more appropriate system than the traditional Bryan-Cox type model which is based on a fixed grid in space (Bryan, 1969, Cox and Bryan, 1984), because water particles in the ocean tend to move on surfaces of constant density (Holland, *et al.*, 1984). It is only in the last fifteen years that isopycnal models have been developed to study the ocean circulation (Bleck and Boudra, 1986, Oberhuber, 1990). An isopycnic coordinate system also allows better numerical handling of the bottom topography of the ocean.

The model code was implemented on the UK Meteorological Office Hadley Centre Cray Y-MP8 computer, and then integrated at intermediate resolution, nominally 0.5 - 1° horizontally and 20 isopycnic layers vertically. This is much coarser horizontal resolution than the Vivaldi data set. Various integrations have been carried out, under different physical conditions. The integration studied here included "realistic" bathymetry and haline forcing, was run for 45 years, and is known as run AW (New, *et al.*, 1993). The model was initialised from the Levitus data set (Levitus, 1982) and some forcing back to Levitus is included in the integration for the mixed layer, while the interior layers were not relaxed towards any climatology. There was no diapycnic mixing, but water could pass to and from the mixed layer through seasonal entrainment and detrainment.

It was possible to extract a particular isopycnic layer, from a particular month and year of the model results, and to put these into a similar format to the Vivaldi data, for ease of comparison. The comparisons used results from year 30, because the model takes a number of years to "spin up" to a realistic state, and this state appeared to have been attained by year 30. The Vivaldi data were gathered mostly during May, which corresponds with month 8 of AIM which was initialised from the month of October in year 1. The top isopycnic layer, layer 1, of AIM is its "mixed layer", and layer 11 of AIM corresponds to a layer with σ_0 of 27.00, and 0.15 kg m^{-3} thick. The AIM output was processed in the same way as the Vivaldi data to derive the Sverdrup IPV. Then, because the AIM results were defined over the whole of the North Atlantic Ocean, they were reduced down to the Vivaldi geographical region. The mixed layer temperature, layer 11 potential temperature and layer 11 Sverdrup IPV from run AW, year 30, month 8 (May) of AIM are shown in Figure C-1.

The range of potential temperature on layer 11 of the model output within the Vivaldi region matched closely the range of potential temperature on level 27.00 of the Vivaldi data, although the model values were skewed towards the higher values (compare Figure C-2a with Figure 3-10b). The mixed layer temperature range of AIM also closely matched the near-surface temperature as measured by thermosalinograph during Vivaldi. The Sverdrup IPV values were also within similar ranges, but the AIM reached greater extremes at the northern and southern limits of the region (again, compare Figure C-2b with Figure 3-10b). This shows that AIM values in the region, at that time of year, are quite realistic.

C.2 COMPARISON OF SVERDRUP PV WITH ISOPYCNIC POTENTIAL TEMPERATURE AND MIXED LAYER TEMPERATURE

Using output from run AW, year 30, month 8 (May) of AIM (Figure C-1), within the Vivaldi geographical region, comparisons were made of Sverdrup IPV on layer 11 ($\sigma_0 = 27.00$) with the layer 11 potential temperature and the mixed layer temperature, as shown in Figure C-2. The correlation between Sverdrup IPV and layer 11 temperature is quite poor (Figure C-2a). The lowest Sverdrup IPV values have a narrow range of corresponding temperature, which increases to include cooler temperatures as the Sverdrup IPV increases. The temperature is highly dependent on latitude, while the Sverdrup IPV is not particularly dependent on geographical position.

The correlation is even poorer with mixed layer temperature (Figure C-2b), where a wide range of temperatures corresponds with the whole range of Sverdrup IPV. This occurs because the temperature is near-constant with longitude, and changes steadily with latitude.

C.3 COMPARISON OF AIM RESULTS WITH VIVALDI RESULTS

Both sets of comparisons, from Vivaldi and AIM, indicate that there exists a functional relationship between Sverdrup IPV and isopycnal potential temperature. Both sets of comparisons show that there is a poorer correlation between Sverdrup IPV and SST, but that some correlation still exists. The AIM output show a poorer correlation between the Sverdrup IPV and isopycnic potential temperature, most probably due to the coarser resolution of the model output, but there is general agreement with the sense of the relationship between Sverdrup IPV and isopycnic potential temperature. Each output value of this run of AIM is smoothed horizontally over an area that is nominally 0.5 - 1° squared. This translates to about 60 km by 60 km in the Vivaldi region, which is not sufficient to resolve many mesoscale features. It is notable too that relative vorticity

makes a significant contribution to IPV at the mesoscale, and so both sets of comparisons might be considerably changed if the full IPV were used in these comparisons. Since this comparison of AIM and Vivaldi data was carried out, finer scale runs of AIM have been executed. It would be interesting to repeat the comparison with the fine-scale output, and this may be done as part of future work.

Fig. C-1 Mixed layer temperature, layer 11 potential temperature and layer 11 Sverdrup PV from run AW, year 30, month 8 (May) of AIM.

(a)

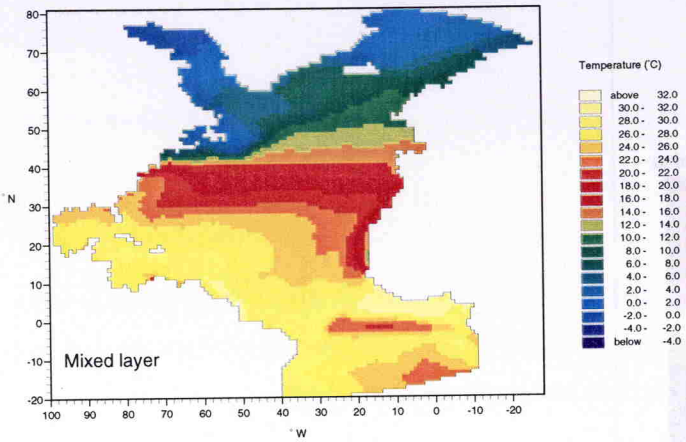

(b)

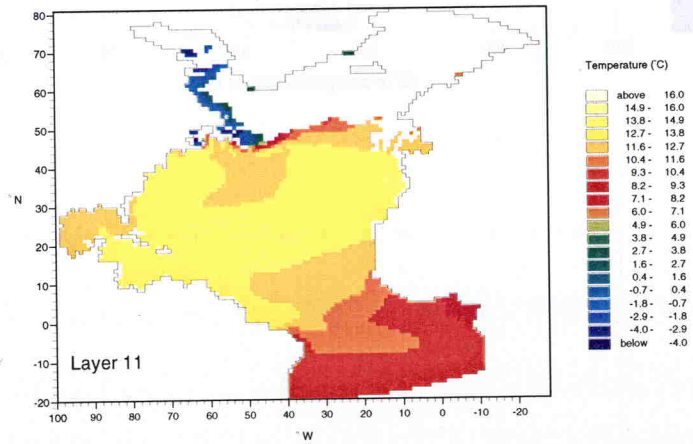

(c)

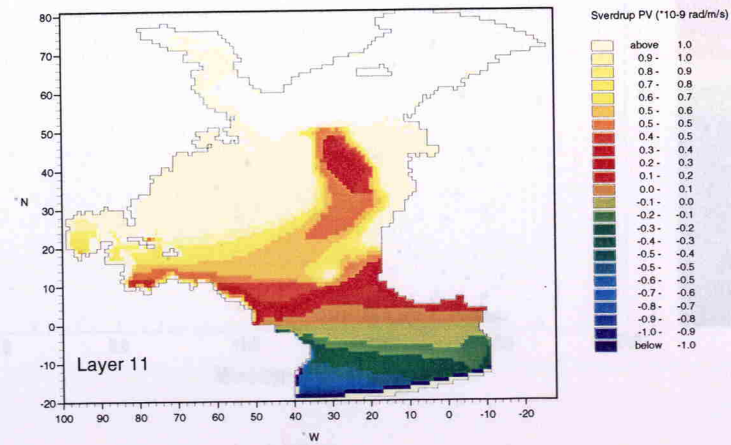

Fig. C-2 Relationship between layer 11 PV and (a) layer 11 potential temperature and (b) mixed layer temperature, from AIM run AW, year 30, month 8.

(a)

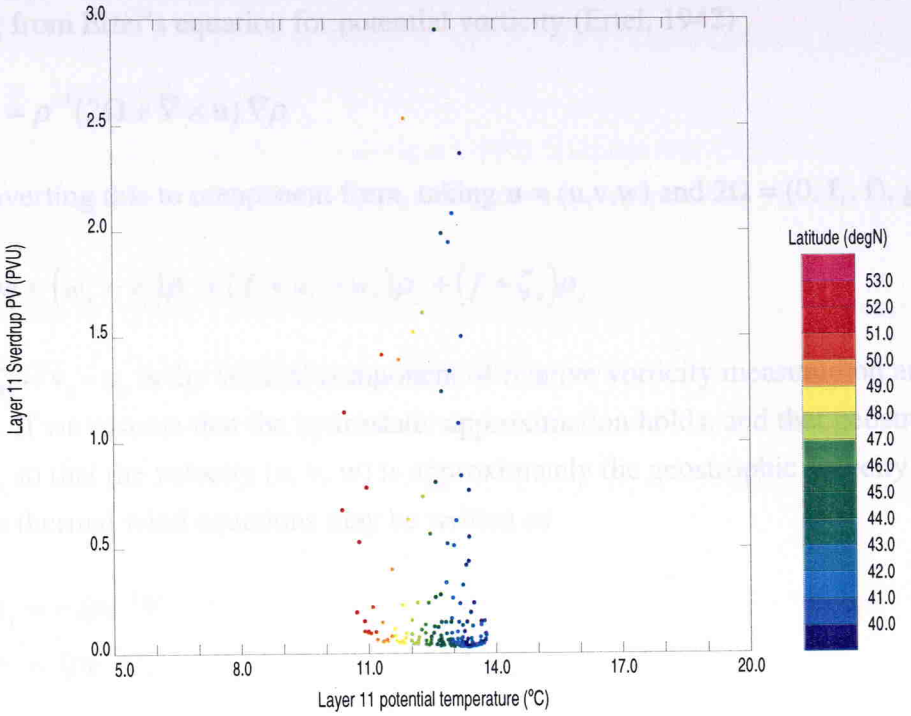

(b)

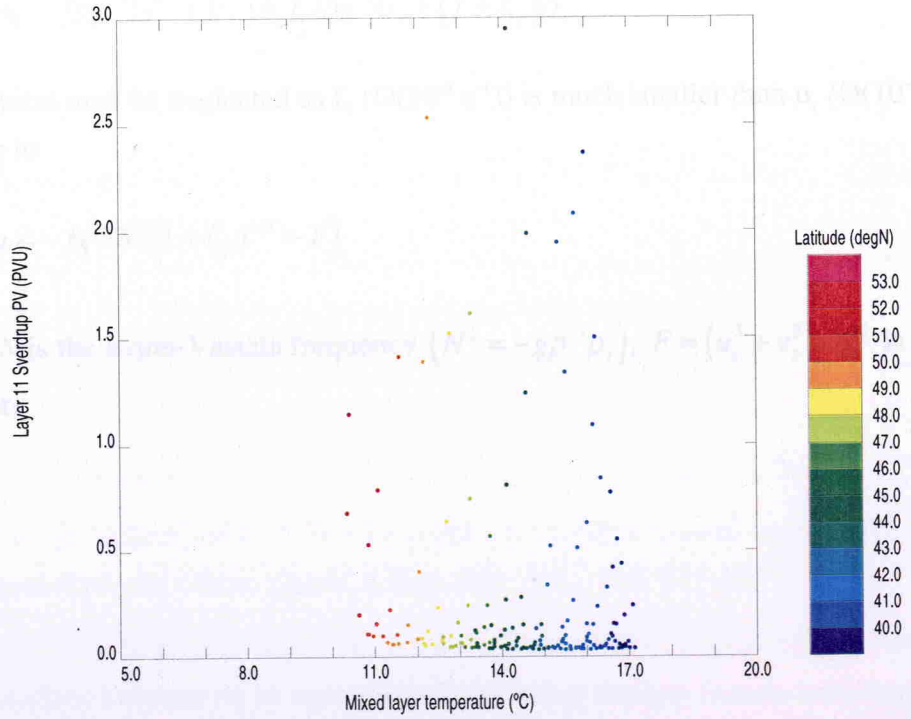

Appendix D. DERIVATION OF ISOBARIC POTENTIAL VORTICITY EQUATION (2.4)

Starting from Ertel's equation for potential vorticity (Ertel, 1942)

$$q = \rho^{-1}(2\Omega + \nabla \times \mathbf{u}).\nabla\rho \tag{D.1}$$

and converting this to component form, taking **u** = (u,v,w) and 2Ω = (0, f_1, f), gives

$$\rho q = (w_y - v_z)\rho_x + (f_1 + u_z - w_x)\rho_y + (f + \zeta_p)\rho_z \tag{D.2}$$

where $\zeta_p = v_x - u_y$ is the vertical component of relative vorticity measured on an isobaric surface. If we assume that the hydrostatic approximation holds, and that geostrophy applies, so that the velocity (u, v, w) is approximately the geostrophic velocity (U, V, 0) , then the thermal wind equations may be written as

$$\begin{aligned} \rho_x &= -f\rho g^{-1} V_z \\ \rho_y &= f\rho g^{-1} U_z \end{aligned} \tag{D.3}$$

Applying (D.3), (D.2) can be reduced down to

$$\rho q = f\rho g^{-1}(V_z^2 + U_z^2) + f_1 f\rho g^{-1} U_z + (f + \zeta_p)\rho_z \tag{D.4}$$

The f_1 term may be neglected as f_1 ($O(10^{-4}\ s^{-1})$) is much smaller than u_z ($O(10^{-2}\ s^{-1})$), leading to

$$q = -fg^{-1}N^2(1 + \zeta_p f^{-1} - F), \tag{D.5}$$

where N is the Brunt-Väisälä frequency $(N^2 = -g\rho^{-1}\rho_z)$, $F = (u_z^2 + v_z^2)/N^2$ is the Froude number.

BIBLIOGRAPHY

Allen, J., R. Pollard and A. New (1991) How do eddies modify the stratification of the thermocline? In: *Ocean variability and acoustic propagation. Proceedings of workshop, La Spezia, Italy, June 4-8, 1990*, Potter, J. and A. Warn-Varnas, editor, Kluwer Academic, Dordrecht, pp. 417-431.

Allen, J. T., J. F. Read and S. G. Alderson (1992) SeaSoar and CTD sections across the Iceland-Faeroes Front and Faeroe Shetland Channel, August 1990. *IOSDL* Report No. 295, 124 pp.

Allen, J. and D. Smeed (1996) Potential vorticity and vertical velocity at the Iceland-Færœs Front. *J. Phys. Oceanogr.*, **26**, 2611-2634.

Apel, J. R. (1987) *Principles of Ocean Physics*, Academic Press, Orlando, 605 pp.

Arhan, M. (1990) The North Atlantic Current and Subarctic Intermediate Water. *J. Mar. Res.*, **48**, 109-144.

Arhan, M. and A. Colin de Verdière (1985) Dynamics of eddy motions in the eastern North Atlantic. *J. Phys. Oceanogr.*, **15**, 153-170.

Ball, F.K. (1960) Control of inversion height by surface heating. *Quart. J. Roy. Met. Soc.*, **86**, 483-494.

Bannehr, L., G. Rohn and G. Warnecke (1996) A functional analytic method to derive displacement vector fields from satellite image sequences. *Inter. J. Remote Sensing* , **17**, 383-392.

Bauer, J. and J. D. Woods (1984) Isopycnic atlas of the North Atlantic Ocean - monthly mean maps and sections. *Institut fur Meereskunde an der Universitat Kiel* Nr. 132, 173 pp.

Behringer, D. W. (1972) Investigation of large scale oceanic circulation patterns using historical hydrographic data. Ph.D. Thesis, University of California, San Diego.

Bleck, R. and D. B. Boudra (1986) Wind-driven spin-up in eddy-resolving ocean models formulated in isopycnic and isobaric coordinates. *J. Geophys. Res*, **91**, 7611-7621.

Bleck, R., R. Onken and J. D. Woods (1988) A two-dimensional model of mesoscale frontogenesis in the ocean. *Quart. J. Roy. Met. Soc.*, **114**, 347-371.

Breaker, L., V. Krasnopolsky, D. Rao and X. Yan (1994) The feasibility of estimating ocean surface currents on an operational basis using satellite feature tracking methods. *Bulletin American Met. Soc.*, **75**, 2085-2095.

Broutman, D. (1990) Spectral multigrid for the vorticity-streamfunction relation. *Ocean Modelling,* **No. 89** , 2-4.

Bryan, K. (1969) A numerical method for the study of the circulation of the world ocean. *J. Comput. Phys.*, **4**, 347-376.

Burren, C. (1993) A numerical modelling investigation of the impact of mesoscale heterogeneity on oceanic primary productivity. PhD Thesis, University of Southampton, 271 pp.

Challenor, P. G., J. F. Read, R. T. Pollard and R. T. Tokmakian (1996) Measuring surface currents in the Drake Passage from altimetry and hydrography. *J. Phys. Oceanogr.*, **26**, 2748-2759.

Charnock, H. and J. A. Businger (1991) The Frontal Air-Sea Interaction Experiment in Perspective. *J. Geophys. Res.*, **96**, 8639-8642.

Cipollini, P. and G. Corsini (1996) The Modular Optoelectronic Scanner MOS: a study of its capabilities for optically active parameter estimation by means of an ocean colour model. *Proc. SPIE* (Ocean Optics XIII), Halifax (Canada), 22-25 October, 1996, **2963**, 6 pp.

Côté, S. and A. Tatnall (1995) A neural network-based method for tracking features from satellite sensor images. *Inter. J. Remote Sensing* , **16**, 3695-3701.

Cox, M. D. and K. Bryan (1984) A numerical model of the ventilated thermocline. *J. Phys. Oceanogr.*, **14**, 674-687.

Csanady, G. T. and G. Vittal (1996) Vorticity balance of outcropping isopycnals. *J. Phys. Oceanogr.*, **26**, 1952-1956.

Cunningham, S. A., M. J. Griffiths, J. Hemmings, S. G. Alderson et al (1992) SeaSoar CTD, fluorescence and scalar irradiance data from RRS Charles Darwin Cruises 58/59, NE Atlantic (Vivaldi 91). *IOSDL* Report No 299, 48 pp.

Denman, K. and M. Miyake (1973) Upper layer modification at ocean weather station Papa; observation and simulation. *J. Phys. Oceanogr.*, **3**, 185-196.

Dickson, R. R., J. Meincke, S.-A. Malmberg and A. J. Lee (1988) The "Great Salinity Anomaly" in the northern North Atlantic 1968-1982. *Prog. Oceanogr.*, **20**, 103-151.

Ellett, D. J., A. Edwards and R. Bowers (1986) The hydrography of the Rockall Channel - an overview. *The Royal Society of Edinburgh.*

Emery, W. J., A. C. Thomas, M. J. Collins, W. R. Crawford and D. L. Mackas (1986) An objective method for computing advective surface velocities from sequential infrared satellite images. *J. Geophys. Res.*, **91**, 12865-12878.

Erikson, C. C., R. A. Weller, D. L. Rudnick, R. T. Pollard and L. A. Regier (1991) Ocean frontal variability in the Frontal Air-Sea Interaction Experiment. *J. Geophys. Res.*, **96**, 8569-8592.

Ertel, H. (1942) On hydrodynamical vorticity equations, *Physikalische Zeitschrift*, **43**, 526-529.

Fedorov, K. (1986) *The physical nature and structure of oceanic fronts*, Springer-Verlag, New York, 333 pp.

Fedorov, K. and N. Kuz'mina (1977) Fronts in the ocean. In: *Mesoscale variability of an oceanic temperature field* , Fedorov, K., editor, IOAN, Moscow, pp. 33-53.

Fischer, J., H. Leach and J. D. Woods (1989) A synoptic map of isopycnic potential vorticity in the seasonal thermocline. *J. Phys. Oceanogr.*, **19**, 519-531.

Follows, M. and J. Marshall (1994) Eddy driven exchange at ocean fronts. *Ocean Modelling*, **No. 102**, 5-9.

Foreman, S. (1990) Meteorological Office Unified Model Documentation, Ocean model, Mixed layer formulation. *UK Meteorological Office* Unified model documentation paper No. 40, 16 pp.

Garcia, C. A. E. and I. S. Robinson (1989) Sea surface velocities in shallow seas extracted from sequential Coastal Zone Color Scanner satellite data. *J. Geophys. Res.*, **94**, 12681-12691.

Gill, A. E. (1982) *Atmosphere-Ocean Dynamics*, Academic Press, San Diego, 662 pp.

Gordon, A. L. (1967) Structure of Antarctic waters between 20°W and 170°W. In: *Ant. Rep. Folio Series, folio 6* , Bushnell, V. C., editor, American Geographic Society, New York, 24 pp.

Haines, K. (1991) A direct method for assimilating sea surface height data into ocean models with adjustments to the deep circulation. *J. Phys. Oceanogr.*, **21(6)**, 843-868.

Haines, K., P. Malanotte-Rizzoli, R. Young and W. Holland (1993) A comparison of two methods for the assimilation of altimeter data into a shallow-water model. *Dynamics of Atmospheres and Oceans*, **17**, 89-133.

Halliwell, G. R., Jr., P. Cornillon, K. H. Brink, R. T. Pollard, D. L. Evans, L. A. Regier, J. M. Tooke and R. W. Schmitt (1991) Descriptive oceanography during the Frontal Air-Sea

Interaction Experiment: medium-to large-scale variability. *J. Geophys. Res.*, **96**, 8553-8568.

Hanson, H. P., P. Cornillon, G. R. J. Halliwell and V. Halliwell (1991) Climatological perspectives, oceanographic and meteorological, on variability in the Subtropical Convergence Zone in the Northwestern Atlantic. *J. Geophys. Res.*, **96(C5)**, 8517-8529.

Harvey, J. (1982) θ-S relationships and water masses in the eastern North Atlantic. *Deep-Sea Research*, **29**, 1021-1033.

Holland, W. R., T. Keffer and P. B. Rhines (1984) Dynamics of the oceanic general circulation: the potential vorticity field. *Nature*, **308**, 698-705.

Hoskins, B. (1982) The mathematical theory of frontogenesis. *Annu. Rev. Fluid. Mech.*, **14**, 131-151.

Hoskins, B. J. and F. P. Bretherton (1972) Atmospheric frontogenesis models: mathematical formulation and solution. *J. Atmos. Sci.*, **29**, 11-37.

Hoskins, B. J., M. E. McIntyre and R. W. Robertson (1985) On the use and significance of isentropic potential vorticity maps. *Quart. J. Roy. Met. Soc.*, **111**, 877-946.

Hua, B., J. McWilliams and W. Brechner Owens (1986) An objective analysis of the POLYMODE Local Dynamics Experiment. Part II: streamfunction and potential vorticity fields during the intensive period. *J. Phys. Oceanogr.*, **16**, 506-521.

Iselin, C. O. (1939) The influence of vertical and horizontal turbulence on the characteristics of waters at mid-depths. *Transactions of the American Geophysical Union*, **3**, 414-417.

Kelly, K. (1989) An inverse model for near-surface velocity from infrared images. *J. Phys. Oceanogr.*, **19 (12)**, 1845-1863.

Kelly, K. A. and P. T. Strub (1992) Comparison of velocity estimates from Advanced Very High Resolution Radiometer in the Coastal Transition Zone. *J. Geophys. Res.*, **97**, 9653-9668.

Klein, P. and B. L. Hua (1988) Mesoscale heterogeneity of the wind-driven mixed layer: Influence of a quasigeostrophic flow. *J. Mar. Res.*, **46**, 495-525.

Klein, P. and B. Hua (1990) The mesoscale variability of the sea surface temperature: an analytical and numerical model. *J. Mar. Res.* **48**, 729-763.

Kraus, E. and J. Turner (1967) A one-dimensional model of the seasonal thermocline. II. The general theory and its consequences. *Tellus*, **19**, 98-105.

Kuo, N. and C. Ho (1996) A satellite feature-tracking method to compute sea surface angular velocities. *Acta Oceanographica Taiwana*, **35**, 55-63.

Leach, H. (1987) The diagnosis of synoptic-scale vertical motion in the seasonal thermocline. *Deep-Sea Res.*, **34**, 2005-2017.

Leese, J. A., C. S. Novak and B. B. Clarke (1971) An automated technique for obtaining cloud motion from geosynchronous satellite data using cross correlation. *J. Appl. Met.*, **10**, 110-132.

Levitus, S. (1982) Climatological atlas of the world ocean. *NOAA* Professional Paper 13, 173 pp.

Levitus, S. and T. Boyer (1994) *World Ocean Atlas, Volume 4 Temperature, NESDIS 4*, NODC, Washington.

Levitus, S., R. Burgett and T. Boyer (1994) *World Ocean Atlas, Volume 3 Salinity, NESDIS 3*, NODC, Washington.

Linden, P. (1991) Dynamics of fronts and eddies. In: *Nonlinear topics in ocean physics* , Osborne, A., editor, Elsevier, Amsterdam, pp. 313-351.

Lukas, R. and E. Lindstrom (1991) The mixed layer of the Western Equatorial Pacific Ocean. *J. Geophys. Res.*, **96 Supp.**, 3343-3357.

Luyten, J., J. Pedlosky and H. Stommel (1983) The ventilated thermocline. *J. Phys. Oceanogr.*, **13(2)**, 292-309.

Marshall, D. (1995) Topographic steering of the Antarctic Circumpolar Current. *J. Phys. Oceanogr.*, **25**, 1636-1650.

Marshall, D. (1997) Subduction of water masses in an eddying ocean. *J. Mar. Res.*, **55**, 201-222.

Marshall, D. and J. Marshall (1995) On the thermodynamics of subduction. *J. Phys. Oceanogr.*, **25**, 138-151.

Marshall, J. C. (1985) Determining the ocean circulation and improving the geoid from satellite altimetry. *J. Phys. Oceanogr.*, **15**, 330-349.

Marshall, J. and A. Nurser (1992) Fluid dynamics of oceanic thermocline ventilation. *J. Phys. Oceanogr.*, **22**, 583-595.

Marshall, J. C. and R. G. Williams (1989) Estimation of balanced velocity and temperature fields from satellite observations of passive scalars. Unpublished note, 4 pp.

McCartney, M. S. (1982) The subtropical recirculation of Mode Waters. *J. Mar. Res.*, **40**, 427-464.

McCartney, M. S. and L. D. Talley (1982) The subpolar mode water of the North Atlantic Ocean. *J. Phys. Oceanogr.*, **12**, 1169-1188.

McDowell, S., P. Rhines and T. Keffer (1982) North Atlantic potential vorticity and its relation to the general circulation. *J. Phys. Oceanogr.*, **12**, 1417-1436.

McWilliams, J. C. (1976) Maps from the Mid-Ocean Dynamics Experiment: Part II. Potential vorticity and its conservation. *J. Phys. Oceanogr.*, **6**, 828-846.

Montgomery, R. (1938) Circulation in upper layers of southern North Atlantic deduced with use of isentropic analysis. *Pap. Phys. Oceanogr. Met.*, **6**, 55 pp.

Mooers, C. (1978) Frontal dynamics and frontogenesis. In: *Oceanic fronts in coastal processes* , Bowman, M., editor, Springer-Verlag, Berlin, pp. 16-22.

Morrison, A. I. (1993) Underway temperatures and salinity during RRS *Discovery Cruise 198. James Rennell Centre for Ocean Circulation* Internal Document No. 9, 14 pp.

NAG FORTRAN Library Manual (1991) *Mark 15*, Numerical Algorithms Group Limited, Oxford.

New, A. L., R. Bleck, Y. Jia, R. Marsh, M. Huddleston and S. Barnard (1993) An isopycnic-coordinate model simulation of the Atlantic Ocean. Unpublished manuscript, 30 pp.

Newton, C. (1978) Fronts and wave disturbances in Gulf Stream and atmospheric jet stream. *J. Geophys. Res.*, **83**, 4697-4706.

Niiler, P. and E. Kraus (1977) One-dimensional models of the upper ocean. In: *Modelling and prediction of the upper layers of the ocean* , Kraus, E., editor, Pergamon, Oxford, 325 pp.

Nurser, A. and J. Marshall (1991) On the relationship between subduction rates and diabiatic forcing of the mixed layer. *J. Phys. Oceanogr.*, **21**, 1793-1802.

Oakey, N. and J. Elliott (1982) Dissipation within the surface mixed layer. *J. Phys. Oceanogr.*, **12**, 171-185.

Oberhuber, J. (1990) Simulation of the Atlantic circulation with a coupled sea ice-mixed layer-isopycnal general circulation model. *Max-Planck-Institute for Meteorology* Report No. 59, 86 pp.

Olbers, D., V. Gouretski, G. Seiss and J. Schröter (1993) *Hydrographic atlas of the Southern Ocean*, Alfred-Wegener Institut für Polar- und Meeresforschung, Bremerhaven, Germany, 82 pp.

Open University (1991) *Ocean Circulation*, Open University/Pergamon Press, Milton Keynes/Oxford, 238 pp.

Owens, N. J. P. (1993) BOFS "STERNA 92" Cruise Report" RRS *James Clark Ross 02 26/11/92-18/12/92. Plymouth Marine Laboratory* , 239 pp.

Parr, A. (1938) Analysis of current profiles by a study of pycnomeric distortion and identifying properties. *J. Mar. Res.*, **1**, 269-290.

Pedlosky, J. (1987) *Geophysical Fluid Dynamics*, 2nd ed., Springer-Verlag, New York, 710 pp.

Pedlosky, J. (1990) The dynamics of the oceanic subtropical gyres. *Science*, **248**, 316-322.

Pollard, R. T. (1986) Frontal surveys with a towed profiling conductivity/temperature/depth measurement package (SeaSoar). *Nature*, **323**, 433-435.

Pollard, R. T., J. T. Allen, G. W. J. Miller, A. I. Morrison, J. F. Read and P. G. Taylor (1993) CTD data collected on RRS Discovery Cruise 198 (STERNA) in the Bellingshausen Sea and along 88°W. *IOSDL* Internal Document No. 321, 65 pp.

Pollard, R. T., M. J. Griffiths, S. A. Cunningham, J. F. Read, F. F. Pérez and A. F. Ríos (1996) Vivaldi 1991 - A study of the formation, circulation and ventilation of Eastern North Atlantic Central Water. *Prog. Oceanog.*, **37**, 167-192.

Pollard, R. T., H. Leach, G. Griffiths and others (1991) RRS Charles Darwin cruises 58 & 59, 25 April - 16 May; 18 May - 10 June 1991. VIVALDI '91. *IOSDL* No.228, 49 pp.

Pollard, R. T. and S. Pu (1985) Structure and Circulation of the Upper Atlantic Ocean Northeast of the Azores. *Prog. Oceanog.*, **14**, 443-462.

Pollard, R., J. Read, J. Allen, G. Griffiths and A. Morrison (1995) On the physical structure of a front in the Bellingshausen Sea. *Deep-Sea Research II*, **42**, 955-982.

Pollard, R. T., J. F. Read and J. Smithers (1986) SeaSoar CTD surveys during FASINEX. *IOSDL* Report No. 230, 111 pp.

Pollard, R. T. and L. A. Regier (1992) Vorticity and vertical circulation at an ocean front. *J. Phys. Oceanogr.*, **22**, 609-625.

Pond, S. and G. L. Pickard (1983) *Introductory Dynamical Oceanography*, Pergamon Press, Oxford, 329 pp.

Read, J. F., J. T. Allen, P. Machin, G. Miller, A. I. Morrison, R. T. Pollard and P. G. Taylor (1993) SeaSoar data collected on RRS Discovery Cruise 198 (STERNA) acrosss Drake Passage and in the Bellingshausen Sea. *IOSDL* Internal Document No. 320, 57 pp.

Read, J. F., R. T. Pollard, A. I. Morrison and C. Symon (1995) On the southerly extent of the Antarctic Circumpolar Current in the southeast Pacific. *Deep-Sea Research II*, **42**, 933-954.

Reid, J. (1965) Intermediate waters of the Pacific Ocean. *Johns Hopkins Oceanogr. Stud.*, **No. 2**, 85 pp.

Rhines, P. (1986) Vorticity dynamics of the oceanic general circulation. *Ann. Rev. Fluid Mech.*, **18**, 433-97.

Rhines, P. and W. Young (1982a) Homogenization of potential vorticity in planetary gyres. *J. Fluid. Mech.*, **122**, 347-367.

Rhines, P. and W. Young (1982b) A theory of wind-driven circulation. I. Mid-ocean gyres. *J. Mar. Res.*, **40 suppl.**, 559-596.

Ríos, A. F., F. F. Pérez and F. Frage (1992) Water masses in the upper and middle North Atlantic ocean east of the Azores. *Deep-Sea Research*, **39**, 645-658.

Robinson, A. (1996) Physical processes, field estimation and an approach to interdisciplinary ocean modeling. *Earth-Science Reviews*, **40(1/2)**, 3-54.

Roden, G. (1975) On North Pacific temperature, salinity, sound velocity and density fronts and their relation to the wind and energy flux field. *J. Phys. Oceanogr.*, **5**, 557-571.

Roden, G. (1976) On the structure and prediction of oceanic fronts. *Naval Research Reviews*, **29(3)**, 18-36.

Rudnick, D. and R. Davis (1988) Frontogenesis in mixed layers. *J. Phys. Oceanogr.*, **18**, 434-457.

Rudnick, D. and R. Weller (1993) The heat budget in the North Atlantic subtropical frontal zone. *J. Geophys. Res.*, **98**, 6883-6893.

Samelson, R. M. and D. C. Chapman (1995) Evolution of the instability of a mixed-layer front. *J. Geophys. Res.*, **100**, 6743-6759.

Sarmiento, J. L., C. G. Rooth and W. Roether (1982) The North Atlantic tritium distribution in 1972. *J. Geophys. Res.*, **87**, 8047-8056.

Schmitt, R., P. Bogden and C. Dorman (1989) Evaporation minus precipitation and density fluxes for the North Atlantic. *J. Phys. Oceanogr.*, **19(9)**, 1208-1221.

Smeed, D. A., J. T. Allen and S. G. Alderson (1992) The form to be taken by feature models in FOAM. *DRA* Technical Memorandum (USSF) 92193.

Smeed, D. A., J. T. Allen and M. A. Brandon (1991) A preliminary report on the use of feature models in FOAM. *DRA* Technical Memorandum (USSF) 91150(C).

Smith, G. D. (1990) *Numerical solution of partial differential equations: finite difference methods*, 3rd edn, Oxford University Press, Oxford, 337 pp.

Spall, M. (1995) Frontogenesis, subduction, and cross-front exchange at upper ocean fronts. *J. Geophys. Res.*, **100**, 2543-2557.

Stage, S. A. and R. A. Weller (1986) The Frontal Air-Sea Interaction Experiment (FASINEX) Part II: experimental plan. *Bulletin American Met. Soc.*, **67**, 16-20.

Stammer, D. and J. D. Woods (1987) Isopycnic Potential Vorticity atlas of the North Atlantic Ocean - monthly mean maps. *Institut fur Meereskunde an der Universitat Kiel* , 108 pp.

Stow, D. A. (1987) Remotely-sensed tracers for hydrodynamic surface flow estimation. *Inter. J. Remote Sensing* , **8**, 261-278.

Strub, P., T. Chereskin, P. Niiler, C. James and M. Levine (1997) Altimeter-derived variability of surface velocities in the California Current System 1. Evaluation of TOPEX altimeter velocity resolution. *J. Geophys. Res.*, **102**, 12727-12748.

Talley, L. D. (1985) Ventilation of the subtropical North Pacific: the shallow salinity minimum. *J. Phys. Oceanogr.*, **15**, 633-649.

Turner, D. (1993) BOFS 'Sterna 92' cruise report, Discovery 198 11/11/92-17/12/92. *Plymouth Marine Laboratory* internal report, 85 pp.

Turner, D. R. and N. J. P. Owens (1995) A biogeochemical study in the Bellingshausen Sea: Overview of the STERNA 1992 expedition. *Deep-Sea Research II*, **42**, 907-932.

Udall, I. (1993) The influence of the mixed layer on the ventilation of the thermocline. MPhil/PhD Upgrading Report, University of Southampton, UK, 54 pp.

Voorhis, A. D. and J. G. Bruce (1982) Small-scale surface stirring and frontogenesis in the subtropical convergence of the western North Atlantic.*J. Mar.Res.*, **40**, 801-821.

Wahl, D. and J. Simpson (1990) Physical processes affecting the objective determination of near-surface velocity from satellite data. *J. Geophys. Res.*, **95**, 13511-13528.

Webb, D. J., P. D. Killworth, A. Coward and S. Thompson (1991) *The FRAM Atlas of the Southern Ocean*, Natural Environment Research Council, Swindon, UK.

Weller, R. A. (1991) Overview of the Frontal Air-Sea Interaction Experiment (FASINEX): A study of air-sea interaction in a region of strong oceanic gradients. *J. Geophys. Res.*, **96 (C5)**, 8501-8516.

Wesseling, P. (1982) MGD1 - a robust and efficient multigrid method. In: *Multigrid methods* , Hackbusch, W. and U. Trottenberg, editor, Springer-Verlag, Berlin, pp. 614-630.

Williams, R. G., M. A. Spall and J. C. Marshall (1995) Does Stommel's mixed layer "demon" work? *J. Phys. Oceanogr.*, **25**, 3089-3102.

Woods, J. (1980) Do waves limit turbulent diffusion in the ocean? *Nature*, **288**, 219-224.

Woods, J. D. (1985) The physics of thermocline ventilation. In: *Coupled ocean atmosphere models* , Nihoul, J. C. J., editor, Elsevier, Amsterdam, pp. 543-590.

Woods, J., W. Barkmann and A. Horsh (1984) Solar heating of the oceans - diurnal, seasonal and meridional variation. *Quart. J. Roy. Met. Soc.*, **110**, 633-656.

Woods, J. and P. Minnett (1979) Analysis of mesoscale thermoclinicity with an example from the tropical thermocline during GATE. *Deep-Sea Research*, **26A**, 85-96.

Wunsch, C. (1996) *The Ocean Circulation Inverse Problem*, Cambridge University Press, Cambridge, 442 pp.

SOUTHAMPTON UNIVERSITY LIBRARY

USER'S DECLARATION

AUTHOR: MORRISON, ANNE INGLIS TITLE: OBSERVATIONS OF OCEANIC POTENTIAL VORTICITY AND ITS RELATIONSHIP WITH OTHER TRACERS

DATE: 1999

I undertake not to reproduce this thesis, or any substantial portion of it, or to quote extensively from it without first obtaining the permission, in writing, of the Librarian of the University of Southampton.

To be signed by each user of this thesis

DATE	SIGNATURE	ADDRESS